



688
2015

Berichte

zur Polar- und Meeresforschung

Reports on Polar and Marine Research

The Expedition PS87 of the Research Vessel POLARSTERN to the Arctic Ocean in 2014

Edited by

Rüdiger Stein

with contributions of the participants

Die Berichte zur Polar- und Meeresforschung werden vom Alfred-Wegener-Institut, Helmholtz-Zentrum für Polar- und Meeresforschung (AWI) in Bremerhaven, Deutschland, in Fortsetzung der vormaligen Berichte zur Polarforschung herausgegeben. Sie erscheinen in unregelmäßiger Abfolge.

Die Berichte zur Polar- und Meeresforschung enthalten Darstellungen und Ergebnisse der vom AWI selbst oder mit seiner Unterstützung durchgeführten Forschungsarbeiten in den Polargebieten und in den Meeren.

Die Publikationen umfassen Expeditionsberichte der vom AWI betriebenen Schiffe, Flugzeuge und Stationen, Forschungsergebnisse (inkl. Dissertationen) des Instituts und des Archivs für deutsche Polarforschung, sowie Abstracts und Proceedings von nationalen und internationalen Tagungen und Workshops des AWI.

Die Beiträge geben nicht notwendigerweise die Auffassung des AWI wider.

Herausgeber

Dr. Horst Bornemann

Redaktionelle Bearbeitung und Layout

Birgit Chiaventone

Alfred-Wegener-Institut
Helmholtz-Zentrum für Polar- und Meeresforschung
Am Handeshafen 12
27570 Bremerhaven
Germany

www.awi.de

www.reports.awi.de

Der Erstautor bzw. herausgebende Autor eines Bandes der Berichte zur Polar- und Meeresforschung versichert, dass er über alle Rechte am Werk verfügt und überträgt sämtliche Rechte auch im Namen seiner Koautoren an das AWI. Ein einfaches Nutzungsrecht verbleibt, wenn nicht anders angegeben, beim Autor (bei den Autoren). Das AWI beansprucht die Publikation der eingereichten Manuskripte über sein Repositorium ePIC (electronic Publication Information Center, s. Innenseite am Rückdeckel) mit optionalem print-on-demand.

The Reports on Polar and Marine Research are issued by the Alfred Wegener Institute, Helmholtz Centre for Polar and Marine Research (AWI) in Bremerhaven, Germany, succeeding the former Reports on Polar Research. They are published at irregular intervals.

The Reports on Polar and Marine Research contain presentations and results of research activities in polar regions and in the seas either carried out by the AWI or with its support.

Publications comprise expedition reports of the ships, aircrafts, and stations operated by the AWI, research results (incl. dissertations) of the Institute and the Archiv für deutsche Polarforschung, as well as abstracts and proceedings of national and international conferences and workshops of the AWI.

The papers contained in the Reports do not necessarily reflect the opinion of the AWI.

Editor

Dr. Horst Bornemann

Editorial editing and layout

Birgit Chiaventone

Alfred-Wegener-Institut
Helmholtz-Zentrum für Polar- und Meeresforschung
Am Handeshafen 12
27570 Bremerhaven
Germany

www.awi.de

www.reports.awi.de

The first or editing author of an issue of Reports on Polar and Marine Research ensures that he possesses all rights of the opus, and transfers all rights to the AWI, including those associated with the co-authors. The non-exclusive right of use (einfaches Nutzungsrecht) remains with the author unless stated otherwise. The AWI reserves the right to publish the submitted articles in its repository ePIC (electronic Publication Information Center, see inside page of verso) with the option to "print-on-demand".

Titel: Das norwegische Hovercraft Sabvabaa auf einer Eisscholle im zentralen Arktischen Ozean bei 87°15'N, 155°E, dem Startpunkt für ein fast einjähriges Driftexperiment durch den Arktischen Ozean bis in die Fram-Straße (Foto von Rüdiger Stein, Alfred-Wegener-Institut, 30. August 2014)

Cover: The Norwegian hovercraft Sabvabaa has been dropped-off from Polarstern on a large ice floe in the central Arctic Ocean at about 87°15'N, 155°E, ready for its about one-year drift through the entire Arctic Ocean towards Fram Strait (picture taken by Rüdiger Stein, Alfred Wegener Institute, 30th August 2014).

The Expedition PS87 of the Research Vessel POLARSTERN to the Arctic Ocean in 2014

Edited by

Rüdiger Stein

with contributions of the participants

Please cite or link this publication using the identifiers

hdl:10013/epic.45337 or <http://hdl.handle.net/10013/epic.45337> and

doi:10.2312/BzPM_0688_2015 or http://doi.org/10.2312/BzPM_0688_2015

ISSN 1866-3192

PS87

(ARK-XXVIII/4)

05 August 2014 – 08 October 2014

Tromsø – Bremerhaven



**Chief scientist
Rüdiger Stein**

**Coordinator
Rainer Knust**

Contents

1.	Zusammenfassung und Fahrtverlauf	3
	Summary and Itinerary	8
2.	Weather Conditions	10
3.	Isotope Signature of Water Vapour over the Arctic Ocean	14
4.	Activities of the Sea Ice Physics Group	19
	4.1 AEM –Ice thickness measurements	19
	4.2 <i>In-situ</i> sea ice observations	22
5.	Physical Oceanography	27
6.	Distribution of Seabirds and Marine Mammals	31
7.	The environmental controls of trace metal ratios recorded in calcareous tests of Arctic deep-sea benthic foraminifera – Culture experiments, modern field data and the long-term geological record	37
8.	Bathymetric Investigations	43
9.	Marine Geophysics	49
	9.1 Seismic Investigations Across the Lomonosov Ridge	49
	9.2 Magnetic measurements	57
	9.3 Gravity measurements	61
	9.4 Marine mammal observation	70
10.	Marine Geology	73
	10.1 Overview of the PS87 Marine Geology Programme	73
	10.2 Marine Sediment Echosounding using PARASOUND	87
	10.3 Physical properties and core logging	97
	10.4 Line-scan imaging and XRF scanning	108
	10.5 Characteristics of surface sediments	113
	10.6 Main lithologies and lithostratigraphy of PS87 sediment cores	119
	10.6.1 Results of smear-slide analysis	119
	10.7 Occurrences of dropstones	148
	10.8 Micropaleontology and biostratigraphy	151
	10.9 Inorganic geochemistry: pore water & sediment	165

APPENDIX	170	
A1	Teilnehmende Institute / Participating Institutions	171
A2	Fahrtteilnehmer / Cruise Participants	174
A.3	Schiffsbesatzung / Ship's Crew	176
A.4	Station list	178
A.5	Marine Geology	191
	A5.1 Lithological description of Giant Box Corer (GKG) and Gravity	192
	A5.2 Tables with data of smear-slide analysis	212
	A5.3 Tables with preliminary data of coarse-fraction analysis	221
	A5.4 Tables with data of dropstone analysis	233
	A5.5 Tables with micropaleontological data	253

1. ZUSAMMENFASSUNG UND FAHRTVERLAUF

Rüdiger Stein (AWI)

Grant-No. AWI-PS87_01

Zusammenfassung

Ziel der Expedition PS87 war die zentrale Arktis, insbesondere die Region des Alpha-Rückens und des südlichen Lomonosov-Rückens (Abb. 1.1), wo schwerpunktmäßig geowissenschaftliche Untersuchungen durchgeführt werden sollten. Übergeordnete Fragestellungen bezogen sich dabei auf die detaillierte Rekonstruktion der kurz- und langfristigen Klimaänderungen und der tektonischen Entwicklung des Arktischen Ozeans. Trotz intensiver Bemühungen war es leider nicht möglich, eines unserer Hauptarbeitsgebiete, den Alpha-Rücken, wo alte Sedimente oberflächennah ausstreichen, zu erreichen, da die extremen Eisverhältnisse in diesem Jahr für *Polarstern* nicht zu bewältigen waren. Wir haben daher unser Forschungsprogramm mit Fokus auf den Lomonosov-Rücken verlagert (Abb. 1.1 und 1.2). Zusammenfassend lässt sich festhalten:

- Insgesamt wurden 3.084 km seismische Profile aufgezeichnet, davon 2058 km Mehrkanal-Seismik mit dem langen 3.000 m Streamer. Diese Daten sind wichtige Grundlage für die Festlegung der genauen Lokationen von IODP-Bohrpunkten, die wir in einem IODP-Proposal vorgeschlagen haben.
- Umfangreiche geologische Beprobungen (6 x Kastenlot, 37 x Schwerelot, 20 x Großkastengreifer, 17 x Multicorer) wurden auf dem zentralen Lomonosov-Rücken durchgeführt. Das gewonnene Kernmaterial z.T. aus Abschnitten, von denen es bisher überhaupt kein Probenmaterial gab (Richtung Grönland), und die Beprobung älterer präquartärer (Miozän und älter?) Sedimente werden einmalige Chancen für die Rekonstruktion der jüngeren und älteren Klimageschichte des Arktischen Ozeans eröffnen.
- Während der Transitstrecken und der gesamten Arbeiten in den Untersuchungsgebieten wurden durchgehend vom 06.08. bis 28.09.14 Hydrosweep- und PARASOUND-Daten aufgezeichnet. Insgesamt konnten so über 10.370 km neue Hydrosweep- und PARASOUND-Profile gewonnen und dabei qualitativ hochwertige bathymetrische Detailvermessungen in Teilgebieten des Lomonosov-Rückens durchgeführt werden.
- Am 30.08.14 haben wir Yngve Kristoffersen und Audun Tholfsen mit ihrem Hovercraft auf einer dickeren Eisscholle ausgesetzt, von der aus sie ihr Drift-Experiment „FRAM-2014/15“ starten – viel Erfolg und gute Heimkehr!
- Neben dem geowissenschaftlichen Schwerpunktprogramm wurden umfangreiche Untersuchungen zur Meereisphysik (1.300 km EM-Bird-Eisdickenmessungen auf Hubschrauberflügen, Ausbringen von 20 Driftbojen zur Bestimmung der Eisdrift), Ozeanographie (50 XCTD zur Bestimmung von Temperatur und Leitfähigkeit in den oberen 1.100 m der Wassersäule) und Polarökologie (1.607 Transekt-Zählungen von Seevögeln und Meeressäugern von der Brücke bzw. während der Hubschraubereinsätze) durchgeführt.

Das herausragende Ereignis dieser Expedition war nicht der Nordpol, den *Polarstern* am 26.08. um 10:23 UTC (zum 4. Mal !) erreichte, sondern sicherlich das Auffinden und detaillierte Auskartieren von riesigen untermeerischen Rutschmassen, die alte Sedimente, die normalerweise in größerer Tiefe liegen und somit für uns nicht erreichbar sind, freigelegt haben. Damit konnten wir doch noch mit unseren Bordmitteln alte Sedimente, die wir uns vom Alpha-Rücken erhofft hatten, beproben. Da die Probenstationen z.T. weniger als eine halbe Schiffslänge auseinanderlagen, erforderte dies eine genaue Positionierung von Schiff und Lot, d.h., exzellente Fähigkeiten der Nautiker und den Einsatz des Posidonia-Systems.

Fahrtverlauf

Polarstern lief am 05.08.2014 gegen Mittag aus Tromsø aus. Mit an Bord waren neben den 44 Besatzungsmitgliedern 50 Wissenschaftler und Techniker aus 11 Nationen. Auf unserem Weg in die zentrale Arktis machten wir in der Nacht vom 07.08.2014 zum 08.08.2014 eine erste geologische Station auf dem Hovgaard-Rücken westlich von Svalbard, wo Großkastengreifer, Multicorer und Schwerelot zu ihren ersten Einsätzen kamen. Von dort aus ging's dann weiter nach NW auf die grönländische Seite des Nordatlantiks, wo wir bei ca. 80°51'N/09°10'W auf einen großen mit Sediment beladenen Eisberg trafen. Mittels Mummy Chair wurden umfangreiche Sedimentproben genommen. Von dort aus dampften wir weiter nach Norden, unser erstes Hauptziel, den Alpha-Rücken, vor Augen. Die Eisverhältnisse wurden dichter, das weitere Vorankommen verlangsamte sich deutlich. Während dieser Tage beschränkten sich die wissenschaftlichen Arbeiten auf Eisdickenmessungen, XCTD-Einsätzen und Beobachtungen von Seevögeln und Meeressäugern von der Brücke. Am 18.08. erreichten wir endlich den Lomonosov-Rücken und machten Station bei 86°38.2'N/44°54'W. Das erste Kastenlot wurde gezogen.

Die Eisverhältnisse wurden schlechter, das Eis dicker und dichter. Am 19.09. steckten wir ganz fest. Trotz intensivster Anstrengungen und mehrfacher Versuche war kein Vorkommen Richtung Westen, über den Lomonosov-Rücken hinweg zum Alpha-Rücken, möglich. Wir mussten so schließlich eines unser Primärziele, die Beprobung der kretazischen Schwarzschiefer auf dem Alpha-Rücken, aufgeben. Unsere Untersuchungen mussten so ganz auf den Lomonosov-Rücken verlagert werden, wo in den Folgetagen in erster Linie geologische Sedimentbeprobungen, XCTD-Einsätze und Meereisvermessungen im Vordergrund unserer Aktivitäten standen.

Während ein Vordringen nach Westen nicht möglich war, war die Weiterfahrt Richtung Norden relativ „einfach“. So erreichten wir am 26.08.14 um 10:23 UTC den Nordpol (89°59.7'N/23°59.8'W). Am 30.08.14 dockten wir bei ca. 87°15'N/155°E an eine große Eisscholle an, auf der wir unsere norwegischen Kollegen aus Bergen, Yngve Kristoffersen und Audun Tholfsen, mit ihrem Hovercraft *Sabvabaa* (Abb. 1.3) aussetzten. Diese starteten von dort mit ihrem FRAM 2014/15-Experiment, d.h., sie wollen mit der Transpolar-Drift in den nächsten Monaten quer durch den Arktischen Ozean driften (Abb. 1.4), auf dieser Driftroute seismische, geologische und ozeanographische Messungen bzw. Beprobungen machen und im nächsten Frühsommer wieder im Nordatlantik ankommen!!

Am 02.09.14 erreichten wir endlich weniger dichte Eisverhältnisse, so dass zum ersten Mal auf unserer Expedition seismische Profilmfahrten im Umfeld einer von uns vorgeschlagenen Lokalität für eine Tiefbohrung im Rahmen von IODP durchgeführt werden konnten. Neben der Geophysik wurden weiterhin detaillierte bathymetrische Vermessungen mittels Hydrosweep gefahren. Durch diese detaillierte Hydrosweep-Kartierung konnte ein erstes Gebiet mit deutlichen Abrisskanten erkannt werden, in dem möglicherweise ältere Sedimente austreichen könnten. Diese Abrisskante wurde intensiv mittels Schwereloteinsätzen beprobt.

Vom 11.-18.09.14, mittlerweile hatten wir eisfreie Bedingungen auf dem Lomonosov-Rücken in einem großen Areal zwischen 84-81°N und 155-130°E, standen seismische Profilmfahrten

mit dem 3.000 m-Streamer im Vordergrund, die zu einem Site-Survey für weitere IODP-Bohrvorschläge auf dem südlichen Lomonosov-Rücken gehörten. In diesem Gebiet konnten wir dann mit Hydrosweep-Detaillkartierungen zeigen, dass durch riesige Rutschungen am Lomonosov-Rücken wahrscheinlich großräumig ältere Sedimentschichten über eine Mächtigkeitsspanne von ca. 500 m freigelegt wurden. Zwischen dem 22. und 26.09.14 wurden diese Sedimente intensiv mittels Schwerelot beprobt.

Am 27.09.14 durchquerten wir das Amundsen-Becken Richtung Gakkel-Rücken, wo wir bei $81^{\circ}21'N/120^{\circ}31.5'E$ in einem ca. 5.200 m tiefen „Rift valley“ eine letzte geologische Station abarbeiteten und eine letzte Hydrosweep-Profilfahrt durchführten. Am 28.09.14, 02:08 UTC, schalteten wir alle Messgeräte ab und beendeten damit die wissenschaftlichen Arbeiten unserer Expedition. Genau eine Stunde später erreichten wir die russische EEZ.

Nach einer z.T. sehr stürmischen Rückfahrt lief *Polarstern* dann am 08.10.2014 gegen 16:00 Uhr in Bremerhaven ein.

Wir möchten uns abschließend ganz herzlich bei Kapitän Schwarze und seiner Besatzung für die große Unterstützung und Hilfsbereitschaft in allen Situationen bedanken.

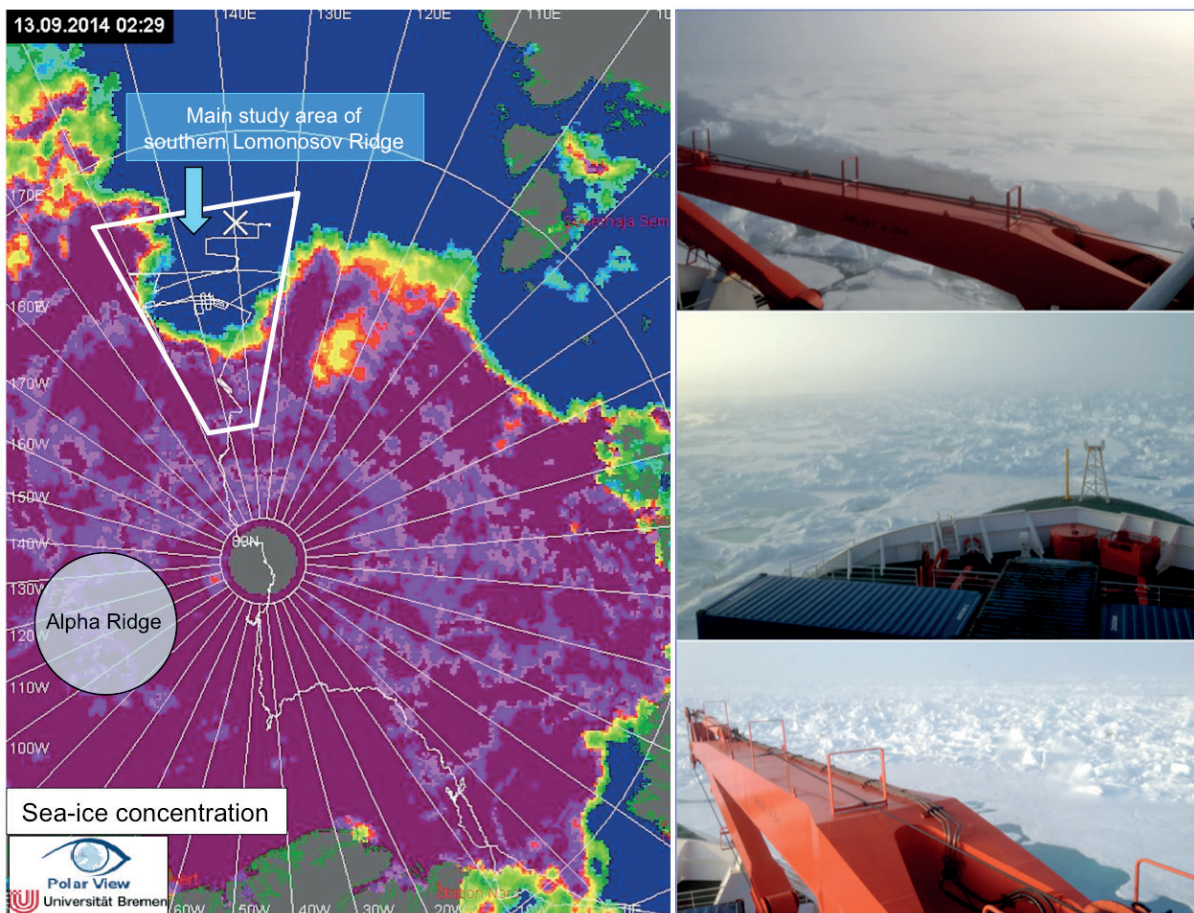


Abb. 1.1: Meereisverbreitung während Expedition PS93.1. Das Gebiet des Alpha-Rückens war wegen zu dichter Eisbedingungen nicht erreichbar, während auf dem südlichen Lomonosov Rücken optimale Eisbedingungen vorherrschten. Fotos zeigen Beispiele aus Regionen mit extremen Eisbedingungen.

Fig. 1.1: Sea-ice concentration during Expedition PS87. The Alpha Ridge area that could not be reached due to too strong ice cover, and the main study on southern Lomonosov Rücken with optimum ice conditions is shown. Photographs are examples of central Arctic Ocean areas with heavy ice conditions.

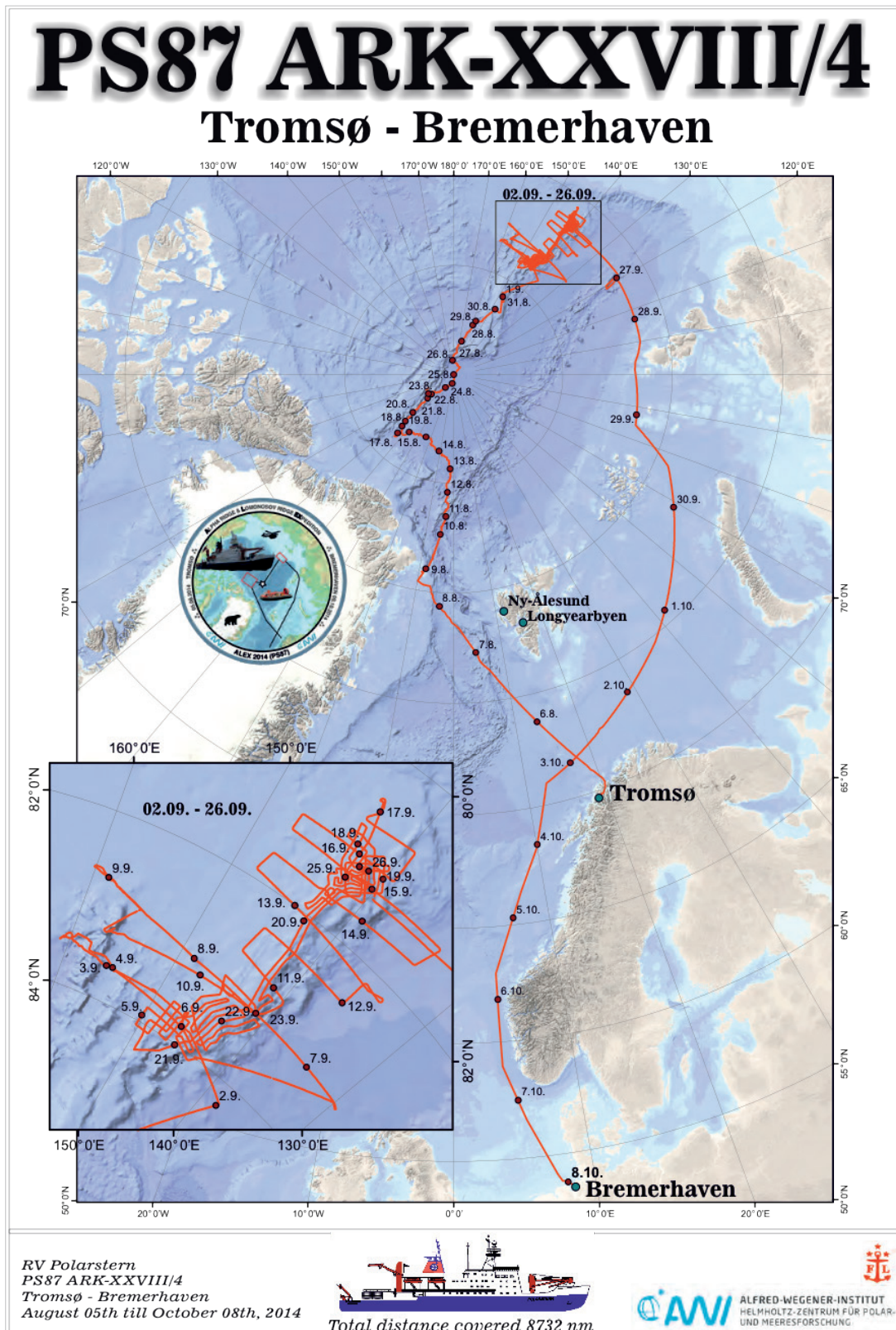


Abb. 1.2: Fahrtroute der PS87(ARK-XXVIII/4)-Expedition

Fig. 1.2: Cruise track of Expedition PS87 (ARK-XXVIII/4)

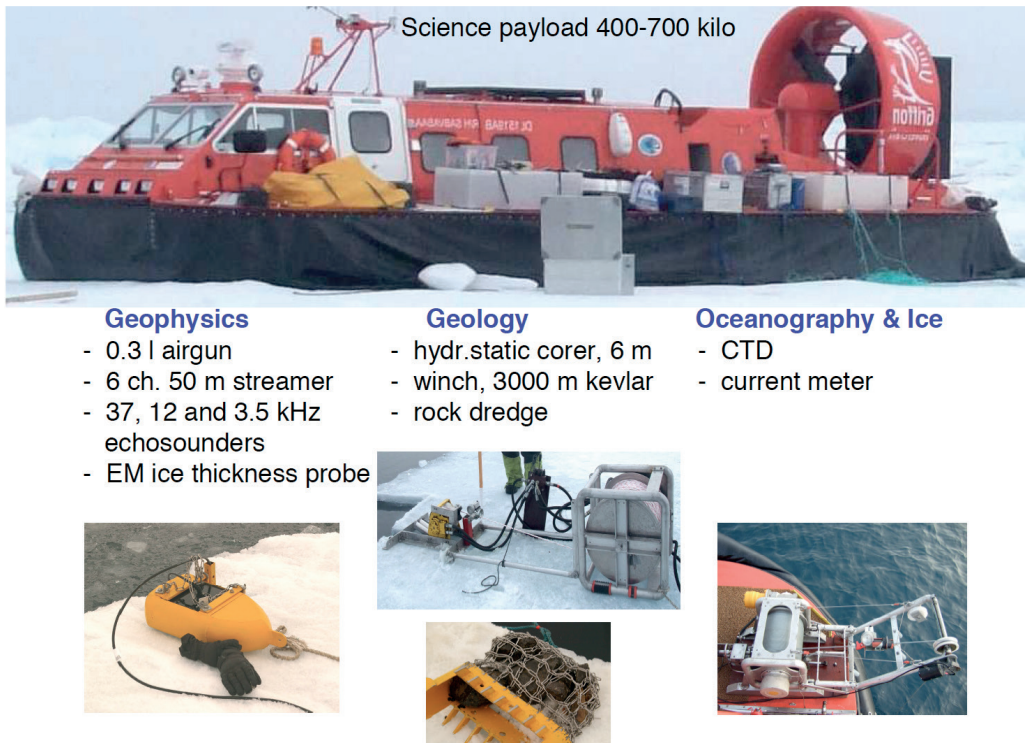


Abb. 1.3: Das Hovercraft Sabvabaa und Auswahl von Geräten für den Einsatz (Foto: Y. Kristoffersen)

Fig. 1.3: The hovercraft Sabvabaa and some of its equipment (Photo: Y. Kristoffersen)

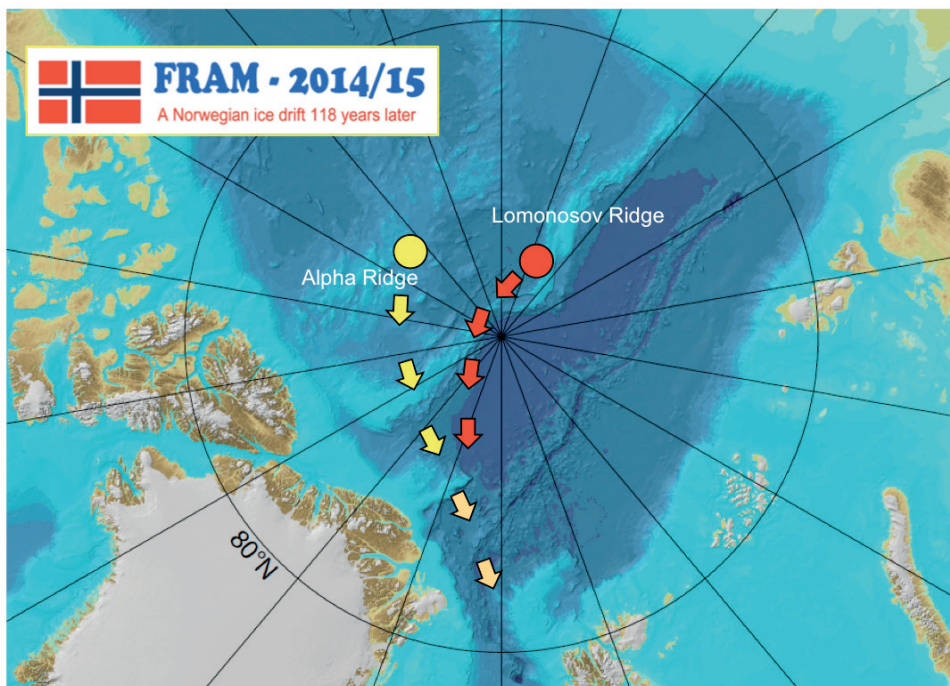


Abb. 1.4: Plan für das FRAM-2014/15 Drift-Experiment (Proposal Y. Kristoffersen); gelber Kreis = ursprünglich geplanter Startpunkt auf dem Alpha-Rücken, roter Kreis = tatsächlicher Startpunkt bei 87°15'N/155°E

Fig. 1.4: Outline of the plan for the FRAM-2014/15 drift experiment (Proposal Y. Kristoffersen); yellow circle = originally starting point on Alpha Ridge, red circle = real starting point at 87°15'N/155°E

SUMMARY AND ITINERARY

Summary

The Expedition PS87 (ARK-XXVIII/4) was mainly related to geoscientific investigations in the central Arctic Ocean, to be carried out on the Alpha Ridge and the Lomonosov Ridge (Fig. 1.1). The overall goal of the research programme was the detailed reconstruction of the short- and long-term climate history as well as the tectonic evolution of the Arctic Ocean. Since ice conditions were too strong to allow reaching the Alpha Ridge, we focused our work on the Lomonosov Ridge (Fig. 1.1 and 1.2). Key activities of the expedition can be summarized as follows:

- In total, 3,084 km of high-quality seismic profiles were recorded, 2,058 km of which are multichannel seismic lines with the 3,000 m long streamer. These data are important for future more detailed planning of IODP drill sites we have proposed for the Lomonosov Ridge area.
- A detailed geological coring programme was carried out on Lomonosov Ridge from the Greenland side across the North Pole towards the Siberian side of the ridge. Areas from where no material was available so far, were sampled as well as old (preglacial?) sediments having an age of probably Late-Middle Miocene and older. These sediments may give us the unique chance to reconstruct past preglacial Arctic climate intervals.
- During transit and within the main working areas, Hydrosweep and PARASOUND were running continuously, resulting in 10,370 km of high-quality profiles. In some key areas, a detailed bathymetry profiling was carried out, and unique and impressive 3D maps of parts of Lomonosov Ridge could be obtained.
- On August 30, we dropped off Yngve Kristoffersen and Audun Tholfsen (University of Bergen/Norway) with their hovercraft on an huge ice floe from where they started their drift experiment “FRAM-2014/15”.
- The geoscientific programme was supplemented by additional activities related to sea ice physics (i.e., 1,300 km of measurements of sea ice thickness, deployment of 20 drift buoys), oceanography (i.e., measurements of temperature and conductivity by 50 XCTD runs), and polar ecology (i.e., 1,607 counting sessions of sea birds and marine mammals).

The outstanding event of this expedition was not the North Pole *Polarstern* that was reached on August 26 at 10:23 UTC for the 4th (!) time, but certainly the discovery and detailed Hydrosweep mapping of large-scale slide scars and mega-slides that occurred along the western slope of Lomonosov Ridge and exposed older in general more deeply buried sediments. Cropping-out at the seafloor, these sediments could be cored by gravity coring from *Polarstern*. As the coring stations at this steep slope of Lomonosov Ridge are located very close to each other (i.e., partly < half of the ship's length!), a precise navigation and the use of a special acoustic pinger (“Posidonia“) system was needed to locate the ship and the gravity corer exactly on the spot.

Itinerary

Polarstern left Tromsø on August 05 around noon, onboard 44 crew members and 50 scientists and technicians from 11 nations. On our way to the central Arctic Ocean we had a first geological station with giant box corer, multicorer and gravity corer on Hovgaard Ridge west of Svalbard during the night August 07/08. From there, we steamed towards NW along the NW Greenland continental shelf. At 80°51'N/09°10'W, we met a huge sediment-laden iceberg that we sampled by using the mummy chair. Then, we continued steaming towards the north, towards our first main target area, the Alpha Ridge. The further to the North, the denser the ice became. During these days our station work was restricted to measurements of sea-ice thickness, XCTD runs and counting activities of sea birds and marine mammals from the bridge. On August 18, we reached Lomonosov Ridge and had the first Kastenlot station.

From day to day, ice conditions became worse. On August 19 we were stuck in the ice. Although trying hard it was not possible for us to cross the Lomonosov Ridge towards the west, towards Alpha Ridge. Thus, finally we had to skip one of our main goals, i.e., reaching Alpha Ridge and sample the Cretaceous blackshales. As a consequence, we had to move all our scientific objectives to Lomonosov Ridge, where several geological stations, XCTD runs and sea-ice measurements were carried out during the coming days.

Whereas steaming towards the west was not possible, the way towards northern direction was relatively „easy“ to handle. Thus, on August 26, 10:23 UTC, we arrived at the North Pole (89°59.7'N/23°59.8'W). On August 30, we docked at a major ice floe at about 87°15'N/155°E where our Norwegian colleagues Yngve Kristoffersen and Audun Tholfsen were dropped off with their hovercraft *Sabvabaa* (Fig. 1.3). From this location they planned to start their FRAM-2014/15 Experiment, i.e., they planned to drift within the Transpolar Drift across the entire Arctic Ocean (Fig. 1.4), doing seismic, geological and oceanographical measurements and sampling, respectively, along the drift route, before they will leave the Arctic Ocean through Fram Strait during next spring/summer.

On September 02, we reached an area with less dense sea-ice conditions, and for the first time seismic profiling could be carried out in the area of a potential location for an IODP drill site. Besides seismic profiling also a detailed Hydrosweep bathymetry survey was carried out. By this activity, an area with huge slide scars could be identified and then sampled by gravity coring.

From September 11 to 18, we concentrated on seismic profiling using the 3,000 m streamer as part of a site survey for a number of IODP drill sites proposed on southern Lomonosov Ridge. Within this area, also a detailed Hydrosweep survey was carried out. By this, large-scale slide scars were identified at the western slope of Lomonosov Ridge where older sediments of about 500 m in thickness are probably cropping-out. These sediments were sampled by means of gravity coring between September 22 and 26.

On September 27 we steamed through the Amundsen Basin towards the Gakkel Ridge where we had a last geological station in the central rift valley at 81°21'N/120°31.5'E and in a water depth of ca. 5,200 m, followed by a final hydrosweep survey across the rift valley. On September 28, 02:08 UTC, we switched-off all our scientific measuring devices, an hour later we entered the Russian EEZ.

After a stormy return track through the North Atlantic, we arrived in Bremerhaven on September 08 at about 14:00 UTC.

Finally, we would like to thank Captain Schwarze and his crew for the excellent cooperation at any time. This cooperation was the basis for the success of Expedition PS87!

2. WEATHER CONDITIONS

Harald Rentsch, Hartmut Sonnabend (DWD)

Aug 05-14, 2014: Tromsø, then strait on to the pack ice

At first two days (Aug 5 and 6) of the expedition PS87 (ARK XXVIII/4) some precipitation occurred, connected to a weakening frontal system north of Tromsø. The wind came from easterly to north-easterly directions of wind force 3-4 Beaufort (Bft).

On 7 August the strong cloudiness of a cold front of a weak Polar Low nearby Denmarkshavn (Eastern Greenland) dominated the weather, but precipitation was missed. Together with northerly-, later north-westerly winds of strength 4 the air temperature dropped down the closer we came to the ice edge. Following days, beginning at 9.8., we moved within areas with high pressure and moist southerly, partly south-easterly wind compounds of strength 4 to 5 Bft. That's why the atmosphere was stabilized by cooling of air in the near-surface boundary layer by the sea-ice more and more, so dense multi-layered clouds, freezing drizzle and fog patches minted this cruise leg.

This situation lasted several days, ending on 12 August. After that, rising pressure nearby our ships track and a reduced wind speed from south-easterly let to dissolving of clouds- thus, very good flight-meteorological conditions enabled some flights for getting ice information with the EM-Bird.

During the following days up to August 15, weak northerly winds dominated, thus colder and dryer air mass dissolved fog patches and low clouds for a while. Some successful flights for ice reconnaissance were carried out. Together with the ice information of the "Bremer Ice chart" we always had a detailed overlook over the ice situation within the vicinity of the ship's track.

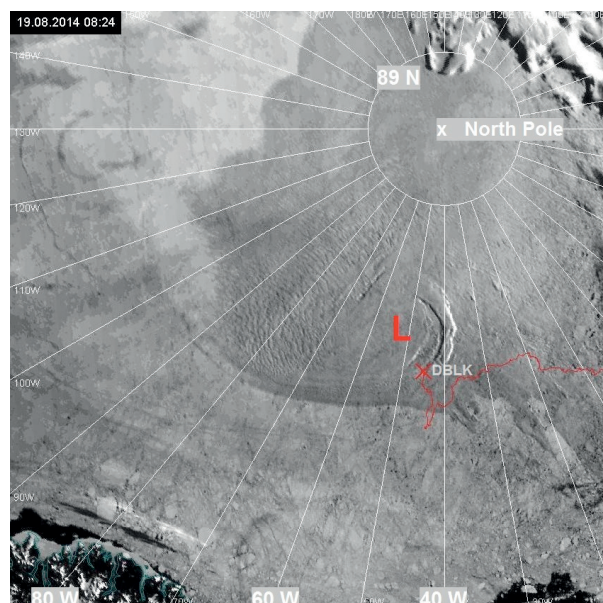


Fig. 1.1: Polar low (L), visible with NOAA 19 (vis) for August 19, 2014, 08:24 UTC. The position of the vessel POLARSTERN is marked by red x and the ships sign DBLK.

Aug 15-26, 2014: Survey to the North Pole

On August 15, a wave-disturbance caused low clouds and fog, which meant insufficient flight-conditions. But one day later, on August 16, we had excellent flyable weather in the area around the ship all the day, a colder and dryer north-westerly airflow of strength 3 Bft brought temperatures of -2°C . This fair weather period continued until 18 August.

Unfortunately, there was no useful information by satellite about the ice situation available. One day later, on 19 August, a Polar low passed our ships track, and together with very low clouds, snow showers and radiation fog all flight movements were prevented (see Fig. 1.1). On its back side dryer and colder air from south-westerly directions caused fair weather for all planned helicopter flights on 20 August. Some broken clouds in upper levels did not disturb so much.

Without significant changes in the general distribution of the pressure features the westerly wind flow abided weak and often multi-layered clouds accompanied the ship through the thick pack ice fields nearby latitude 88.5°N . Cyclonic influences were forced by crossing of some fronts causing drifting snow and freezing drizzle in connection with moderate winds up to nearly 6 wind forces on 25 August. Ice thickness of nearly 1.5 m and snow coverage on it stopped the ship often during their track towards the North Pole. One day later, on August 26, the short stop for a North Pole-“party” took place on a big floe nearby 90° north below a grey sky and we had windy weather together with wind-chill temperatures of about -16°C .

Aug 27- Sep 09, 2014: North Pole to the border of Arctic ice

Until the next passage of fronts and upcoming snowfalls on 29 August we had to deal with fog and low stratus clouds. Northerly, later on north-westerly winds of around 3 Bft brought moist and moderate cold-air-masses with thick hoar frost to the ship. Such low temperatures up to -8°C and stronger winds caused wind-chill temperatures up to around -25°C . In the period August 30 (a hovercraft left the ship for drifting on a floe) to 2 September, weak frontal influences with snow and freezing drizzle as well as calmed winds of less than 3 Bft from southerly directions dominated the weather nearby the ship. Under influence of a high pressure system and an unstable boundary layer, snow grain and low stratus clouds were produced every day until September 4. During this time scale the sea was nearly calm in ice-free waters.

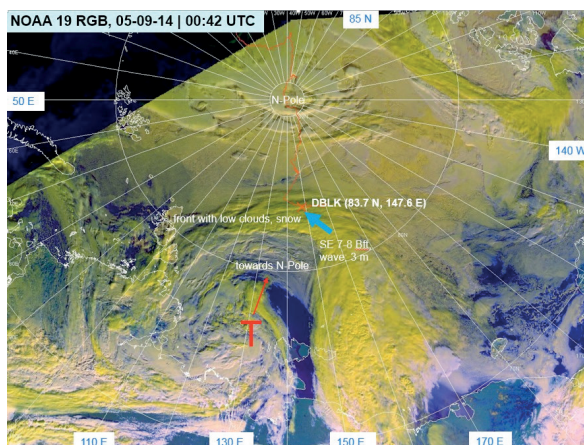


Fig. 2.2: Depression (T) moves towards North Pole, observed by NOAA 19 (RGB), Sep 05 2014, 00:42 UTC. The position of the vessel Polarstern is marked by x DBLK, and its coordinates: 83.7°N , 147.6°E .

On Sep 5, a gale “T” (see Fig. 2.2), which weakened during its track northwards noticeably, came from Eastern Siberia, moved towards the North Pole and changed the general weather situation completely. There were seen windy, unsettled conditions; snow showers with gusty south-easterly winds up to 7 Bft. Icing conditions had prevented all helicopter flights for 2 to 3 days. The marine work on *Polarstern* was not influenced by wave-heights of 2 to 3 m because the close ice-edge led to a weakening and smoothing of the peak waves.

Not until three days later on the back side of the low “T” we had wind from north and 5 wind-forces together with isolated showers, but also good flight conditions. During this period, including the 8th of September, some more Polar lows approached towards our working areas, driven by westerly winds in upper levels, causing insufficient flight weather conditions and partly intense snowfalls.

Sep 10-27, 2014: Research in ice-free Arctic Ocean

Between 11 and 13 September numerous depressions and Polar lows brought overcast conditions and often snowfall or showers, at what the near-surface inversion of temperature in the boundary layer was dissolved only seldom. That’s why sunny moments had trodden for not more than 90 minutes as a total sum during a nearly 20-days period. The airflow reached its maximum at south-westerly directions nearby 7-8 Bft in connection with total wave heights of 3 m. On Sep 10 nearby 82.6° N 161° E we left the Arctic pack ice zone finally for this cruise.

During the period from Sep 16 to 19 an unstable strati-formed boundary layer dominated with moist air the weather nearby the ship. At this time southerly winds of 3 Bft, later easterly winds of 6-7 wind forces raised the sea up to 3 m and brought snow grain showers to us. The main reason for that was a cold air mass (-2 to -3°C) laying over a warm sea surface (SST: 0° -1°C), thus, producing a continuously moist- and warm air flux from the sea surface to the lowest air levels. – Finally on September 21 we observed clear sky conditions and sunshine for more than 3 hours on the edge of a high pressure system, the wind came from east of force 5. At the sunset time, around 15:07 ships time, we could see one of the most beautiful sunsets of this expedition.

After weak winds and changeable weather on 23 September, one day later fronts of a low brought snow, heavy south-westerly winds up to 8 Bft towards 81° N 141° E. The sea raised only up to 2.5 m because of the nearby smoothing ice edge.- Also, on September 26, 2014, a complex low pressure system hit the ship, wind force 8 to 9 and a sea of 2.5 m were measured. A long lasting snowfall postponed all scientific research for some hours, because only a nearly calmed sea could allow the necessary precise ships movement’s for marine work on the seafloor.

Until one day after the end of scientific research, 28 September, more fronts and its precipitation reached the ship nearby the Russian EEZ and close to ice edge. Consequently, despite strong southerly winds 6-7 Bft, the waves could not reach more than 2 m.

Sep 28–Oct 9, 2014: The voyage to get home to Bremerhaven

The time after passing Severnaya Zemlya was characterized by ongoing cyclonic wind flow and often moderate southerly to north-westerly winds up to Bft 6-7, which enforced wave heights of in average not more than 2.5 m. Besides, the rainy, windy days were clearly the winner during this period of the expedition. From October 6 to 7 we got stormy winds around 10 Bft straight against the ships course, causing some trouble for the ships' speed, which was reduced significantly. The highest sea was measured nearby Utsira, when the ship was hit by waves of more than 7 m.

On Thursday, October 8 2014, *Polarstern* reached the Harbour of Bremerhaven, one day earlier as planned together with south-westerly winds 6 to 7 Bft.

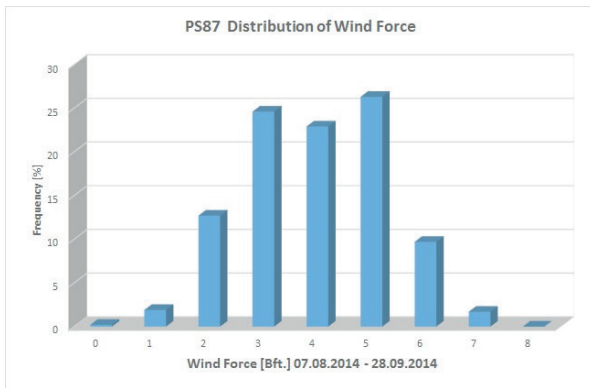


Fig. 2.3: Distribution of wind force during expedition PS87

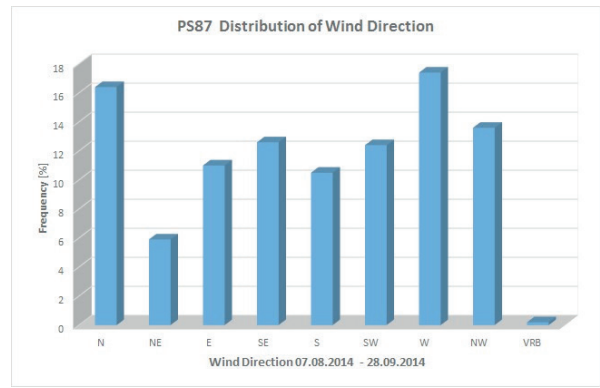


Fig. 2.4: Distribution of wind direction during expedition PS87

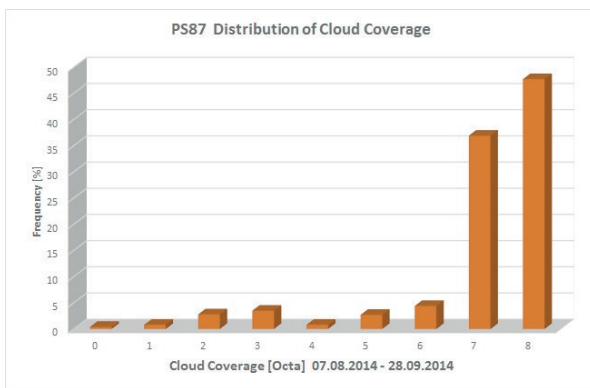


Fig.2.5: Distribution of cloud coverage during expedition PS87

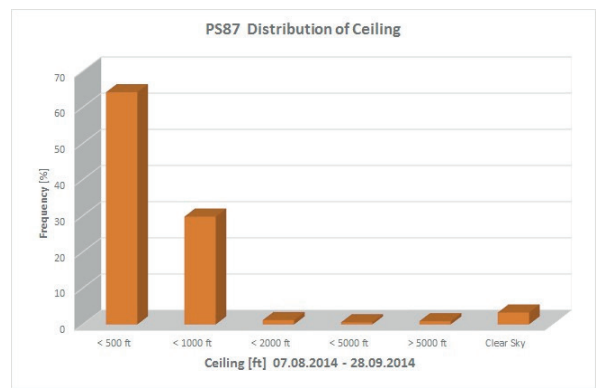


Fig. 2.6: Distribution of ceiling during expedition PS87

3. ISOTOPE SIGNATURE OF WATER VAPOUR OVER THE ARCTIC OCEAN

François Ritter¹,
not onboard: Sepp Kipfstuhl¹, Martin Werner¹
Hans-Christian Steen-Larsen²

¹AWI
²LSCE

Grant-No. AWI-PS87_02

Objectives

Polarstern has recently been considered to be a good candidate for hosting continuous measurements of stable water isotopes in the air with new laser-based isotope analysers. The isotopic data collected during the research vessel's cruises through the Arctic Sea every boreal summer can be compared with isotopic data from stations placed in Iceland (by Hans Christian Steen-Larsen, LSCE) and Svalbard (by Valérie-Masson Delmotte, LSCE). The conservation of the second-order isotope parameter d-excess ($\delta D - 8 \cdot \delta^{18}O$) can be used to localize and isolate the sources and the sinks of humidity in Arctic air masses, which improves our understanding of the hydrological cycle over the Arctic.

Guided by these considerations, Martin Werner, Sepp Kipfstuhl, Hans Christian Steen-Larsen, and co-workers have initiated the project IsoArc, which is one of the first projects funded by AWI's strategy funds. The project will include continuous isotopic measurements on *Polarstern* during the period 2015-2017. As a pilot study, continuous isotopic measurements of specific humidity, $\delta^{18}O$ and δD had been successfully performed for over 1 month, with a Los Gatos Research (LGR) isotope analyser during PS87 (ARK-XXVIII/4). This instrument was removed from the ship after the cruise and will be replaced by a new Picarro analyser for the IsoArc project in 2015.

Work at sea

The Los Gatos Research instrument requires several calibrations to correct the raw data. An external device called Water Vapour Isotope Standard Source (WVISS) was brought onto the vessel, with four different types of water standards: TD1, NZE, OCEAN3 and a "Working Standard" (WS). The WVISS is able to suck water from a bottle of water standard and then vaporize it to produce a vapour stream. Assuming no fractionation during the complete vaporization, the stream has the same isotopic composition as the water standard. Therefore, the measured value by the Los Gatos Research Analyzer (Water Vapor Isotope Analyzer – WVIA) can be compared with the known value from the water standard.

Three types of calibration were performed:

1. Humidity-isotope-function calibration on the dates 2014/08/09, 2014/08/24, 2014/08/31 and 2014/09/07

By mixing the standard stream with dry air produced by an air drier included in the WVISS, the level of humidity is changed but the isotopic composition is kept constant. An instrumental humidity dependency is recorded during the ~24 hours of calibration. The humidity values are kept between 3,500 ppmv and 8,000 ppmv, which is equivalent to the level of humidity over the Arctic Ocean. Two water standards have been used for comparison: TD1 and WS. Each

humidity response curve presented in Fig. 3.1 corresponds to a moving average fit, calculated every 50 ppmv over a range of 1,000 ppmv.

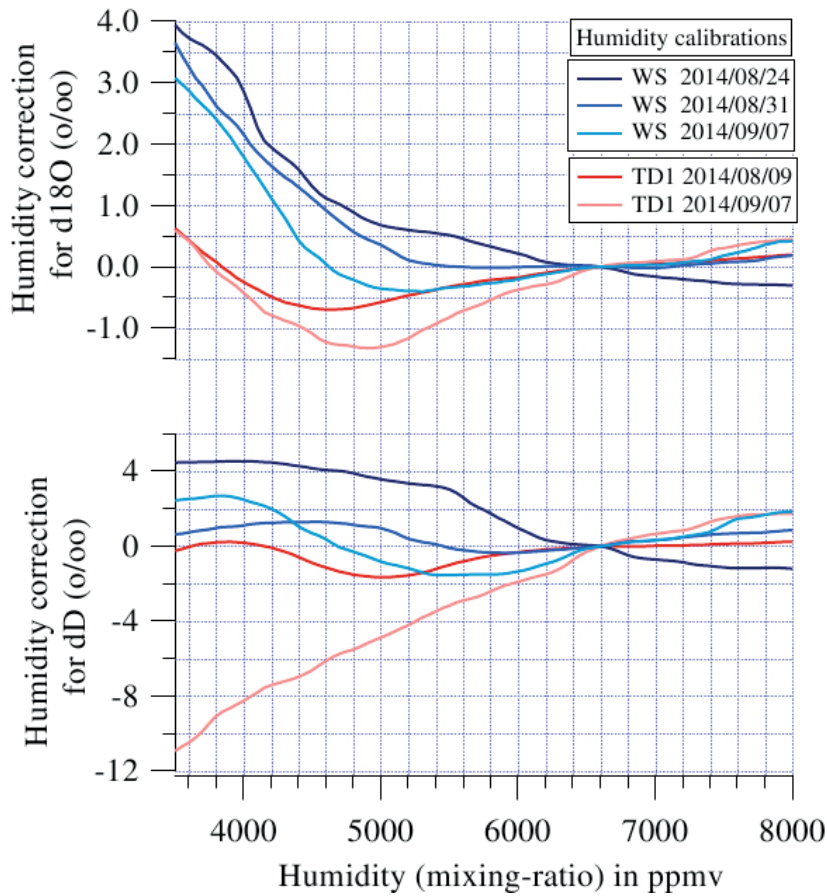


Fig. 3.1: Humidity-isotope-functions against humidity at different dates (performed with the standard TD1 in red and the Working Standard in blue)

2. VSMOW calibration on 2014/08/09

This calibration converts the isotope data on the international VSMOW scale by fitting the measured values of the standards TD1, NZE and OCEAN3 against their known value. Every standard has been measured during 20 minutes at a stable humidity (6,000 ppmv) and the WVISS has been cleaned with dry air between two measurements to avoid any memory effect (i.e. molecules of a previous probe are still trapped in the system). Fig. 3.2 shows the known values of the 3 used standards (denoted as “theoretical values” on the y-axis) against the average of the measured values (corrected in humidity).

3. Drift calibration, 12 minutes measurements of the WS every 111 minutes

The humidity is kept constant around 6000 ppmv and the different 12 minutes averages show a drift in the signal in Fig. 3.3. This drift is corrected by simple linear time-interpolation between two consecutive drift calibrations.

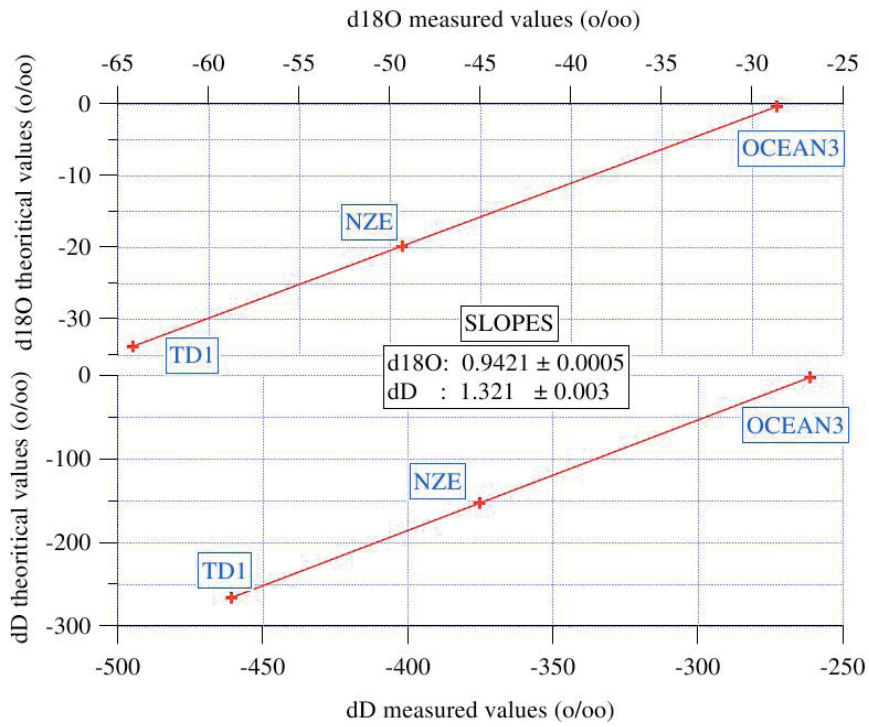


Fig. 3.2: VSMOW-slopes given by plotting the known values of the standards TD1, NZE and OCEAN3 against their measured values

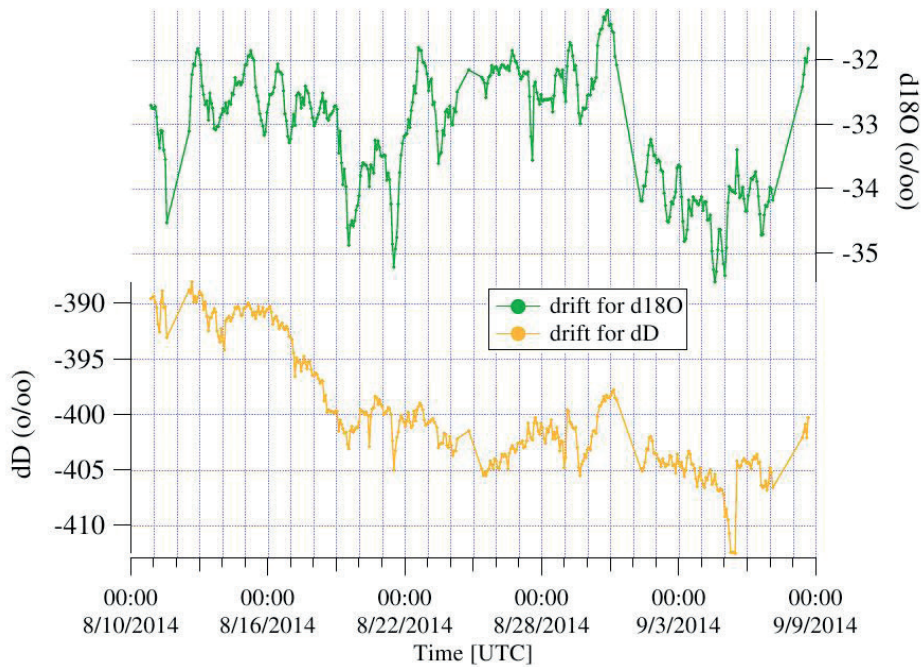


Fig. 3.3.: Drift of the instrument over one month for both isotopes, at constant humidity ($q=6,000$ ppmv) and constant isotopic composition

Preliminary results

Unfortunately, two compressors were already broke after 1 month of PS87 (ARK-XXVIII/4). A plastic ring from the first compressor was damaged after the first week and a piece inside the spare compressor was broken after 3 weeks, although this compressor had been used continuously at Kohnen Station on Antarctica without problem. These compressors were part of the calibration unit as they had produced a difference of pressure used to suck the water standard from the bottle.

Analyses of the calibrations

An unusual result is that the humidity calibrations performed with the TD1 water standard have different trends than the humidity calibrations performed with the Working Standard (WS). We decided to compare the data with the two different corrections from TD1 and WS to see the impact of this difference. Further calibrations will be needed in Bremerhaven to choose the best correction.

The VSMOW correction shows a very good error on the slope (0.0003 for $\delta^{18}\text{O}$ and 0.001 for δD), and similar slopes have been calculated 6 months before at Kohnen Station with the same instrument: 1.425 for δD and 0.996 for $\delta^{18}\text{O}$.

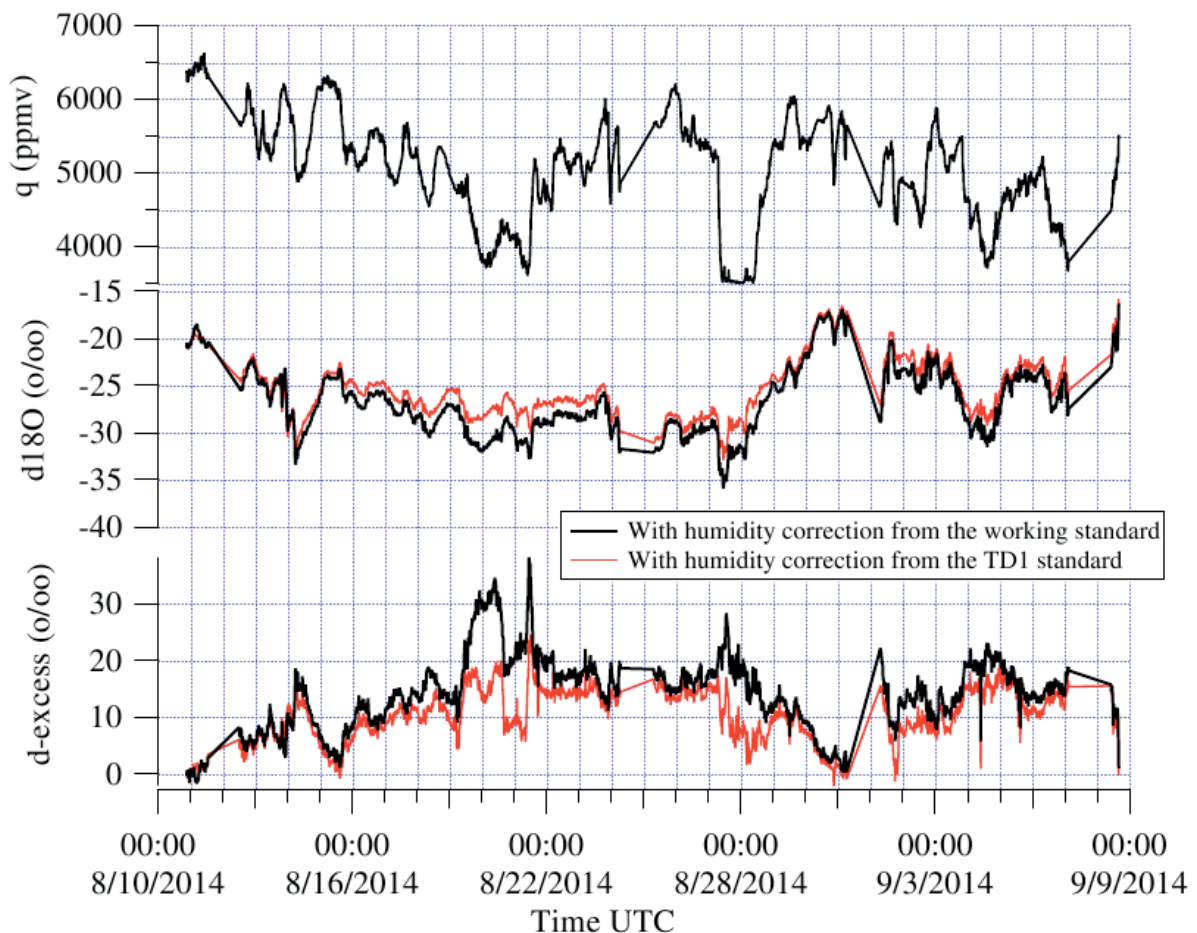


Fig. 3.4: Humidity, $\delta^{18}\text{O}$ and $d\text{-excess}$ against time (10 min average) after correction in VSMOW, drift and humidity (black curve: correction given by the humidity calibration performed with the Working Standard, red curve: with the TD1 standard)

Analyses of the calibrated measurements

The calibrated measurements are presented in Fig. 3.4, after applying VSMOW, drift and humidity correction functions. We can observe the impact of a different humidity correction based on the standard TD1 or WS.

The natural variability is remarkable, especially during the event between the 2014/08/17 and 2014/08/31, which shows a constant increase in $\delta^{18}\text{O}$ of nearly 20‰, whereas comparable measurements at Kohnen Station, Antarctica show diurnal cycles with an amplitude of 8‰. Some diurnal cycles seem to be observed in the humidity at the beginning of the cruise, however the cloud cover was systematically between 70-100%. The local evaporation of water or sea ice is supposed to be strongly diminished. The linear relation between δD and $\delta^{18}\text{O}$ gives a slope of 6.55 ± 0.02 . This slope is very similar to the slope calculated at NEEM in Greenland: 6.47 ± 0.07 .

Other parameters of the LGR Analyzer instrument seem to be more stable during PS87 (ARK-XXVIII/4) than during a previous field campaign at Kohnen Station, Antarctica. Stable pressure and temperature inside the cavity and stable velocity of the laser ray indicate that such type of isotope analyzers can resist to the strong movements of the ship. These findings are very promising for the envisaged permanent installation of such instrument on *Polarstern* during the Iso-Arc project in 2015-2017.

Data Management

Isotope data will be processed and quality controlled after the cruise and will then be made available in the PANGAEA Data Publisher for Earth & Environmental Science.

4. ACTIVITIES OF THE SEA ICE PHYSICS GROUP

Anne Bublitz¹, Maria Winkler² ¹AWI
not on board: Christian Haas² ²YUoT
Marcel Nicolaus¹, Stefan Hendricks¹

Grant-No. AWI-PS87_02

4.1 AEM –Ice thickness measurements

Objectives

Global sea ice area accounts for more than a quarter of the total cryospheric surface and contributes to positive short wave feedback cycles, intensifying existing natural variations and global warming. Therefore changes in sea ice cover are strongly connected to climate change. The minimum of the summer sea ice extent in the Arctic is mainly controlled by the thickness distribution of the sea ice at the start of the melting season. The last decade showed a series of record lows of summer sea ice extent which imply an increasing loss in sea ice volume, whose magnitude is poorly quantified due to a lack of sea ice thickness information by remote sensing data.

The ice thickness distribution in summer can only be measured during ship cruises or aircraft surveys, since ice thickness estimates from satellite data are mostly restricted to colder times of the year due to ice conditions. To minimize ship time, those ice surveys in the summer are preferable done by means of airborne surveys. Since 1991 sea ice thickness data have been collected during *Polarstern* cruises using electromagnetic induction devices. Since 2001 surveys with helicopters have used airborne electromagnetic induction (AEM) systems. The objective of the AEM survey on this cruise was to continue the time series of ice thickness measurements in the Arctic carried out on earlier *Polarstern* cruises.

Work at sea

For the AEM sea ice thickness measurements we used the AEM Bird from York University (Toronto). The bird is 3.5 m long with a diameter of 0.35 m and a weight of 105 kg. The components inside the bird's Kevlar shell include EM coils, a laser altimeter, DGPS system, INS, and a laser scanner. The Bird is towed 20 m below the helicopter and flies at altitudes of 15 m to 20 m above the ice surface. The method takes advantage of the conductivity contrast between sea ice and sea water to estimate sea ice thickness (including snow thickness).

Preliminary results

During the cruise we were able to conduct 6 AEM surveys covering about 1,300 km of sea ice. The surveys were conducted in 40 nm x 40 nm x 40 nm triangles from the ship. Flight operations were strongly dependent on weather conditions; therefore most of the flights were done within the same region near Greenland and Canada, covering mostly older multi-year ice. Fig. 4.1.1 and Table 4.1.1 provide an overview of the AEM flights made during this cruise.

4.1 AEM –Ice thickness measurements

Tab. 4.1.1: List of AEM sea ice thickness surveys during PS87 (ARK-XXVIII/4)

Station	Latitude	Longitude	Start Date (UTC)
AEM - 1	84.464	-02.629	11.08.2014
AEM - 2	86.710	-37.426	15.08.2014
AEM - 3	86.281	-43.884	16.08.2014
AEM - 4	87.611	-53.436	19.08.2014
AEM - 5	88.302	-48.176	20.08.2014 </td
AEM - 6	83.738	159.375	03.09.2014

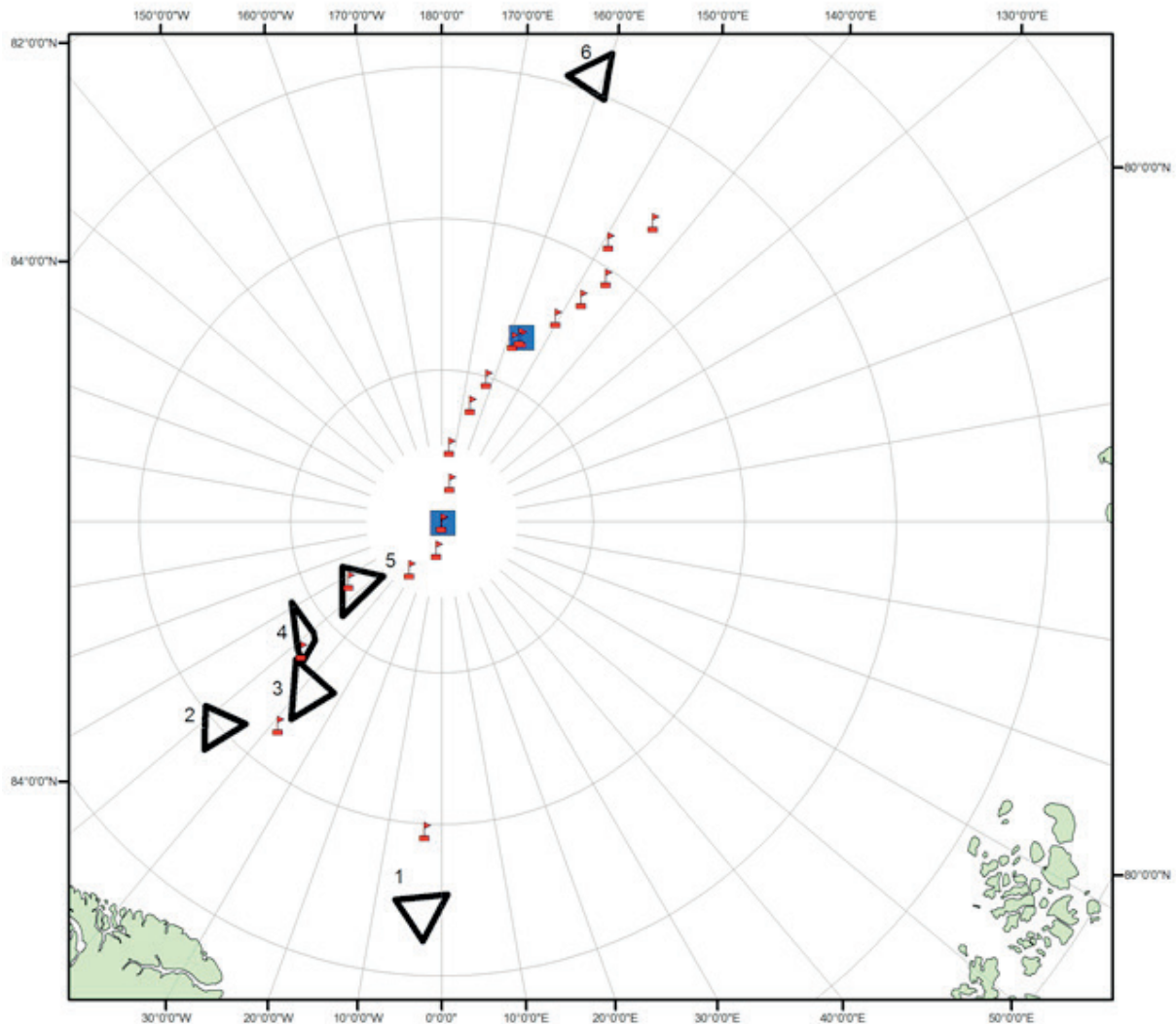


Fig. 4.1.1: Map of activities of the sea ice physics group during ARK - XXVIII/4 including AEM surveys (black lines), buoy deployments (red flags) and ice stations (blue squares).

Preliminary ice thickness results of AEM flight 3 and 6 are shown in Fig. 4.1.2 and Fig. 4.1.3. To estimate the ice thicknesses shown here, a 1D sea ice model with sea ice conductivities of 0 mS/m and sea water conductivity of 2,400 mS/m was used. To compare the ice conditions for for AEM flight 2-6, the preliminary ice thickness distributions are shown in Fig. 4.1.4.

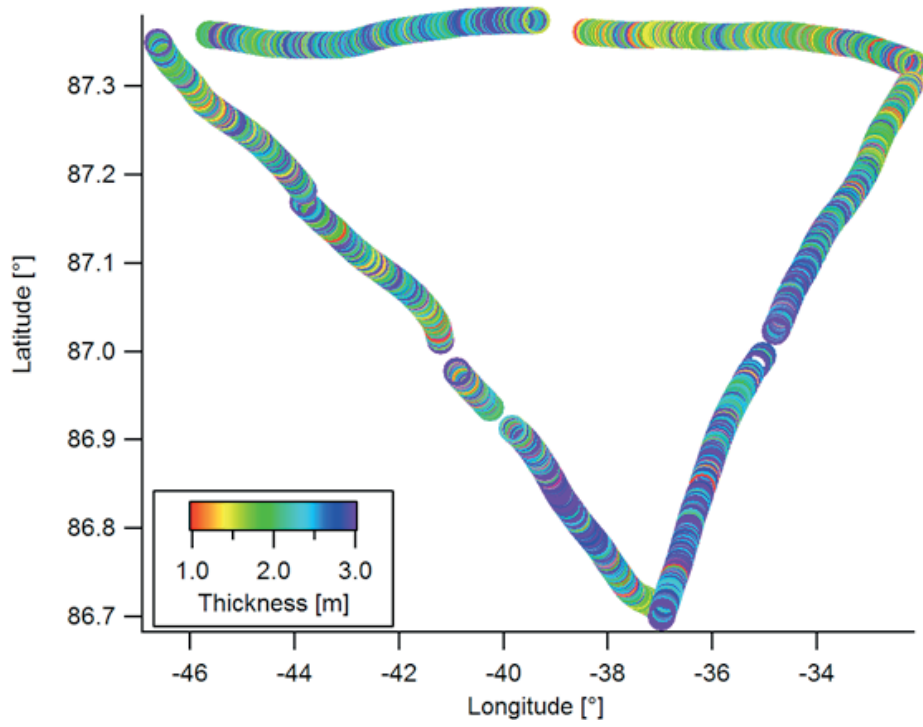


Fig. 4.1.2: Map of sea ice thickness estimates for AEM – 3

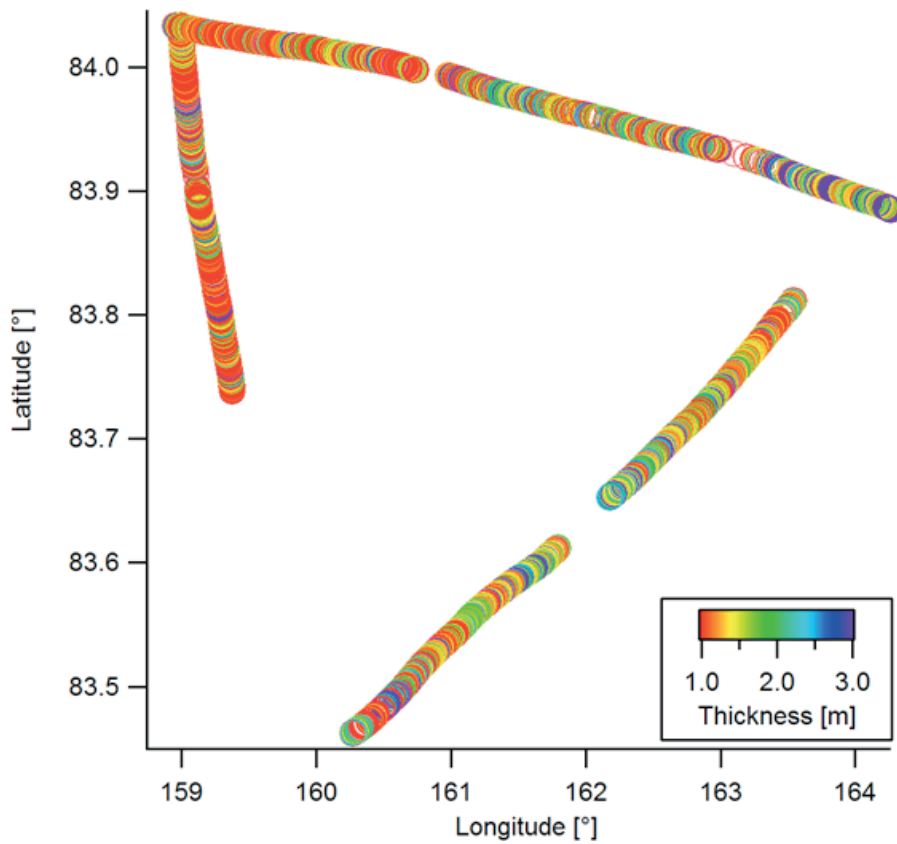


Fig. 4.1.3: Map of sea ice thickness estimates for AEM – 6

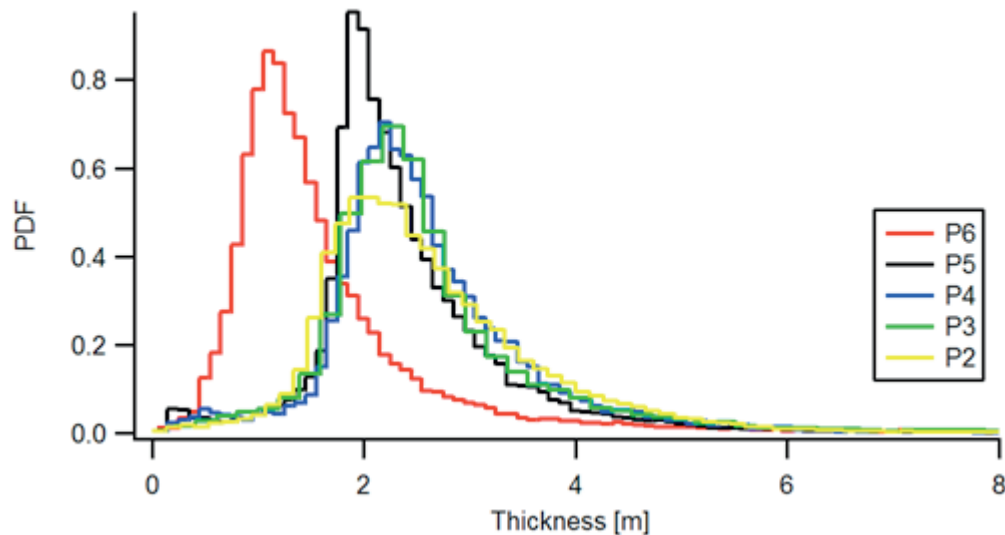


Fig. 4.1.4: Sea ice thickness distribution for AEM flights 2-6. The modal thicknesses range from 2.20 m to 1.80 m on the Canadian side of the Arctic Ocean and 1.05 m for AEM flight 6 on the Russian side.

Data management

AEM ice thickness data require further processing after the cruise and will be available upon request as point data with an average spacing of 3 to 4 meters and a footprint of approximately 50 m. The sea ice thickness data will be released following final processing and analysis after the cruise in the PANGAEA Data Publisher for Earth & Environmental Science and international databases like the Sea Ice Thickness Climate Data Record (Sea Ice CDR).

4.2 In-situ sea ice observations

Objectives

The drift of sea ice plays an important role in the climate system. The sea ice cover of the ocean is not stationary because sea ice floes are subject to winds and currents. Deformation due to convergence and shear motions can increase the ice thickness and change the surface roughness, providing larger working surfaces for the atmospheric and oceanic drag. The formation of leads and polynyas due to divergent drift has a direct effect on the oceanic heat balance. We have deployed 21 drifting buoys to monitor ice drift and deformation.

In addition, during ice stations ground-based EM and drill-hole thickness measurements were performed to gather validation data for the AEM surveys. *In-situ* measurements were also valuable to provide information when no airborne surveys could be performed due to poor weather conditions.

General ice conditions can be well documented with visual observations from the ship's bridge. As part of international efforts to standardize visual ice observations, the Climate in the Cryosphere (CliC) Committee standardized ice observation protocol for Arctic sea ice was established for the use of all ice-going ships.

Work at sea

21 buoys were deployed on ice floes during ARK XXVIII/4. The majority of these were deployed on the ice using the mummy chair and a crane of *Polarstern*, or during helicopter landings a few kilometres off the ships track. Three types of buoys were deployed: 1) 14 Surface Velocity Profilers (SVP) which report position, air temperature and pressure. 2) 4 Seasonal ice mass balance buoys (SIMB) which report position, air temperature and pressure as well as ice and snow thickness. 3) 1 Snow buoy which gives information about position, air temperature, pressure and snow thickness. 4) 2 UptempO buoys, which report position, air temperature, pressure and water temperature in the upper 60 m of the water column. The 4 SIMBs were deployed during the two ice stations where ice thickness and snow depth measurements were made.

Standardised ship based ice observations were made hourly from the bridge of *Polarstern* according to the ASSIST protocol (Arctic Shipborne Sea Ice Standardization Tool). The observations were made during normal working hours between 8 am and 9 pm.

Preliminary results

As part of the International Arctic Buoy Programme IABP we were able to deploy 21 buoys during the cruise. These were contributed by different international partners. For each buoy one thickness measurement was made at the deployment site. The 4 SIMBs were deployed during the ice stations. Table 4.2.2 gives an overview of all the buoy types and deployment positions. Fig. 4.1.1 shows a map of the buoy deployment sites as well as the positions of the ice stations.

At the two ice stations we conducted ice thickness surveys on a 50 m x 50 m cross-profile. Each ice station includes 9 direct snow and ice thickness measurements (drilling) and an electromagnetic (EM) ice thickness survey on and around the profile using an EM-31 (Geonics) towed on a sled.

Tab. 4.2.1: List of ice stations during PS87 (ARK-XXVIII/4)

Ice Station	Latitude	Longitude	Date	EM instrument
Ice - 1	89.893	46.709	26.08.2014	EM31
Ice - 2	87.310	154.92	30.08.2014	EM31, GEM-2

The second ice station included additional ice thickness measurements with an electromagnetic multi-frequency device (GEM-2) to resolve the thickness and conductivity structures at different sounding depths. Table 4.2.1 gives information about the position of the ice stations and methods used.

4.2 In-situ sea ice observations

Tab. 4.2.2: List of buoys and deployment dates and positions during ARK - XXVIII/4

Anzahl	Buoy type	Institution	IMEI	Serialnr.	Date	Lat itude	Longitude
2	UptempO buoy with 60m cable	University of Washington	300 2340 6023 3150	233150	02.10.2014	73° 42.426N	29° 55.815E
			300 2340 6023 3160	233160	02.09.2014	85° 9.522N	144° 33.956E
2	MetOcean Polar iSVP drifter buoy	Environment Canada	300 2340 6089 4080		27.08.2014	89° 0.818N	173° 13.068E
			300 2340 6089 0090		25.08.2014	89° 37.132N	8° 38.187W
10	Argos-2 SVP-B/RTC/GPS drifter with drogue	University of Washington		137804	13.08.2014	85° 54N	2° 58W
				137805	20.08.2014	87° 29.13N	47° 9.62W
				137806	01.09.2014	85° 41.458N	149° 1.322E
				137807	28.08.2014	88° 24.99N	165° 38.868E
				137808	16.08.2014	86° 33.142N	38° 32.724W
				137809	31.08.2014	86° 31.599N	147° 38.959E
				137810	23.08.2014	88° 32.878N	57° 07.787W
				137811	31.08.2014	86° 55.08N	150° 25.174E
				137812	01.09.2014	86° 7.104N	145° 47.436E
				137813	27.08.2014	89° 28.7N	166° 44.7E
2	SVP buoy	Finnish Meterological Institute	300 2340 1008 5650		29.08.2014	87° 26.057N	158° 15.652E
			300 2340 1008 7650		24.08.2014	89°14.478N	32° 54.74W
2	S-IMB	Finnish Meterological Institute		FMI15	26.08.2014	89° 58.00N	29° 38.29E
				FMI17	30.08.2014	87° 21.1758N	156° 9.3466E
2	S-IMB	AWI	300 2340 6176 4860	215:153	30.08.2014	87° 21.2268N	156° 59.2254E
			300 2340 6176 6880	217:158	26.08.2014	89° 58.934 N	24° 50.781E
1	Snow buoy	AWI	300 2340 6151 9990		29.08.2014	88° 1.684N	162° 10.682E

Fig. 4.2.1 and Fig. 4.2.2 show the sea ice thickness results for the EM31 survey done for Ice – 1. The thicknesses range from 1.20 m to 3.50 m with a modal thickness of 1.55 m. The sea ice thickness results for the EM31 survey from Ice – 2 range from 1.0 m to 3.50 m, with a modal thickness of 1.05.

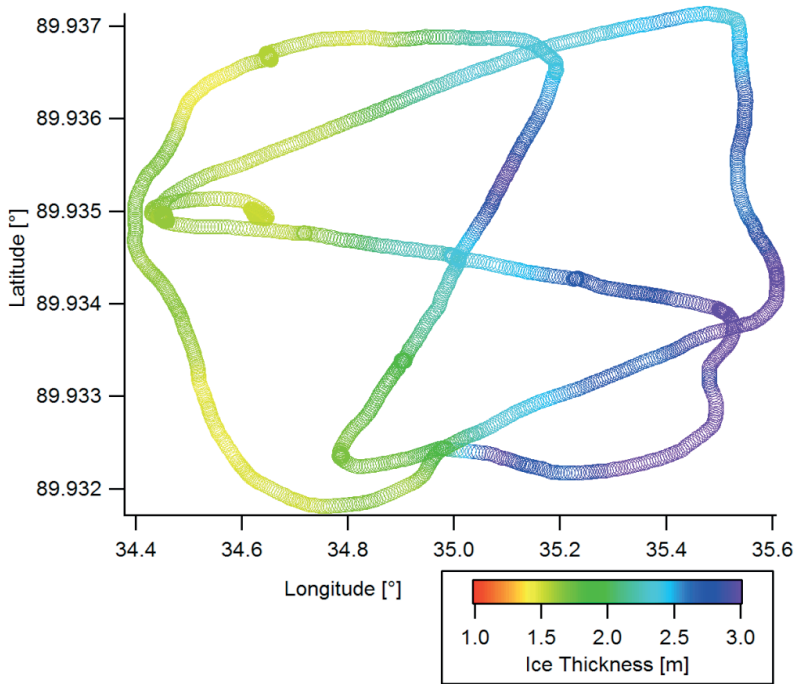


Fig. 4.2.1: Map of sea ice thickness estimates at ice station Ice – 1

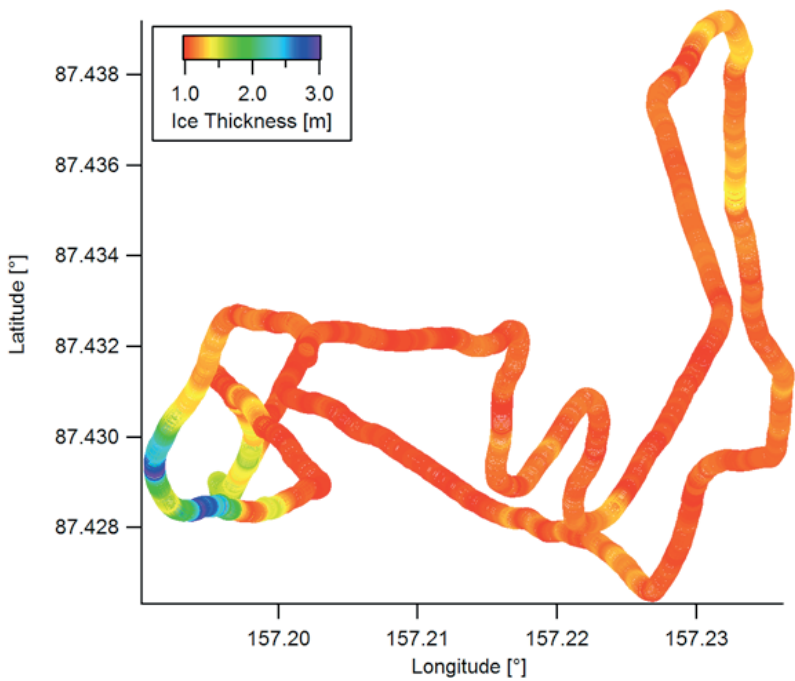


Fig. 4.2.2: Map of sea ice thickness estimates at ice station Ice - 2.

Data management

The ice observations will be archived at <http://doi.pangaea.de/10.1594/PANGAEA.803221> and are distributed by the International Arctic Research Center (IARC) of the University of Alaska, Fairbanks.4.

Ice thickness data from the electromagnetic induction device will be published in the PANGAEA Data Publisher for Earth & Environmental Science after final processing if appropriate. The positions and meteorological data of buoys are automatically transmitted to and stored by the WMO GTS system in near-real time. They are also uploaded to the database of the IABP, which is publicly accessible.

5. PHYSICAL OCEANOGRAPHY

Albrecht Roloff
not on board: Benjamin Rabe, Ursula Schauer

AWI
AWI

Grant-No. AWI-PS87_02

Objectives

During the past decade, the circulation and water masses of the Arctic Ocean have experienced considerable changes. The waters advected from the Atlantic and the Pacific became much warmer, the Atlantic inflow became saltier. On the other hand, the upper Arctic waters freshened since the 1990s. The aim of the oceanography programme was to use the occasion of a trans-arctic cruise to collect hydrographic data by expandable CTDs (XCTDs) and to measure the upper ocean currents with the ship-borne ADCP. Taken together with data from the planned *Polarstern* expedition TransArc II in 2015, the data from this cruise will enable tracing the further evolution of the water mass distribution and the circulation in the Eurasian Arctic and the Makarov Basin. The observations will eventually serve to distinguish between variability and long-term trends in the Arctic.

Warm and saline North-Atlantic waters are imported to the Arctic Ocean in two branches flowing through the Fram Strait and the Barents Sea. They are subject to transformation in different extent by surface processes and thus submerge below the fresh polar surface layer. There they circulate in cyclonic sense along the continental slope but also return to the Fram Strait along topographic features such as the Lomonosow Ridge. On this cruise the properties of the branch returning along the Lomonosov Ridge should be captured.

In the central Arctic, stratification is strong due to fresh water in the surface mixed layer originating from continental runoff, Pacific inflow and ice melt. This fresh water overlies the warm Atlantic-derived waters and thus hampers the release of heat from the latter to the atmosphere. Changes in the fresh water distribution might therefore modify the upward diffusion of Atlantic water heat and have an influence on the ice cover. Driven mainly by the wind and ice drag, it circulates anticyclonically in the Beaufort Gyre and crosses the Arctic Ocean from the Pacific sector towards the Atlantic sector in the Transpolar Drift. Since the early 1990s the fresh water content has increased by about 20 %. Since this change might reverse within the next years the aim of this cruise was to measure the current fresh water distribution in the Transpolar Drift.

To address these questions hydrographic observations (temperature and salinity) were taken using expendable devices. This was a collaboration between the AWI and the Japan Agency for Marine Earth Science and Technology (JAMSTEC). In addition, one cast was carried out with the CTD (Conductivity Temperature Depth) rosette.

Work at sea

An XCTD-1 system by Tsurumi-Seiki Co. Ltd. (Yokohama, Japan) was used to obtain 50 temperature and salinity profiles down to 1,100 m water depth. The system consists of a launcher for expendable CTD probes and a mobile deck-unit for data acquisition. The profiles were taken during sailing without stopping the ship.

One profile was taken with a CTD/rosette water sampler system from Sea-Bird Electronics Inc. The SBE9+ CTD (S/N 937) was equipped with duplicate temperature (S/N 1373 and 1338) and conductivity (S/N 1198 and 1199) sensors, a Digiquartz 410K-134 pressure sensor (S/N 113135) and was connected to a SBE32 Carousel Water Sampler (S/N 718) with 22 Niskin 12-liter bottles. Additionally, a Benthos Altimeter (S/N 1229), a Wetlabs C-Star Transmissometer (S/N 1220), a Wetlabs FLRTD Fluorometer (S/N 1853) and an SBE 43 dissolved oxygen sensor (S/N 734) were mounted on the carousel.

Underway velocity measurements with a vessel-mounted narrow-band 150 kHz ADCP from RD instruments were obtained down to ca. 400 m depth. Two Sea-Bird SBE45 thermosalinographs, installed at 6 m depth in the bow thruster tunnel and at 11 m depth in the keel, provided continuous temperature / salinity data. The bow system was switched off while the ship was crossing sea ice. The salinity of both instruments was regularly calibrated by analysing water samples with the salinometer. The ADCP worked well throughout most of the cruise with very few data gaps. All underway measurements were stopped during transit through the Russian EEZ.

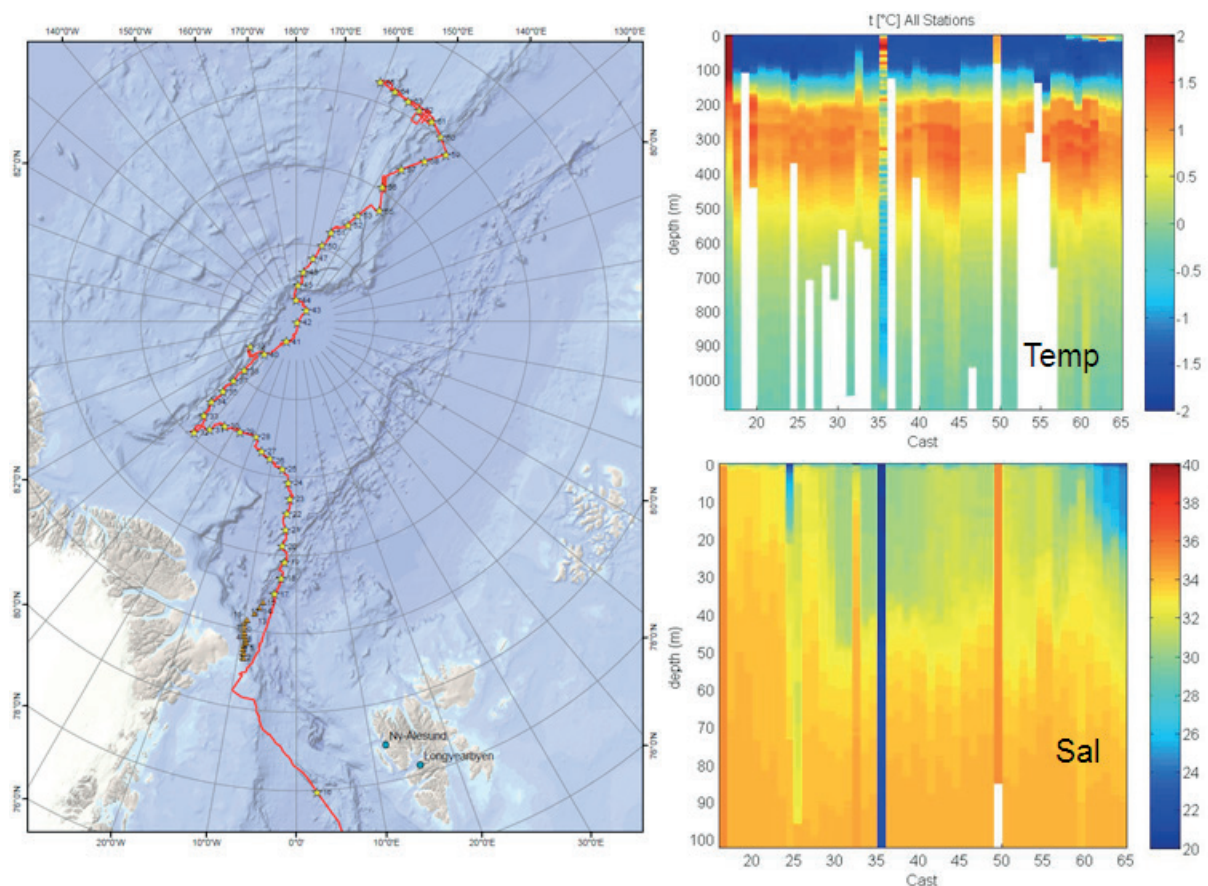


Fig. 5.1: Map of the XCTD stations (left) and temperature and salinity distribution along the cruise track (right). Erroneous stations have not yet been removed.

Preliminary results

The preliminary XCTD profiles trace the path of warm and saline Atlantic water along the Lomonosov Ridge (Fig. 5.1). Crossings of the warm core show similar high temperatures from

the East Siberian side up to the downstream end off Greenland indicating weak to no dilution with colder ambient waters along the flow.

The section across the Lomonosov Ridge (Fig. 5.2) shows at the surface a thin warm lense. The region has been ice-free for several weeks and thus been exposed to considerable insolation and warming in that region. On the Amundsen Basin side (left) the warm intermediate core centered at 300 m reaches maximum values of 1.5°C; it extends down to 1000 m water depth. This deep warm water did not cross the Ridge to the Makarov Basin side (right), and there the temperature maximum at 300 m is only ca. 1°C.

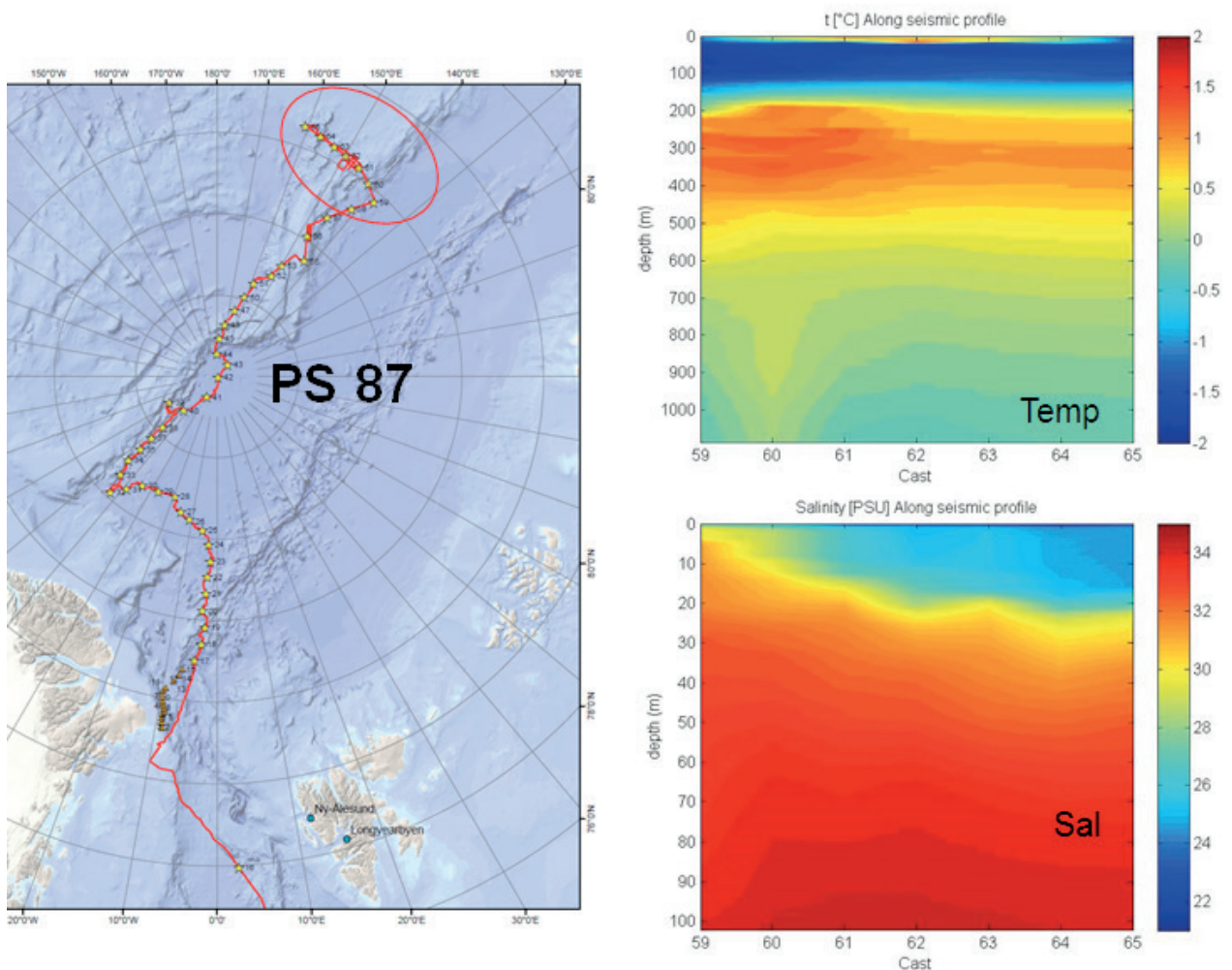


Fig. 5.2: Section across the Lomonosov Ridge (red circle, left panel). Right panel: Temperature and salinity distribution along the section from west (left side) to east (right side). Note the difference in the depth scale.

The salinity distribution shows clearly the position of the front between fresh waters on the Makarov basin side, probably originating from Pacific inflow and from ice melt, and the more saline waters in the Amundsen Basin.

Integration to national and international programmes

The oceanographic work of the cruise was a contribution to the HGF Programme PACES II, Topic 1 WP4: "Arctic sea ice and its interaction with ocean and ecosystems" and the BMBF funded project RACE ("Arktische Zirkulation als Teil des Nordatlantischen Stromsystems").

It was part of a co-operation between AWI and the Japan Agency for Marine Earth Science and Technology (JAMSTEC). It was a contribution to ArcticROOS and IAOOS (International Arctic Ocean Observing System).

Data management

XCTD data as well as ADCP data will be processed and quality controlled after the cruise and will then be made available in the PANGAEA Data Publisher for Earth & Environmental Science.

6. DISTRIBUTION OF SEABIRDS AND MARINE MAMMALS

Oria Jamar de Bolsée, Dominik Nachtsheim PoE
not on board: Claude Joiris PoE

Grant-No. AWI-PS87_02

Objectives

This research programme is part of a long-term study on the at-sea distribution of seabirds and marine mammals in the Arctic and Antarctic polar regions, led by the Laboratory for Polar Ecology (PoE). The main objective is to improve the knowledge on distribution and densities of higher trophic levels, in relation to influencing environmental factors, such as water masses, fronts and ice conditions (Joiris & Falck 2011, Joiris et al. 2013). Additionally, the integration of these data into a time series running since 1973 might allow to detect possible changes in the distribution of seabirds and marine mammals due to climate changes and decreasing sea ice extent, especially in the Arctic (Joiris 2012).

Work at sea

Seabirds and marine mammals were recorded during continuous transect counts of 30 minutes. The observations were conducted from the bridge of *Polarstern* (approximately 18 meters above sea level) at a 90° angle on portside, visibility and light conditions allowing. For counts to be valid the vessel should sail at a minimum speed of 5 knots. Species were detected without width limitation first by naked eye, followed by detailed observation with binoculars (8 – 10 fold magnification). Additionally, photographic documentation was used for a more thorough identification of some specimens. Furthermore, additional observations were carried out during helicopter flights, in order to cover a larger area and investigate the potential impact of the ship's presence on certain species. Environmental parameters, such as water temperature and salinity, were recorded continuously by the ship's integrated devices and extracted from the DShip data system on board.

Preliminary results

A total of 1,607 half hour transect counts were conducted, representing 803.5 hours of observation. During those counts 25 seabird and 9 marine mammal species (5 cetaceans, 3 seals and polar bears) were sighted. Due to large geographical differences and ice conditions (other expeditions did not spend much time in close ice coverage), this data set is hardly comparable to previous legs and will this be analysed per hydrographical areas.

Overall 11,742 seabirds were counted (Tab. 6.1). The most abundant bird species was the Atlantic puffin ($n = 4,533$; Fig. 6.1) although most sightings occurred along the Norwegian coast, during the first days of the expedition. This could be explained by the fact that they are breeding on the Scandinavian coast and fly between breeding and feeding grounds to care for their chicks (Sale 2006). The main alcid species is the little auk, which is very abundant in the Arctic. During this leg they were mostly seen at the ice edge of the Greenland Sea. Closely related is the black guillemot. Most individuals of this species were observed above the Siberian part of the Lomonosov Ridge. Juveniles, non-breeding as well as breeding adults were seen.

The northern fulmar mostly occurred in Norwegian and Greenland Seas. Almost equal numbers of the two morphs, light and dark, were counted. Usually light morph individuals occur more south whereas dark ones tend to occur further north (Sale 2006). One dark specimen was even spotted near the North Pole, at 89.95°N.

The most abundant gull species was the black-legged kittiwake, seen throughout the whole expedition, showing the largest distributional range. Additionally, a high number of ivory gulls were sighted, mainly under ice conditions. The total number exceeded the record of PS80 (ARK-XXVII/1) during which 840 individuals were encountered. On several occasions, an adult ivory gull travelling together with a juvenile was observed. An interesting sighting was an iceberg covered with sediments at 80.85°N 8.99°W which provided a breeding ground for ivory gulls (Fig. 6.2). Juveniles at different stages of their growth were observed. Above the Siberian part of the Lomonosov Ridge many Ross's gulls were seen. This rare species was often observed flying high in the sky. One unique encounter was a Sabine's gull (Fig. 6.3) following *Polarstern* for a while, together with a swarm of kittiwakes. Several seabird species are known for following ships. During this expedition mostly kittiwakes and fulmars were attracted by *Polarstern*. In sea ice conditions these followers took advantage of the freshly broken ice in order to feed, mainly on polar cods.

A total of 100 marine mammals were observed (Tab. 6.2). Cetaceans were only seen in Norwegian and Greenland Seas, with one exception of small whales in the Siberian part of the Lomonosov Ridge, although 25 days were spent in this area. Generally, no whales were sighted under dense sea ice conditions. One group of 7 narwhals, consisting of 5 adults and 2 calves, was sighted near the vessel, which is an unusual encounter for a species known for avoiding ships.

Seals were mostly sighted under ice conditions. Interestingly, several individuals were seen far north, as far as 86.11°N, in dense sea ice areas with limited access to open waters. An exceptional sighting was the presence of 17 harp seals, swimming through freshly formed pancake ice. A total of 21 seals could not be identified down to species level since they were only seen at distance in the water.

Finally, several polar bears were encountered: solitary animals, including one feeding on a seal carcass, and a mother with three cubs (Fig. 6.4). The latest was rather unusual since mother polar bears commonly raise one or two cubs, offering better chances of survival to her young. In fact one of the observed cubs was significantly smaller than the other two. The number of polar bear tracks was one order of magnitude higher than the number of sighted bears. Thus, tracks provide important additional information on their occurrence. Many tracks were seen under dense sea ice conditions, almost up to the North Pole (88.56°N).

In total, four helicopter flights were used for wildlife observation, three in dense sea ice conditions and one in open waters at the Siberian part of the Lomonosov Ridge. They were helpful in confirming the general absence of endotherm animals.

Worth mentioning are two out of count records: one adult male walrus (*Odobenus rosmarus*) swimming around the ship, far from any land or ice, during a geological station work (83.21°N 141.08°E) and one pechora pipit (*Anthus gustavi*) who stayed on board for several days.

Tab. 6.1: List of seabird species encountered during PS87 (ARK-XXVIII/4)

English name	Scientific name	Numbers
Atlantic Puffin	<i>Fratercula arctica</i>	4533
Little Auk	<i>Alle alle</i>	568
Black Guillemot	<i>Cephus grylle</i>	76
Brünnich's Guillemot	<i>Uria lomvia</i>	163
Common Guillemot	<i>Uria aalge</i>	1
Guillemot sp.		18
Razorbill	<i>Alca torda</i>	51
Auk sp.		58
Northern Fulmar – Light	<i>Fulmarus glacialis</i>	347
Northern Fulmar – Dark	<i>Fulmarus glacialis</i>	337
Black-legged Kittiwake	<i>Rissa tridactyla</i>	2960
Ross's Gull	<i>Rhodostethia rosea</i>	1771
Ivory Gull	<i>Pagophila eburnea</i>	344
European Herring Gull	<i>Larus argentatus</i>	98
Glaucous Gull	<i>Larus hyperboreus</i>	13
Great Black-backed Gull	<i>Larus marinus</i>	2
Lesser Black-backed Gull	<i>Larus fuscus</i>	1
Black-backed Gull sp.		9
Mew Gull	<i>Larus canus</i>	4
Sabine's Gull	<i>Xema sabini</i>	1
Gull sp.		322
Great Skua	<i>Stercorarius skua</i>	5
Arctic Skua	<i>Stercorarius parasiticus</i>	15
Pomarine Skua	<i>Stercorarius pomarinus</i>	3
Skua sp.		2
Northern Gannet	<i>Sula bassana</i>	3
Great Cormorant	<i>Phalacrocorax carbo</i>	1
Arctic Tern	<i>Sterna paradisea</i>	2
Tern sp.		21
Fork-tailed Storm-petrel	<i>Oceanodroma furcata</i>	10
Phalarope sp.	<i>Phalaropus sp.</i>	1
Greylag goose	<i>Anser anser</i>	2
		11742

Tab. 6.2: List of marine mammal species encountered during PS87 (ARK-XXVIII/4)

English name	Scientific name	Numbers
Polar Bear	<i>Ursus maritimus</i>	8
Polar Bear track	<i>Ursus maritimus</i>	120
Arctic fox track	<i>Alopex lagopus</i>	3
Harp Seal	<i>Pagophilus groenlandica</i>	18
Hooded Seal	<i>Cystophora cristata</i>	4
Ringed Seal	<i>Pusa hispida</i>	2
Seal sp.		21
Fin Whale	<i>Balaenoptera physalus</i>	3
Humpback Whale	<i>Megaptera novaeangliae</i>	1
Northern Minke Whale	<i>Balaenoptera acutorostrata</i>	3
Whale sp.		5
Narwhal	<i>Monodon monoceros</i>	7
White-beaked Dolphin	<i>Lagenorhynchus albirostris</i>	24
Smaller Whale sp.		4



Fig. 6.1: Atlantic puffin (Fratercula arctica)



Fig. 6.2: One adult and three juvenile ivory gulls (*Pagophila eburnea*) on a sediment covered iceberg



Fig. 6.3: Sabine's gull (*Xema sabini*)



Fig. 6.4: Polar bear (*Ursus maritimus*) with three cubs

Data management

All seabird and marine mammal data are available in the PoE dataset (contact: crjoiris@gmail.com).

References

- Joiris CR, Falck E (2011) Summer at-sea distribution of little auks *Alle alle* and harp seals *Pagophilus (Phoca) groenlandica* in the Fram Strait and the Greenland Sea: impact of small-scale hydrological events. *Polar Biology*, 34, 541-548.
- Joiris CR (2012) Possible impact of decreasing Arctic pack ice on the higher trophic levels – seabirds and marine mammals. *Advances in Environmental Research*, 23, 207-221.
- Joiris CR, Humphries GRW, De Broyer A (2013) Seabirds encountered along return transects between South Africa and Antarctica in summer in relation to hydrological features. *Polar Biology*, 36, 1633-1647.
- Sale R (2006) *A complete guide to Arctic wildlife*. Firefly Books Ltd., Ontario, Canada.

7. THE ENVIRONMENTAL CONTROLS OF TRACE METAL RATIOS RECORDED IN CALCAREOUS TESTS OF ARCTIC DEEP-SEA BENTHIC FORAMINIFERA – CULTURE EXPERIMENTS, MODERN FIELD DATA AND THE LONG-TERM GEOLOGICAL RECORD

Stefanie Kaboth¹

¹UoU)

not on board: Jutta Wollenburg²

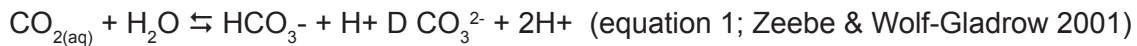
²AWI

Grant-No. AWI-PS87_01

Objectives

The Arctic Ocean shows a strong positive feedback to present day climate change. Hereby, the rise in northern hemisphere air temperature is amplified in the Arctic Ocean by a factor of 2 to 4 (Miller et al. 2010; Seereze & Barry 2011). This so-called Arctic amplification is the result of a collection of positive feedbacks to temperature rise with the strongest and quickest being melt of sea-ice and snow coverage, one of the slowest the melting of continental ice sheets (Seereze & Barry 2011). Over the last decades Arctic amplification has led to a significant rise in Arctic Ocean surface temperature of 0.5°C, of advected Atlantic Water by 1°C and a dramatic loss in summer sea-ice extend of 7.5 % per decade (Otto-Bliesner et al. 2006; Serreze et al. 2007; Comiso et al. 2008; Kwok & Rothrock 2009). As consequence of seasonal sea-ice retreat, primary production and via the continental shelf pump the uptake and export of anthropogenic CO₂ increases (Anderson et al. 2010). Exchange of carbon dioxide (CO₂) between atmosphere and ocean is a critical process of the polar oceans carbon cycle (Orr et al. 2009; McNeill et al. 2008) and an important determinant of past and future climate change (Tripathi et al. 2005). The polar oceans are the global sites of deep-water formation. Here production of dense water is supposed to occur preferably on the broad continental shelves where water not only is cooled to its freezing point, but also increases its salinity due to the accumulation of brine rejected during freezing of sea ice (Rudels & Quadfasel 1991). This dense water flows gravitatively down the slope and contributes to and ventilates the respective deep and bottom waters. Since ice-free surface waters are in equilibrium with the atmosphere large areas of ice-free water, sea-ice formation and deep convection are favourable for a high CO₂ uptake/deep-water storage in the polar oceans. The Arctic Ocean is a mediterranean sea with limited communications with the major ocean basins (Pacific, Atlantic). Because of its geographical constrains and the comparably small volume (1 % of the worlds ocean), its global role as present CO₂ sink is comparably small (2 % of the global ocean anthropogenic CO₂ inventory) (Tanhua et al. 2009; Jutterström & Anderson 2010).

The present increase in anthropogenic CO₂ emissions and attendant increase in ocean acidification and sea ice melt decrease the pH and saturation state of carbonate ion concentrations in the Arctic Ocean (Orr et al. 2009; McNeill et al. 2008; Yamamoto-Kawai et al. 2009; Tanhua et al. 2009; Hauck et al. 2010). Hereby, the uptake of CO₂ by seawater increases the concentration of hydrogen ions, which lowers pH and, in changing the chemical equilibrium of the inorganic carbon system, reduces the concentration of carbonate ions (CO₃²⁻). If the CO₂ concentration changes, the carbonate ion concentration and pH change as a result of shifts in the equilibrium (see equation 1).



Modern Arctic Ocean abyssal-waters (>2,000 m) are saturated with respect to calcite (Jutterström & Anderson 2005; Jutterström et al. 2010). However, because the Arctic Ocean deep-water ventilation is largely dependent on its own deep-water production and the latter one a by-product of sea-ice formation/brine release, the glacial increase of perennial sea-ice may have led to a drop in bottom and deep-water pH. At Arctic sites >2,000m water depths extended sediment sequences from peak glacial intervals are barren in microfossils indicating an accumulation under the influence of corrosive or hostile deep waters. Isochronously, at shallower sites strongly corroded calcareous foraminifera test indicate a peak glacial calcite lysocline at about 800m (Wollenburg et al. 2001, 2004, 2007).

The formation of deep-water in the Greenland Sea, one of the driving forces of Atlantic Meridional Circulation, decreases since the late 1970s (Schlosser et al. 1991). In its northernmost position of the Atlantic Meridional Circulation the Arctic Ocean's vulnerability to climate changes has consequences far beyond the Arctic Ocean.

Employment of effective and fossilisable proxies on changes in the physical and geochemical properties is essential to assess glacial-interglacial variability, modern and future changes in polar deep-waters. In this respect, analyses on trace metal (Mg/Ca, U/Ca, B/Ca) ratios recorded in tests of foraminifers to estimate calcification temperatures, alkalinity, carbonate ion saturation, and pH are common methods. However, for the Arctic Ocean deep-sea benthic foraminifer calibration curves constrained by either core-top samples or culture experiments are lacking. Newly developed high-pressure aquaria have recently facilitated the first efficient cultivation (producing offspring) of our most trusted palaeodeep-water recorder *Cibicides wuellerstorfi*. In different experimental set-ups the same facilities will be used to cultivate these foraminifera and associated species at different temperatures and in waters with different carbonate chemistries to establish the first species-specific trace metal calibration curves for both Polar Oceans. Core top analyses will verify the experimental results.

Benthic foraminifera are the most abundant calcareous deep-water microfossils. The distribution of modern and fossil deep-sea benthic foraminifera in Arctic Ocean is controlled by the availability of food, oxygen, and pH (e.g. Wollenburg & Kuhnt 2000). Whereas the variability in faunal composition is a good monitor of the amount and seasonality of carbon fluxes, and/or the prevalence of corrosive bottom waters, precise information on deep-water ventilation, pH, alkalinity and carbonate ion concentration as well as the calcification temperature of shells can only be assessed by analysing the geochemical composition of their calcareous shells.

As the $\delta^{18}\text{O}$ ratios recorded in both water masses and foraminiferal tests are determined by both salinity and temperature, and Mg/Ca mainly by temperature both proxies can be combined to distinguish between salinity and temperature effects. Therefore, in an area where salinity effects exceed temperature effects on the $\delta^{18}\text{O}$, trace metal analyses on shells of foraminifers may, after calibration, provide a reliable palaeotemperature proxy. Apart from simple dissolution indices (e.g. Anderson & Archer 2002), trace metal ratios are furthermore the only potential proxy for the palaeodeep-water carbonate chemistry, and as such pH. We will culture the 15 sediment cores retrieved during this expedition at different pH-values. The results will contribute to the calibration for trace metal ratios in foraminiferal calcite versus temperature and pH/alkalinity in a running long-term bipolar study. This results from this study should enable not only a reconstruction of palaeotemperatures and palaeodeep-water carbonate chemistries, but also provide insight in the extent of palaeosea-ice variability, deep-water formation and exchange, and thus, the polar oceans present and past role in climate change.

Trace metal/Calcium ratios

The substitution of calcium by magnesium in the calcite lattice is mainly a function of temperature. Thus, simplified highest Mg/Ca ratios are observed in warm water foraminifers. Over the last two decades Mg/Ca analyses on calcareous shells of foraminifers for to estimate calcification temperature from marine became a widely used tool in palaeoceanography. Because Mg/Ca of foraminifers are biologically mediated and often species specific, empirical calibrations studies are essential to determine temperature sensitivity and the role of other contributing factors. An exponential relationship between planktonic foraminifera Mg/Ca and temperature (about 9-10 % Mg/Ca increase per °C) has been demonstrated in cultivation experiments, sediment traps/nets and core top samples (Elderfield & Ganssen 2000; Anand et al. 2003; Groeneveld & Chiessi 2011). Benthic Mg/Ca calibrations are based almost exclusively on core-top studies (Elderfield et al. 2006, 2010; Bryan & Marchitto 2008; Raitzsch et al. 2008). Cultivation experiments on Mg/Ca recorded in benthic foraminifera are rare (Hintz et al. 2006; Segev & Erez 2006; Dissard et al. 2010a/b; Alison et al. 2010; Filipsson et al. 2010) and restricted to shallow water species. Only Filipsson et al. (2010) cultured foraminifers from water depths of <800 m. However, only *Bulimina marginata/aculeata* formed new chambers during their experiments. Thus, up to date only the environmental controls on the Mg/Ca ratios recorded in tests of *Ammonia tepida*, *Elphidium williamsoni*, *Rosalina vilardeboana*, *Amphistegina* spp. and *B. marginata/aculeata* were experimentally verified. Since, until recently it has been impossible to culture barophilic deep-water foraminifera under *in-situ* (high-pressure) conditions (Wollenburg & Tiedeman subm.), The temperature dependency of Mg/Ca of deep-water foraminifera, especially those of our most trusted palaeodeep-water recorders *Cibicides* (*Cibicidoides*, *Planulina*) *wuellerstorfi* and *Uvigerina peregrina* is still not verified by culture experiments. Calibrations constructed on Mg/Ca recorded in deep-water benthic foraminifera from core-top samples revealed that: 1) Benthic species show a similar temperature dependency (6-11% Mg/Ca increase per °C) to planktonic foraminifera, 2) As deep-water species live within a small temperature range, the calibration of Mg/Ca to these small-scale temperature variability is not straightforward besides temperature Mg/Ca is also dependent on the carbonate ion saturation state (Raitzsch et al. 2008). Since the Mg/Ca ratio recorded in calcareous deep-water foraminifera is dependent on both temperature and the carbonate ion saturation state, temperature-independent carbonate system proxies (B/Ca and U/Ca) can potentially be used to correct the Mg/Ca temperature effect for the carbonate ion concentration effect (Raitzsch et al. subm.). Because at present this is still just a qualitative verification, culture experiments on multiple trace metal ratios and variable environmental controls are needed to calculate relationships. The boron composition of marine carbonates is a suitable tracer for the carbonate system, since the fractionation between the two aqueous boron species $B(OH)_4^-$ and $B(OH)_3$ in seawater is controlled by the carbonate ion concentration (CO_3^{2-}) and pH (Yu et al., 2010). Herein the fraction of $B(OH)_4^-$ decreases in favour of increasing $B(OH)_3$ with decreasing sea water pH. Because foraminifera only incorporate $B(OH)_4^-$ the B/Ca ratio recorded in their shells can be used to estimate seawater pH and other related CO_2 system variables. Since secondary effects such as temperature or dissolution appear to be minimal, the B/Ca ratio in benthic foraminifera seems a robust tool for estimating past deep-water $\Delta(CO_3^{2-})$ (Yu & Elderfield 2007; Yu et al. 2010). Compared with boron, little attention has been paid to the uranium content in foraminiferal shells. Similarly to boron, uranium exists as different species in seawater, whose relative amounts are also dependent on pH. Culture experiments on planktonic foraminifera species provide evidence that shell U/Ca is strongly influenced by pH in a way that U/Ca decreases exponentially with increasing pH or (CO_3^{2-}) (Russell et al. 2004, Raitzsch et al. subm.). For benthic foraminifera culture experiments on the B/Ca and U/Ca ratios recorded in foraminiferal calcite have not been performed yet.

The accuracy of core-top based calibrations for trace metal/calcium measurements can be significantly biased by other factors than just temperature or the carbonate system (e.g. Hintz et al. 2006). Boyle (1995) suggested four mechanisms for the observed inter-individual variability in field-collected material: (1) bioturbative mixing of sediments altering depositional age, (2) individual variation (e.g., size, growth rate, age and genetic factors), (3) microhabitat variation, and (4) unknown post-depositional processes altering test chemistry. Culturing under stringent physicochemical controlled conditions provides the ability to experiment on specific vital effects, elucidating some of the biomineralization effects on the preserved trace metal/Ca ratios in foraminiferal calcite.

Trace metal analyses on benthic foraminiferal shells have not yet been applied to sediments from the Arctic Ocean (>70°N). Core-top and related culture experiments to determine calibrations on trace metal ratios in deep-sea foraminifera are unavailable. Therefore, this study has the potential to provide an important contribution to the use of trace metal/Ca ratios in benthic foraminifera for the polar oceans.

Work at sea and preliminary results

We have successfully operated three multiple corer casts and transferred the surface sediments into push-cores for the transport in the cold lab at the AWI (Table 7.1). Here pushcores will be transferred into 5 high-pressure aquaria running at 130 bar and 10 mesocosms running at atmospheric pressure. We will culture these sediments for 5 months in calcein-tagged water. Hereby, new experimental offspring can be visualised by fluorescence analyses. The cultures will be kept at site-alike environmental conditions, and different but within the individual experiment stable pH-values of 7.9 to 8.5. Analyses on newly formed tests will start approximately 6 months after the expedition. The obtained results will be compared to results of comparable experiments from the last 2 years and from the Arctic and Antarctic Ocean

Trace metal analyses on foraminifera from surface samples from 16 additional multiple corer casts accomplish the data set. These results will be related to DIC analyses on water samples from CTD casts and additional samples from the water covering the sediments in the respective multiple corer tubes.

Tab. 7.1: Multicorer casts

Samples for culturing					
Date	Station	Gear	Latitude	Longitude	Depth [m]
26.09.2014	PS87/109-3	Multi corer	81° 07.67' N	140° 34.91' E	1303,1
26.09.2014	PS87/109-5	Multi corer	81° 07.69' N	140° 34.94' E	1302,6
26.09.2014	PS87/109-6	Multi corer	81° 07.67' N	140° 35.13' E	1304,6

Data management

All data will be uploaded to the PANGAEA Data Publisher for Earth & Environmental Science. Unrestricted access to the data will be granted after about three years, pending analysis and publication.

Acknowledgements

This study is funded by DFG grant WO 742/2-1 of SPP 1158.

References

- Alison N, Austin W, Paterson D, Austin H (2010) Culture studies of the benthic foraminifera *Elphidium williamsoni*: Evaluating pH, $\Delta(\text{CO}_3^{2-})$ and inter-individual effects on test Mg/Ca, *Chemical Geology*, 274, 87-93.
- Anand P, Elderfield H, Conte MH (2003) Calibration of Mg/Ca thermometry in planktonic foraminifera from a sediment trap time series, *Paleoceanography*, 18(2), 1050, doi:10.1029/2002PA000846.
- Anderson DM, Archer D (2002) Glacial-interglacial stability of ocean pH inferred from foraminifer dissolution rates, *Nature*, 416, 70-
- Anderson LG, Tanhua T, Björk G, Hjalmarrsson S, Jones EP, Jutterström S, Rudels B, Swift J H, Wåhlström I (2010) Arctic Ocean shelf – basin interaction, an active continental shelf CO_2 pump and its impact on the degree of calcium carbonate dissolution, *Deep Sea Res. I*, 57, 869–879 doi:10.1016/j.dsr.2010.03.012.
- Bryan SP, Marchitto TM (2008) Mg/Ca-temperature proxy in benthic foraminifera: new calibrations from the Florida Straits and a hypothesis regarding Mg/Li. *Paleoceanography*, 23. doi:10.1029/2007PA001553 PA2220.
- Comiso JC (2006) Abrupt decline in the Arctic winter sea ice cover. *Geophys. Res. Lett.*, 33, L18504, doi:10.1029/2006GL027341.
- Dissard D, Nerke G, Reichert GJ, Bijma J (2010a) The impact of salinity on the Mg/Ca and Sr/Ca ratio in the benthic foraminifera *Ammonia tepida*: Results from culture experiments, *Geochimica et Cosmochimica Acta*, 74, 928-940.
- Dissard D, Nerke G, Reichert GJ, Bijma J (2010b). Impact of seawater $p\text{CO}_2$ on calcification and Mg/Ca and Sr/Ca ratios in benthic foraminifera calcite: results from culturing experiments with *Ammonia tepida*, *Biogeosciences*, 7, 81-93.
- Elderfield H, Ganssen (2000) Past temperature and $\delta^{18}\text{O}$ of surface ocean waters inferred from foraminiferal Mg/Ca ratios, *Nature*, 405, 442–445, doi:10.1038/35013033.
- Elderfield H, Yu J, Anand P, Kiefer T, Nyland B (2006) Calibrations for benthic foraminiferal Mg/Ca paleothermometry and the carbonate ion hypothesis. *Earth Planet Sci Lett.*, 250, 633–649.
- Elderfield H, Greaves M, Barker S, Hall R, Tripathi A, Ferretti P, Crowhurst S, Booth L, Daunt C (2010) A record of bottom water temperature and seawater $\delta^{18}\text{O}$ for the Southern Ocean over the past 440 kyr based on Mg/Ca of benthic foraminiferal *Uvigerina* spp., *Quat. Sci. Rev.*, 29, 160–169.
- Erez J (2003) The source of ions for biomineralization in foraminifera and their implications for paleoceanographic proxies. *Rev Mineral Geochem*, 54, 115–149.
- Filipsson HL, Bernhard J M, Lincoln SA, McCorkle DC (2010) A culture-based calibration of benthic foraminiferal paleotemperature proxies: $\delta^{18}\text{O}$ and Mg/Ca results, *Biogeosciences discuss.*, 7, 351-385.
- Groeneveld J, Chiessi CM (2011) Mg/Ca of *Globorotalia inflata* as a recorder of permanent thermocline temperatures in the South Atlantic, *Paleoceanography*, 26, PA2203, doi:10.1029/2010PA001940.
- Groeneveld J, Steph S, Tiedemann R, Garbe-Schönberg D, Nürnberg D (2006) 13. Pliocene mixed layer oceanography for Site 1241, using combined Mg/Ca and $\delta^{18}\text{O}$ analyses of *Globigerinoides sacculifer*, *Proceedings Ocean Drilling Program Scientific Results*, 202, 1-27.

- Groeneveld J, Nürnberg D, Tiedemann R, Reichart G-J, Steph S, Reuning L, Crudeli D, Mason P (2008), Foraminiferal Mg/Ca increase in the Caribbean during the Pliocene: Western Atlantic Warm Pool formation, salinity influence, or diagenetic overprint?, *Geochemical Geophysical Geosystems* 9, Q01P23.
- Hauck J, M Hoppema, RGJ Bellerby, C Völker, Wolf-Gladrow D (2010) Data-based estimation of anthropogenic carbon and acidification in the Weddell Sea on a decadal timescale, *J. Geophys. Res.*, 115, C03004, doi:10.1029/2009JC005479.
- Hintz CJ, Shaw TJ, Chandler TG, Bernhard JM, McCorkle DC, Blanks JK (2006) Trace/minor element:calcium ratios in cultured benthic foraminifera. Part I: Inter-species and inter-individual variability, *Geochimica et Cosmochimica Acta*, 70 (8), 1952-1963.
- Jutterström S, Anderson LG (2005) The saturation of calcite and aragonite in the Arctic Ocean, *Marine Chemistry*, 94, 101-110.
- Jutterström S, Anderson LG (2010) Uptake of CO₂ by the Arctic Ocean in a changing climate, *Marine Chemistry*, doi:10.1016/j.marchem.2010.07.002.
- Kwok R, Rothrock DA (2009) Decline in Arctic sea ice thickness from submarine and ICESat records: 1958–2008. *Geophys. Res. Lett.*, 36, L15501. doi:10.1029/2009GL039035.
- Lawrence DM, Slater AG, Tomas RA, Holland MM, Deser C (2008) Accelerated Arctic land warming and permafrost degradation during rapid sea ice loss. *Geophys. Res. Lett.*, 35, L11506. doi:10.1029/2008GL033894.
- Rudels B, Quadfasel D (1991) Convection and deep water formation in the Arctic Ocean-Greenland Sea System. *J. Mar. Syst.*, 2, 435-450.
- Schlosser P, Böhnisch G, Rhein M, Bayer R (1991) Reduction of deep water formation in the Greenland Sea during the 1980s: evidence from tracer data. *Science*, 251, 1054–1056.
- Segev E, Erez J (2006) Effect of Mg/Ca ratio in seawater on shell composition in shallow benthic foraminifera, *Geochem. Geophys. Geosyst.*, 7, Q02P09, doi:10.1029/2005GC000969.
- Tripathi A, Backman J, Elderfield H, Ferretti P (2005) Eocene bipolar glaciation associated with global carbon cycle changes. *Science*, 436, doi:10.1038.
- McNeil BI, Metzl N, Key RM, Matear RJ, Corbiere A (2007) An empirical estimate of the Southern Ocean air-sea CO₂ flux, *Global Biogeochem. Cycles* 21, GB3011, doi:10.1029/2007GB002991.
- McNeil BI, Matear RJ (2008) Southern Ocean acidification: A tipping point at 450-ppm atmospheric CO₂, *PNAS*, 105(48), 18860-18864.
- Miller GH, Alley EB, Brigham-Grette J, Fitzpatrick JJ, Polyak L, Serreze MC, White JWC (2010) Arctic amplification: can the past constrain the future? *Quatern. Sci. Rev.*, 29, 1779–1790.
- Orr JC, Jutterström S, Bopp L, Anderson LG, Cadule P, Fabry V J, Frölicher T, Jones EP, Joos F, Lenton A, Maier-Reimer E, Segschneider J, Steinacher M, Swingedouw D (2009) Amplified acidification of the Arctic Ocean, *IOP Conf.Series: Earth and Environmental Science*, 6, doi:10.1088/1755-1307/6/6/462009.
- Raitzsch M, Kuhnert H, Groeneveld J, Bickert T (2008) Benthic foraminifer Mg/Ca anomalies in South Atlantic core top sediments and their implications for paleothermometry, *Geochemistry, Geophysics, Geosystems*, 9, Q05010, doi:10.1029/2007GC001788.
- Russel AD, Hönisch B, Spero HJ, Lea, DW (2004) Effects of seawater carbonate ion concentration and temperature on shell U, Mg, and Sr in cultured planktonic foraminifera, *Geochim. Cosmochim. Acta* 68, 4347-4361.

8. BATHYMETRIC INVESTIGATIONS

Laura Jensen, Mirjam Cahnbley,
Clara Stolle

AWI

Grant-No. AWI-PS87_01

Objectives

The main task of the bathymetry group on this expedition was the collection and processing of high-resolution seafloor topography data in the research area with the multibeam echo sounder. Multibeam data is sparse in the high Arctic and existing bathymetric models are mainly derived from satellite altimetry with limited spatial resolution. Thus, mapping the seafloor in these inaccessible regions gives valuable basic information for understanding and interpreting several geophysical processes in the Arctic. Despite data recording and processing, the bathymetry group provided detailed seafloor maps to the geological working group supporting sampling site collection and station planning. During the expedition, it was possible to perform extended bathymetric surveys at two locations of the Siberian part of the Lomonosov Ridge, which will contribute to the reconstruction of the climate history in that region.

Work at sea

Technical settings

Multibeam data was recorded with the ATLAS Hydrographic Hydrosweep DS3 multibeam echo sounder, permanently installed on *Polarstern*. using the ATLAS Hydromap Control (AHC) software version 2.6.6.0 with the following relevant parameter settings: Swath width portside/starboard mainly “250 %”, in heavy sea ice conditions sometimes reduced to “200 %”, which results in a coverage of 4-5 times the water depth. Beam spacing was set to “Equal Footprint”, desired number of beams to “920”, C-keel source to “System C-keel”, and the transmission sequence to “Equidistant Transmission”, with a desired time interval of mainly 450 ms, which triggers the system to ping as often as possible. However, in shallow water depths (<300m) the desired time interval was increased to 1,000 ms to reduce the data amount.

For online visualisation of the raw data, the Hypack software package version 13.0.0.6 was used. Raw data was stored in *.asd-format in 30 minute blocks using the ATLAS Parastore software version 3.3.17.0. In addition it was stored in *.hsx-format with Hypack (in 30 minute blocks as well). No water column data was collected. As no significant artefacts caused by interferences between PARASOUND PS70 and Hydrosweep DS3 were visible in the data of both systems, Hydrosweep did not trigger PARASOUND on this expedition.

During station work, the data recording was not stopped but the Wait Time in the acquisition control was set to 120s, so that every 2 minutes one ping was stored. This was done to avoid data gaps at the geological stations due to drifting of the vessel (especially within sea ice). For the sound velocity corrections sound velocity profiles were obtained from 50 XCTD measurements (see Chapter 5), three Valeport SVP casts and one CTD cast (Table 8.1). As the Valeport SVP was tied to the wire during Multicorer casts no additional ship's time

was needed for the operation. The sound velocities were applied in AHC, Hypack and during postprocessing.

Tab. 8.1: Valeport SVP and CTD casts

Station	Device	Date	Time [UTC]	Latitude	Longitude	Depth [m]
PS87/074-2	SVP (MUC)	09/09/14	9:00	82°43'26" N	158°37'31" E	2743
PS87/076-3	SVP (MUC)	09/09/14	22:48	82°53'47" N	154°57'47" E	2555
PS87/079-3	SVP (MUC)	09/10/14	18:41	83°12'05" N	141°22'29" E	1331
PS87/109-1	CTD	09/26/14	15:47	81°07'38" N	140°35'09" E	1251

Operation

Data acquisition started on August 6, 2014 at 07:37 UTC when leaving the Norwegian shelf and lasted until September 28, 2014, 02:18 UTC shortly before entering the Russian exclusive economic zone (EEZ). After leaving the Russian EEZ, on October 1, 2014 at 18:09 UTC the system was switched on again and data was collected until October 4, 2014, 09:32 UTC off the Norwegian coast south of Tromsø. The echo sounder was operated fully supervised by three operators in a 24/7 shift mode. During dedicated bathymetric surveys, the system was partly operated from the bridge via Ultra VNC win32 remote desktop.

Generally, the system was stable and continuous data recording was possible. However, during the cruise the system had to be restarted several times, which caused data gaps with a total duration of about 10 hours. Table 8.2 summarizes the times and reasons for system restarts.

Tab. 8.2: Times and reasons for system restarts

Date	Time (UTC)	Durat- ion (h)	Reason	Solution
06.08.	15:50	0.75	After starting the system: Warning: SPM:Slot1:DSP POST error->0x20 (pops up every few seconds); Several system restarts due to ATLAS remote maintenance (J. Reuter)	Taking out card 1 of SPM, restart; taking out card 2 of SPM, restart; placing both cards back, restart.
07.08.	8:50	1.25	Several system restarts due to ATLAS remote maintenance (J. Reuter)	
13.08.	7:37	2.00	Cannot connect to database (You have to start the UDP Inbound Server!)	Switch on/off echo sounder, restart mcpc1ds3
27.08.	7:56	1.50	CM Recovery Action: SPM failed. (Data not sent properly to sounder!); Afterwards: Warning: SPM:Slot1:DSP POST error->0x20 (pops up every few seconds)	Switch on/off echo sounder
27.08.	12:36	0.75	(changing cards of SPM)	Taking out card 1 of SPM, restart; taking out card 2 of SPM, restart; placing both cards back, restart.
09.09.	7:59	2.50	Driver 'ATLAS HYDROSWEEP DS-3' is not sending telegrams. (Data not sent properly to sounder!)	Replacing power supply of CM with spare part.

Date	Time (UTC)	Duration (h)	Reason	Solution
10.09.	11:10	0.75	Driver 'ATLAS HYDROSWEEP DS-3' is not sending telegrams. (Data not sent properly to sounder!)	Switch on/off echo sounder
12.09.	4:35	0.50	Driver 'ATLAS HYDROSWEEP DS-3' is not sending telegrams. (Data not sent properly to sounder!)	Switch on/off echo sounder
12.09.	5:18	0.25	Driver 'ATLAS HYDROSWEEP DS-3' is not sending telegrams. (Data not sent properly to sounder!) Afterwards: no tracking windows!	Switch on/off echo sounder
Sum		10.25		

For data processing, the *.asd-files were imported in the software CARIS HIPS&SIPS Version 8.1. All raw data (except the data collected at the end of the cruise after leaving the Russian EEZ) were already processed during the cruise. Data were corrected for refraction errors using the sound velocity profiles and cleaned from coarse depth errors using the “Swath Editor”, a ping-by-ping data-cleaning editor. Occasionally the “Subset Editor” was used for data cleaning, where data can be viewed and cleaned region-based in a 3D-view. The processed data was exported to ASCII-files, gridded and – for data access, station planning and further use – integrated into an ESRI ArcGIS project. Furthermore, maps were produced with Generic Mapping Tools (GMT) and 3D-visualizations were obtained with QPS Fledermaus.

Preliminary results

During PS87, an area of about 80,935 km² with a track length of about 5,600 nm was mapped within 54 days (excluding the data collected from October 1 to October 4). Fig. 8.1 shows an overview of the acquired multibeam data coverage.

In the main research area, five dedicated bathymetric surveys were conducted, with a total duration of nearly 5 days (Fig. 8.2, Table 8.3). Except for Survey 1 and 2 the survey data was collected during ice free conditions. Survey 3 and 4 were not purely bathymetric surveys but performed in addition to data collected earlier, during seismic profiles. For that reason, the tracks had to be planned to fill as many data gaps as possible leading to only limited systematic ship's tracks.

Tab. 8.3: Bathymetric survey times and coverage

	Station	Start date	Start time [UTC]	End date	End time [UTC]	Duration [h]	Coverage [km ²]
Survey 1	PS87/052	31.8	13:40	2.9	0:05	34.0	982
Survey 2	PS87/077	9.9	23:45	10.9	4:18	4.5	246

	Station	Start date	Start time [UTC]	End date	End time [UTC]	Duration [h]	Coverage [km ²]	
Survey 3	PS87/071	6.9	12:09	6.9	17:24	5.5	16,363	
	PS87/082	21.9	19:58	23.9	7:36	36.0		
	PS87/084	23.9	13:23	23.9	16:36	3.0		
					<i>Sum</i>	44.5		
		+ several seismic profiles from 2.9. - 8.9., 10.9. - 11.9., and 20.9. - 21.9.						
Survey 4	PS87/091	24.9	11:25	25.9	0:15	13.0	12,616	
	PS87/098	25.9	8:42	25.9	10:58	2.5		
	PS87/101	25.9	17:10	26.9	4:51	12.0		
					<i>Sum</i>	27.5		
		+ several seismic profiles from 13. - 20.9.						
Survey 5	PS87/111	27.9	17:04	28.9	2:07	9.0	2,722	
					<i>Sum</i>	119.5		

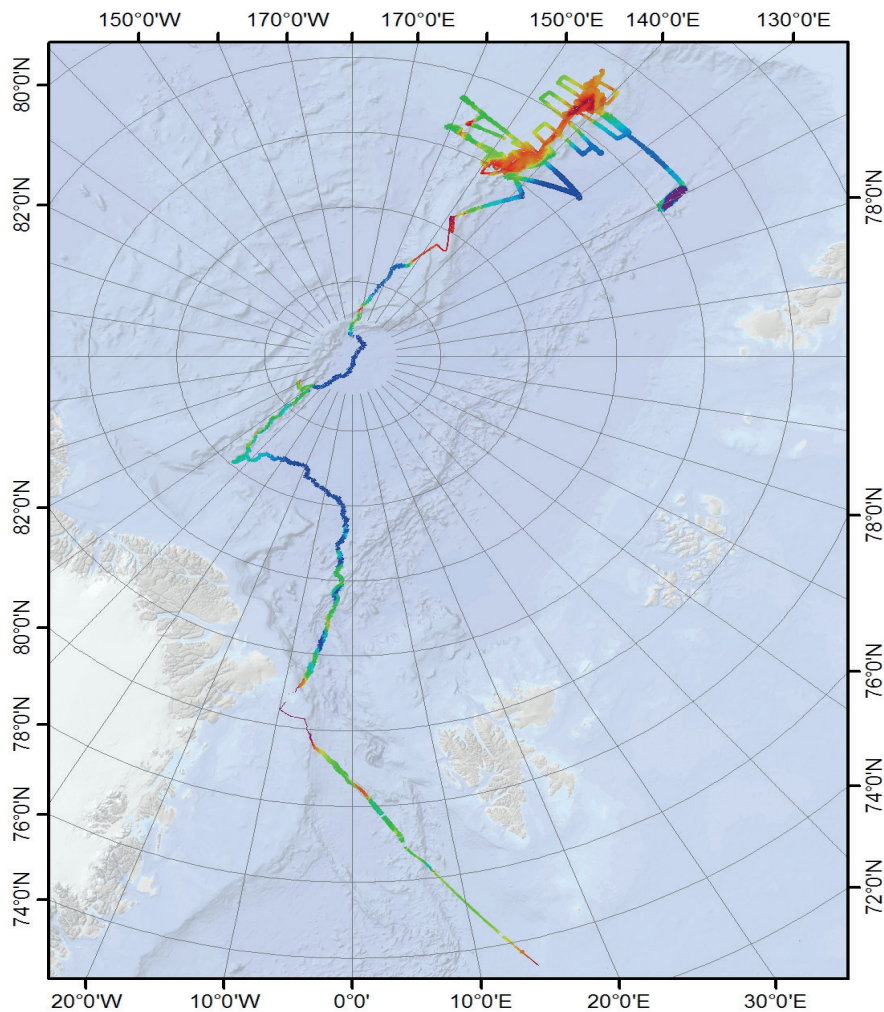


Fig. 8.1: Overview map of the multibeam data coverage for PS87

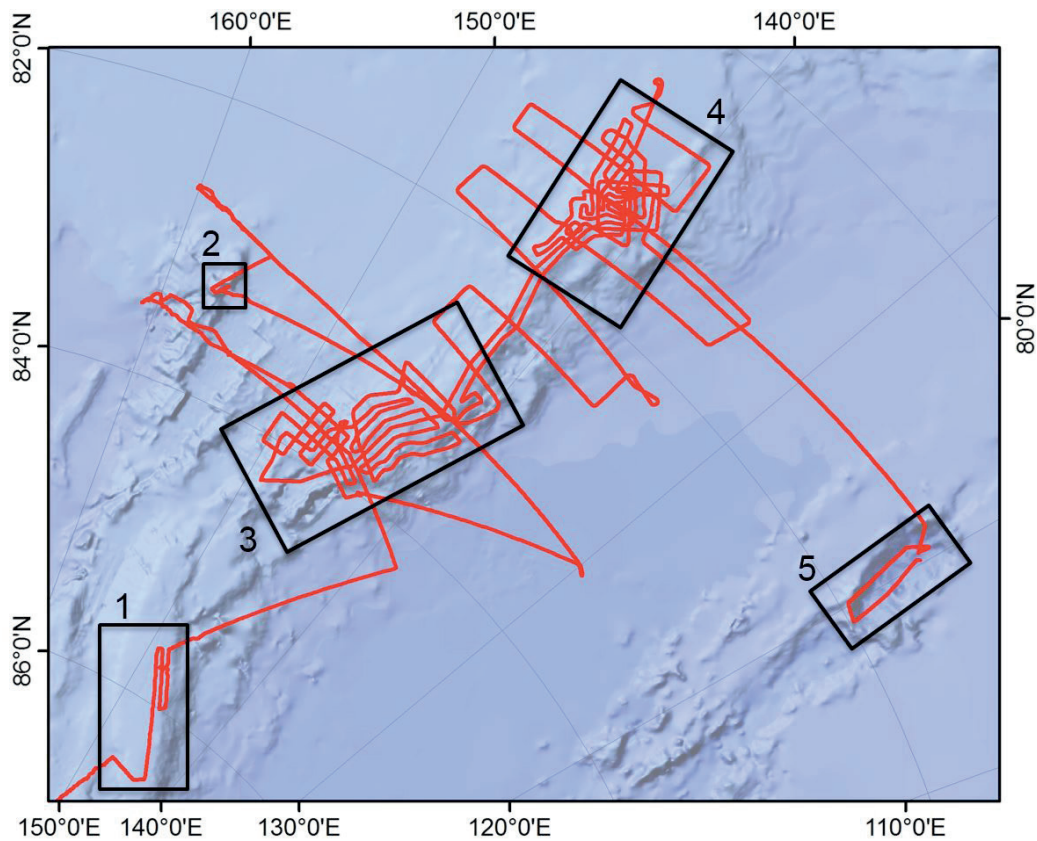


Fig. 8.2: Bathymetric surveys in the main research area

From August 13 in the evening until the early morning of September 2, the ship was operating in sea ice, which lead to a reduced data quality. Nevertheless, the data collected while ice breaking is still useful and can be interpreted. Fig. 8.3 shows two examples of the data quality of Hydrosweep DS3, one collected within sea ice, one without sea ice.

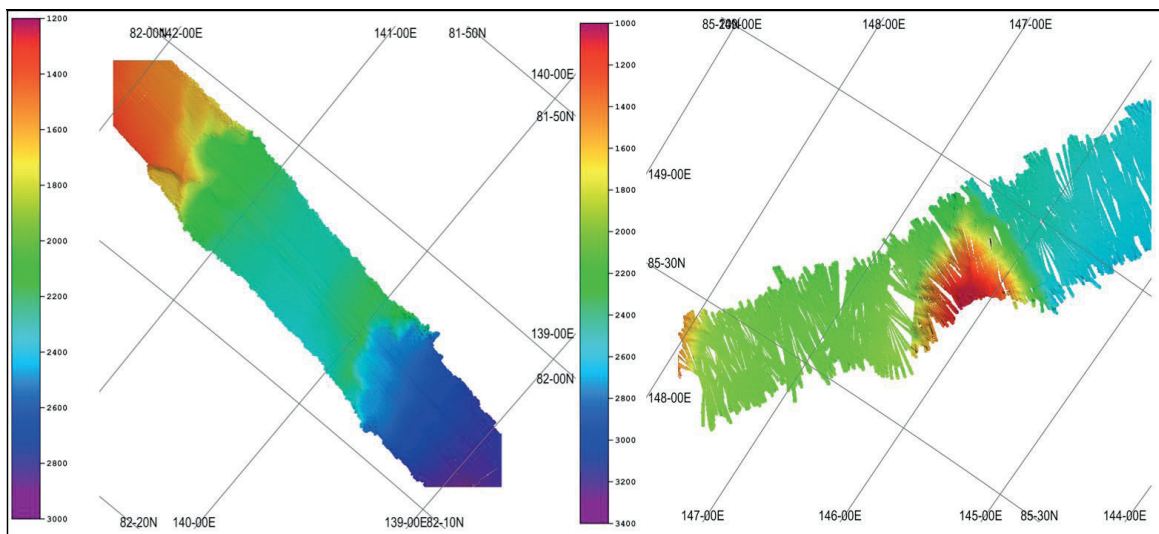


Fig. 8.3: Examples for the data quality of Hydrosweep DS3 (Grids with 50m resolution). Left: without sea ice. Right: with sea ice.

Data management

The acquired multibeam raw data will be stored in the long-term archive PANGAEA Data Publisher for Earth & Environmental Science and will be available on request. The processed data will be archived in the bathymetric archive of the AWI bathymetry group. Furthermore, the data will contribute to global datasets such as IBCAO (International Bathymetric Chart of the Arctic Ocean) and GEBCO (General Bathymetric Chart of the Oceans).

9. MARINE GEOPHYSICS

9.1 Seismic Investigations Across the Lomonosov Ridge

Wilfried Jokat ¹ , Wolfram Geissler ¹ , Bernhard	¹ AWI
Coakley ³ , Graeme Eagles ¹ , Hannes Eisermann ⁵ ,	² ESYS
Catalina Gebhardt ¹ , Tanja Fromm ¹ , Bastian	³ UoAF
Kimme ⁵ , Conrad Kopsch ² , Norbert Lensch ¹ ,	⁴ UoBr
Florian Riefstahl ⁴ , Isabel Sauermilch ⁴	⁵ UoH

Grant-No. AWI-PS87_01

Objectives

Geophysical investigation over the past decade has concentrated on the sedimentary and tectonic history of the Arctic Ocean. Here, especially the Lomonosov and Alpha-Mendeleev ridges play an important role. While the evolution of the continental Lomonosov Ridge as a consequence of the rifting event along the Barents and Siberian shelves and subsequent drift history of the Eurasian Basin, is well understood, the origin and history of the Alpha Mendeleev Ridge remains less clear (e.g., Kristoffersen 1990; Jokat et al. 1995; Jokat 2004, 2005). In general, this feature is interpreted as a large igneous province, which erupted sub-aerially between 100 and 85 Myr. As this period was part of the geomagnetic normal Cretaceous, no marine magnetic seafloor spreading anomalies can be expected to provide definite constraints on the age of any mid-ocean ridge system that may have been active along with the province's formation.

Furthermore, there is a general paucity of basement samples and long sediment cores that might help to understand the evolution and relevance of the two ridges for the geological evolution of the Arctic Ocean. A site near the North Pole on the Lomonosov Ridge was subject of an IODP drilling campaign in 2004, which recovered sedimentary rocks dating back to 56 Ma. However, recovery was incomplete. Thus, a new proposal was submitted to the IODP system for drilling close to the East Siberian/Laptev shelf to achieve a more complete sedimentary record for the Miocene/Oligocene. With this in mind, part of the geophysical programme was to provide additional data to support the drilling proposal.

The geophysical programme originally had two main scientific targets:

- Gather new seismic data on the Alpha and Lomonosov ridges to provide an appropriate database for future scientific deep sea drilling. This database should consist of a small seismic network with cross lines at the proposed site location, with control provided from shallow geological samples. Since the Alpha Ridge could not be reached at all, no new geophysical data were acquired in that remote area. Efforts during the remaining geophysical research were therefore concentrated on gathering new seismic data in several transects across the Lomonosov Ridge. The absence of sea ice over the Lomonosov Ridge south of 85°N meant that this part of the cruise was very successful.
- Gather additional seismic data in an alternative surveying area at the junction of the Mendeleev Ridge with the East Siberian Sea. Here, we planned to densify a seismic

9.1 Seismic investigations across the Lomonosov Ridge

network gathered in the 2008 season. The priority was to collect seismic lines running from the shelf deep into the Makarov Basin and lines crossing the Mendeleev Ridge as far north as possible. Dense sea ice in the region and the time constraints introduced by the difficulties of transit to the Alpha Ridge mean that this plan could not be conducted.

Work at sea

Seismic investigations were not possible before September 2 because of the severe ice conditions encountered during the transit towards Alpha Ridge. Since the first lines (20140250/260/280/281) were located close to the ice rim, only the analog streamers with active lengths of 300 m and 600 m were used (Fig. 9.1.1).

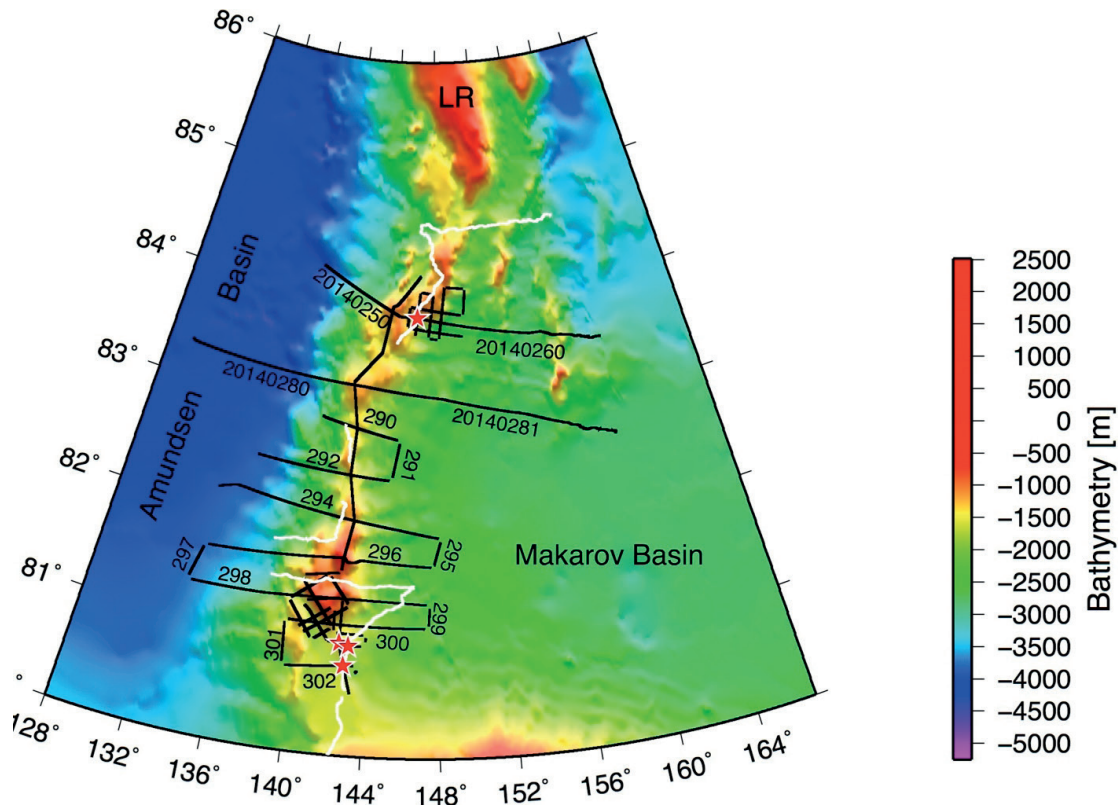


Fig. 9.1.1: Siberian part of the Lomonosov Ridge. The black lines indicate the seismic reflection data gathered during this cruise. The numbers are the profile names. The line numbers are shortened in the very south to the last three digits. White lines: Seismic profiles acquired in 1998; red stars: proposed IODP drill sites, LR-Lomonosov Ridge.

The 3,000 m digital Sercel streamer was operated for the remaining profiles further south where sea ice was not encountered. In summary, we gathered seismic data with the following setups (details in Table 9.1.1):

		Shots	Length
300 m Prakla streamer (48 channels)	4 G-guns	7,134	287 km
600 m Prakla streamer (96 channels)	3 G-guns	10,505	429 km
600 m Prakla streamer (96 channels)	2 GI-guns	10,925	310 km
3,000 m Sercel streamer (240 channels)	3 G-guns	50,426	2,058 km
Total quantity of seismic data (333 h)		78,990	3,084 km

The number of airguns was restricted to three when gathering data on 96 channels or more, since real-time quality control showed that the source energy was sufficient to detect the acoustic basement. The small survey with 2 GI-guns (34 ms delay between injector and generator) was conducted to increase the vertical resolution in the imaged sediment column around the proposed IODP alternate site LORI-5B (Fig. 9.1.2).

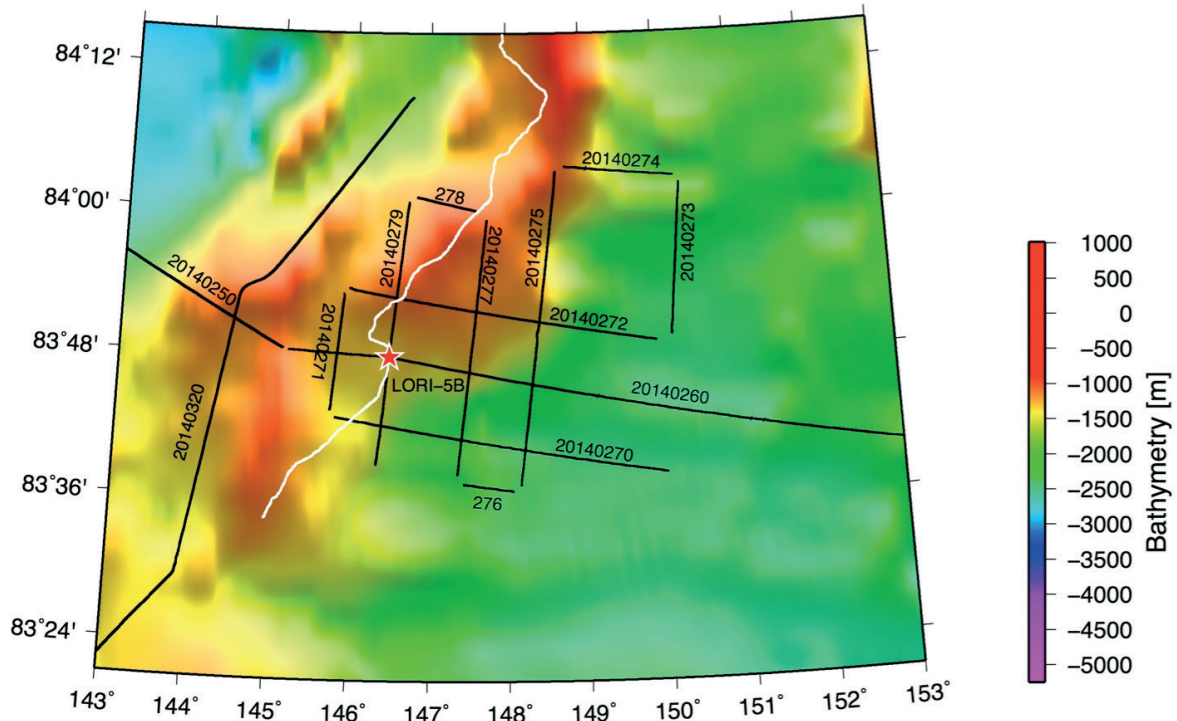


Fig. 9.1.2: Detailed survey in the area of a proposed alternate IODP drilling site. White line: seismic data gathered in 1998; black lines: seismic data gathered during this cruise.

We did not use any tail buoys with the streamer in order to avoid entanglements with drifting sea ice, although in the southern part of our research area no major drifting ice fields were sighted, much to our surprise. A detailed seismic survey was conducted without any problems around the primary drill site LORI-1 and its alternate (Fig. 9.1.3). Here, the tracks are somewhat irregular as a consequence of our search for locations that would allow deeper horizons to be drilled by shallow holes. The resulting ongoing revision of planned tracks within a finite available survey time meant that gathering of data on a more regular grid was not possible. Outcrops of older strata were interpreted from the first crossing of a NW-trending channel, and several lines were designed to cross this feature and map it in more detail. The lines in the north of the channel were gathered to test whether the Miocene sedimentary cover is less thick but complete. Several crossing lines in this area were acquired in order that the primary proposed hole, LORI-1, might be shifted without the need to gather new seismic data in the event that the drilling setup allows only a shallow hole.

9.1 Seismic investigations across the Lomonosov Ridge

Tab. 9.1.1: Profile statistics for the seismic lines gathered during this cruise

Profile	Start of Profile Date	Time	End of Profile Date	Time	Start Lon E	Lat (N)	End Lon E	Lat (N)	Shots	Length [km]	FFID Start	FFID End	Streamer [m]	Lead In [m]	Airgun	Chan dx Chan [m]	Dist. Source - 1st Receiver [m]	Sample rate [ms]	
20140250	02.09.2014	13:04:29	02.09.2014	22:15:59	138.491	84.194	145.108	83.810	2200	89	10070	12269	300	44	6°G	48	6.25	187	2
20140260	02.09.2014	22:20:59	03.09.2014	18:54:57	145.171	83.808	160.578	83.489	4934	198	12289	17222	300	44	6°G	48	6.25	187	2
20140270	04.09.2014	22:08:58	05.09.2014	3:34:58	150.023	83.638	145.788	83.716	1957	53	17685	19641	600	44	2°G1	96	6.25	194	1
20140271	05.09.2014	3:42:58	05.09.2014	5:36:58	145.726	83.724	145.884	83.887	685	18	19689	20373	600	44	2°G1	96	6.25	194	1
20140272	05.09.2014	5:47:58	05.09.2014	10:36:57	145.950	83.895	149.941	83.821	1735	49	20439	22173	600	44	2°G1	96	6.25	194	1
20140273	05.09.2014	10:52:59	05.09.2014	13:17:59	150.132	83.828	150.305	84.041	871	24	22269	23140	600	44	2°G1	96	6.25	194	1
20140274	05.09.2014	13:26:59	05.09.2014	15:09:59	150.239	84.059	148.766	84.064	617	17	23193	23809	600	44	2°G1	96	6.25	194	1
20140275	05.09.2014	15:19:59	05.09.2014	20:17:58	148.658	84.059	148.164	83.622	1785	49	23869	25653	600	44	2°G1	96	6.25	194	1
20140276	05.09.2014	20:27:58	05.09.2014	21:15:58	148.072	83.614	147.428	83.624	289	8	25713	26001	600	44	2°G1	96	6.25	194	1
20140277	05.09.2014	21:27:58	06.09.2014	1:35:59	147.355	83.636	147.741	83.992	1320	40	26073	27392	600	44	2°G1	96	6.25	194	1
20140278	06.09.2014	1:48:59	06.09.2014	1:46:59	147.625	84.003	146.815	84.023	346	10	27470	27815	600	44	2°G1	96	6.25	194	1
20140279	06.09.2014	2:56:59	06.09.2014	7:09:59	146.716	84.017	146.325	83.649	1320	41	27875	29390	600	44	2°G1	96	6.25	194	1
20140280	07.09.2014	5:47:59	08.09.2014	2:47:58	129.653	83.319	144.929	83.156	4939	203	29500	34500	600	44	4°G	96	6.25	187	2
20140281	08.09.2014	6:20:59	09.09.2014	5:36:43	144.555	83.162	160.090	82.649	5566	226	34586	40151	600	44	4°G	96	6.25	187	2
20140290	11.09.2014	10:01:57	11.09.2014	18:06:56	139.967	82.906	145.307	82.743	1941	77	41260	43200	3000	75	4°G	240	12.50	183	1
20140291	11.09.2014	18:29:57	11.09.2014	22:04:57	145.440	82.718	145.024	82.418	861	34	43292	44152	3000	75	4°G	240	12.50	183	1
20140292	11.09.2014	22:31:57	12.09.2014	11:54:57	144.847	82.392	136.038	82.489	2632	107	44260	47472	3000	75	3°G	240	12.50	183	1
20140293	12.09.2014	19:44:57	13.09.2014	18:31:58	133.994	82.147	147.996	81.970	5469	220	47547	53015	3000	75	3°G	240	12.50	183	1
20140294	13.09.2014	18:58:57	13.09.2014	21:24:58	148.130	81.872	147.723	81.602	585	24	53123	53707	3000	75	3°G	240	12.50	183	1
20140296	13.09.2014	21:48:57	14.09.2014	20:24:43	147.545	81.651	134.205	81.640	5424	219	53803	59226	3000	75	3°G	240	12.50	183	1
20140297	14.09.2014	20:49:58	15.09.2014	0:07:58	134.016	81.619	133.541	81.343	793	32	59327	60119	3000	75	3°G	240	12.50	183	1
20140298	15.09.2014	0:43:00	16.09.2014	0:39:59	133.708	81.311	147.308	81.328	5749	230	60259	66007	3000	75	3°G	240	12.50	183	1
20140299	16.09.2014	1:07:58	16.09.2014	02:55:58	147.469	81.302	147.411	81.145	433	18	66119	66551	3000	75	3°G	240	12.50	183	1
20140300	16.09.2014	3:27:58	16.09.2014	17:16:59	147.200	81.121	139.510	81.130	3317	133	66679	69995	3000	75	3°G	240	12.50	183	1
20140301	16.09.2014	17:44:58	16.09.2014	21:49:58	139.341	81.107	139.472	80.759	981	39	70107	71087	3000	75	3°G	240	12.50	183	1
20140302	16.09.2014	22:18:59	17.09.2014	05:56:14	139.632	80.731	143.543	80.742	878	68	71203	72885	3000	75	3°G	240	12.50	183	1
20140303	17.09.2014	05:56:59	17.09.2014	06:14:59	143.550	80.744	143.442	80.721	73	3	73035	73107	3000	75	3°G	240	12.50	183	1
20140304	17.09.2014	06:15:59	17.09.2014	06:14:59	143.231	80.537	142.476	81.338	2301	92	73305	75605	3000	75	3°G	240	12.50	183	1
20140305	17.09.2014	20:56:59	18.09.2014	00:13:59	142.286	81.359	140.441	81.313	789	32	75717	76505	3000	75	3°G	240	12.50	183	1
20140306	18.09.2014	00:55:59	18.09.2014	05:24:59	140.344	81.270	141.800	80.990	1077	40	76673	77749	3000	75	3°G	240	12.50	183	1
20140307	18.09.2014	05:32:59	18.09.2014	08:56:29	141.852	80.984	143.672	80.951	815	33	77781	78595	3000	75	3°G	240	12.50	183	1
20140308	18.09.2014	09:37:59	18.09.2014	10:04:59	143.931	80.991	143.929	81.028	109	4	78632	78740	3000	75	3°G	240	12.50	183	1
20140309	18.09.2014	10:26:59	18.09.2014	13:14:59	143.802	81.049	142.276	81.054	673	27	78828	79500	3000	75	3°G	240	12.50	183	1
20140310	18.09.2014	13:40:59	18.09.2014	15:40:59	142.110	81.077	142.083	81.247	481	19	79604	80084	3000	75	3°G	240	12.50	183	1
20140311	18.09.2014	16:16:59	18.09.2014	19:56:59	141.837	81.266	140.170	81.085	881	35	80228	81108	3000	75	3°G	240	12.50	183	1
20140312	18.09.2014	20:17:00	18.09.2014	20:32:00	140.139	81.060	140.217	81.042	61	2	81188	81248	3000	75	3°G	240	12.50	183	1
20140313	18.09.2014	20:58:14	19.09.2014	01:59:00	140.435	81.037	142.764	81.280	1204	49	81353	82556	3000	75	3°G	240	12.50	183	1
20140314	19.09.2014	02:23:59	19.09.2014	05:18:00	142.813	81.314	141.688	81.530	697	31	82656	83352	3000	75	3°G	240	12.50	183	1
20140315	19.09.2014	05:47:59	19.09.2014	10:03:30	141.447	81.538	139.536	81.320	1023	40	83472	84494	3000	75	3°G	240	12.50	183	1
20140316	19.09.2014	10:26:59	19.09.2014	14:33:59	139.513	81.290	140.843	80.999	989	40	84588	85576	3000	75	3°G	240	12.50	183	1
20140317	19.09.2014	15:00:00	19.09.2014	16:47:00	141.053	80.992	141.892	81.086	429	18	85660	86108	3000	75	3°G	240	12.50	183	1
20140318	19.09.2014	17:12:00	19.09.2014	22:34:00	141.944	81.122	140.095	81.490	1289	52	86208	87496	3000	75	3°G	240	12.50	183	1
20140319	19.09.2014	23:10:00	20.09.2014	02:33:00	140.177	81.531	142.132	81.574	813	33	87640	88452	3000	75	3°G	240	12.50	183	1
20140320	20.09.2014	02:53:00	20.09.2014	3:39:00	142.266	81.596	142.306	81.664	185	8	88532	88716	3000	75	3°G	240	12.50	183	1
20140321	20.09.2014	6:58:00	20.09.2014	11:26:45	142.285	81.664	142.779	82.032	1076	42	89153	90228	3000	75	3°G	240	12.50	183	1
20140322	20.09.2014	11:27:00	20.09.2014	15:59:00	142.779	82.033	142.300	82.417	1089	44	90229	91317	3000	75	3°G	240	12.50	183	1
20140323	20.09.2014	15:59:15	20.09.2014	20:38:45	142.299	82.418	142.467	82.625	1123	46	91318	92440	3000	75	3°G	240	12.50	183	1
20140324	21.09.2014	1:08:30	21.09.2014	1:08:15	142.468	82.826	141.979	83.215	1074	44	92441	93514	3000	75	3°G	240	12.50	183	1
20140325	21.09.2014	1:08:30	21.09.2014	5:05:15	141.978	83.216	143.842	83.487	948	39	93515	94462	3000	75	3°G	240	12.50	183	1
20140326	21.09.2014	5:05:30	21.09.2014	9:45:15	143.844	83.487	144.510	83.876	1120	44	94463	95562	3000	75	3°G	240	12.50	183	1
20140327	21.09.2014	9:45:30	21.09.2014	14:06:15	144.511	83.877	146.769	84.162	1044	42	95563	96626	3000	75	3°G	240	12.50	183	1

Several lines were shot across the originally proposed drill sites. The additional high quality data confirm the selection of these locations. There is no indication of any erosion of the younger Miocene sediments. No major mass wasting events are interpretable in the seismic data that might have disturbed the sequences at LR-01A.

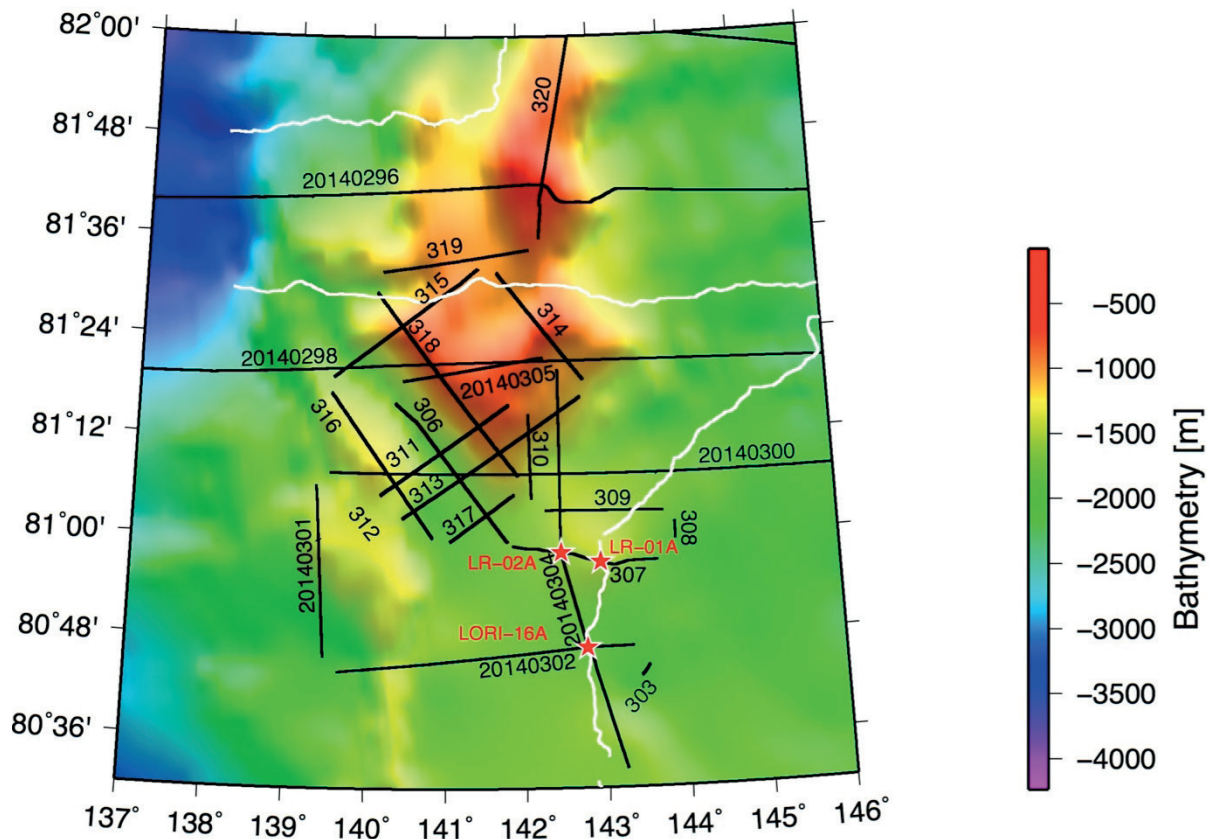


Fig. 9.1.3: Seismic profiles on the southernmost Siberian part of the Lomonosov Ridge, gathered to provide additional information around the primary drilling site LR-01A. White lines: seismic data gathered in 1998; black lines: seismic data gathered during this cruise; red stars: proposed IODP drilling sites.

The seismic data acquisition was supplemented by coincident magnetic, gravity, sediment echosounder (PARASOUND) and swath bathymetric data, which will be described in other chapters of this report. Besides QC, some basic processing was conducted whilst still underway, including demultiplexing and CDP sorting.

Preliminary (expected) results

The seismic network started at the southern rim of the sea ice edge (Figs. 9.1.1, 9.1.2). A long line was acquired to map the Makarov-facing margin of the Lomonosov Ridge (Fig. 9.1.4) and investigate the complex structure of the ridge towards the Makarov Basin. The bathymetry shows that the margin of the ridge widens and becomes more complex. Horst and graben structures are interpreted to belong to the Marvin Spur, which runs mostly parallel to the ridge closer to the Canadian margin. At approximately 85°N, where the Lomonosov Ridge bends slightly to the south, the spur's strike remains unchanged and the shape of the ridge becomes more complex.

9.1 Seismic investigations across the Lomonosov Ridge

A more detailed seismic survey was performed around a proposed IODP drill site in addition to this long transect across the Lomonosov Ridge. The site selection might be questioned on the basis of the swath bathymetric data, which show the products of small mass wasting events in the vicinity of the site. Slides on this small scale were hitherto unknown from Lomonosov Ridge, and could only be discovered by technical advances of the Hydrosweep swath system.

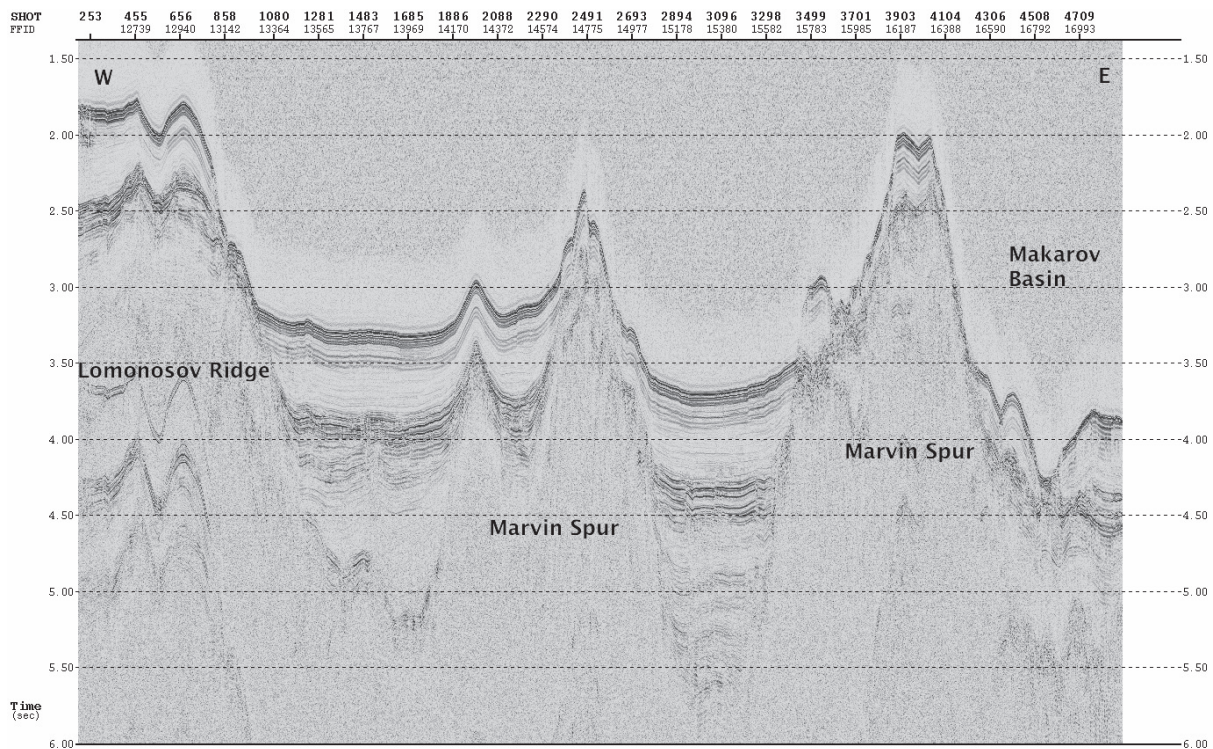


Fig. 9.1.4: Seismic line 20140260 (channel 16) across the Lomonosov Ridge at approximately 85°N.

Moran et al. (2006) confirmed the presence of an erosional unconformity during scientific drilling of the Lomonosov Ridge in 2004. The unconformity is a product of the regional basement level changes that occurred as a consequence of the ridge's breakup from the Siberian Margin (Jokat et al. 1992). However, until now only a few transects across the ridge existed to confirm that the unconformity is present along its entire length. Furthermore, the images of Mesozoic strata below the unconformity were rather poor for unknown reasons. Profile 20140290 crosses the ridge at ~83°N (Fig. 9.1.1), imaging both the erosional unconformity and the older sediments with excellent quality (Fig. 9.1.5). In contrast to the older seismic line 91091, gathered close to the pole, no eroded half-grabens are interpretable. Moreover, the Mesozoic sedimentary rocks are slightly folded/disturbed just below the unconformity. Here, only weak indications for an eroded surface are visible. However, the complex structure of the seismic reflectors forming the unconformity suggests that its deposition close to sea level was highly influenced by waves/currents. The deeper basement signals show indications of intensive faulting (Fig. 9.1.5, 3.5 s TWT). This faulting might be as old as the Mesozoic rifting event in which the Amerasia Basin formed in Mesozoic times, and may have been overprinted during the later unconformity-forming event that initiated the Amundsen Basin. The ridge finally separated from the Siberian shelf during this later event. In this interpretation, all of our data should show evidence for these two rifting events where they image the ridge.

At the current stage of processing, no information is available on seismic velocities. Thus, we currently cannot confirm or disprove the presence of a similar jump in seismic velocities at this unconformity as that found further north (Jokat et al. 1992).

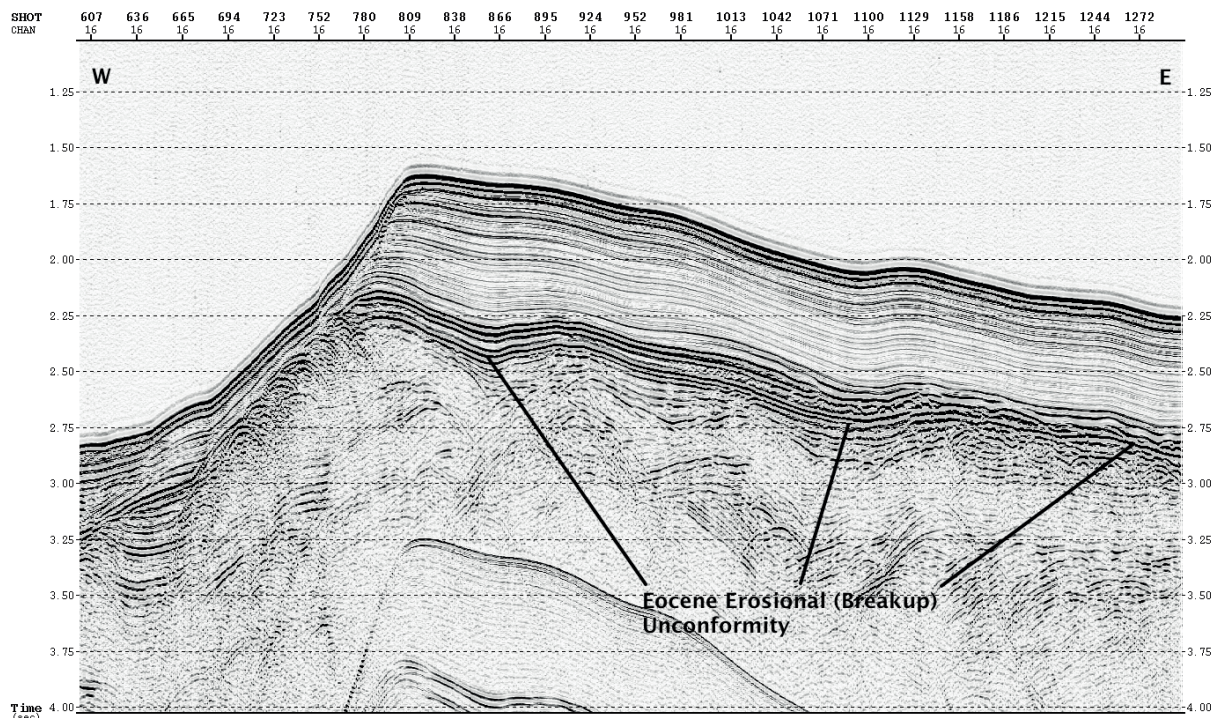


Fig. 9.1.5: Part of seismic line 20140290 (channel 16) across the Lomonosov Ridge at $\sim 83^{\circ}\text{N}$. The position of the erosional breakup unconformity is indicated. Note the strongly faulted deeper basement of the ridge.

The final parts of the seismic survey programme concentrated on gathering additional seismic data around the primary IODP drilling location (Fig. 9.1.3). The seismic data are supplemented by swath bathymetric and PARASOUND sediment echosounder data. The survey had two objectives:

- To confirm by additional seismic data that the site selection is suited to achieve the scientific goals. If this is not possible, to gather additional data suitable for making a decision about where to shift the site to. Thus, sufficient crossing lines had to be acquired to fulfil some minimum requirements of the IODP programme.
- To search for a location where Oligocene sediments can be reached by shallow drill holes. The original IODP proposal requested a 1,300 m deep drill hole to reach these sediments and the layers below.

While the new seismic data confirm the selection of the primary IODP site LR-01A (Fig. 9.1.6), the search for a better location to drill into Oligocene sediments was more difficult. It turned out that the Miocene sediment cover has an almost constant thickness in the research area.

9.1 Seismic investigations across the Lomonosov Ridge

However, at the northern end of a topographic channel the seismic data imaged a 500 m high slide scarp. For details of the scarp itself see Chapter 7 (Bathymetry). At the scarp, the entire sedimentary column is exposed down to the proposed Oligocene, and might be easily accessible by offset drilling. Together with the swath bathymetry, several lines show that the slide scar is present along the channel's entire northern flank. However, the depth of exposure that it affords into the older sediments varies. Based on this information, several gravity cores were taken to access the older material. The coring results are reported elsewhere in this report, and will not be repeated here.

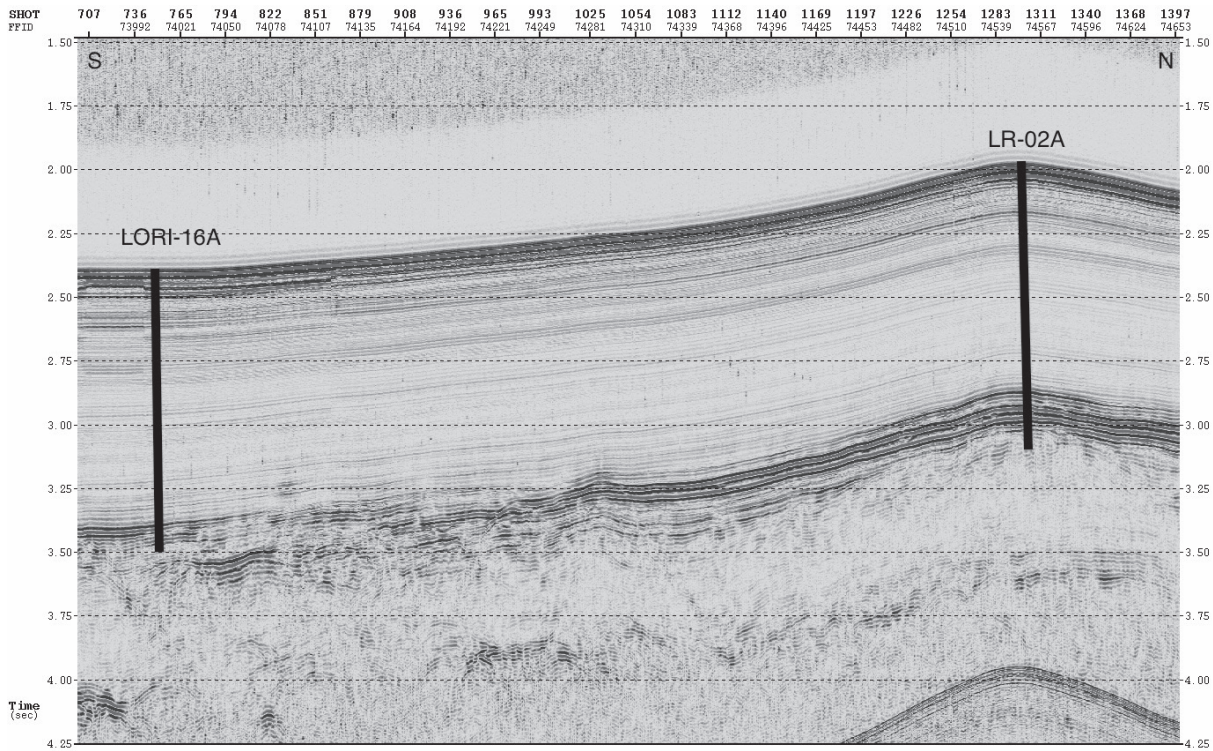


Fig. 9.1.6: Part of seismic line 20140304 (Channel 16) across one of the primary IODP drill sites (LR-02A) and an alternate site (LORI-16A). Note that this is a single channel record section, which will be enhanced by future seismic data processing.

Data management

The seismic data will be processed within the geophysical department and archived at AWI. After publication, the data are available on specific request.

9.2 Magnetic measurements

Graeme Eagles¹, Conrad Kopsch²

¹AWI

²ESYS

Objectives

Magnetic data were collected throughout expedition PS87 using *Polarstern's* vector magnetometer system as part of ongoing reconnaissance. The system is permanently installed midships in the crow's nest. Above decks, it consists of two orthogonal three-component digital fluxgate sensors from MAGSON GmbH in (Fig. 9.2.1). Data from the magnetometers reach an industrial PC in the ship's computer room via a fibre optic connection. From here they are forwarded to the DSHIP system. Data are displayed in real time on the computer's monitor (Fig. 9.2.2).



Fig. 9.2.1: Fluxgate magnetometer system (two sensors) on *Polarstern*

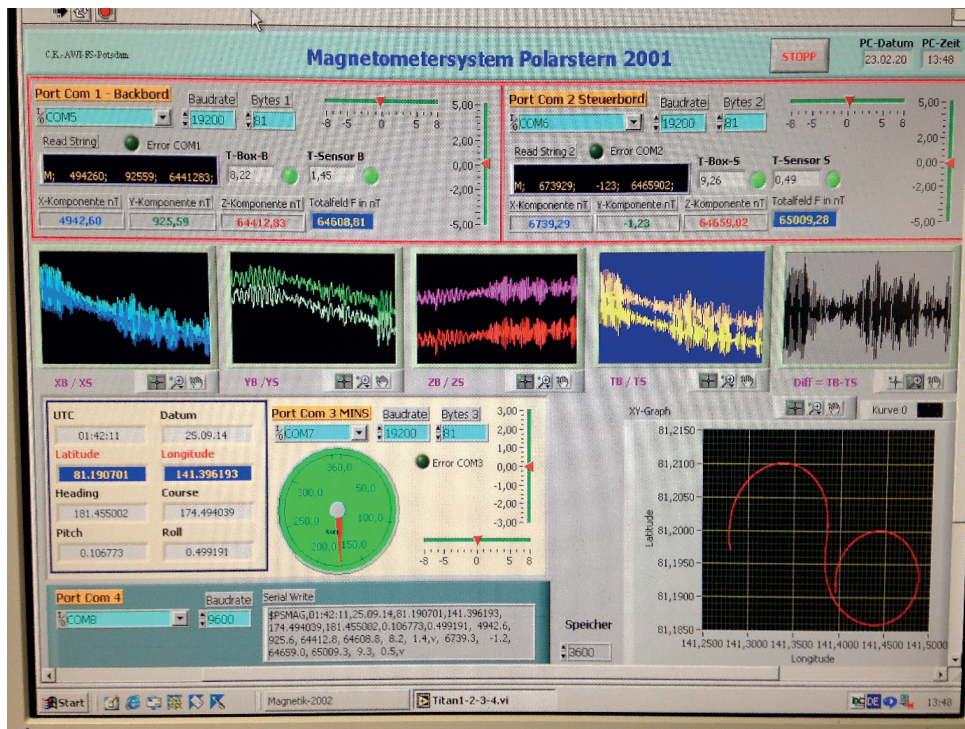


Fig. 9.2.2: Magnetometer data capture and display in the computer room

Key technical specifications of the system are as follows:

3 component ringcore sensors:

noise level	<10 pT/sqrt(Hz)
long term stability	<10 nT/year
dynamic range	+/-100000 nT in all components
resolution	+/-10 pT
temperature measurement	separately for electronics and sensor
housing for electronics and sensor	waterproof aluminium box
power supply	12-20V DC
input current	200mA
signal processor	TMS320F206
tilt meter	dual axis inclinometer SSY0090C

Work at sea

Magnetic data from the two magnetometers were recorded and logged continuously at 1 Hz. No planned magnetic survey track pattern was followed, as the main aims of the leg were seismic surveying and geological sampling. Data were logged everywhere except where permission to do so is normally required, but had not been sought or granted. Fig. 9.2.3 shows the locations of logged data.

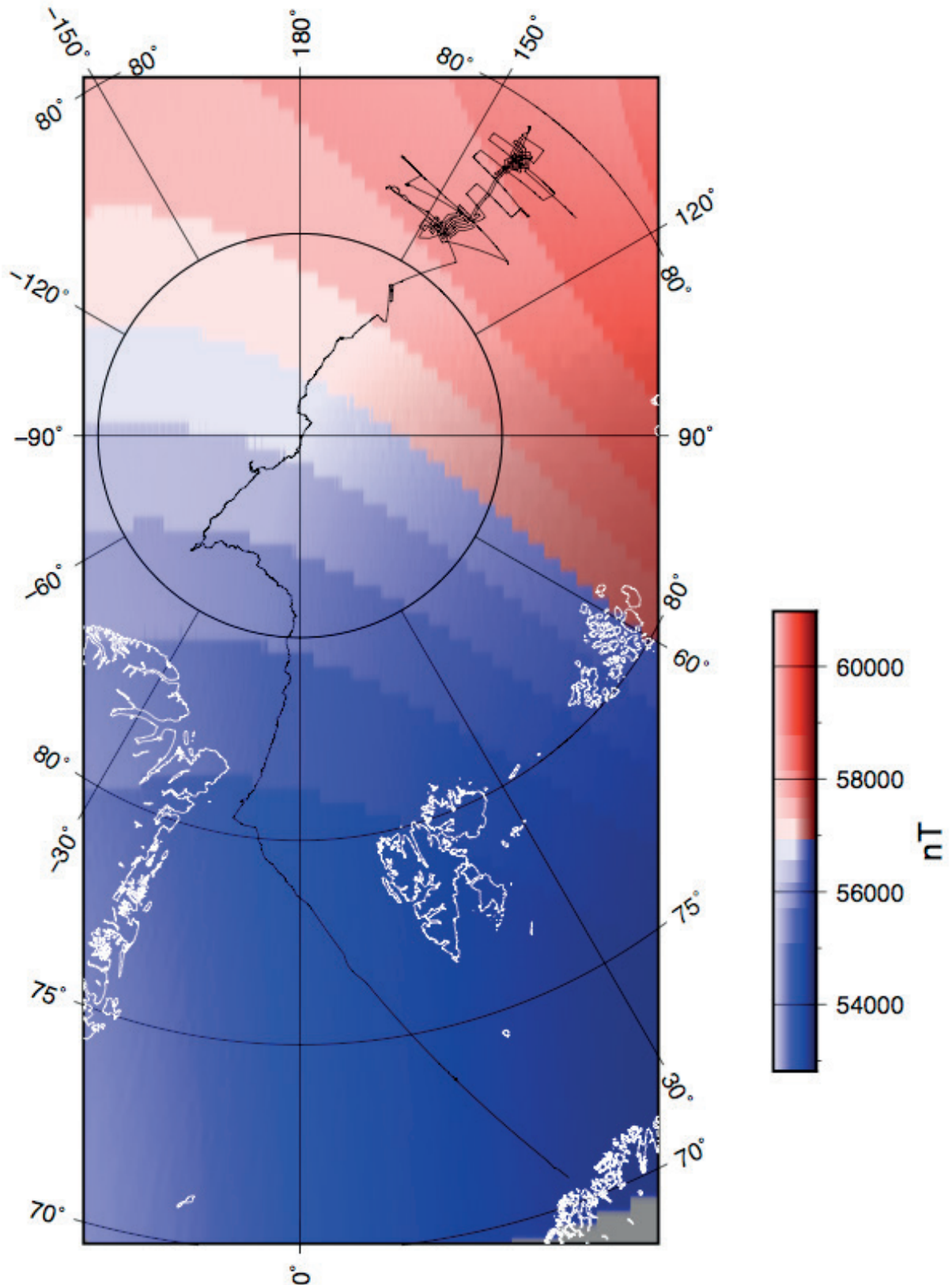


Fig. 9.2.3: Track with locations of fluxgate readings overlain on IGRF model field for August 2014

Preliminary results

Working with the system involves the important step of compensating for transient effects on the data that come from induced and remanent magnetic fields related to the ship’s ferromagnetic bulk and its movement within Earth’s magnetic field. Four calibration loops were completed at several different locations in order to calculate the coefficients that are necessary for this compensation (see table 9.2.1 for locations and Fig. 9.2.4 for an example). It is advisable to complete loops like these at regular intervals in order to be able to compensate for slow changes in the ship’s permanent magnetisation or in the eddy fields brought about by changes in the ship’s cargo placement.

Tab. 9.2.1: Summary of calibration circles for compensating ships magnetic field

Date	Longitude	Latitude
06 Aug. 2014	013°34.955’ E	73°42.043’ N
09 Aug. 2014	009°08.584’ W	80°51.346’ N
07 Sep. 2014	143°02.511’ E	83°59.696’ N
25 Sep. 2014	141°43.000’ E	81°12.630’ N

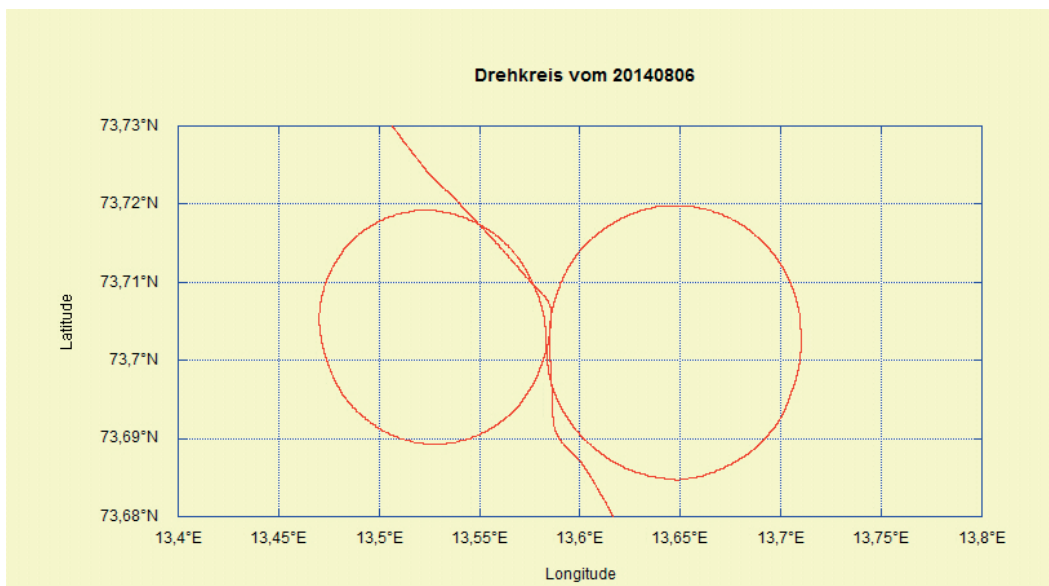


Fig. 9.2.4: Example of a compensation loop ship track (from 6 August 2014)

In the compensation process, the IGRF model is used to determine the inducing field the ship moved in. It is important to realise that the model is a prediction made with reference to irregularly-spaced observatory records, near to which it is most accurate. It is advisable therefore that, where possible, calibration loops are completed close to a magnetic observatory.

The IGRF varies in the range 57,300—59,200 nT in the survey area (Fig. 9.2.3).

Data management

All of the fluxgate data were downloaded from the Dship system at the end of the leg. Calculation of compensated magnetic profile values will be completed in Bremerhaven at a later date. Data acquisition was stopped before entering the Russian EEZ.

9.3 Gravity measurements

Graeme Eagles¹, Bernard Coakley³

¹AWI, ³UoAF

Objectives

Polarstern's permanently-installed Bodenseewerk KSS-32 gravimeter measured relative gravity throughout leg PS87 as part of its ongoing reconnaissance gravity surveying effort. Data were logged at all locations except in Danish and Russian waters where permission to do so was not sought or granted. Two sets of onshore tie measurements were made at the very beginning and very end of the leg, in Tromsø and in Bremerhaven. Together with measurements made earlier in Tromsø, these measurements allow us to convert the shipboard data to absolute gravity values and correct them for instrument drift.

Work at sea

Tie and drift measurements in Tromsø & Bremerhaven

Measurements were made before the leg with the portable LaCoste and Romberg gravity meter G-1031 next to the ship at the port of Tromsø, and at the IGSN absolute gravity points at the Nordnorsk Kunstmuseum (formerly the Police Station) and Tromsø Museum (Figs. 9.3.1—9.3.3). A tie measurement was also completed at the Nordnorsk Kunstmuseum in Tromsø on July 4th, 2014 at the start of the preceding cruise leg. A further tie was completed with measurements next to the ship and at AWI's building D after *Polarstern*'s return to Bremerhaven, using the portable LaCoste and Romberg gravity meter G-877. No measurement was possible at the quayside location in Bremerhaven before this season's activities, as *Polarstern* had been in dry dock and the ship's gravity meter not logging for long periods.

The KSS-32 instrument logged continuously during the periods of tie measurements in order to use the G-1031 and G-877 measurements for estimating dockside tie values.

The measurements were used to determine an acceleration of $g=982555.59$ mGal next to *Polarstern* in the harbour in Tromsø, and of $g=981356.76$ mGal next to *Polarstern* in Bremerhaven. Once corrected for the differences in height between the quayside and the ship's KSS-32 gravimeter, the absolute accelerations at the ship's gravimeter was determined to be 982556.46 mGal in Tromsø and 981347.22 mGal in Bremerhaven. The corresponding ship's gravimeter readings during the measurement were 2337.51 scu (scale units) in Tromsø and 1132.90 scu in Bremerhaven.

9.3 Gravity measurements



Fig. 9.3.1: Gravity tie point outside Nordnorsk Kunstmuseum in central Tromsø. (Photo: W. Geissler).



Fig. 9.3.2: Top left: Bolt Q measurement point at Tromsø Museum. Top Right: Bolt R measurement point at Tromsø Museum. Bottom Right: Office with ante-room where Bolt R is located. Bottom left: Outside view of the Tromsø Museum. (Photos: W. Geissler)

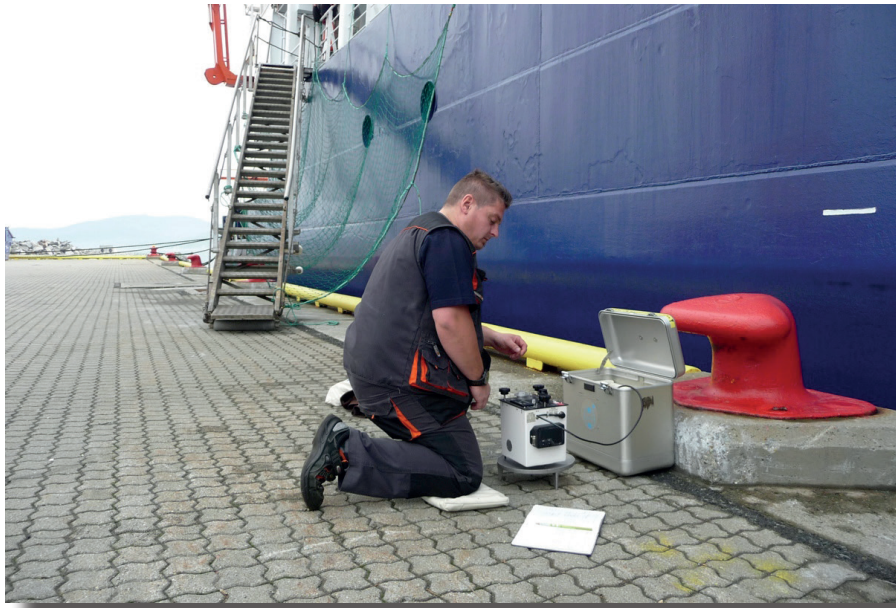


Fig. 9.3.3: Tie point at Kai 25, Breivika, next to Polarstern on August 5 2014 (Photo: W. Geissler)

Details of the tie measurements made at stations with known absolute g values are given below:

Measurement 1 (Table 9.3.1).

Instrument : LaCoste & Romberg gravimeter, G-1031 with feedback
 Location: Tromsø, Nordnorsk Kunstmuseum, BGI008019 (former Police Station)
 Date: 5. August 2014
 Conditions: Calm, no wind, no precipitation
 Abs. gravity: 982552.47 mGal
 Present : W. Geissler, W. Jokat

Tab. 9.3.1: Gravity measurements at Nordnorsk Kunstmuseum. The average value from all measurements is 6216.94 mGal. The scaling factor for transfer from scale units (scu) to mGal, was 1.02123.

UTC	Counter [scu]	Type	Counter [mGal]	feedback [mGal]	Total. gravity [mGal]
07:09	6088	Feedback	6222.01	-5.028	6216.98
07:11	6089	Feedback	6223.03	-6.050	6216.98
07:13	6090	Feedback	6224.05	-7.082	6216.97
07:14	6087	Feedback	6220.99	-4.088	6216.90
07:15	6086	Feedback	6219.97	-3.070	6216.90
??	6084.59	Manual	6218.52	-1.630	6216.89

Five measurements were done with the feedback unit and on the plate. One measurement was completed manually. The temperature inside the instrument was a constant 53.5°C.

9.3 Gravity measurements

Measurement 2 (Table 9.3.2)

Instrument : LaCoste & Romberg gravimeter, G-1031 with feedback
 Location : Tromsø, Tromsø Museum Bolt Q (Tromsø Q)
 Date : 5. August 2014
 Conditions : Indoors, calm
 Abs. g : 982551.448 mGal
 Present : W. Geissler, W. Jokat

Five measurements were done with the feedback unit and on the plate. One measurement was completed manually. The temperature inside the instrument was a constant 53.5°C.

Tab. 9.3.2: Gravity measurements at Tromsø Museum Bolt Q. The average value from all measurements is 6215.82 mGal. The scaling factor for transfer from scale units (scu) to mGal, was 1.02123.

UTC	Counter [scu]	Type	Counter [mGal]	feedback [mGal]	Total. gravity [mGal]
08:00	6083.505	Manual	6217.42	-1.621	6215.80
08:01	6085	Feedback	6218.94	-3.060	6215.88
08:03	6086	Feedback	6219.97	-4.081	6215.88
08:04	6087	Feedback	6220.99	-5.142	6215.85
08:05	6084	Feedback	6217.92	-2.155	6215.77
08:06	6083	Feedback	6216.90	-1.134	6215.77

Measurement 3 (Table 9.3.3)

Instrument : LaCoste & Romberg gravimeter, G-1031 with feedback
 Location : Tromsø, Tromsø Museum Bolt R (Tromsø R)
 Date : 5. August 2014
 Conditions : Indoors, instrument read unstable accelerations at start
 Abs. gravity : 982552.140 mGal
 Present : W. Geissler, W. Jokat

Three measurements were done with the feedback unit and on the plate. One measurement was completed manually. The temperature inside the instrument was a constant 53.5°C.

Tab. 9.4.3: Gravity measurements at Tromsø Museum Bolt R. The average value from all measurements is 6216.56 mGal. The scaling factor for transfer from scale units (scu) to mGal, was 1.02123.

UTC	Counter [scu]	Type	Counter [mGal]	feedback [mGal]	Total. gravity [mGal]
08:23	6084.202	Manual	6218.13	-1.614	6216.52
08:26	6085	Feedback	6218.94	-2.342	6216.60
08:27	6086	Feedback	6219.97	-3.366	6216.60
08:28	6082	Feedback	6215.88	0.633	6216.51

Measurement 4 (Table 9.3.4)

Instrument : LaCoste & Romberg gravimeter, G-877 with feedback
 Location : Building D, Alfred Wegener Institute, Bremerhaven
 Date : 8. October 2014
 Conditions : Indoors, instrument read unstable accelerations
 Abs. gravity : 981356.72 mGal
 Present : H. Kirk

Six measurements were done manually with the instrument on the plate. No measurement was successfully completed with feedback. The temperature inside the instrument was a constant 49.8°C.

Tab. 9.4.4: Gravity measurements at AWI Building D in Bremerhaven. The average value from all measurements is 5018.85 mGal. The scaling factor for transfer from scale units (scu) to mGal, was 1.02462.

UTC	Counter [scu]	Type	Counter [mGal]	feedback [mGal]	Total. gravity [mGal]
14:03	4903.71	Manual	5018.85		5018.85
14:05	4903.71	Manual	5018.85		5018.85
14:07	4903.71	Manual	5018.85		5018.85
14:08	4903.71	Manual	5018.85		5018.85
14:10	4903.71	Manual	5018.85		5018.85
14:11	4903.71	Manual	5018.85		5018.85

As described below, harbour values were determined using the different tie possibilities that the various absolute stations offer.

Measurement 5.1: Before visiting the tie stations in Tromsø (Table 9.3.5.1)

Instrument : LaCoste & Romberg gravimeter, Model G-1031 with feedback
 Location : 69.67962°N, 18.99687°E, Kai 25 Breivika, next to *Polarstern*
 Date : 5. August 2014
 Conditions : calm, no wind, no precipitation
 Present : W. Geissler, W. Jokat, O. Hüttebraucker

Four measurements were done with the feedback unit and on the plate. Four measurements were completed manually. The temperature inside the instrument was a constant 53.5°C. The KSS-32 gravimeter inside the ship was determined to be situated 2.01 m below the LaCoste & Romberg instrument on the quayside.

9.3 Gravity measurements

Tab. 9.3.5.1: Gravity measurements at Kai 25, Breivika, next to *Polarstern*. The average value from all measurements is 6220.10 mGal. The scaling factor for transfer from scale units (scu) to mGal, was 1.02123.

UTC	Counter [scu]	Type	Counter [mGal]	feedback [mGal]	Total. gravity [mGal]
06:18	6084	Feedback	6217.92	2.128	6220.05
06:20	6085	Feedback	6218.94	1.201	6220.15
06:23	6086	Feedback	6219.97	0.170	6220.14
06:25	6087	Feedback	6220.99	-0.844	6220.14
06:29	6087.78	Manual	6221.78	-1.730	6220.05
06:35	6087.73	Manual	6221.73		6221.73
06:36	6087.73	Manual	6221.73		6221.73
06:39	6087.71	Manual	6221.71	-1.664	6220.05

Measurement 5.2: After visiting the tie stations in Tromsø (Table 9.3.5)

Instrument : LaCoste & Romberg gravimeter, Model G-1031 with feedback
 Location : 69.67962°N, 18.99687°E, Kai 25 Breivika, next to *Polarstern*
 Date : 5. August 2014
 Conditions : calm, no wind, no precipitation
 Present : W. Geissler, W. Jokat, O. Hüttebraucker

Four measurements were done with the feedback unit and on the plate. Four measurements were completed manually. The temperature inside the instrument was a constant 53.5°C. The KSS-32 gravimeter inside the ship was determined to be situated 2.36 m below the LaCoste instrument on the quayside.

Tab. 9.3.5.2: Gravity measurements at Kai 25, Breivika, next to *Polarstern*. The average value from all measurements is 6220.10 mGal. The scaling factor for transfer from scale units (scu) to mGal, was 1.02123.

UTC	Counter [scu]	Type	Counter [mGal]	feedback [mGal]	Total. gravity [mGal]
06:18	6084	Feedback	6217.92	2.128	6220.05
06:20	6085	Feedback	6218.94	1.201	6220.15
06:23	6086	Feedback	6219.97	0.170	6220.14
06:25	6087	Feedback	6220.99	-0.844	6220.14
06:29	6087.78	Manual	6221.78	-1.730	6220.05
06:35	6087.73	Manual	6221.73		6221.73
06:36	6087.73	Manual	6221.73		6221.73
06:39	6087.71	Manual	6221.71	-1.664	6220.05

Measurement 6: After visiting the tie station at Building D in Bremerhaven (Table 9.3.6)

Instrument : LaCoste & Romberg gravimeter, Model G-877 with feedback
 Location : Lloydwerft Bremerhaven, Quayside of *Polarstern*
 Date : 8. October 2014
 Conditions : calm weather, busy harbour activities
 Present : H. Kirk

Eight measurements were completed manually and seven with feedback, all with the instrument on the plate. The temperature inside the instrument was a constant 49.7°C. The KSS-32 gravimeter inside the ship was determined to be situated 1.50 m below the LaCoste instrument on the quayside. Continuous display whilst operating in feedback mode showed the measurements to be unstable by <0.1 mGal during measurement period.

Tab. 9.3.6: Gravity measurements at the Lloydwerft in Bremerhaven, next to *Polarstern*. The average value from manual measurements is 5018.90 mGal and the average from feedback measurements is 5018.13 mGal. The scaling factor for transfer from scale units (scu) to mGal, was 1.02462.

UTC	Counter [scu]	Type	Counter [mGal]	feedback [mGal]	Total gravity [mGal]
06:18	4903.77	Manual	5018.91		5018.91
06:20	4903.74	Manual	5018.88		5018.88
06:23	4903.76	Manual	5018.90		5018.90
06:25	4903.76	Manual	5018.90		5018.90
06:29	4903.73	Manual	5018.87		5018.87
06:35	4903.77	Manual	5018.91		5018.91
06:36	4903.76	Manual	5018.90		5018.90
06:39	4903.76	Manual	5018.90		5018.90
06:39	4906	Feedback	5021.20	-3.050	5018.15
06:39	4905	Feedback	5020.17	-2.035	5018.14
06:39	4904	Feedback	5019.15	-1.030	5018.12
06:39	4903	Feedback	5018.12	0.000	5018.12
06:39	4902	Feedback	5017.10	1.020	5018.12
06:39	4901	Feedback	5016.07	2.050	5018.12
06:39	4900	Feedback	5015.05	3.070	5018.12

Using these tie points, and correcting for the height differences between the quayside and the KSS-32 gravimeter inside the ship, absolute gravity at the quay in Tromsø was determined as $g=982556.30$ mGal before the tie measurements and $g=982556.40$ mGal afterwards. The corresponding ship's gravimeter measurement readings were 2337.82 and 2337.94 CU. Quayside absolute gravity in Bremerhaven at the end of the leg was determined as 981357.22 mGal for ship's gravimeter readings of 1132.9 scu.

Preliminary results

During this leg, we have tailored and tested a set of shell scripts for reduction and plotting of gravity data that were originally written by Bernard Coakley for Bell gravimeters operating on USCGS *Healy*, and that he has subsequently adapted for gravimeter data collected on other vessels with other gravimeter types. Starting with output files taken daily from DShip, the raw data were reformatted and processed to estimate the gravity anomalies. Reduction was accomplished with the UNIX/GMT script *Air-Sea-gravReduction*. Reduction consists of combining the gravimeter output with synchronized ship's navigation (Trimble1) to eliminate the effects of Earth's symmetric mass distribution (latitude correction) and to correct for ship's motion across the surface of a rotating earth (Eötvös correction).

The reduction and plotting process for a typical day's surveying takes a few minutes. No significant problems with the data were recognized during the cruise. Fig. 9.3.4 shows an example of a daily plot, comparing reduced data from the KSS-32 to bathymetry, a key influence on measured gravitational accelerations at sea.

The KSS-32 accepts GPS input, which is utilized to control the platform and maintain a level orientation through turns. During long, broad turns (e.g. at hour 17 in Fig. 9.3.4), such as were done while towing the 3 km streamer, the GPS adjustments maintain the platform level, resulting in smooth gravity anomaly data. During sharper turns, the inbuilt compensation does not work as effectively, leaving a small residual anomaly that is unrelated to any geological source. *Air-Sea-gravReduction* automatically and successfully edits most of these undesired anomalies out of the data set.

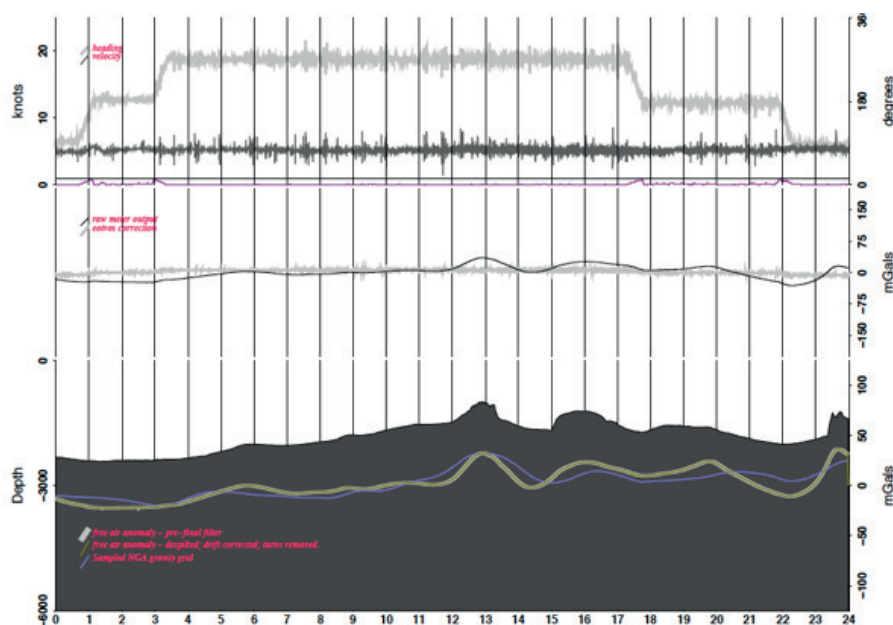


Fig. 9.3.4: Gravity data from Julian day 259. Broad, gentle turns, seen as slopes in the heading, do not seem to affect the gravity anomaly at all, indicating successful internal compensation in this instance.

Arctic Gravity Project data (Kenyon et al. 2008) are shown for comparison. The similar levels and positions of anomalies indicate that the gravity tie in Tromsø was good and that meter drift during the cruise was minimal.

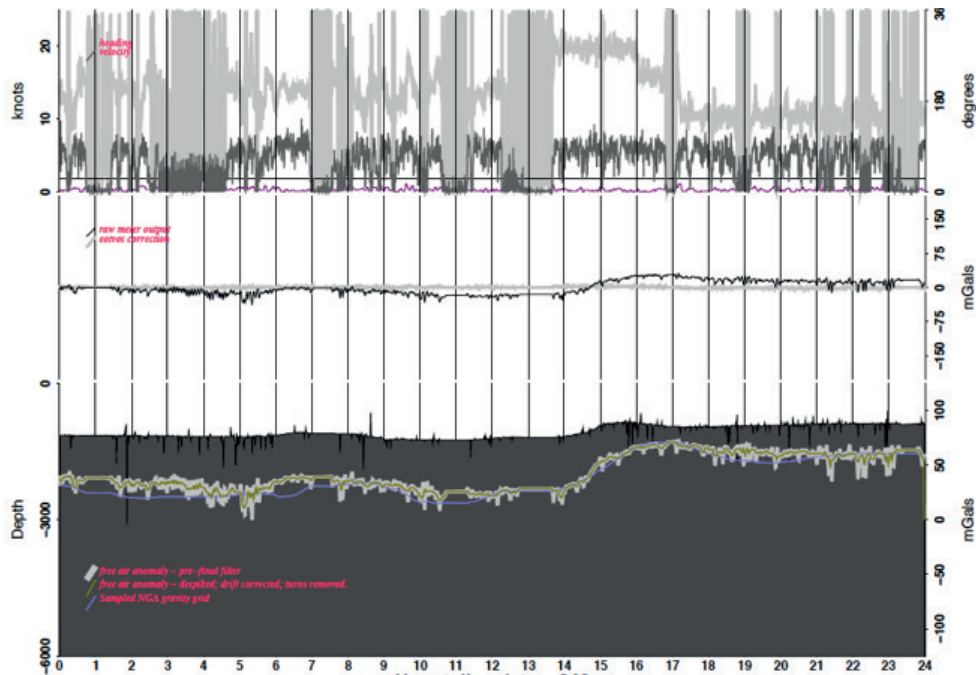


Fig. 9.3.5: Data collected during backing and ramming. Note short, low amplitude, negative excursions of the gravity caused by the velocity spikes and rapid heading changes encountered whilst breaking ice. The final filtering was partly successful in eliminating these features as indicated by the reduced amplitude of the excursions in the final filtered data, compared to the unfiltered data.

The results in Fig. 9.3.4 were produced with data collected whilst operating in open water. Previous experience has shown that good data can also be collected while making steady way during icebreaking. The heavy ice encountered during much of the early part of PS87 however required extensive, regular backing and ramming. These manoeuvres contaminate the estimated gravity anomaly signal at short wavelengths (Fig. 9.3.5) and complicate utilization of these data either for gravity modelling or for compilation to create a gridded data set. These data follow the level and form of the sampled AGP grid, suggesting that with some further processing, it should be possible to eliminate their flaws.

While underway, some experimentation was done to attempt to eliminate the short wavelength gravity lows associated with backing and ramming. This was done by using both shorter and longer filters and attempting to eliminate bad data based on the horizontal accelerations output from the KSS-32 and changes in the Eötvös correction. None of these methods was fully satisfactory. The wavelength of these distortions is much shorter than the underlying gravity anomalies, suggesting that frequency domain filtering of the processed data might be the best approach for eliminating this noise.

Data management

With the end of PS87 scientific activities on September 28, *Polarstern* passed into the Russian EEZ and the gravimeter measurements were stopped. By this point, all of the leg's gravity data had been reduced, plotted and saved in a format ready for further processing, in the case of significant instrument drift, in Bremerhaven.

9.4 Marine mammal observation

Wilfried Jokat¹, Wolfram Geissler¹, Bernhard Coakley³, Graeme Eagles¹, Hannes Eisermann⁵, Catalina Gebhardt¹, Tanja Fromm¹, Bastian Kimmel⁵, Oria Jamar⁶, Conrad Kopsch², Norbert Lensch¹, Dominik Nachtsheim⁶, Florian Riefstahl⁴, Isabel Sauermilch⁴

¹AWI, ²ESYS, ³UoAF, ⁴UoBr, ⁵UoH, ⁶PoIE

Objectives

Specific marine mammal observations were conducted from 4 September 2014 to 21 September 2014 during the seismic measurements across the Lomonosov Ridge. The aims of the observation were

- to get more data about the distribution of whale species in the Arctic Ocean
- to minimize the effect from underwater noise caused by seismic sources during the acquisition of seismic reflection data to marine mammals.

Work at sea

Observations were undertaken from the bridge of *Polarstern*. Between 4 and 12 September 2014, we could perform our observations continuously for 24 h per day, since we had polar days. From 13 September onwards, observations were carried out during daylight only. On the 16 m high bridge, a good and clear view of the sea surface around the ship is ensured. The two observers in charge used naked eye and binoculars (Fujinon 7-50 FTM/MT Field of view 7-300) to scan the sea surface. The reticle scale of the binoculars was used for distance estimation of detected marine mammals.

The marine mammal observer was supported by member of the PoIE, who performed such investigations for the entire cruise. All observers were scientists trained onboard by other team members, who already are experienced in marine mammal observation and certified to JNCC standards.

Observation during airgun operation

Several actions were undertaken in order to minimize the risk of disturbing marine mammals by seismic data acquisition.

- A pre-shooting search was carried out by the observers on the bridge prior to any seismic action (Table 9.4.1). Ramp-up of the airguns could only start after 60 min without sightings of marine mammals.
- For the ramp-up, we started with one single gun, and added one additional gun every 3 min until all guns were shooting and full acoustic power for the planned seismic profile was reached.
- All seismic actions were to stop immediately in case of sighting of a marine mammal within a zone of 500 m distance to the seismic source (mitigation zone) during ramp-up or airgun operation. After a 30 min delay from the sighting, shooting could be restarted with a ramp-up.

During the pre-shooting search, ramp up and acquisition of the seismic reflection profiles, no marine mammals were sighted within the mitigation zone or further away by the observers (see chapter “Sea birds and marine mammals”). Nevertheless, during days where no seismic data were acquired, a number of sightings were reported by the bird observers. For a list of all sightings of marine mammals, refer to chapter “Sea birds and marine mammals” and table 6.1 herein.

Tab. 9.4.1: Marine mammal observation before and during airgun operation

Date	Time [UTC]	Operation	Sightings during operation?
4.9.2014	19:34	Start of pre-shooting search	no
4.9.2014	21:01	Start of ramp-up	no
4.9.2014	21:04	Full power; begin of profile	no
6.9.2014	07:15	End of profile	
7.9.2014	03:01	Start of pre-shooting search	no
7.9.2014	05:35	Start of ramp-up	no
7.9.2014	05:44	Full power; begin of profile	no
8.9.2014	02:58	End of profile	
8.9.2014	02:58	Start of pre-shooting search	no
8.9.2014	06:07	Start of ramp-up	no
8.9.2014	06:16	Full power; begin of profile	no
9.9.2014	05:40	End of profile	
11.9.2014	08:00	Start of pre-shooting search	no
11.9.2014	08:58	Start of ramp-up	no
11.9.2014	09:07	Full power; begin of profile	no
12.9.2014	11:55	End of profile	
12.9.2014	17:25	Start of pre-shooting search	no
12.9.2014	19:28	Start of ramp-up	no
12.9.2014	19:34	Full power; begin of profile	no
17.9.2014	06:30	End of profile	
17.9.2014	08:33	Start of pre-shooting search	no
17.9.2014	10:20	Start of ramp-up	no
17.9.2014	10:26	Full power; begin of profile	no
20.9.2014	03:59	End of profile	
20.9.2014	03:59	Start of pre-shooting search	no
20.9.2014	05:26	Start of ramp-up	no
20.9.2014	05:35	Full power; begin of profile	no
21.9.2014	11.30	End of observation (night)	
21.9.2014	14.07	End of profile	

References

- Jokat W, Uenzelmann-Neben G, Kristoffersen Y, Rasmussen T (1992) ARCTIC '91: Lomonosov Ridge - a double-sided continental margin, *Geology*, 20, 887-890
- Jokat W, Weigelt E, Kristoffersen Y, Rasmussen TM, (1995) New insights into the evolution of Lomonosov Ridge and the Eurasia Basin. *Geophys. J. Int.* 122, 378-392.
- Jokat W (2004) The tectonic evolution of the Arctic Ocean: Overview and perspectives, in: Stein, R., Macdonald, R.W. (Eds.), *The Organic Carbon Cycle in the Arctic Ocean*, Springer Verlag, Heidelberg, pp. 21-24.
- Jokat W (2005) The sedimentary structure of the Lomonosov Ridge between 88°N and 80°N: Consequences for tectonic and glacial processes, *Geophysical Journal International*, 163, 698-726. doi:10.1111/j.1365-246X.2005.02786.x
- Kenyon S, Forsberg R, Coakley B, (2008) New Gravity Field for the Arctic, *Eos Trans. AGU*, 89(32), 289, doi: 10.1029/2008EO320002.
- Kristoffersen Y (1990) Eurasian Basin, in: Grantz, A., Johnson, L., Sweeny, J.F. (Eds.), *The Arctic Ocean Region, Geology of North America Vol. L.*, Geol. Soc. Am., Boulder, Colorado, pp. 365-378.
- Moran K, Backman J, Brinkhuis H, Clemens SC, Cronin T, Dickens GR, Eynaud F, Gattacceca J, Jakobsson M, Jordan RW, Kaminski M, King J, Koc N, Krylov A, Martinez N, Matthiessen J, McInroy D, Moore TC, Onodera J, O'Regan A M, Pälike H, Rea B, Rio D, Sakamoto T, Smith DC, Stein R, St. John K, Suto I, Suzuki N, Takahashi K, Watanabe M, Yamamoto M, Frank M, Jokat W, Kristoffersen Y (2006). The Cenozoic palaeo-environment of the Arctic Ocean, *Nature*, 441, 601-605, doi:10.1038/nature04800

10. MARINE GEOLOGY

Rüdiger Stein¹, Jens Matthiessen¹, Frank Niessen¹, Evgenia Bazhenova², Laura Castro de la Guardia³, Anne de Vernal⁴, Matthias Forwick⁵, Tanja Hörner¹, Haiyan Jin⁶, Stefanie Kaboth⁷, Mike Kaminski⁸, Henriette Kolling¹, Anne Kremer¹, Anna Kudryavtseva², Norbert Lensch¹, Seung-il Nam⁹, Anna Katharina Prim¹⁰, Albrecht Roloff¹, Michael Schreck⁹, Robert Spielhagen¹¹, Jessica Volz¹², Mike Zwick¹²

AWI¹
UoStP²
UoAE³
GEOTOP⁴
UoT⁵
SIOA⁶
UoU⁷
KFU⁸
KOPRI⁹
UoM¹⁰
GEOMAR¹¹
UoBr¹²

Grant-No. AWI-PS87_01

10.1 Overview of the PS87 Marine Geology Programme

Rüdiger Stein¹, Jens Matthiessen¹, Frank Niessen¹, Evgenia Bazhenova², Laura Castro de la Guardia³, Anne de Vernal⁴, Matthias Forwick⁵, Tanja Hörner¹, Haiyan Jin⁶, Stefanie Kaboth⁷, Mike Kaminski⁸, Henriette Kolling¹, Anne Kremer¹, Anna Kudryavtseva², Norbert Lensch¹, Seung-il Nam⁹, Anna Katharina Prim¹⁰, Albrecht Roloff¹, Michael Schreck⁹, Robert Spielhagen¹¹, Jessica Volz¹², Mike Zwick¹²

AWI¹
UoStP²
UoAE³
GEOTOP⁴
UoT⁵
SIOA⁶
UoU⁷
KFU⁸
KOPRI⁹
UoM¹⁰
GEOMAR¹¹
UoBr¹²

Objectives

Despite the importance of the Arctic Ocean in the global climate/earth system, this region is one of the last major physiographic provinces on Earth where the short- and long-term geological history is still poorly known. This lack in knowledge is mainly due to the major technological/logistical problems in operating within the permanently ice-covered Arctic region which makes it difficult to retrieve long and undisturbed sediment cores. Prior to 1990, the available samples and geological data from the central Arctic Basins were derived mainly from drifting ice islands such as T-3 (Clark et al., 1980) and CESAR (Jackson et al. 1985) (Fig. 10.1.1). During the last ~20 years, several international expeditions, have greatly advanced our knowledge on central Arctic Ocean paleoenvironment and its variability through Quaternary times (for review see Stein 2008). Prior to 2004, however, in the central Arctic Ocean piston and gravity coring was mainly restricted to obtaining near-surface sediments, i.e., only the upper 15 m could be sampled. Thus, all studies were restricted to the late Pliocene/Quaternary time interval, with a few exceptions (Fig. 10.1.1). These include the four short cores obtained by gravity coring from drifting ice floes over the Alpha Ridge, where older pre-Neogene organic-carbon-

10.1 Overview of the PS87 Marine Geology Programme

rich muds and laminated biosiliceous oozes were sampled. These were the only samples recording the late Cretaceous/early Cenozoic climate history and depositional environment. In general, these data suggest a warmer (ice-free) Arctic Ocean with strong seasonality and high paleoproductivity, most likely associated with upwelling conditions (Jackson et al. 1985; Clark et al. 1986; Firth & Clark 1998; Jenkyns et al. 2004; Davies et al. 2011). Continuous central Arctic Ocean sedimentary records, allowing a development of chronologic sequences of climate and environmental change through Cenozoic times and a comparison with global climate records, however, were missing prior to the IODP Expedition 302 (Arctic Ocean Coring Expedition – ACEX; Backman et al. 2006, 2008; Moran et al. 2006). With ACEX, for the first time a scientific drilling expedition in the permanently ice-covered Arctic Ocean was carried out, penetrating 428 meters of Quaternary, Neogene, Paleogene and Campanian sediment on the crest of Lomonosov Ridge close to the North Pole between 87 and 88°N.

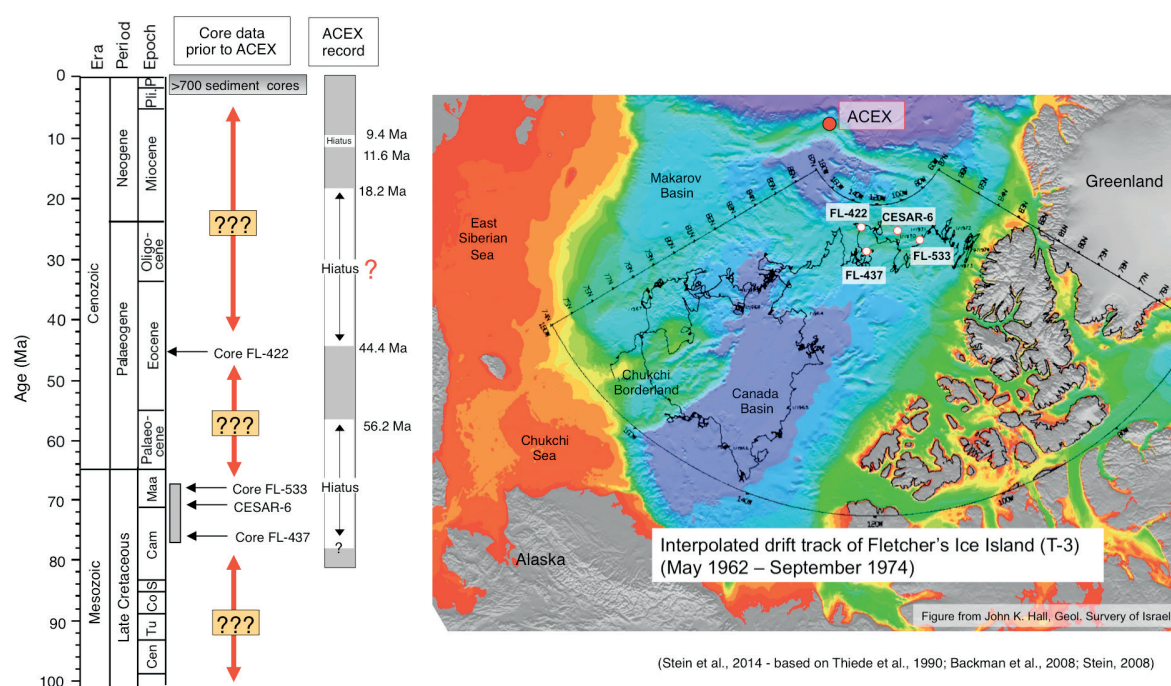


Fig. 10.1.1: Stratigraphic coverage of existing sediment cores in the central Arctic Ocean prior to IODP-ACEX (based on Thiede et al. 1990; Stein 2008) and the section recovered during the ACEX drilling expedition (Backman et al. 2006, 2008). The middle Eocene sediments recovered at Core FL-422 are arbitrarily placed at 45 Ma, the three Late Cretaceous (Maastrichtian/Campanian) cores are arbitrarily placed on the time axis as well. The map shows the Amerasian Basin and surrounding continents (shallower-water areas in red, orange and yellow colors, deep-water areas in green and blue colors) and the drift track of the Ice Island T3 with locations of cores FL-422, FL-437, FL-533, and CESAR-6 (Fig. from Stein et al. 2014).

By studying the unique ACEX sequence, a large number of scientific discoveries that describe previously unknown Arctic paleoenvironments, were obtained during the last decade (for most recent review and references see Stein et al. 2014). While these results from ACEX were unprecedented, key questions related to the climate history of the Arctic Ocean on its course from Greenhouse to Icehouse conditions during early Cenozoic times remain unanswered, in part because of poor core recovery, and in part because of the possible presence of a major mid-Cenozoic hiatus within the ACEX record. Furthermore, the ACEX sites remain the one and only drill holes in the entire central Arctic Ocean to date. In order to decipher the paleoclimatic and tectonic history of this unique and sensitive, but still not well known region on Earth,

future scientific Arctic drilling campaigns are certainly needed. For the precise planning of such future drilling activities including site selection, evaluation of proposed drill sites for safety and environmental protection aspects, etc., however, comprehensive site survey data are needed first. Here, the marine-geological programme (this chapter) as well as the geophysics programme (Chapter 9) of expedition PS87 have also to be regarded a major contribution to these site-survey activities.

The overall goals of the marine-geological research programme were (1) high-resolution studies of changes in paleoclimate, paleoceanic circulation, paleoproductivity, and sea-ice distribution in the central Arctic Ocean and the adjacent continental margin during Late Quaternary (especially postglacial-Holocene) times, and (2) the long-term history of the Mesozoic and Cenozoic Arctic Ocean and its environmental evolution from a warm (Greenhouse) to an ice-covered polar (Icehouse) ocean. In areas such as the Alpha- Ridge, the original main target area of Expedition PS87, pre-Quaternary sediments are cropping out, which could even be cored with coring gears aboard *Polarstern* and which would allow to study the Mesozoic/Tertiary history of the (preglacial) Arctic Ocean. Unfortunately, too strong ice conditions did not allow to reach the Alpha Ridge area (see Chapter 1). Thus, the main target area of the expedition has been shifted to the Lomonosov Ridge (Fig. 1.2).

The main objectives of PS87 marine geological studies include:

Stratigraphic analyses of the sediment sequences

As basis for all further reconstructions of paleoenvironmental changes, a stratigraphic framework as precise as possible has to be established. This work will include oxygen and carbon stable isotopes, absolute age dating, biostratigraphy, magnetostratigraphy, natural radionuclides, physical properties, XRF scanning, cyclostratigraphy, and correlation to other existing (dated) Arctic Ocean records.

The terrigenous sediment supply, sedimentary processes, and ice-sheet history

The research will concentrate on the quantification and characterization of terrigenous supply and its change through late Cenozoic times. This study will allow estimates of chemical and sedimentary budgets, identifications of major transport processes and pathways, and reconstructions of circum-Arctic ice-sheet history. Of major interest is a detailed sedimentological, geochemical, mineralogical, and micropaleontological study of surface sediments and sediment cores. Methods should include determinations of grain size, clay minerals, heavy minerals, major, minor, trace and rare earth elements, organic carbon fractions, and physical properties. Mapping of sediment echotypes from PARASOUND profiles will allow an extrapolation of point information from core data into spatial facies pattern. Furthermore, MSCL-logging and XRF-scanning records will be determined.

Organic carbon flux and surface-water characteristics (sea ice, temperature, salinity, etc.)

Data on spatial and temporal changes in the central Arctic Ocean organic-carbon budget are still rare, though the global importance for organic carbon storage in these areas is apparent (see Stein & Macdonald 2004 and Stein 2008 for review and further references). Thus, one of the major goals is to quantify the flux of organic carbon, to characterize the mechanisms controlling organic carbon deposition (i.e., surface-water productivity vs. terrigenous input) and their changes through late Quaternary and Mesozoic/Cenozoic times, and to reconstruct surface-water temperature, surface-water salinity, and sea-ice cover from biomarker records (e.g., n -alkanes, sterols, alkenones; U_{37}^k Index, TEX_{86} Index, IP_{25} Index).

Foraminifers and stable isotopes

The distribution and variability of planktonic and benthic (calcareous and agglutinated) foraminifers and their stable isotope signal will be determined to reconstruct changes in paleoenvironment such as water mass properties, surface-water productivity etc. through time.

Palynological proxies

The temporal distribution of organic-walled microfossils (dinoflagellate cysts, acritarchs, freshwater algae) will be used to establish a biostratigraphic framework of Neogene to Mesozoic sediments and to provide information on sea-surface conditions through time.

Inorganic geochemistry of pore water and sediments

Geochemical investigations of PS87 pore water and sediment samples will be carried out to document biogeochemical processes. Of special interest will be the characterization of inorganic compounds related to the degradation of organic matter and early diagenesis in the sediment.

Work at sea

In order to reach the main goals of the marine-geological programme, the recovery of undisturbed sediment sequences by means of Giant Box Corer (GKG), Multicorer (MUC), Gravity Corer (SL) and Kastenlot Corer (KAL) was one of the main foci of the shipboard geological work. Sampling was performed along and across the Lomonosov Ridge (Fig. 10.1.2). Of interest are areas of high sedimentation rates for the high-resolution studies of late Quaternary (postglacial-Holocene) paleoenvironment and areas where older strata are cropping-out (for studying Cenozoic sequences of paleoenvironmental change). Coring positions have been collected carefully using detailed bathymetric mapping and sub-bottom profiling systems (i.e., Hydrosweep and PARASOUND, respectively) to avoid areas of sediment redeposition (turbidites and slumps) and erosion, and to identify areas where preglacial sediments are cropping out.

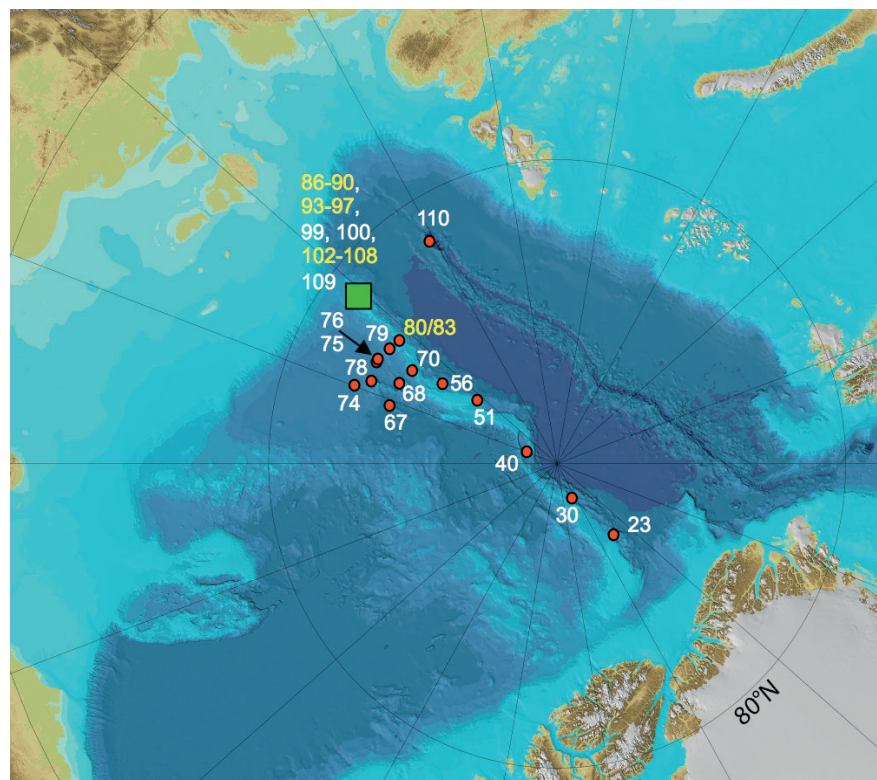


Fig. 10.1.2: Geological stations of Expedition PS87 (23 = PS87/023, 30 = PS87/030, etc.). Green square indicates location of „Super Coring Event“ (see Fig. 10.6.23), yellow numbers locations where probably old sediment are cropping out.

In total, geological coring was carried out at 46 stations, using the following gears: Giant Box Corer (GKG), Multicorer (MUC), Gravity Corer (SL), and/or Kastenlot Corer (KAL) (Table 10.1.1).

Tab. 10.1.1: Locations and gears of the geological stations. GC – Gravity Corer, MUC-Multicorer, GKG – Giant Box Corer, KAL – Kastenlot Corer.

Station	Gear	Latitude	Longitude	Water depth [m]
PS87/003-1	GKG	78° 24.12' N	1° 2.88' E	1170.8
PS87/003-2	GC	78° 24.08' N	1° 2.77' E	1173.2
PS87/023-1	KAL	86° 38.23' N	44° 53.98' W	2444.8
PS87/023-2	GKG	86° 37.86' N	44° 52.45' W	2439
PS87/026-1	GKG	87° 26.95' N	46° 33.95' W	3339
PS87/029-1	GKG	88° 29.01' N	48° 5.81' W	2903
PS87/029-2	MUC	88° 28.91' N	48° 4.55' W	2905.1
PS87/029-3	MUC	88° 28.73' N	48° 2.88' W	2911.9
PS87/030-1	KAL	88° 39.72' N	61° 32.52' W	1276.8
PS87/030-2	GKG	88° 39.56' N	61° 29.20' W	1278.4
PS87/030-3	MUC	88° 39.39' N	61° 25.55' W	1277.8
PS87/035-2	GKG	89° 58.97' N	19° 28.74' E	4183.1
PS87/035-3	MUC	89° 58.61' N	31° 53.17' E	4184.9
PS87/040-1	KAL	88° 59.31' N	171° 53.20' E	2614.1
PS87/040-2	GKG	88° 59.18' N	171° 44.50' E	2618.4
PS87/040-3	MUC	88° 58.96' N	171° 37.55' E	2621.4
PS87/051-1	GC	86° 26.98' N	147° 20.31' E	1190.7
PS87/055-1	GKG	85° 41.47' N	148° 59.47' E	730.7
PS87/056-1	KAL	85° 45.15' N	147° 57.24' E	835.8
PS87/056-2	GKG	85° 45.07' N	147° 55.85' E	836
PS87/067-1	GC	83° 29.47' N	160° 34.29' E	2862.3
PS87/067-2	GKG	83° 29.65' N	160° 35.36' E	2857
PS87/067-3	MUC	83° 29.90' N	160° 34.48' E	2867.1
PS87/068-1	GC	83° 37.89' N	154° 46.50' E	2708.9
PS87/068-2	GKG	83° 37.70' N	154° 46.87' E	2711
PS87/068-3	MUC	83° 37.41' N	154° 45.27' E	2712.6
PS87/070-1	KAL	83° 48.17' N	146° 7.01' E	1339.8
PS87/070-1	GKG	83° 48.16' N	146° 6.77' E	1340.4
PS87/070-3	MUC	83° 48.18' N	146° 7.04' E	1340.2
PS87/074-1	GKG	82° 43.39' N	158° 37.49' E	2816.5
PS87/074-2	MUC	82° 43.44' N	158° 37.54' E	2815.7
PS87/074-3	GC	82° 43.12' N	158° 36.88' E	2772

10.1 Overview of the PS87 Marine Geology Programme

Station	Gear	Latitude	Longitude	Water depth [m]
PS87/075-1	GC	82° 51.49' N	155° 45.19' E	2711.5
PS87/076-1	GC	82° 53.80' N	154° 57.93' E	2762.2
PS87/076-2	GKG	82° 53.81' N	154° 57.88' E	2763
PS87/076-3	MUC	82° 53.78' N	154° 57.79' E	2764.9
PS87/078-1	GC	83° 15.14' N	156° 48.17' E	784.2
PS87/079-1	KAL	83° 12.06' N	141° 22.77' E	1360.8
PS87/079-2	GKG	83° 12.09' N	141° 22.92' E	1359.6
PS87/079-3	MUC	83° 12.09' N	141° 22.54' E	1358.6
PS87/079-4	MUC	83° 12.09' N	141° 22.48' E	1360.8
PS87/080-1	GC	83° 12.26' N	141° 4.97' E	1471.8
PS87/080-2	GC	83° 12.28' N	141° 4.41' E	1508.9
PS87/080-3	GC	83° 12.27' N	141° 5.05' E	1468.8
PS87/080-4	GC	83° 12.30' N	141° 4.45' E	1512.1
PS87/083-1	GC	83° 12.26' N	141° 5.55' E	1448.6
PS87/083-2	GC	83° 12.23' N	141° 4.72' E	1486.9
PS87/083-3	GC	83° 12.24' N	141° 4.18' E	1537.8
PS87/086-1	GKG	81° 13.04' N	141° 22.99' E	901.8
PS87/086-2	MUC	81° 13.04' N	141° 22.98' E	901.7
PS87/086-3	GC	81° 13.04' N	141° 23.02' E	901
PS87/087-1	GC	81° 12.29' N	141° 15.92' E	1407.6
PS87/088-1	GC	81° 12.31' N	141° 16.40' E	1378.2
PS87/089-1	GC	81° 12.35' N	141° 16.47' E	1364.8
PS87/090-1	GC	81° 12.37' N	141° 16.87' E	1313
PS87/093-1	GC	81° 12.48' N	141° 17.62' E	1215.7
PS87/094-1	GC	81° 12.57' N	141° 18.49' E	1167.6
PS87/095-1	GC	81° 12.64' N	141° 19.21' E	1125.9
PS87/096-1	GC	81° 12.73' N	141° 20.04' E	1071.4
PS87/097-1	GC	81° 12.37' N	141° 16.88' E	1327.8
PS87/099-1	GC	81° 25.50' N	142° 14.43' E	740.4
PS87/099-2	GC	81° 25.49' N	142° 14.24' E	739.5
PS87/099-3	GKG	81° 25.48' N	142° 14.49' E	741.3
PS87/099-4	MUC	81° 25.50' N	142° 14.33' E	741.2
PS87/100-1	GKG	81° 21.42' N	142° 35.46' E	951
PS87/100-2	GC	81° 21.41' N	142° 35.56' E	951.1

Station	Gear	Latitude	Longitude	Water depth [m]
PS87/102-1	GC	81° 12.86' N	141° 11.38' E	1330.6
PS87/103-1	GC	81° 12.84' N	141° 11.12' E	1369.7
PS87/104-1	GC	81° 12.80' N	141° 10.85' E	1417.8
PS87/105-1	GC	81° 12.78' N	141° 10.65' E	1448.3
PS87/106-1	GC	81° 12.76' N	141° 10.47' E	1471.8
PS87/107-1	GC	81° 12.74' N	141° 10.25' E	1496.3
PS87/108-1	GC	81° 12.79' N	141° 10.70' E	1439.6
PS87/109-2	GC	81° 7.70' N	140° 34.99' E	1306.9
PS87/109-3	MUC	81° 7.67' N	140° 34.91' E	1303.1
PS87/109-4	GKG	81° 7.69' N	140° 34.95' E	1303.3
PS87/109-5	MUC	81° 7.69' N	140° 34.94' E	1302.6
PS87/109-6	MUC	81° 7.67' N	140° 35.13' E	1304.6
PS87/110-1	GC	81° 21.02' N	120° 31.47' E	5071.9
PS87/110-2	GKG	81° 21.03' N	120° 31.48' E	5129.5

Surface sediment sampling

Surface and near-surface sediment sampling was carried out by using a Giant Box Corer and a Multicorer. The Giant Box Corer (weight of ca. 500 kg; volume of sample 50*50*60 cm; manufactured by Fa. Wuttke, Henstedt-Ulzburg, Germany) was successfully used 19 times at 20 stations. At the last station, there was no recovery due to the surface conditions of the sea floor.

From the Box Corer surface sediments and usually two archive tubes (diameter 12 cm) and two boxes (10 x 50 and 7 x 50 cm) were taken. Usually the smaller archive box was logged (MSCL, see Chapter 10.3). Further samples were obtained from the surface sediments:

- Sample water from box core surface with silicon hose and bucket
- 10 x 10 cm frame, ca. 1-2 cm sediment depth (Benthic foraminifera Kaminski)
 - 50 ml NUNC (Palynology: de Vernal/Matthiessen)
 - 50 ml NUNC (Geochemistry: Bazhenova)
 - 100 ml NUNC (Sedimentology/Mineralogy: Matthiessen/Stein)
 - 100 ml NUNC (Planktic foraminifera, stable isotopes: Nam/Spielhagen)
 - 50 ml NUNC (fill half) (Algae: de Vernal/Matthiessen)
 - 50 ml glass (Org. Geochemistry: Stein/Hörner)
 - X-ray slabs from the side
 - 10 ml syringes for dry bulk density (1, 5, 10, 15, 20, 30, 40, 50 cm)
 - Sampling of drop stones (Bazhenova)

10.1 Overview of the PS87 Marine Geology Programme

The standard 8-tubes-version Multicorer (manufactured by Fa. Wuttke, Henstedt-Ulzburg, Germany) with an inner tube diameter of 10 cm was used. The penetration weight was always 250 kg. The Multicorer was successfully used 14 times at 12 stations, and usually recovered undisturbed surface sediments and overlying bottom water.

From the recovered 8 tubes 3 tubes were sampled at 1 cm steps down to 10 cm and stained with an ethanol-bengal rose mixture for living/dead foraminiferal assemblage studies (Wollenburg/Kaboth). The 100 – 200 ml of the residual water of the MUC tubes were additionally sampled and mixed with 150 – 300 µl of mercuric-chloride to preserve the *in-situ* isotopic composition of the near bottom water for further study.

- One tube was used for pore water chemistry analyses (J. Volz; see Chapter 10.9).
- One tube was sampled at 1 cm interval for TOC/N and $\delta^{13}\text{C}_{\text{org}}$ analyses (H. Jin). These samples will also be used for chlorophyll degradation product analyses as an index of paleo-productivity and phytoplankton diagnostic pigments will be analyzed as tracers of the structure of phytoplankton communities.
- One tube was sampled at 1 cm interval for palynology with the primary objective of qualitatively and quantitatively characterizing the organic microfossil assemblages as well as dinoflagellate cyst populations (A. de Vernal).
- Two tubes were sampled at 1 cm steps as archive back-up for the AWI and the Organic Geochemistry Department of the AWI (R. Stein et al.).

Sampling of long sediment cores

Long sediment cores were taken by a Gravity Corer and a Kastenlot Corer. The Gravity Corer (GC or "Schwerelot", SL) has a penetration weight of 1.5 t. It was successfully used with variable barrel lengths of 3, 5 or 10 m at 31 stations (37 cores; see Table 10.1.2). The recovery of the gravity corer varied between 0.88 and 7.12 m (Fig. 10.1.3).

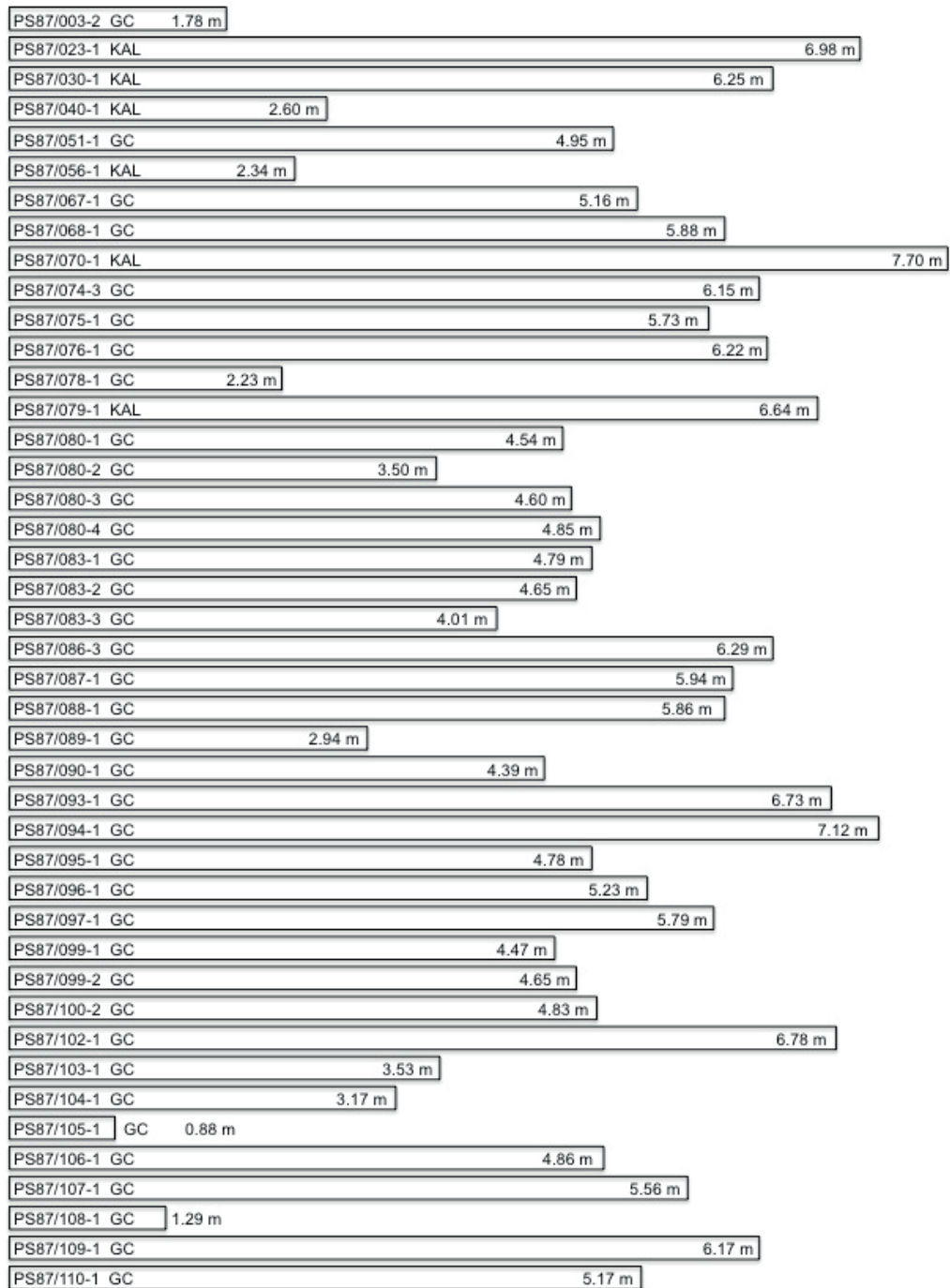


Fig. 10.1.3: Core lengths (Recovery) of gravity- and kastenlot cores.

10.1 Overview of the PS87 Marine Geology Programme

Tab. 10.1.2: Recovery and penetration of kastenlot- and gravity cores taken during Expedition PS87.

Station	Gear	Latitude	Longitude	Water depth	Recov.
PS87/003-2	GC-10	78° 24.08' N	1° 2.77' E	1173.2	178
PS87/023-1	KAL-10	86° 38.23' N	44° 53.98' W	2444.8	698
PS87/030-1	KAL-10	88° 39.72' N	61° 32.52' W	1276.8	625
PS87/040-1	KAL-10	88° 59.31' N	171° 53.20' E	2614.1	260
PS87/051-1	GC-10	86° 26.98' N	147° 20.31' E	1190.7	495
PS87/056-1	KAL-10	85° 45.15' N	147° 57.24' E	835.8	234
PS87/067-1	GC-10	83° 29.47' N	160° 34.29' E	2862.3	516
PS87/068-1	GC-10	83° 37.89' N	154° 46.50' E	2708.9	588
PS87/070-1	KAL-10	83° 48.17' N	146° 7.01' E	1339.8	770
PS87/074-3	GC-10	82° 43.12' N	158° 36.88' E	2772	615
PS87/075-1	GC-10	82° 51.49' N	155° 45.19' E	2711.5	573
PS87/076-1	GC-10	82° 53.80' N	154° 57.93' E	2762.2	622
PS87/078-1	GC-10	83° 15.14' N	156° 48.17' E	784.2	223
PS87/079-1	KAL-10	83° 12.06' N	141° 22.77' E	1360.8	664
PS87/080-1	GC-5	83° 12.26' N	141° 4.97' E	1471.8	454
PS87/080-2	GC-10	83° 12.28' N	141° 4.41' E	1508.9	350
PS87/080-3	GC-10	83° 12.27' N	141° 5.05' E	1468.8	460
PS87/080-4	GC-10	83° 12.30' N	141° 4.45' E	1512.1	485
PS87/083-1	GC-10	83° 12.26' N	141° 5.55' E	1448.6	479
PS87/083-2	GC-10	83° 12.23' N	141° 4.72' E	1486.9	465
PS87/083-3	GC-10	83° 12.24' N	141° 4.18' E	1537.8	401
PS87/086-3	GC-10	81° 13.04' N	141° 23.02' E	901	629
PS87/087-1	GC-10	81° 12.29' N	141° 15.92' E	1407.6	594
PS87/088-1	GC-10	81° 12.31' N	141° 16.40' E	1378.2	586
PS87/089-1	GC-10	81° 12.35' N	141° 16.47' E	1364.8	294
PS87/090-1	GC-10	81° 12.37' N	141° 16.87' E	1313	439
PS87/093-1	GC-10	81° 12.48' N	141° 17.62' E	1215.7	673
PS87/094-1	GC-10	81° 12.57' N	141° 18.49' E	1167.6	712
PS87/095-1	GC-10	81° 12.64' N	141° 19.21' E	1125.9	478

Station	Gear	Latitude	Longitude	Water depth	Recov.
PS87/096-1	GC-10	81° 12.73' N	141° 20.04' E	1071.4	523
PS87/097-1	GC-10	81° 12.37' N	141° 16.88' E	1327.8	578.5
PS87/099-1	GC-10	81° 25.50' N	142° 14.43' E	740.4	447
PS87/099-2	GC-10	81° 25.49' N	142° 14.24' E	739.5	464.5
PS87/100-2	GC-10	81° 21.41' N	142° 35.56' E	951.1	483
PS87/102-1	GC-10	81° 12.86' N	141° 11.38' E	1330.6	678
PS87/103-1	GC-10	81° 12.84' N	141° 11.12' E	1369.7	353
PS87/104-1	GC-10	81° 12.80' N	141° 10.85' E	1417.8	317
PS87/105-1	GC-10	81° 12.78' N	141° 10.65' E	1448.3	88
PS87/106-1	GC-10	81° 12.76' N	141° 10.47' E	1471.8	486
PS87/107-1	GC-10	81° 12.74' N	141° 10.25' E	1496.3	556
PS87/108-1	GC-5	81° 12.79' N	141° 10.70' E	1439.6	129
PS87/109-2	GC-10	81° 7.70' N	140° 34.99' E	1306.9	617
PS87/110-1	GC-10	81° 21.02' N	120° 31.47' E	5071.9	517

The Kastenlot (Kögler 1963), a Gravity Corer with a rectangular cross section of 30 x 30 cm, has a penetration weight of 3.5 t and a core box segment sized 30 x 30 x 575 cm (manufactured by Hydrowerkstätten Kiel). The length of the Kastenlot boxes used was 11.75m plus about 30 cm for the core catcher. The great advantage of the Kastenlot is a wall-thickness of the barrel of only 2 mm.

Because of the great cross-sectional area (900 cm²) and the small thickness of the barrels, the quality of the cores was generally excellent. The Kastenlot was successfully used at 6 stations. The recovery of the Kastenlot cores varied between 2.34 and 7.70 m (Table 10.1.2, Fig. 10.1.3). All Kastenlot sediments were sampled and stored in plastic boxes (three sizes: (1) 100 x 12, (2) 100 x 8, and (3) 100 x 10), in general in 6 series per interval:

- Series I Archive (1)
- Series II Sedimentology (1)
- Series III Physical Properties (2)
- Series IV Organic Geochemistry (2)
- Series V Mineralogy/Geochemistry (1)
- Series VI GEOMAR (3)

From the remaining sediments, samples of about 50 cm³ (ca. every 5 cm) were taken for biostratigraphy that were analysed on board.

All gravity cores were logged before they were opened whereas plastic boxes of two series of the Kastenlot cores (Series III and IV) were logged (MSCL; Chapter 10.3). After opening, from all core sections (archive half) photographs were taken (see below). From a large number of core sections, a detailed visual core description was carried out. Colour of sediments was described using the Munsell Soil Colour Chart as well as spectral reflectance analysis using a spectrophotometer. For main lithologies, smear-slide analysis was performed for rough evaluation of grain-size composition, preliminary determination of mineralogical composition (quartz, feldspars, carbonates, opaques), and content of biogenic components (foraminifers, coccoliths, diatoms, sponge spicules). Sediment slabs were taken from all opened cores for X-ray photography to be carried out later at the AWI (see below). For coarse-fraction analysis, the fraction $>63\ \mu\text{m}$ was isolated by means of wet sieving, and the abundance of the major sediment components (siliciclastics, detrital carbonates, planktic and benthic foraminifers, ostracods, etc.) were estimated by using a binocular microscope (see annex for details).

Photographs of sediment cores

The cores have been photographed with the photographic system that was set up on board (Fig. 10.1.4). A Nikon D700 camera (AF-S Nikon 24-70mm objective) was used for all pictures. To preserve the original colour impression the flash light system was not used, all pictures have been taken with room light only. Compared to the LineScan Camera that was also used during this cruise to take photographs of the sediment cores, this system has a much lower resolution. It has to be noted that the colour impression varies between both systems, probably caused by the different light settings.

The Kastenlot (KAL) cores have been photographed with a exposure time of 4 seconds and a diaphragm of 1:22. Light correction was set with +5LW. For the gravity (SL) cores, the exposure time had to be increased to 6 seconds, they where placed deeper in the core table.

All the digital images are organized separately for each sediment core under the respective station and gear number

Sediment slabs and X-Ray photographs

X-Ray images were produced to study sedimentary and biogenic structures and to determine the number of coarse-grained particles ($>2\ \text{mm}$) in order to evaluate the content of IRD. Therefore, sediment slabs (250 x 100 x 8 mm) were taken continuously from every opened sediment core (GKG, SL, KAL) for X-Ray film processing. Plastic slabs with a size of 252 x 103 x 12 mm were slowly pushed into the smoothed sediment surface and carefully removed. To avoid any damages, the slabs were sealed in a plastic cover and the air was removed. The sealed slabs were placed on 100 x 300 mm large film stripes (Industrial X-Ray Film Agfa-Gevaert Structurix D4 FW 30 x 40) in a cabinet X-Ray system (Hewlett-Packard Faxitron Series) and were exposed on the average for 10 minutes at 35 kV. The films were developed for 3 minutes (Agfa-Gevaert Developer Structurix G 128), washed for 1 minute and then fixed for 3 minutes (Agfa-Gevaert Fixing Bath Structurix G335). After washing in a water bath for 10



Fig. 10.1.4: Photographic system that was used on board. 1: Camera (Nikon D700), 2: Flash Lights, 3: Core table

minutes the film negatives were dried and stored in a transparent cover. The X-Ray negatives will be scanned after the expedition at AWI, all images and the gravel counts will be stored for each sediment core under the respective station and gear number in the data bank PANGAEA Data Publisher for Earth & Environmental Science (WDC-mare).

Shear strength

For shear strength measurements, a hand held shear vane (Geovane GEO 709) with a 19 mm blade which was calibrated on 30th August 2006 (Geotechnics, Auckland, New Zealand), was used. The shear strength of Kastenlot PS87/056-1 and gravity core PS87/078-1 were measured in about 10 cm intervals at the split cores and was converted by a calibration chart published by the company into undrained vane shear strength in kPa. Values between 0 and 140 can be reached. Changes in lithology cause different shear strength, so that sediments that have a higher density (e.g. debris flows) show a higher shear strength. The shear strength in both cores is increasing with depth due to normal consolidation processes (Fig. 10.1.5).

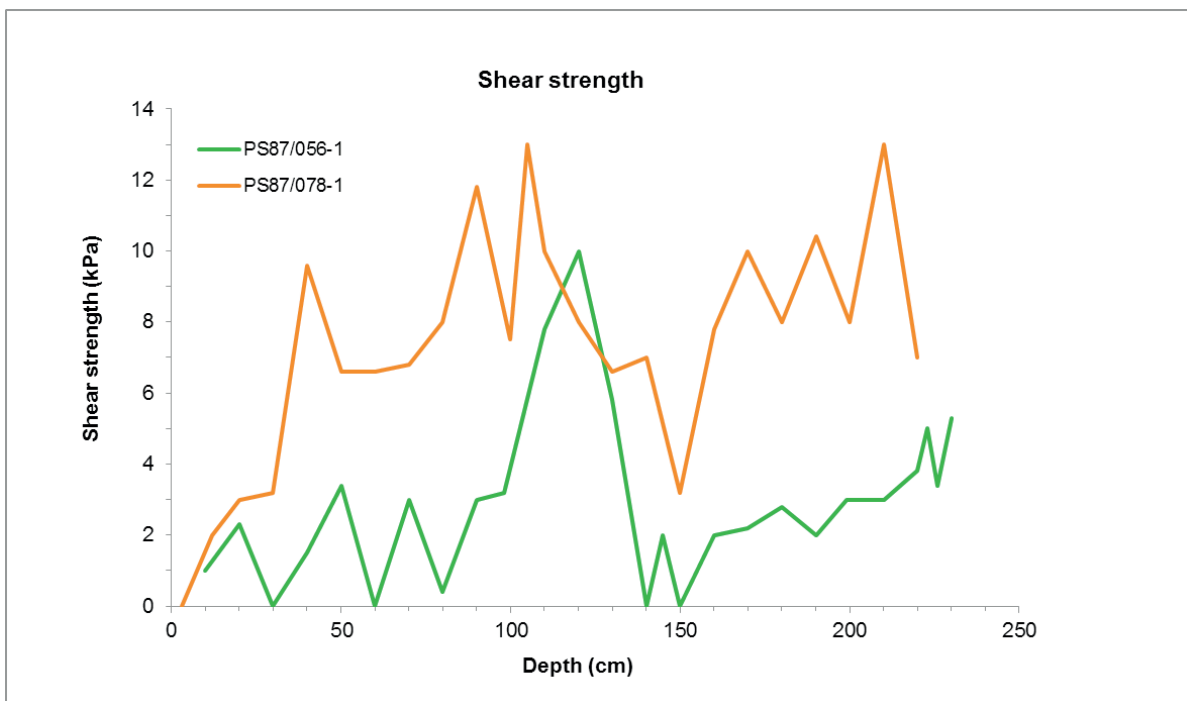


Fig. 10.1.5: Shear strength of Kastenlot core PS87/056-1 and gravity core PS87/078-1

Preliminary results

Preliminary results of the shipboard studies of surface sediments as well as selected sediment cores are presented and discussed in the following subchapters 10.2 to 10.9 and the annex.

Data management

Raw data and processed data (shipboard and shorebased) will be made available in PANGAEA.

References

- Backman J, Jakobsson M, Frank M, Sangiorgi F, Brinkhuis H, Stickley C, O'Regan M, Løvlie R, Pälike H, Spofforth D, Gattacecca J, Moran K, King J, Heil C (2008) Age Model and Core-Seismic Integration for the Cenozoic ACEX Sediments from the Lomonosov Ridge. *Paleoceanography*, doi:10.1029/2007PA001476.
- Backman J, Moran K, McInroy DB, et. al. (2006) Proceedings IODP, 302, College Station, Texas (Integrated Ocean Drilling Program Management International, Inc.). doi:10.2204/iodp.proc.302.104.2006.
- Clark DL (1988) Early history of the Arctic Ocean. *Paleoceanography*, 3, 539-550.
- Clark DL, Byers CW and Pratt LM (1986) Cretaceous black mud from the central Arctic Ocean. *Paleoceanography*, 1, 265-271. Firth and Clark, 1998
- Clark DL, Whitman R.R, Morgan KA and Mackey SC (1980) Stratigraphy and glacial-marine sediments of the Amerasian Basin, central Arctic Ocean. GSA Special Paper, 181, 57 pp.
- Davies A, Kemp AES, Pälike H (2011) Tropical ocean-atmosphere controls on inter-annual climate variability in the Cretaceous Arctic. *Geophys. Res. Lett.*, 38, doi: 10.1029/2010GL046151
- Firth JV and Clark DL (1998) An early Maastrichtian organic-walled phytoplankton cyst assemblage from an organic-walled black mud in Core F1-533, Alpha Ridge: evidence for upwelling conditions in the Cretaceous Arctic Ocean. *Mar. Micropaleont.*, 34, 1-27.
- Jackson HR, Mudie PJ and Blasco SM (1985) Initial geological report on CESAR - The Canadian Expedition to study the Alpha Ridge, Arctic Ocean. *Geol. Surv. Canada, Paper 84-22*, 177 pp.
- Jenkyns HC, Forster A, Schouten S, Sinninghe Damsté JS (2004) High temperatures in the late Cretaceous Arctic Ocean. *Nature*, 432, 888-892.
- Moran K, Backman J, Brinkhuis H, Clemens SC, Cronin T, Dickens GR, Eynaud F., Gattacecca J, Jakobsson M, Jordan RW, Kaminski M, King J, Koc N, Krylov A, Martinez N, Matthiessen J, McInroy D, Moore TC, Onodera J, O'Regan AM, Pälike H, Rea B, Rio D, Sakamoto T, Smith DC, Stein R, St. John K, Suto I, Suzuki N, Takahashi K, Watanabe M, Yamamoto M, Frank M, Jokat, W, Kristoffersen Y (2006) The Cenozoic palaeoenvironment of the Arctic Ocean. *Nature*, 441, 601-605.
- Stein R (2008) Arctic Ocean Sediments: Processes, Proxies, and Palaeoenvironment. *Developments in Marine Geology*, Vol. 2, Elsevier, Amsterdam, 587 pp..
- Stein R and Macdonald RW (Eds.) (2004) *The Organic Carbon Cycle in the Arctic Ocean*, Springer-Verlag, Berlin, 363 pp.
- Stein R, Weller P, Backman J, Brinkhuis H, Moran K, Pälike H (2014) Cenozoic Arctic Ocean Climate History: Some highlights from the IODP Arctic Coring Expedition (ACEX). In: Stein, R., Blackman, D. Inagaki, F., and Larsen, H.-C. (Eds.), *Earth and Life Processes Discovered from Subseafloor Environment - A Decade of Science Achieved by the Integrated Ocean Drilling Program (IODP)*, *Developments in Marine Geology*, Vol. 7, Elsevier Amsterdam/New York, pp. 259-293 ([doi:10.1016/B978-0-444-62617-2.00011-6](https://doi.org/10.1016/B978-0-444-62617-2.00011-6)).
- Thiede J, Clark DL, Hermann Y (1990) Late Mesozoic and Cenozoic paleoceanography of the northern polar oceans, in: *The Geology of North America*, Vol. L, The Arctic Ocean Region, pp. 427-458.

10.2 Marine Sediment Echosounding using PARASOUND

Frank Niessen¹, Florian Petersen²

¹AWI

²UoK

Objectives

In the Arctic Ocean, bottom and sub-bottom reflection patterns obtained by PARASOUND characterize the uppermost sediments in terms of their acoustic behavior down to about 100 m below the sea floor. This can be used to study depositional environments of unknown areas on larger scales in terms of space and time, of which the uppermost sediments may also be sampled. The general objectives of sediment echosounding during PS87 (ARK-XXVIII/4) were:

- to provide the data base for an acoustic facies interpretation indicative for different sedimentary environments,
- to obtain different pattern of high-resolution acoustic stratigraphy useful for lateral correlation over shorter and longer distances thereby aiding correlation of sediment cores retrieved during the cruise,
- to select coring stations based on acoustic pattern and reflection amplitude, and
- to provide a high-resolution counterpart for the uppermost sections of seismic profiles recorded during the cruise.

Cruise and area specific objectives of the sediment echosounding of PS87 include:

- to identify and interpret older sediments (Early Pleistocene to Mesozoic), which crop out at or near the sediment surface in the context of planned deep ocean drilling projects (IODP, MEBO),
- to identify and interpret truncation and sedimentation related to local or large-scale erosion and reworking by grounded ice (icebergs or ice shelves).

Work at sea

The Deep Sea Sediment Echo Sounder PARASOUND (ATLAS HYDROGRAPHIC, Bremen, Germany) was upgraded from DS II to DS III-P70 during the shipyards stay of *Polarstern* in Bremerhaven in May 2007. This upgrade included a complete installation of new hardware and software and replaced the original system installed on *Polarstern* in 1989 (e.g. Spiess 1992). Meanwhile, several sea-trial phases including final software updating and testing at sea were carried out, and, a number of research cruises used the DS III-P70 successfully. Finally, the system has gained a satisfactory stability during operation and revealed some excellent results (e.g. Niessen et al. 2010, 2013). For a summary of the development and technical specification of the DS III-P70 the reader is referred to Niessen in Macke (2009) and Jokat (2009). For more technical details the reader is referred to the system manuals provided by the manufacturer (ATLAS Hydrographic, 2007a,b).

The hull-mounted PARASOUND system generates two primary frequencies, of which the lower frequency is selectable between 18 and 23.5 kHz transmitting in a narrow beam of 4° at high power. As a result of the non-linear acoustic behavior of water, the so-called “Parametric Effect”, two secondary harmonic frequencies are generated of which one is the difference (e.g. 4 kHz) and the other the sum (e.g. 40 kHz) of the two primary frequencies, respectively.

10.2 Sediment Echosounding using PARASOUND

As a result of the longer wavelength, the difference parametric frequency allows sub-bottom penetration up to 100 m in the Arctic Ocean (depending on sediment conditions) with a vertical resolution of about 30 cm. The primary advantage of parametric echosounders is based on the fact that the sediment-penetrating pulse is generated within the narrow beam of the primary frequencies, thereby providing a very high lateral resolution compared to conventional 4 kHz-systems. This capability, however, limits good survey results on sea-floor slopes, which are inclined to more than 4° relative to horizontal. The reason is that the energy reflected from the small inclined footprint on the seafloor is out of the lateral range of the receiving transducers in the hull of the vessel. As a consequence, the survey results are poor over longer lateral distances along the slopes of ridges in the Arctic Ocean such as the Gakkel Ridge and the Lomonosov Ridge, which were major targets of the PS87 cruise.

Tab. 10.2.1: Settings of ATLAS HYDROMAP CONTROL for operating PARASOUND during cruise PS87

Used Settings	Selected Options	Selected Ranges
Mode of Operation	P-SBP/SBES	PHF, (SHF), SLF
Frequency	PHF SHF SLF	20 kHz (44 kHz) 4 kHz
Pulselength	No. of Periods Length	2 0.5 ms
Transmission Source Level	Transmission Power Transmission Voltage	100% 159 V
Beam Steering	none	
Mode of Transmisson	Single Pulse Quasi-Equidistant Pulse Train	Auto according to water depth Interval 400-1200 ms none
Pulse Type	Continuous Wave	
Pulse Shape	Rectangular	
Receiver Band Width	Output Sample Rate (OSR) Band Width (% of OSR)	6.1 kHz 66%
Reception Shading	none	
System Depth Source	Fix Min/Max Depth Limit or Variable Min/Max Depth	Manual Other (Atlas Hydrosweep) Atlas Parastore
Water Velocity	C-Mean C-Keel	Manual 1500 m/s System C-keel
Data Recording	PHF SLF	Full Profile Full Profile

PARASOUND DS III-P70 is controlled by two different operator software packages plus server software running in the background. These processes are running simultaneously on a PC under Windows-7. (i) ATLAS HYDROMAP CONTROL is used to run the system by an operator. The selected modes of operation, sounding options and ranges used during the cruise are summarized in Table 10.2.1. A list of abbreviations is given at the end of this chapter. (ii) ATLAS PARASTORE-3 is used by the operator for on-line visualization (processing) of received data on PC screen, for data storage and printing. It can also be used for replaying of recorded data, post-processing and further data storage in different output formats (PS3 and/or SEG-Y). For any further details the reader is referred to the operator manuals of Atlas Hydromap Control and Atlas Parastore and some basic descriptions given by Niessen et al. in Schiel 2009.

As a result of several problems with online-printing in the past, a PNG-creator was installed on the operator-PC during the previous cruise PS86, which created files instead of hard-copy prints (Boetius in prep.). During PS87 an additional PNG-creator was created for auxiliary data files instead of hard-copy prints. The PNG files of PHF, SLF and AUX data can later be used for printing and storage.

During PS87 digital data acquisition and storage were switched on during the transect from Tromsø to the first waypoint on the Hoovgaard Ridge at the northern end of the Boreas Abyssal Plain on August 06 at 11:08 UTC and was switched off after the last HYDROSWEEEP survey (PS87-111) leaving the Gakkel Ridge on October 3 at 02:16 UTC towards the EEZ of Russia. In addition, PARASOUND data were acquired during the journey back to Bremerhaven on the western slope of the Barents Sea for a site survey requested by Geomar between the waypoints HS_Geomar01 71° 32.5' N 16° 38.8' E to HS-Geomar02 70° 57' N 12° 46' E.

Acquisition included PHF and SLF data during the entire cruise. Both PHF and SLF traces were visualized as online profiles on screen. SLF profiles (200m depth window) and online status (60s intervals) were saved as PNG files and printed on A4 pages. The PHF profiles (200m depth window) were saved only as PNG files.

Preliminary (expected) results

Some PARASOUND records from coring stations are selected as data examples from the different areas under investigation. These areas include the Fram Strait, the Greenland side of the Lomonosov Ridge (LR), the Central LR, the Siberian side of the LR and the Gakkel Ridge.

The Hoovgaard Ridge was investigated in the context of recently published iceberg plough marks along the crest of the ridge (Arndt et al. 2014). The profile exhibits a pelagic drape over the ridge, which has been overprinted by grounded icebergs in places (Fig. 10.2.1). These are indicated by morphological incision and transparent lenses in the record, which form the berms of the plough marks. A core was recovered between the two time marks 21:20 and 23:20 UTC, in order to gain stratigraphic constrain, when the ice groundings might have occurred.

10.2 Sediment Echosounding using PARASOUND

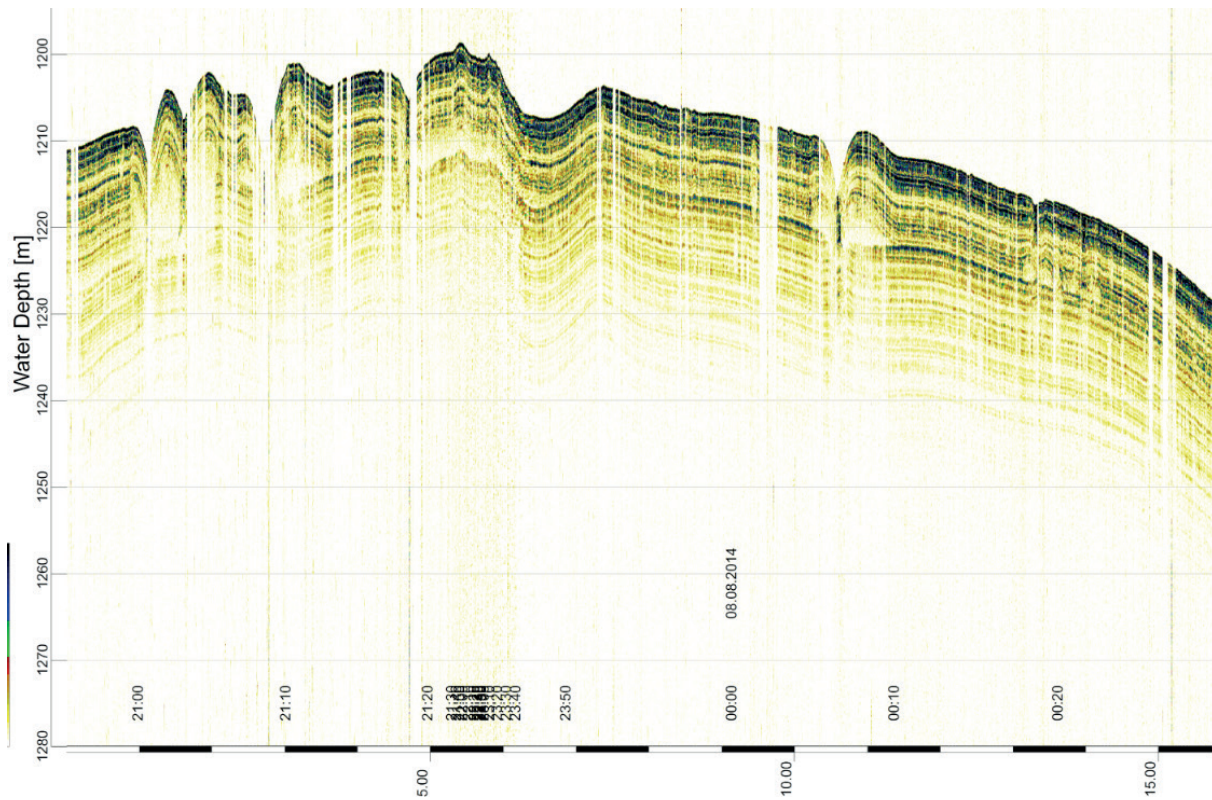


Fig. 10.2.1: PARASOUND example from the Hovgaard Ridge (Fram Strait). Position of coring location PS79/287 is between the time markers 21:20 and 23:40 UTC. The black and white bars at the bottom give lateral distance in km. The depth has been determined by the PARASOUND system.

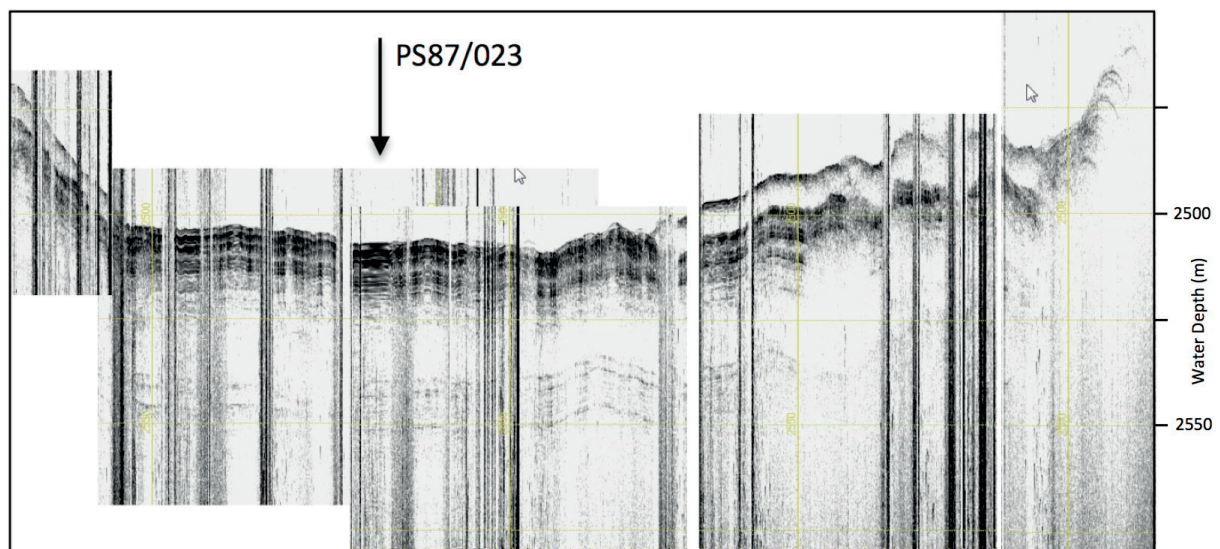


Fig. 10.2.2: PARASOUND example from the Lomonosov Ridge (Greenland side). Position of coring location PS87/023 is marked by an arrow. The yellow and black bars at the bottom give lateral distance (1 km per bar). The depth has been determined by the PARASOUND system.

Near the southernmost point of the cruise on the LR towards Greenland, a Kastenlot (PS87/023) was retrieved at a slope location on the Amundsen Sea side of the ridge. The PARASOUND record (Fig. 10.2.2) is strongly affected by secondary noise created from breaking sea-ice by the hull of the vessel. At the coring location (Fig. 10.2.2) the profile exhibits an acoustic sub-bottom penetration of about 40 m into pelagic sediments. Acoustic stratigraphy suggests three different units. The uppermost unit (1) is about 13 m thick and has strong reflectors overlying a featureless almost transparent unit, which is about 20 m thick. This is underlain by a unit with more distinct reflectors similar in geometry to those of unit 1 but showing weaker reflectors. Towards both lateral ends of the profile, debris-flow deposits lens out, which cover most of unit 1 sediments draped by a thin veneer of pelagic deposits. The coring location is not covered by debris flows (Fig. 10.2.2).

Core PS87/040 (KAL) was retrieved from an intra-basin of the central LR relatively close to the North Pole. The PARASOUND profile (Fig. 10.2.3) shows the coring location between the time markers 22:20 UTC and 03:50 UTC towards the eastern end of the basin. The record is well stratified and has two acoustic units, an upper one with strong reflectors and a lower one with weaker reflections. The relative sedimentation rate at the eastern (left and shallower) end of the profile is about 20% lower than at the right and deeper end. This suggests that the basin is affected by lateral sediment transport and sediment focussing into the basin possibly related to gravity induced re-deposition and/or currents.

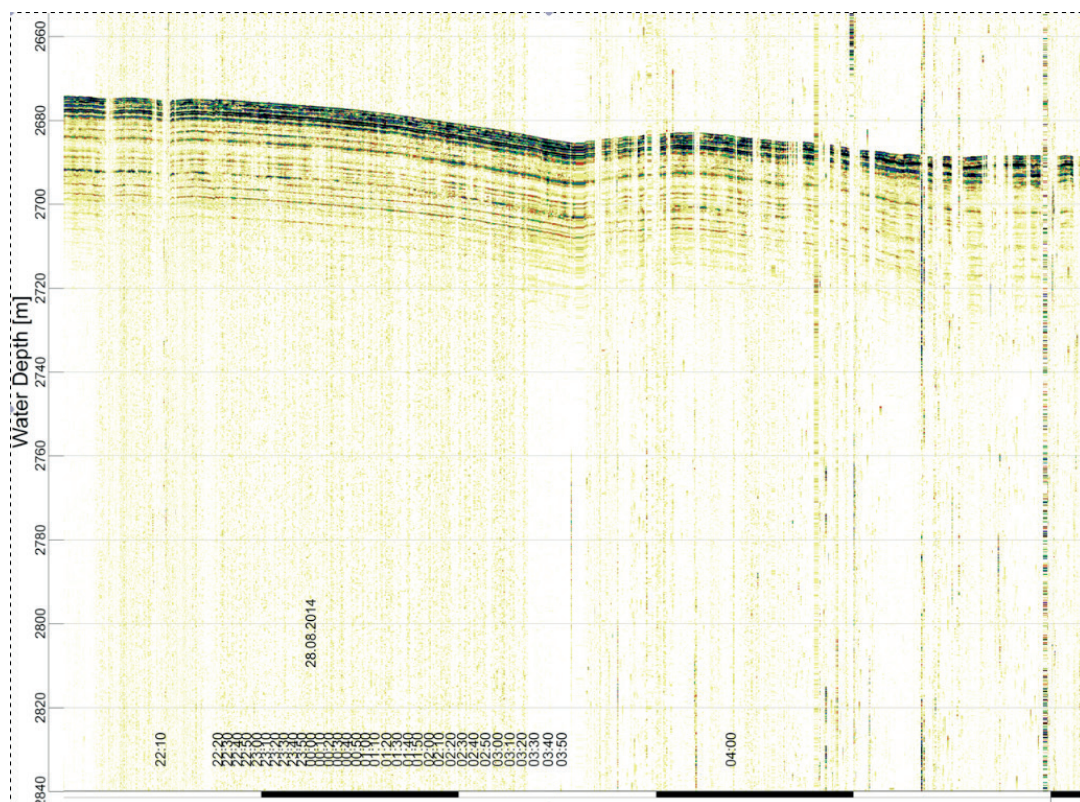


Fig. 10.2.3: PARASOUND example from the central Lomonosov Ridge. Position of coring location PS87/040 is between the time markers 22:20 and 03:50 UTC. The black and white bars at system.

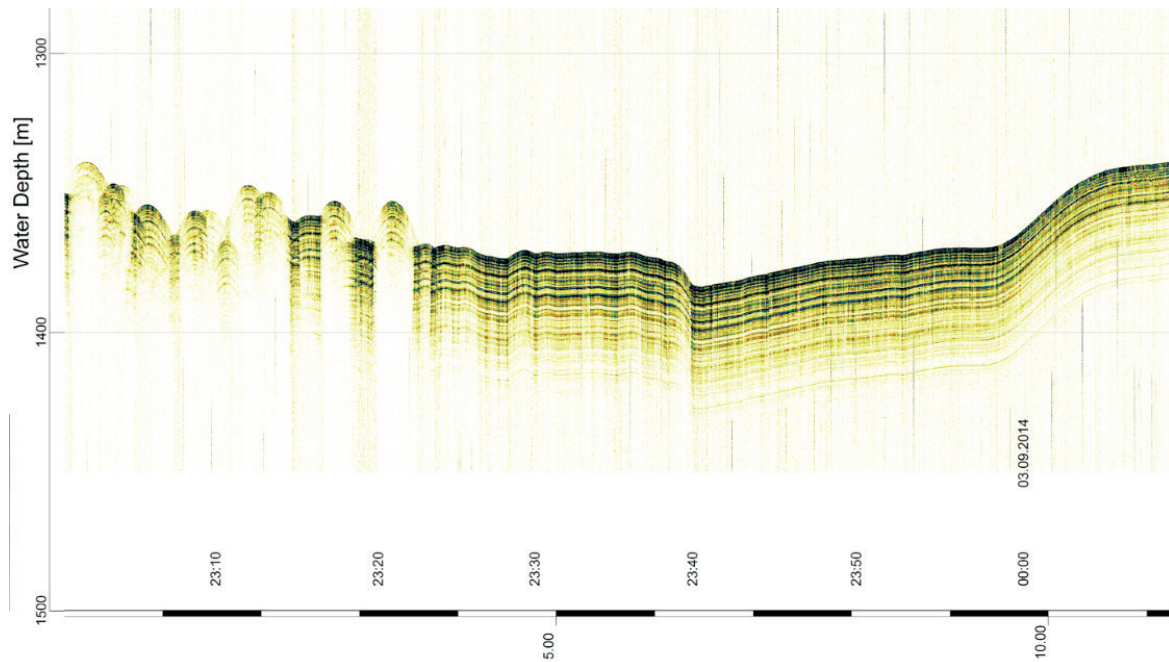


Fig. 10.2.4: PARASOUND example from the central Lomonosov Ridge. Position of coring location PS79/287 is close to the time marker 23:30 UTC. The black and white bars at the bottom give lateral distance in km. The depth has been determined by the PARASOUND system.

Along a PARASOUND profile across the LR at about 84° N, the sediments appear mostly well stratified and drape sub-bottom topographies (Fig. 10.2.4). Here the acoustic stratigraphy is less distinct compared to the profiles described above. Stronger reflectors in the upper 15 m thickness are underlain by a transitional zone of 5 m and then followed by weaker reflectors. The location of core PS87/070 was selected between the time marks of 23:30 and 23:40 UTC. The left end of the profile is characterized by slump hummocks covered by pelagic sediments.

Along a PARASOUND profile across the LR at about 83° N, the sediments exhibit slide scars in places near the crest of the LR (Fig. 10.2.5). Between coring stations PS87/079 /080 and /083, which were selected along the profile, about 200 m thick packages of a formerly well-stratified pelagic drape were removed and re-deposited onto the slope of the Amundsen Basin (left of time mark 21:20 UTC in Fig. 10.2.5). Coring location PS87/079 was selected at about 1,400 m water depth on the undisturbed part of the profile. Cores PS87/080-1 to /080-4 as well as cores PS87/083-1 to /083-3 were selected along the slide scar between about 1,480 m and 1,560 m water depth (Fig. 10.2.5).

At the southern end of the LR on the Siberian side (about 81°N), near a sill encouraging water-mass exchange between the Amundsen and Makarov basins, coring site PS87/109 was selected in about 1,350 m water depth at time mark 15:20 UTC (Fig. 10.2.6). The PARASOUND profile exhibits a hemi-pelagic drape on a mount of the LR. Again, the acoustic stratigraphy consists of an upper unit with stronger reflections to a sediment depth of about 11 m underlain but well-stratified sediments forming weaker reflectors. Lateral sedimentation rates decrease towards deeper water suggesting stronger winnowing towards the sill below 1,300 m of water (Fig. 10.2.6).

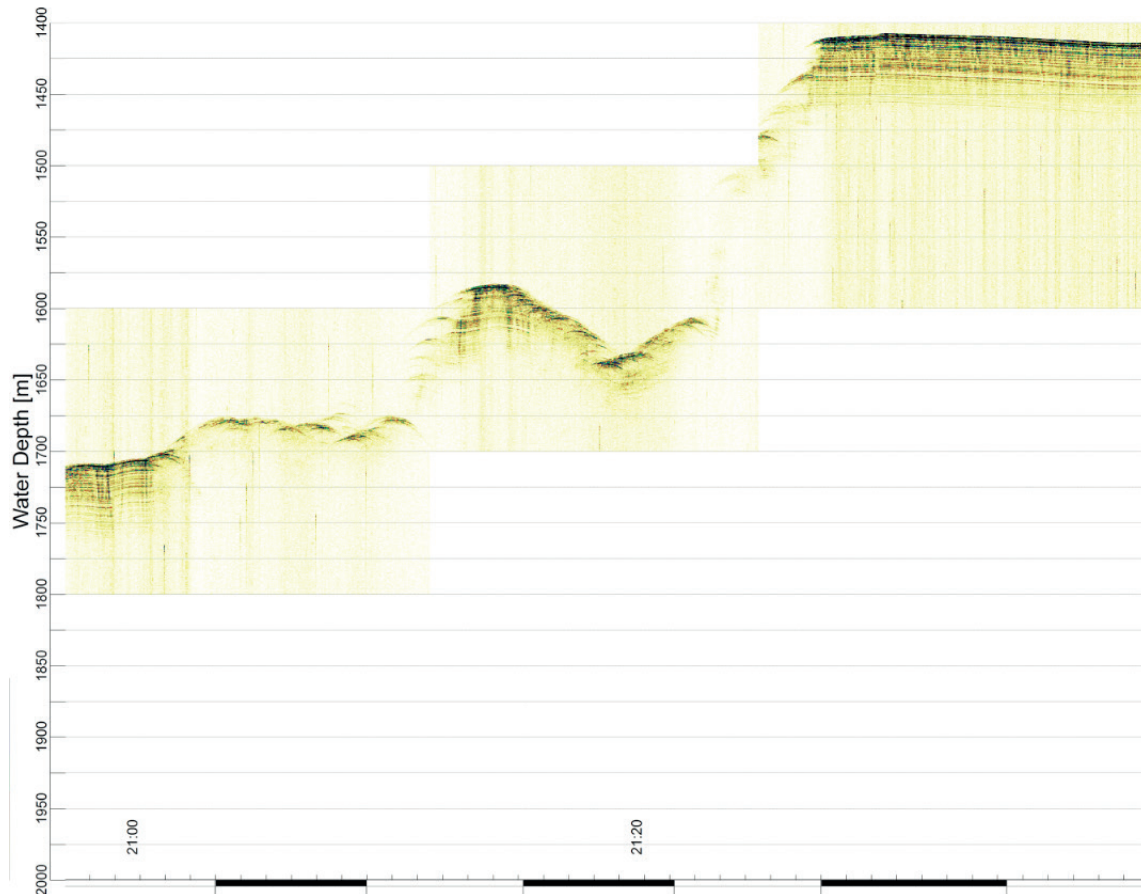


Fig. 10.2.5: PARASOUND example from the central Lomonosov Ridge. Positions of coring locations are described in text. The black and white bars at the bottom give lateral distance (1 km per bar). The depth has been determined by the PARASOUND system.

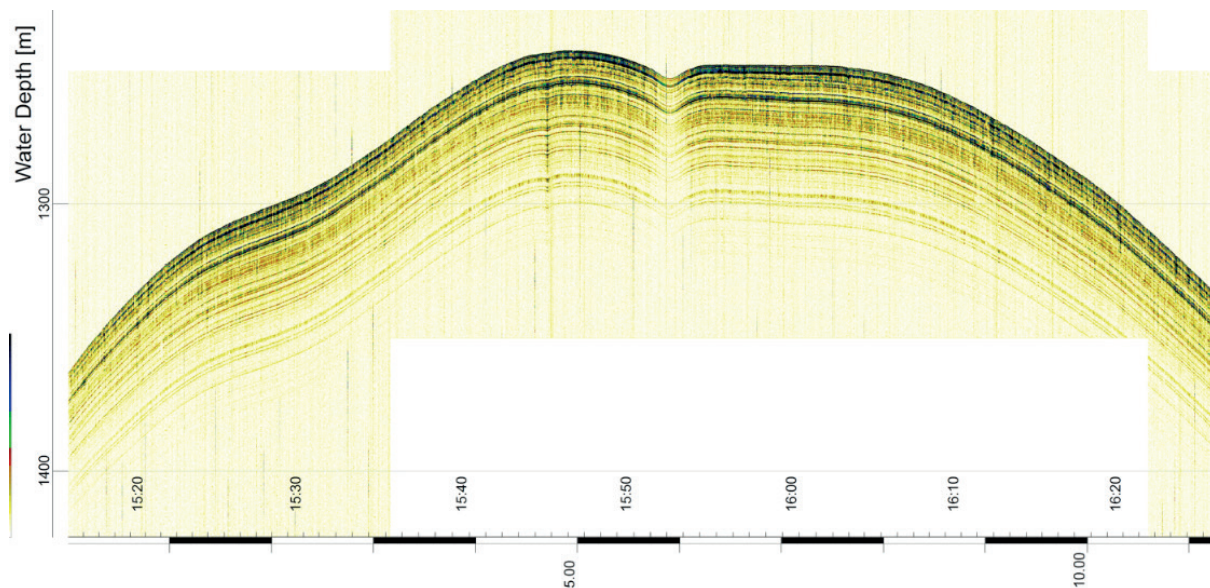


Fig. 10.2.6: PARASOUND example from the southern Lomonosov Ridge (Siberian side). Position of coring location PS87/109 is at the time marker 15:20 UTC. The black and white bars at the bottom give lateral distance in km. The depth has been determined by the PARASOUND system.

10.2 Sediment Echosounding using PARASOUND

On the Gakkel Ridge coring station PS87/110 was selected in one of the small deep basins, which characterize the ridge between 83° and 84° north. The position of the core is slightly above the deepest spot of the basin in 5,100 m water depth at the 12:00 time mark (Fig. 10.2.7). The echo character of the sediments in the basin is somewhat diffuse probably as a result of interfingering of bottom and side echoes. However, some stratification in the upper 20 m of the sedimentary record is visible at the coring site.

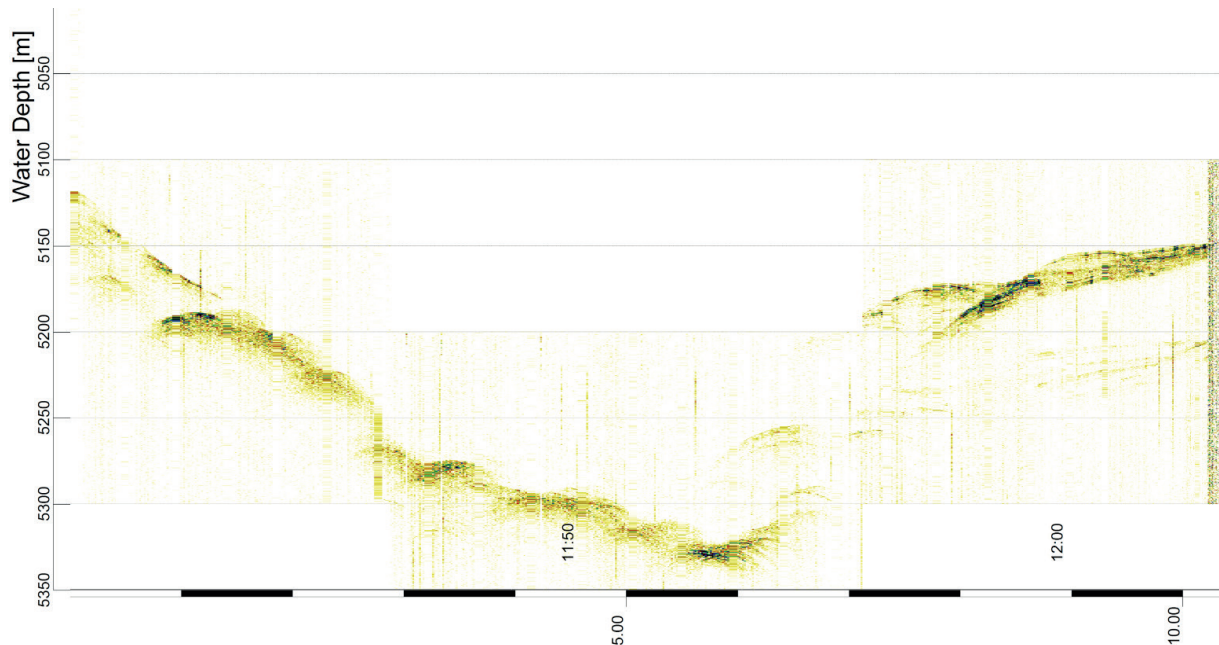


Fig. 10.2.7: PARASOUND example from the southern end of the Gakkel Ridge (Siberian side). Position of coring location PS87/110 is close to the time marker 12:00 UTC. The black and white bars at the bottom give lateral distance in km. The depth has been determined by the PARASOUND system.

For the time after the cruise it is expected that major results can be achieved with respect to correlating the acoustic (PARASOUND) stratigraphy of PS87 with those of previous *Polarstern* cruises in the same area. This will allow to transfer existing age models from cores of previous cruises into the PS87 sediment-echosounding records. Consequently this will aid to constrain the interpretation of spacial and temporal facies changes in the central Arctic Ocean. In particular, this will become important for the shallower parts of the LR, where hints were noted in the PARASOUND data, which will confirm and modify the view that ice has grounded on the LR in places, eroded older strata, and formed diamicton (e.g. Jakobsson et al. 2014).

Data Management

For the entire period of data acquisition five different types of data files were stored on hard disc:

- PHF data in ASD format
- PHF data in PS3 format
- SLF data in ASD format
- SLF data in PS3 format
- Navigation and Auxiliary data (60s intervals) in ASCII format
- ATLAS PARASTORE 3 settings in XML files

In total, 5 system crashes were observed during the cruise for no obvious reasons. Some data were lost (Tab. 10.2.2).

Tab. 10.2.2: PARASOUND system crashes and data gaps during PS87

Date	UTC Time	Remarks
16.08.14	14:22 - 15:00	ATLAS PARASTORE 3 crash
21.08.14	04:18 - 06:30	ATLAS PARASTORE 3 crash
29.08.14	14:37 - 15:37	maintenance on operator pc
16.09.14	14:47 - 15:02	ATLAS PARASTORE 3 crash
24.09.14	02:00 - 04:48	ATLAS Hydromap Server crash

All ASD data are automatically packed into “cabinet files” by Atlas software. The files are named according to date and time of recording (containing 10 minutes of acquired data per file). The data have been sorted by the operator into folders according to data type and recording dates (0 to 24 hours UTC), copied to the storage PC via LAN and checked for completeness and readability (ATLAS PARASTORE-3 in replay mode, selectively only). Once checked, the data folders were copied to *Polarstern* mass storage for daily back ups and final transfer into the AWI database after the end of cruise. In total data with a total volume of 538 GB were transferred. The data was ordered for final storage in the AWI data base (to be linked through PANGAEA) as illustrated in the following link (<https://spaces.awi.de/confluence/display/PSdevices/Sedimentecholot>).

During the entire period of acquisition the system was operator controlled (watch keeping). Book keeping was carried out including basic PARASOUND system settings, some navigation information, various kinds of remarks as well as a low-resolution hand-drawn bathymetry plot with preliminary data interpretation of SLF online profiles, which provides an overview about echo types and specific findings during the cruise.

Time windows with data of specific interest (e.g. geological situations at or near stations, special observations, key examples for different types of facies or stratigraphy) were selected and replayed during the cruise using optimal settings of ATLAS PARASTORE-3 and Software SeNT (courtesy of Hanno Keil, MARUM, University of Bremen).

List of Abbreviations

ASD	Atlas Sounding Data
PHF	Primary High Frequency
P-SBP	Parametric Sub-bottom Profiling
PS3	Export format of PARASOUND data
SBES	Single-Beam Echo-Sounder
SHF	Secondary High Frequency
SLF	Secondary Low Frequency
PNG	Portable Network Graphic

References

- Arndt JE, Niessen F, Jokat W, Dorschel B (2014) Deep water paleo-iceberg scouring on top of Hovgaard Ridge–Arctic Ocean, *Geophysical Research Letters*, 41 (14), pp. 5068-5074.
- Boetius A (in prep) The expedition of the research vessel "*Polarstern*" to the Arctic in 2014 (PS86) / Ed. by Antje Boetius with contributions of the participants. Reports on Polar and Marine Research.
- ATLAS Hydrographic (2007a) ATLAS HYDROMAP CONTROL Operator Manual. Doc.-Id.: ED 1060 G 312, File: ED-1060-G-312_V5-0. Edition: 04.2007. ATLAS HYDROGRAPHIC, Bremen, Germany.
- ATLAS Hydrographic (2007b) ATLAS PARASTORE-3 Operator Manual. Doc. Id.: ED 6006 G 212:/ Version: 4.0 / Edition: 05/2007. ATLAS HYDROGRAPHIC, Bremen, Germany.
- Jakobsson M, Andreassen K, Rún Bjarnadóttir L, Dove D, Dowdeswell JA, England JA, Funder S, Hogan K, Ingólfsson Ó, Jennings A, Krog-Larsen N, Kirchner N, Landvik JY, Mayer L, Mikkelsen N, Möller P, Niessen F, Nilsson J, O'Regan M, Polyak L, Nørgaard Petersen N, Stein R (2014) Arctic Ocean glacial history, *Quat. Sci. Rev.*, 92, 40-67
- Jokat W (2009) The expedition of the research vessel "*Polarstern*" to the Arctic in 2008 (ARK-XXIII/3) / Ed. by Wilfried Jokat with contributions of the participants. Reports on Polar and Marine Research, 597, pp 15-22.
- Macke A (2009) The expedition ANTARKTIS-XXIV/4 of the research vessel "*Polarstern*" in 2007 / Ed. by Andreas Macke with contributions of the participants. Reports on Polar and Marine Research, 591, pp 46-48.
- Niessen F, Matthiessen J, Stein R (2010) Sedimentary environment and glacial history of the Northwest Passage (Canadian Arctic Archipelago) reconstructed from high-resolution acoustic data, *Polarforschung*, 79(2), 65-80.
- Niessen F, Hong J K, Hegewald A, Matthiessen J, Stein R, Kim H, Kim S, Jensen L, Jokat W, Nam SI, Kang SH (2013) Repeated Pleistocene glaciation of the East Siberian continental margin, *Nature Geoscience*, 6 (10), pp. 842-846.
- Schiel S (2009) The expedition ANTARKTIS-XXIV/1 of the research vessel "*Polarstern*" in 2007 / Ed. by Siegrid Schiel with contributions of the participants. Reports on Polar and Marine Research, 592, pp 68-81.
- Spieß V (1992) Digitale Sedimentechographie - Neue Wege zu einer hochauflösenden Akustostratigraphie. Berichte aus dem Fachbereich Geowissenschaften der Universität Bremen, Nr.35, 199pp.

10.3 Physical properties and core logging

Frank Niessen¹, Michael Schreck²,
Tanja Hörner¹, Jens Matthiessen¹

¹AWI
²KOPRI

Objectives

Physical properties and spectral photometric data of sediments provide initial core characterization with a very high vertical resolution. Commonly physical properties and spectral photometric characteristics are measured with automated multi-sensor tracks such as the Multi Sensor Core Logger (MSCL) manufactured by GEOTEK Ltd. (UK). However, whereas physical properties are determined on whole cores, the spectral photometric characteristics are measured on the split core surface. Physical properties and reflectance spectra can be used to define and interpret stratigraphical patterns, including a comparison with lithology and other properties such as data obtained from XRF scanning. They are also useful to link the cores to high-resolution echosounding profiles obtained by systems such as the Parasound DSIII-P70 on *Polarstern* thereby aiding the projection of core data from a single spot into larger spatial and temporal scales.

During cruise PS87 a major goal of MSCL core logging is to provide high-resolution records of 1) density, sonic velocity, and loop magnetic susceptibility, and 2) of point magnetic susceptibility and spectral information. In the area of investigation, similar data were determined on cores retrieved during previous *Polarstern* cruises such as PS19 (Fuetterer 1992), PS36 (Rachor 1997), PS58 (Thiede 2002), PS78 (Schauer 2012). In combination with other data, down-core pattern of physical properties and spectral characteristics provide a powerful tool for lateral core correlation. The overall goal is to improve the stratigraphic framework along the Lomonosov Ridge as well as between the adjacent Amundsen and Makarov basin for a better understanding of the glacial and paleoceanographic history in this area of the Arctic Ocean.

In the following chapters we briefly describe the acquisition of the data for both whole core and split core logging during PS87, and provide a few examples based on preliminary results. For a more detailed description of the physical properties data acquisition the reader is referred to the cruise report of the RV *Araon* expedition ARA03B (Kang 2012). Descriptions of detailed analysis and core-to-core correlation are beyond the scope of this report and will be carried out after the cruise.

Work at sea

The physical properties have been measured on whole cores whereas spectral photometric characteristics and point magnetic susceptibility have been determined on split cores after opening, thus the following chapter is subdivided to account for the two different logging methods. Table 10.3.1 summarizes all logging activities carried out for the different cores onboard *Polarstern* during Expedition PS87.

10.3 Physical properties and core logging

Tab. 10.3.1: Summary of logging activities carried out during Expedition PS87

Station	Date	Time	Latitude	Longitude	Gear	Rec. [cm]	MSCL Logging	Geotek processed	K postprocessed	Excel Sheet
PS87/003-1	07.08.14	21:53	78° 24.12' N	1° 2.88' E	GKG		x	x		
PS87/003-2	07.08.14	23:12	78° 24.08' N	1° 2.77' E	GC	178	x	x		
PS87/023-1	18.08.14	16:00	86° 38.23' N	44° 53.98' W	KAL	698	x	x	x	
PS87/023-2	18.08.14	17:44	86° 37.86' N	44° 52.45' W	GKG		x	x		
PS87/026-1	20.08.14	07:54	87° 26.95' N	46° 33.95' W	GKG		x	x		
PS87/030-1	23.08.14	01:09	88° 39.72' N	61° 32.52' W	KAL	625	x	x	x	
PS87/030-2	23.08.14	02:11	88° 39.56' N	61° 29.20' W	GKG		x	x		
PS87/040-1	27.08.14	23:10	88° 59.31' N	171° 53.20' E	KAL	260	x	x		
PS87/040-2	28.08.14	00:45	88° 59.18' N	171° 44.50' E	GKG		x	x		
PS87/051-1	31.08.14	13:08	86° 26.98' N	147° 20.31' E	GC	495	x	x	x	
PS87/055-1	01.09.14	07:13	85° 41.47' N	148° 59.47' E	GKG		x	x		
PS87/056-1	01.09.14	20:31	85° 45.15' N	147° 57.24' E	KAL	234	x	x		
PS87/056-2	01.09.14	21:17	85° 45.07' N	147° 55.85' E	GKG		x	x		
PS87/067-1	03.09.14	21:33	83° 29.47' N	160° 34.29' E	GC	516	x	x		
PS87/067-2	03.09.14	23:09	83° 29.65' N	160° 35.36' E	GKG		x	x		
PS87/068-1	04.09.14	13:08	83° 37.89' N	154° 46.50' E	GC	588	x	x		
PS87/068-2	04.09.14	15:01	83° 37.70' N	154° 46.87' E	GKG		x	x		
PS87/070-1	06.09.14	09:26	83° 48.17' N	146° 7.01' E	KAL	770	x	x		
PS87/070-2	06.09.14	10:22	83° 48.16' N	146° 6.77' E	GKG		x	x		
PS87/074-1	09.09.14	08:11	82° 43.39' N	158° 37.49' E	GKG		x	x		
PS87/074-3	09.09.14	11:15	82° 43.12' N	158° 36.88' E	GC	615	x	x	x	
PS87/075-1	09.09.14	17:34	82° 51.49' N	155° 45.19' E	GC	573	x	x	x	
PS87/076-1	09.09.14	19:43	82° 53.80' N	154° 57.93' E	GC	622	x	x	x	
PS87/076-2	09.09.14	21:10	82° 53.81' N	154° 57.88' E	GKG		x	x		
PS87/078-1	10.09.14	05:39	83° 15.14' N	156° 48.17' E	GC	223	x	x	x	
PS87/079-1	10.09.14	17:26	83° 12.06' N	141° 22.77' E	KAL	664	x	x	x	x
PS87/079-2	10.09.14	18:22	83° 12.09' N	141° 22.92' E	GKG		x	x		
PS87/080-1	11.09.14	00:40	83° 12.26' N	141° 4.97' E	GC	454	x	x	x	
PS87/080-2	11.09.14	02:23	83° 12.28' N	141° 4.41' E	GC	350	x	x	x	
PS87/080-3	11.09.14	03:43	83° 12.27' N	141° 5.05' E	GC	460	x	x	x	
PS87/080-4	11.09.14	05:01	83° 12.30' N	141° 4.45' E	GC	485	x	x	x	
PS87/083-1	23.09.14	09:11	83° 12.26' N	141° 5.55' E	GC	479	x	x	x	
PS87/083-2	23.09.14	10:30	83° 12.23' N	141° 4.72' E	GC	465	x	x		
PS87/083-3	23.09.14	11:56	83° 12.24' N	141° 4.18' E	GC	401	x	x		
PS87/086-1	24.09.14	03:35	81° 13.04' N	141° 22.98' E	GKG		x	x		
PS87/086-3	24.09.14	04:28	81° 13.04' N	141° 23.02' E	GC	629	x	x	x	x
PS87/087-1	24.09.14	05:55	81° 12.29' N	141° 15.92' E	GC	594	x	x	x	x
PS87/088-1	24.09.14	07:22	81° 12.31' N	141° 16.40' E	GC	586	x	x	x	x
PS87/089-1	24.09.14	08:44	81° 12.35' N	141° 16.47' E	GC	294	x	x	x	x
PS87/090-1	24.09.14	10:01	81° 12.37' N	141° 16.87' E	GC	439	x	x	x	x
PS87/093-1	25.09.14	02:57	81° 12.48' N	141° 17.62' E	GC	673	x	x	x	x
PS87/094-1	25.09.14	04:16	81° 12.57' N	141° 18.49' E	GC	712	x	x	x	x
PS87/095-1	25.09.14	05:42	81° 12.64' N	141° 19.21' E	GC	478	x	x	x	x
PS87/096-1	25.09.14	06:51	81° 12.73' N	141° 20.04' E	GC	523	x	x	x	x
PS87/097-1	25.09.14	08:03	81° 12.37' N	141° 16.88' E	GC	578,5	x	x		
PS87/099-1	25.09.14	11:34	81° 25.50' N	142° 14.43' E	GC	447	x	x	x	
PS87/099-2	25.09.14	12:21	81° 25.49' N	142° 14.24' E	GC	464,5	x	x	x	
PS87/099-3	25.09.14	13:05	81° 25.48' N	142° 14.49' E	GKG		x	x		
PS87/100-1	25.09.14	15:52	81° 21.42' N	142° 35.46' E	GKG		x	x		
PS87/100-2	25.09.14	16:42	81° 21.41' N	142° 35.56' E	GC	483	x	x		
PS87/102-1	26.09.14	05:47	81° 12.86' N	141° 11.38' E	GC	678	x	x	x	
PS87/103-1	26.09.14	07:00	81° 12.84' N	141° 11.12' E	GC	353	x	x		
PS87/104-1	26.09.14	09:05	81° 12.80' N	141° 10.85' E	GC	317	x	x		
PS87/105-1	26.09.14	10:16	81° 12.78' N	141° 10.65' E	GC	88	x	x		
PS87/106-1	26.09.14	11:23	81° 12.76' N	141° 10.47' E	GC	486	x	x		
PS87/107-1	26.09.14	12:53	81° 12.74' N	141° 10.25' E	GC	556	x	x		
PS87/108-1	26.09.14	14:26	81° 12.79' N	141° 10.70' E	GC	129	x	x		
PS87/109-2	26.09.14	17:24	81° 7.70' N	140° 34.99' E	GC	617	x	x		
PS87/109-4	26.09.14	19:42	81° 7.69' N	140° 34.95' E	GKG		x	x		
PS87/110-1	27.09.14	13:08	81° 21.02' N	120° 31.47' E	GC	517	x	x		

A) Whole core logging

Whole core measurements in the ship laboratory included non-destructive, continuous determinations of core geometry (diameter), wet bulk density (WBD), P-wave velocity (Vp), and loop sensor magnetic susceptibility (MS) at 10 mm intervals on all cores obtained during the cruise. A standard MSCL track (GEOTEK Ltd., UK, Ser. No. 25) was used to measure temperature, core diameter, P-wave travel time, gamma-ray attenuation, and MS. The technical specifications of the MSCL system are summarized in Table 10.3.2. The principle of logging cores is described in more detail in the GEOTEK manual “Multi-Sensor Core Logging”, which

can be downloaded from the web (<http://www.geotek.co.uk>). The orientation of the P-wave and gamma sensors was horizontal. Gravity cores (SL) were measured in coring liners including end caps, whereas Kastenlot (KAL) cores were measured in sub-cores retrieved from the original core using length-wise open transparent plastic boxes of 1,000 mm nominal length (this also applies to the split core logging). In the following we summarize the data acquisition of the different sensors, data conversion to standard parameters and the calculation of secondary physical properties.

Geometry

The core diameter (SL including liner) and core width (KAL including sub-sample box) is measured as the distance between the faces of the Vp-transducers by using rectilinear displacement transducers coupled to the Vp transducers. The sediment thickness is measured as the deviation from a core reference similar in length as the core diameter/core width minus a user-defined constant value of two times the liner-wall thickness and box thickness, respectively. In case the cores are measured including the section caps, the thickness deviation caused by caps is added to the sediment thickness, because the software does not allow an extra input for wall thickness of the caps (plus tape). This has important implications for the determination of Vp and WBD at the end caps (see below). The geometry constants used to process the data are given in Table 10.3.3.

Three to five plastic cylinders were used to calibrate the core-diameter logging (Table 10.3.3). Using the GEOTEK Utility Software A/D readings were obtained from the test panel for each of these cylinders and plotted as a function of the deviation from the reference (Table 10.3.3). The resulting linear regression is put into the logger settings (<http://www.geotek.co.uk>) in order to log core-thickness deviation in mm as saved in the raw-data.

Tab. 10.3.2: Technical specifications of the GEOTEK MSCL-14 used during PS87

P-wave velocity and core diameter Displacement transducer orientation: horizontal Plate-transducer diameter: 40 mm Transmitter pulse frequency: 500 kHz Pulse repetition rate: 1 kHz Received pulse resolution: 50 ns Gate: 5000 Delay: 0 s
Density Radiation beam orientation: horizontal Gamma ray source: Cs-137 (1983) Activity: 356 Mbq (1993) Energy: 0.662 MeV Collimator diameter: 5.0 mm Gamma detector: Gammasearch2, Model SD302D, Ser. Nr. 3043, John Count Scientific Ltd., 15 s counting time
Temperature Sensor: PT-100
Magnetic susceptibility Loop sensor: BARTINGTON MS-2C Loop sensor diameter: 14 cm Alternating field frequency: 565 Hz, counting time 10 s, precision $0.1 \cdot 10^{-5}$ (SI) Magnetic field intensity: ca. 80 A/m RMS Counting time: 10 s

Tab. 10.3.3: Core-thickness calibration parameter used during PS87 (RCT = reference core thickness, W = wall thickness of liner or box, CYL = calibration cylinder).

	SL [mm]	KAL transparent [mm]	KAL grey [mm]
RCT	125.25	77.9	98.8
W	2 x 2.5	2 x 3	2 x 2.13
CYL 1	120.2	66.4	94
CYL 2	125.25	71.4	98.8
CYL 3	130.2	77.9	104
CYL 4		83	
CYL 5		88	

Density

Wet Bulk Density (WBD) was determined from attenuation of a gamma-ray beam transmitted from a radioactive source (^{137}Cs). A collimator was used to focus the radiation through the core-centre into a gamma detector (Table 10.3.2). To calculate density from gamma counts, GEOTEK-MSCL software was used (www.geotek.co.uk), which applies a 2nd order polynomial function to describe the relationship between the natural logarithm of gamma counts per second and the product of density and thickness of the measured material. For calibration, the three constants of the equation are determined empirically for each day by logging a standard core consisting of different proportions of aluminum and water as described in Best and Gunn (1999). The data of the standard stair-shaped blocks of aluminum logged in a liner (SL) or in transparent and gray boxes (KAL) filled with water are given in Tables 10.3.4 to 10.3.6.

One problem of the WBD data of SL is that there is no way in the GEOTEK software to correct for errors in the data introduced along the end caps of the liners. These errors are related to the increased diameter caused by the caps and by additional gamma attenuation by the caps (see geometry above). The GEOTEK processing software adds the thickness of the caps to the sediment thickness although the actual sediment core diameter will hardly vary at the caps compared to the rest of the core. This has the effect that the thickness in the product of density and thickness is too high and the calculated density is too low along the end caps. In order to correct the underestimated density we have defined the following approach:

$$\text{WBD}_c = \text{WBD} + ((x-d)/(d/100)*\text{WBD}/100-0.015)$$

WBD_c = corrected WBD (Fig. 10.3.1);

x = software determined sediment thickness along the end caps (after GEOTEK processing, Fig. 10.3-1);

d = as the mean sediment thickness of a core between the end caps (Fig. 10.3.1);

WBD = the bulk density along the end caps (after GEOTEK processing, Fig. 10.3.1);

0.015 is the assumed constant proportion of the WBD, which is related to increased attenuation through the walls of the caps (and tape).

Tab. 10.3.4: Thickness and density of gamma-attenuation calibration box (KAL, transparent) filled with stair-shaped block of aluminum in water. Density of aluminum: 2.71 g/cm³, density of water: 0.998 g/cm³, internal box width along gamma ray: 7.14 mm.

Aluminium Thickness [cm]	Average Density [g/cm³]	Av. Den. * Thickness [g/cm²]
7.02	2.68	19.14
6.58	2.57	18.38
5.76	2.38	16.98
4.93	2.18	15.56
4.12	1.98	14.17
3.29	1.79	12.75
2.48	1.59	11.37
1.65	1.39	9.95
0.93	1.22	8.72
0.00	1.00	7.13

For correcting the WBD of SL cores, software Kaleidagraph has been used. After determination of the mean core thickness between the caps (Fig. 10.3.1) core-thickness values along the caps were isolated using the graphical editor (> 11.81 mm in Fig. 10.3.1). The correction as described above was then only applied using the isolated values of sediment thickness so that all WBD values between the caps remained in their original values. The effect of the correction is illustrated in Fig. 10.3.1. WBD of SL retrieved during PS87 and given in final Kaleidagraph and Excel tables has been corrected for section-end caps.

Tab. 10.3.5: Thickness and density of gamma-attenuation calibration box (KAL, gray) filled with stair-shaped block of aluminum in water. Density of aluminum: 2.71 g/cm³, density of water: 0.998 g/cm³, internal box width along gamma ray: 9.45 mm.

Aluminium Thickness [cm]	Average Density [g/cm³]	Av. Den. * Thickness [g/cm²]
7.02	2.26	21.54
6.58	2.18	20.77
5.76	2.03	19.37
4.93	1.88	17.95
4.12	1.74	16.56
3.29	1.59	15.14
2.48	1.44	13.76
1.65	1.29	12.34
0.93	1.17	11.11
0.00	1.00	9.52

10.3 Physical properties and core logging

Tab. 10.3.6: Thickness and density of gamma-attenuation calibration liner (SL) filled with stair-shaped block of aluminum in water. Density of aluminum: 2.71 g/cm³, density of water: 0.998 g/cm³, internal liner diameter along gamma ray: 12.25 mm.

Aluminium Thickness [cm]	Average Density [g/cm³]	Av. Den. * Thickness [g/cm²]
10.00	2.40	29.35
9.01	2.26	27.65
8.01	2.12	25.94
7.01	1.98	24.22
6.00	1.84	22.49
5.01	1.70	20.80
4.00	1.56	19.08
3.01	1.42	17.37
2.00	1.28	15.64
1.01	1.14	13.96
0.00	1.00	12.23

Porosity

Fractional Porosity (FP) is the ratio of the total volume over the volume of the pores filled with water. FP determined by MSC-L-logging is not an independent data-acquisition parameter but can be calculated from the WBD as follows:

$$FP = (dg - WBD) / (dg - dw)$$

dg = grain density (2.7gcm-3);

dw = pore-water density (1.03gcm-3).

This approach makes the assumption that grain density and pore-water density are constant.

Temperature

Temperature (T) was measured as room temperature in air 20 cm above the floor of the logging lab, where the cores were stored for 24 hours before logging. The sensor was calibrated using water samples of known temperatures ranging from 15° to 35°C in a similar way than described for displacement transducers above. Temperature is measured to monitor core-temperature, which is needed by the GEOTEK Software to normalized Vp to 20°C.

Velocity

Sonic Compressional Velocity (Vp) was calculated from the core diameter/core width and travel time after subtraction of the P-wave travel time through the core liner wall (see geometry above), transducer, electronic delay, and detection offset between the first arrival and second zero-crossing of the received waveform (see GEOTEK Manual for details), where the travel time can be best detected. This travel-time offset was determined using a SL/KAL-liner filled with freshwater (Vp = 1481 m/s). There was no correction of Vp values possible along the end caps of core sections, because the arrival time of the acoustic pulse was not detectable through end caps. All false values at caps were eliminated.

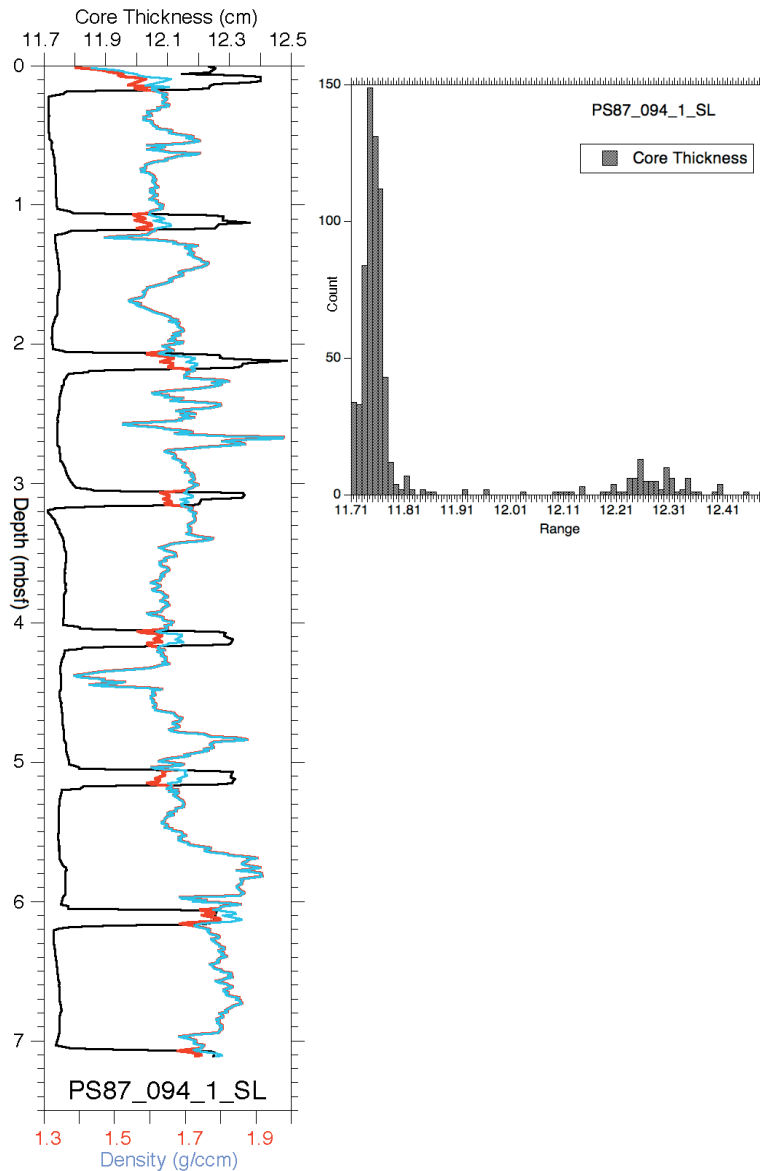


Fig. 10.3.1: Left: Core thickness (sediment thickness) and WBD (red curve is uncorrected, blue is corrected) of SL PS87/094-1 as a function of depth. Right: Range of core thicknesses of the same core to determine the mean core thickness between section end caps. Note that the section end caps are clearly indicated by increased thickness values > 11.81 mm.

Magnetic Susceptibility (MS)

The specifications of the Bartington MS-2 loop sensor used on board are summarized in Table 10.3.2. The MS-2 meter was set to zero 200 mm before the core reached the MS sensor. Sensor was checked for possible drift above the top and below the bottom of the core by logging a 200 mm long liner (SL) and a 500 mm long box (KAL), respectively, filled with water as initial and final calibration piece. Any drift observed, which was larger than 1 or -1, was corrected assuming a linear drift over the entire core length.

10.3 Physical properties and core logging

$$MS_{dc} = MS - CD \cdot (\text{Drift/Core Length})$$

MS_{dc} = the drift corrected MS;

MS = the MS raw data;

CD = depth in core (mbsf).

In order to calculate volume-specific magnetic susceptibility data are corrected for loop-sensor and core diameter as follows:

$$MS (10^{-6} \text{ SI}) = \text{measured value} (10^{-5} \text{ SI}) / K\text{-rel} \cdot 10$$

with K-rel empirically determined by GEOTEK (www.geotec.co.uk):

$$K\text{-rel} = 4.8566(d/D)^2 - 3.0163(d/D) + 0.6448$$

D = diameter of the MS-2 meter core loop (140 mm)

d = reference diameter of the core (Table 10.3.3).

For KAL-cores, the rectangular cross section of the core was equalized to a size-equivalent circular section, of which a fictive core diameter was calculated as input parameter for loop-sensor correction coefficient:

$$d_{KAL} = 2 \sqrt{a \cdot b / \pi}$$

The sediment height of KAL-cores (a) was measured for each section of KAL cores. The average height per core was used to calculate d_{KAL} . The width of KAL-cores (b) was averaged per core from the measured width at each logging interval by the MSCL.

B) Split core logging

Split core measurements in the shipboard laboratory included non-destructive, continuous determinations of point magnetic susceptibility (pMS) and reflectance spectra at 10 mm intervals on a standard MSCL-XZ track (GEOTEK Ltd., UK, Ser. No. 116). Split core logging was conducted only on selected box cores (GKG), gravity cores (SL), and Kastenlot (KAL) cores. The split core surface has been cleaned and smoothed, and covered by a standard foil to avoid contamination of the pMS sensor and spectrophotometer. To assure acquisition of high quality data, wrinkles and bubbles under the foil have been removed before the measurements.

Point magnetic susceptibility

The Bartington MS2 E point sensor provides high down core spatial resolution, as the active portion of the sensor is a narrow rectangle with a field of influence of approximately 5 mm. The measurement time was set to 10 seconds and the sensor was zeroed before every reading. Point magnetic susceptibility is reported in SI^{-5} with an accuracy of $\pm 4 \%$. For several reason

(see discussion below) it is not straightforward to calculate volume-specific susceptibility (e.g. SI⁻⁶) from point-sensor data. Calibration procedure for the point sensor includes a zeroing of the magnetic susceptibility and the measurement of a calibration sample with given magnetic signal (438×10^{-5} SI at 22°C).

Reflectance spectra

Reflectance spectra have been collected in 39 successive 10 nm spectral bands from the near UV through the visible and into the near IR range between 360 and 740 nm using the Konica Minolta colour spectrophotometer CM-2600d. To acquire reflectance data, a \varnothing 8 mm aperture (MAV) has been used. The spectrophotometer is calibrated internally by a white calibration tile and a zero reflectance 'free-air' reading. The internal software contains all necessary colorimetric equations to convert spectra into colour spaces, e.g. RGB, L*a*b*, XYZ and Munsell as output files.

Preliminary results

MS, pMS, WBD and reflectance spectra logs provide nearly complete records in all cores. Thus these parameters offer a good database for core correlation. Minor gaps of data are at or near the end of individual liner sections (see above). In case of split core logging for example, the first 2 and the last 2 measurements of each section had to be removed on average. Vp data have gaps of up to 80% in some cores mostly because sound propagation was not always possible through the core for reasons not yet known. In most cases, cross-correlations of data pairs of FP and Vp exhibit a negative correlation suggesting the relationship of second order polynomial functions (Fig. 10.3.2). This is similar to results from cores analyzed during the cruise ARK-XXIII/3 (Niessen et al. 2009). If determined for each individual core these functions can be used to calculate missing Vp data from porosity.

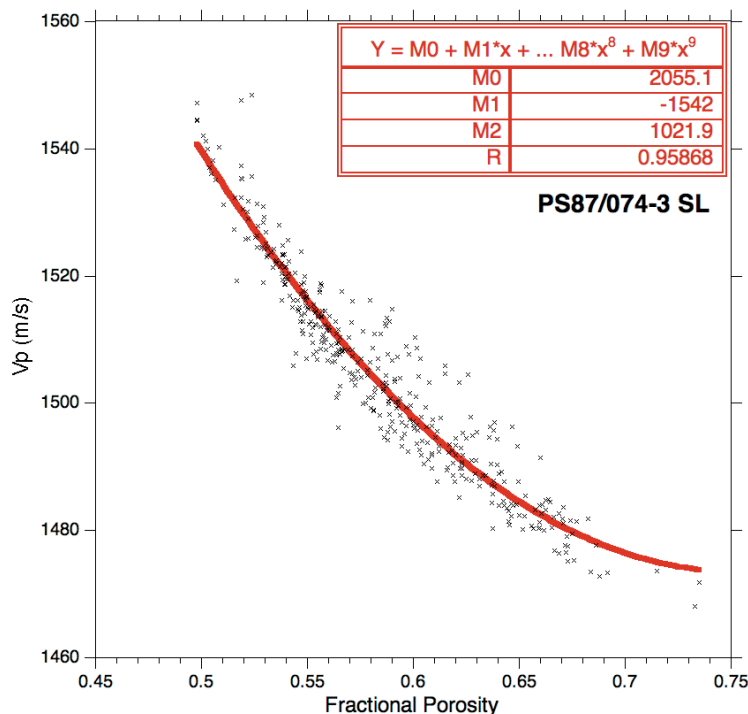
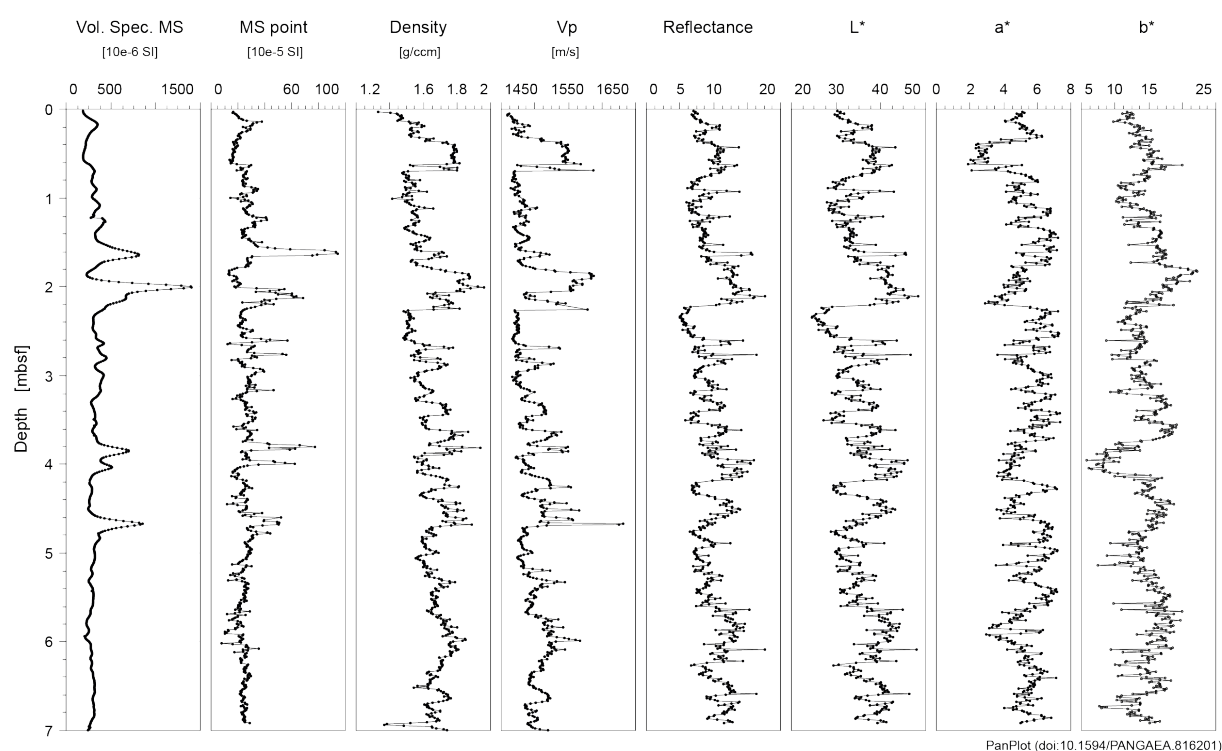


Fig. 10.3.2: Left: Core velocity (Vp) as a function of fractional porosity (FP) of SL core PS87/074-3. Note that there are in total 607 reliable values of FP but only 393 values of Vp (plotted versus FP) in this example.

10.3 Physical properties and core logging

In the following, Kastenlot core PS87/023-1 from the southern Lomonossov Ridge has been selected as an example to highlight the potential and application of these on-board generated, continuous high-resolution data (Fig. 10.3.3). Visual comparisons of point sensor data with those obtained by the loop sensor generally show a good correlation. However, a perfect correlation cannot be expected because the loop data is obtained from a larger core volume as the point data so that data from different material is compared. Also the effect of clasts in the core is more pronounced in loop data than in point data, because clasts may have been removed after splitting or are not directly measured with the point sensor. For this reason it is not straightforward to calculate volume-specific susceptibility from point-sensor data. The downcore variations in WBD are somewhat mirrored in the spectral data, with increased density corresponding to higher L^* (lightness) values but minima in the a^* (green-red) colour space. The combination of L^* and a^* values are particularly useful to identify the so called brown layers (Mn-rich interglacial deposits), which are of (litho-)stratigraphic importance in the Arctic Ocean, and a synthesis of spectral information and geochemical data as generated by continuous XRF scanning (see Chapter 10.4) may provide a good correlation tool. For a lateral correlation of cores in the Arctic Ocean, a combination of MS (point or loop), WBD and spectral information is therefore most promising.



PanPlot (doi:10.1594/PANGAEA.816201)

Fig. 10.3.3: Physical properties, reflectance spectra and $L^*a^*b^*$ values of Kastenlot core PS87/023-1 from the southern Lomonossov Ridge.

Data management

Data acquisition and processing of whole cores went through several steps:

- MSCL Raw-data acquisition of whole cores using GEOTEK software.
- First processing of whole-core data using GEOTEK software. This includes the calculation of core thickness, V_p , and WBD. MS sensor response remained in raw-data state (10^{-5} SI).

- - Second processing of whole-core data using software Kaleidagraph™. This includes a data quality control on calibration sections logged on top and below the bottom of the core (200 mm liner filled with water) and a removal of these data from the core. It also includes the removal of the liner caps from the depth scale and data cleaning for effects caused by liner caps on Vp and correcting WBD along the end caps. In addition, MS is corrected for sensor drift converted to volume specific MS (10⁻⁶ SI). Finally the impedance is calculated from Vp and WBD and the fractional porosity is calculated from the WBD data.
- - Conversion of the final K-graph table into an Excel sheet (xlsx or txt).

Data acquisition and processing of split cores went through following steps:

- MSCL-XZ raw-data acquisition of split cores using GEOTEK MSCL-XZ software.
- Export (as ASCII file) of split core data using GEOTEK software.
- Visual processing of split core data using software Kaleidagraph™. This includes a depth correction, e.g. the removal of the liner caps from the depth scale, and data cleaning for effects caused by gaps between successive liners, polystyrene fillings of coring gaps, or other disturbances of the split core surface (e.g. holes caused by drop stones etc.). Obvious outliers have been deleted from the data set.
- Plotting of core data using software Kaleidagraph™ and Adobe Illustrator

All data will be available to the shipboard science party for joint publication. In addition the data is stored as a function of core depth in the databank PANGAEA Data Publisher for Earth & Environmental Science (www.pangaea.de).

References

- Best AI, Gunn DE (1999) Calibration of marine sediment core loggers for quantitative acoustic impedance studies. *Marine Geology*, 160, 137-146.
- Fuetterer D (1992) ARCTIC'91: The expedition ARK-VIII/3 of RV *Polarstern* in 1991.
- Kang S-H 2012 Cruise Report: RV Araon ARA03B, August 1 – September 10, 2012: Chukchi Borderland and Mendeleev Ridge.
- Niessen F, Poggemann D, Schulte-Loh S (2009) Multi-sensor core logging. In: Jokat, W. (ed): The Expedition of the Research Vessel “*Polarstern*” to the Arctic in 2008 (ARK-XXIII/3). *Rep. Polar Mar. Res.*, 597.
- Rachor E (1997) Scientific cruise report of the Arctic Expedition ARK-XI/1 of RV “*Polarstern*” in 1995: German-Russian Project LADI: Laptev Sea - Arctic Deep Basin Interrelations.
- Schauer U (2012) The expedition of the research vessel “*Polarstern*” to the Arctic in 2011.
- Thiede J (2002) *Polarstern* Arktis XVII/2 - Cruise Report: Amore 2001.

10.4 Line-scan imaging and XRF scanning

Matthias Forwick¹,
Henriette Kolling²

¹UoTr
²AWI

10.4.1 Line-scan imaging

Objectives

Line-scan imaging was performed to document e.g. sediment colour, structures and lithological boundaries of split gravity cores, as well as kastenlot cores and box cores. The results shall be used for stratigraphic correlation (based on colour), as well as correlation with other proxies, e.g. micropalaeontology, element geochemistry or physical properties.

Work at sea

Line-scan images were acquired with a Jai CV L107 camera with RGB (red-green-blue) channels at 630 nm, 535 nm and 450 nm, respectively, mounted to an Avaatech XRF core scanner. The camera contains three CCD sensors and a beam splitter to separate the RGB signal. Images were acquired with a down-core resolution of approx. 70 μm . They were stored in *.bmp and *.jpg formats. The images have a fixed width of 15 cm and their lengths were adjusted depending on the lengths of the sections to be photographed. A total of 203 core sections was imaged, equaling approx. 180 meters. Section lengths varied between 12 and 101 cm. In addition to the virtual colour images, RGB, CIE-L*, a* and b* are available as *.txt files. However, these informations are obtained from the entire image width, i.e. they include also areas that were not covered with sediment core (e.g. ruler and core holders).

The light source was switched on at least 30 minutes prior to image acquisition to allow the light bulbs to warm up and stabilize. Furthermore, a white calibration, using a white tile, was carried out prior to every series of image acquisition. All images were acquired with aperture 11 and 10 ms exposure time. A ruler with mm-scale was placed along the imaged sections. Whenever possible, measurements were performed during transit in open water or during station work in the ice to minimize the negative effect of vibrations on image quality.

The sediment surfaces were cleaned and smoothed with a plastic card (credit card) across-core prior to image acquisition. The corners of the plastic cards were smoothed as thoroughly as possible. However, it could occasionally not be avoided that small incisions in the cards remained, resulting in thin visible stripes across the image, particularly in very fine grained and water-rich intervals (see example on Fig. 10.4.1C). Such stripes can easily be misinterpreted as lamination and caution should be given when analyzing images of such intervals.

Preliminary results

The quality of the images is generally very good. The majority of the imaged sediment is brown (see example on Fig. 10.4.1A). Beige, grey and green are sub-ordinate colours. The surfaces of intervals with high clast contents appear more irregular than intervals where clast numbers are low or absent (Fig. 10.4.1B).

In case sub-mm analyses of the images are planned, it should be noted that the vibrations of the ship led to quasi-continuous distortions of 3-5 pixels, i.e. up to 350 μm (Fig. 10.4.1D). Furthermore, it should be noted that the width of the gravity-core liners did not allow the numbers of the ruler to be entirely visible on the image. However, the upper parts of the numbers are visible and the distances between these are 10 mm (see example of ruler on Fig. 10.4.1D).

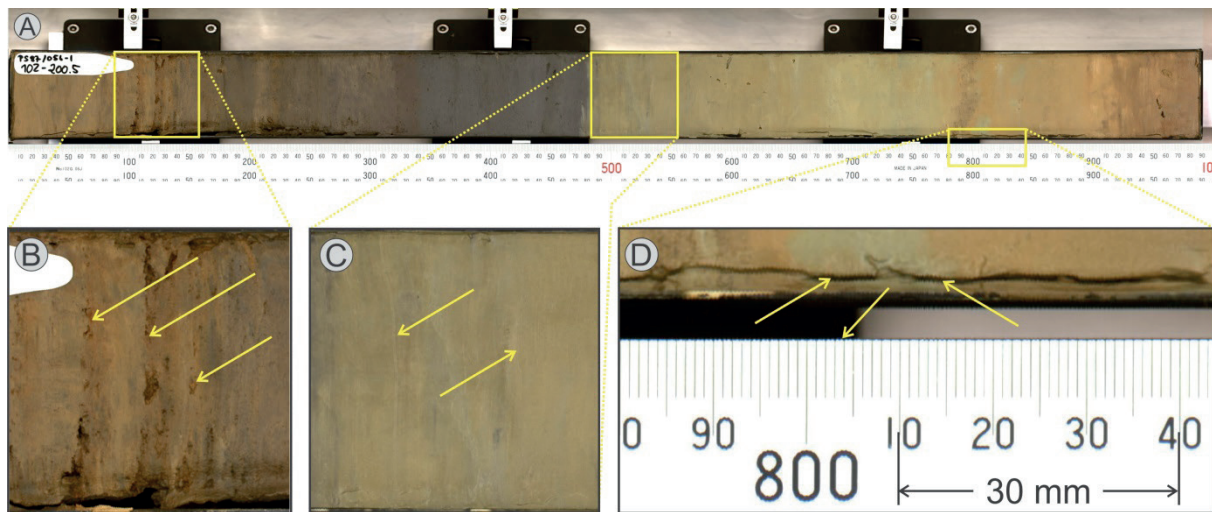


Fig. 10.4.1: A) Example of line-scan image from core PS87/056-1-KAL-OG-0102-0200.5 cm. B) Irregular sediment surface due to coarser sediment composition. C) Thin stripes resulting from irregularities in plastic card used for cleaning of surface. D) Irregularities caused by vibrations of the vessel.

Data management

The *.bmp, *.jpg and *.txt files will be made available in PANGAEA Data Publisher for Earth & Environmental Science .

10.4.2 XRF core scanning

Objectives

X-ray fluorescence (XRF) core scanning was performed to obtain an overview of the qualitative element-geochemical composition of sediment cores recovered during the expedition. The results shall contribute to multi-proxy reconstructions of palaeo-environmental conditions, as well as to identify sediment input from various circum-Arctic sediment sources. In geographically restricted areas, the results should provide a useful tool to establish chemo-stratigraphies that can be used for core correlation.

Work at sea

XRF core scanning was performed with an Avaatech XRF core scanner installed in a 20-foot container that was placed in the container storage room below deck in the front of *Polarstern*. Primary radiation was emitted from an Oxford 100 Watt water cooled X-ray source with a Rhodium anode and a 125 μm Beryllium window. The secondary radiation was detected with a digital Canberra X-PIPS detector with an electrically cooled Peltier system allowing an energy resolution down to 190 eV at 5.9 keV. Measurements were carried out through a helium-

flushed triangle system landing on the sediment surface to avoid measurement through air, the latter exposing much higher friction on the radiation than He, thus, leading to a reduction of the detected signal.

All measurements were carried out with a down-core resolution of 10 mm and cross-core resolution of 12 mm. The step sizes between the measurements were 10 mm, thus, providing continuous records. Measurements including core PS87/080-4-SL were carried out in three runs to excite light, medium and heavy elements, using the following settings: 10 kV, 1000 μ A, 10 seconds count time, no filter (1. run); 30 kV, 2000 μ A, 10 seconds count time, Pd-thick filter (2. run); 50 kV, 2000 μ A, 10 seconds count time, Cu filter (3. run; Tab. 10.4.1). However, due to time constraints, the measurement settings for the cores PS87/086-3-SL to PS87/096-1-SL had to be modified. For those cores, two runs with reduced count times were carried out to exclusively excite light and medium elements: 10 kV, 1000 μ A, 5 seconds, no filter (1. run); 30 kV, 2000 μ A, 5 seconds, Pd-thick filter (2. run; Tab. 10.4.1).

The X-ray source was turned on at least 30 minutes before the start of the measurements to provide sufficient time for heat-up. Prior to and after each measurement series three pressed pellets were measured to control the stability of the measuring setup, i.e. the stability of the X-ray source, the absence of leakage from the He-chamber and the function of the detector.

The sediment cores were stored in the container at least one day prior to the measurements allowing the material to adjust to room temperature. The surfaces were cleaned with a plastic card and covered with a 4 μ m thick ultralene foil to avoid contamination of the measurement triangle affecting further measurement.

A total of 203 core sections were scanned, resulting in approx. 47,800 point measurements. Section lengths varied between 12 and 101 cm.

After the measurements, the raw data were processed using WinAxil. The following models were applied:

PS87-10kV.Afm (including Mg, Al, Si, P, S, Cl, K, Ca, Ti, Cr, Mn, Fe, Rb, Rh)

PS87-30kV.Afm (including Cu, Zn, Ga, Br, Rb, Sr, Y, Zr, Nb, Mo, Ir, Pb, Bi)

PS87-50kV.Afm (including Ag, Cd, Sn, Te, Ba)

Preliminary results

The XRF core scanner performed very well, despite of the constant vibrations of the vessel, as well as repeatedly strong shaking during ice breaking. Only during very strong collisions with ice floes, the X-ray source turned off automatically (Tab. 10.4.1). The intensity of the X-ray source was only marginally reduced during the expedition. Communication errors between Scanner PC and the instrument occurred rarely (Tab. 10.4.1). Measurements were resumed from the depth where the X-ray source turned off or where communication errors occurred.

Tab. 10.4.1: Summary of PS87 cores that have been scanned onboard *Polarstern*. Different measurement settings are listed.

XRF core scanning	Measurement settings		Comments
	Setting 1	Setting 2	
Core no.			
PS87/003-1-GKG	X		
PS87/003-2-SL	X		
PS87/023-1-KAL-OG	X		X-ray source stopped repeatedly during the measurements at 10, 30 and 50 kV of section 0122-0221, due to very hard hits of ice floes. Measurements were resumed from the depth of the last reliable data point.
			X-ray source stopped repeatedly during the measurements at 30 and 50 kV of section 0221-0320, due to very hard hits of ice floes. Measurements were resumed from the depth of the last reliable data point.
			Communication error with scanner at 220 mm during 10 kV run of section 0320-0419 -> re-start of scanner and PC; X-ray source stopped at 850 mm during the 30 kV run, due to a very hard hit of an ice floe. Measurements were resumed from that depth.
			Communication error with scanner at 460 mm during 30 kV run of section 0420-0518.5 -> resumed scanning at that level
			X-ray source stopped 590 mm during the 30 kV run of section 0618-0698, due to a very hard hit of an ice floe. Measurements were resumed from that depth.
PS87/023-1-KAL-PP	X		The section 0501.5-0600 was scanned upside down on 20140822, due to wrong labelling. It was re-scanned on 20140825
			X-ray source stopped 730 mm during the 50 kV run of section 0600.5-0699, due to a very hard hit of an ice floe. Measurements were resumed from that depth.
PS87/023-2-GKG	X		
PS87/026-1-GKG	X		
PS87/029-1-GKG	X		
PS87/030-1-KAL-OG	X		
PS87/030-1-KAL-PP	X		
PS87/030-2-GKG	X		
PS87/040-1-KAL-OG	X		The section 0013-0061.5 was scanned upside down on 20140829, due to wrong labelling. It was re-scanned on 20140903
PS87/040-1-KAL-PP	X		
PS87/040-2-GKG	X		
PS87/051-1-SL	X		Scan interrupted & resumed at 30 kV, 290 mm during scanning of section 0000-0095 due to communication error
PS87/055-1-GKG	X		
PS87/056-1-KAL-OG	X		
PS87/056-1-KAL-PP	X		
PS87/056-2-GKG	X		
PS87/067-1-SL	X		
PS87/067-2-GKG	X		
PS87/068-1-SL	X		
PS87/068-2-GKG	X		
PS87/070-1-KAL-OG	X		Re-scan from 680 during 50 kV during measurement of section 0013-0111, due to X-ray turn-off after hitting an ice floe
			The section 0194-0272.5 was scanned upside down on 20140910, due to wrong labelling. It was re-scanned on 20140913
PS87/070-1-KAL-PP	X		
PS87/070-2-GKG	X		
PS87/074-1-GKG	X		
PS87/074-3-SL	X		
PS87/075-1-SL	X		The measurements with the file names "0000-0172" contained sections 0000-0080 and 0080-0172. The transition between the sections occurred around 800/810 mm
PS87/076-1-SL	X		The measurements with the file names "0000-0132" contained sections 0000-0034 and 0034-0132. The transition between the sections occurred around 350/360 mm
			Scan interrupted and resumed at 30 kV, 170 mm during scanning of section 0132-0221 due to communication error
PS87/076-2-GKG	X		
PS87/078-1-SL	X		
PS87/079-1-KAL-OG	X		Re-start of scanner and PC after communication error during scanning of section 0090.5-0189.5. The communication error was probably a result of too short distance between the sediment surface and the landing triangle when it was lifted up. The measuring unit skipped originally every second measurement over certain intervals. After the sediment surface was lowered, no measurements were skipped
			The section 0288.5-0387 was originally scanned up-side down due to wrong labelling. As this mistake was first observed after the core was frozen, a re-scan could not be performed. Therefore, all depths were re-calculated manually
PS87/079-1-KAL-PP	X		
PS87/079-2-GKG	X		
PS87/080-1-SL	X		
PS87/080-2-SL	X		
PS87/080-3-SL	X		The landing triangle did not find the surface at various depths in the interval 40-150 for all three runs during scanning of section 0000-0058 on 20140915. Therefore, this interval was re-scanned on 20140916
PS87/080-4-SL	X		
PS87/086-3-SL		X	
PS87/087-1-SL		X	
PS87/088-1-SL		X	Scan interrupted and resumed at 10 kV, 840 mm during scanning of section 0385-0486
PS87/089-1-SL		X	
PS87/090-1-SL		X	
PS87/093-1-SL		X	The measurements with the file names "0000-0171" contained sections 0000-0071 and 0071-0171. The transition between the sections occurred around 720/730 mm
PS87/094-1-SL		X	
PS87/095-1-SL		X	
PS87/096-1-SL		X	Scan interrupted and resumed at 30 kV, 90 mm during scanning of section 0000-0026
Setting 1: 10 kV, 1000 µA, 10 seconds count time, no filter (1. run); 30 kV, 2000 µA, 10 seconds count time, Pd-thick filter (2. run);			
50 kV, 2000 µA, 10 seconds count time, Cu filter (3. run)			
Setting 2: 10 kV, 1000 µA, 5 seconds, no filter (1. run); 30 kV, 2000 µA, 5 seconds, Pd-thick filter (2. run)			

Count rates varied during the measurements, particularly at section boundaries (Fig. 10.4.2B). However, decreases in count rates occurred also in relatively porous/coarse intervals or where the sediment surface was irregular so that the contact between the landing triangle and the sediment surface was reduced forcing the primary and/or secondary radiation to travel through air. To minimize the negative influence of such matrix effects, ratios or log-ratios of elements should be applied for future analyses (see Tjallingii et al. 2007; Weljite & Tjallingii 2008).

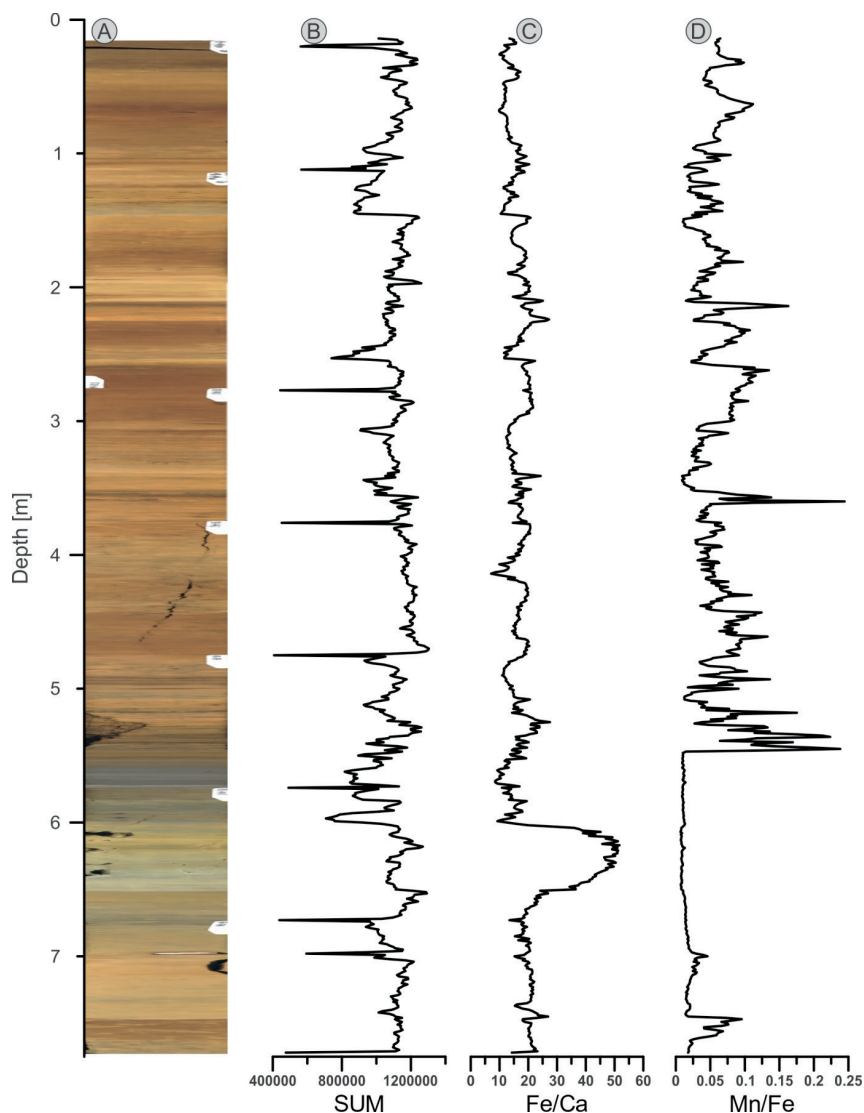


Fig. 10.4.2: A) Line-scan image of core PS87-070-1-KAL-OG. B) Sum of the 12 most abundant elements. C) Fe/Ca-ratio. D) Mn/Fe-ratio.

Certain correlation of sediment colour and changes in element ratios can be observed. Whereas the Mn/Fe ratio increases in dark brown intervals, the Fe/Ca ratio increases in light grey/beige intervals (see example from core PS87/070-1-KAL, Fig. 10.4.2C, 2D). However more extensive post-cruise work is needed to properly address the objectives mentioned above.

Data management

Raw data, processed data and models applied for data processing will be made available in PANGAEA Data Publisher for Earth & Environmental Science.

References

- Tjallingii R, Röhl U, Kölling M, Bickert T (2007) Influence of the water content on X-ray fluorescence core-scanning measurements in soft marine sediments. *Geochemistry, Geophysics, Geosystems*, 8, doi:10.1029/2006GC001393.
- Weltje GJ, Tjallingii R (2008) Calibration of XRF core scanners for quantitative geochemical logging of sediment cores: Theory and application. *Earth and Planetary Science Letters*, 274, 423-438.

10.5 Characteristics of surface sediments

Evgenia Bazhenova¹, Seung-il Nam²,
Robert Spielhagen³, Mike Zwick⁴

¹UoStP
²KOPRI
³GEOMAR
⁴UoBr

Objectives

Since there is a number of factors controlling provenance, accumulation and type of terrigenous input, understanding and quantification of these factors and their fingerprints in the sedimentary record of surface sediments provides the very basis for comparison with downcore data. In addition a detailed assessment of spatial and depth related changes of organism occurrence, abundance, diversity and potential for preservation is needed as a reference for palaeoenvironmental studies. Semi-quantitative analysis onboard and especially the following quantitative studies in the different labs will provide a valuable reference for downcore studies. Moreover this data will help to determine pelagic fluxes, benthic productivity and offer a first estimate in terms of selective dissolution.

Work at sea

During the PS87 (ARK-XXVIII/4) expedition near-surface sediments were taken by the giant box corer (GKG) at 20 geological stations from water depths of 730 to 3339 m (for locations see Fig. 10.1.2; Table 10.1.1). Recovery of the GKG cores ranged between 23 and 43 cm. Surface sediments were mostly undisturbed except PS87/023-2 and PS87/076-2.

After removal of excess water, pictures of the surface were taken, followed by the selection of organisms and fossils of size >2 mm. A preliminary description of the lithology was done visually, followed by a determination of colour using the Munsell Soil Colour Chart (1954). A detailed description of colour and lithology of all box cores is given in the Annex. The characteristics of surface sediments (0-1 cm) recovered by GKG are summarised in Table 10.5.1.

Surface sediments were sampled using iron or plastic (for future geochemical analysis) spoons and 50-1,000 ml beakers according to the needs of each scientist. The coarse fraction (>63 µm) was isolated by means of wet sieving. Results of preliminary coarse-fraction analysis are summarized in Table 10.5.2 and 10.5.3. The biogenic composition of surface samples is plotted in Fig. 10.5.1, followed by the abiogenic content in Fig. 10.5.2.

Preliminary (expected) results

Surface sediments in most cases were dark brown and in a few cases dark greyish brown (PS87/003-1, PS87/076-2) and very dark greyish brown (PS87/026-1) whereas no spatial or depth-related pattern is recognisable (Table 10.5.1). The lithology of most cores is silty clay with some sand or sand admixture, with the exception of PS87/003-1 (silty clay, gravel), PS87/023-2 (silty clay, sand admixture, dropstones up to 12 cm Ø) and PS87/026-1, PS87/055-1, PS87/086-1 (silty clay, at the latter station with very small amounts of sand).

Tab. 10.5.1: GKG surface description with lithology, colour and remarks

Station	Depth [m]	Location	Recovery [cm]	Description of GKG surface sediments		
				Colour	Lithologie	Remarks
PS87/003-1	1170	Hovgaard Ridge	34	dark greyish brown (10 YR 4/2)	silty clay, gravel	polychaetes, ophiurid
PS87/023-2	2439	Lomonosov Ridge (Amundsen Basin)	36	dark brown (10 YR 3/3)	silty clay, sand admixture, dropstones up to 12 cm Ø	bivalve shells, organisms living on stones, surface disturbed
PS87/026-1	3339	Lomonosov Ridge (Amundsen Basin)	40	very dark greyish brown (10 YR 3/2)	silty clay	Water-saturated, bivalve shells
PS87/029-1	2901	Lomonosov Ridge (Amundsen Basin)	41	dark brown (10 YR 3/2)	silty clay, sand admixture	fragment of calcareous shell
PS87/030-2	1278	Lomonosov Ridge (Amundsen Basin)	36	dark brown (10 YR 3/3)	silty clay, sand admixture	water-saturated, polychaets, bivalvia shells, gastropod shells, dropstones with remains of organisms on the surface, dropstones up to 6 cm Ø, clasts of biogenic ooze?
PS87/035-2	-	Lomonosov Ridge (Amundsen Basin)	-	-	-	-
PS87/040-2	2618	Lomonosov Ridge (Intrabasin)	37	dark brown (10 YR 3/3)	silty clay, some sand	water-saturated, fragments of shells
PS87/055-1	730	Lomonosov Ridge (central)	39	dark brown (10 YR 3/3)	silty clay	polychaets, bivalve/brachiopod shells
PS87/056-2	836	Lomonosov Ridge (central)	40	dark brown (10 YR 3/3)	silty clay with some sand	rich fauna: polychaets, bivalve, gastropod scaphopod and brachiopod shells
PS87/067-2	2857	Lomonosov Ridge (Makarov Basin)	37	dark brown (10 YR 3/3)	silty clay, some sand	very soft, bivalve shells, foraminifers, bioturbated (worm traces, clasts)
PS87/068-2	2711	Lomonosov Ridge (Makarov Basin)	23	dark brown (10 YR 3/3)	silty clay, some sand	mud clasts, bivalve shells up to 1.5 cm Ø, polychaets.
PS87/070-2	1340	Lomonosov Ridge (central)	42	dark brown (10 YR 3/3)	silty clay, some sand	water-saturated, sea cucumber; shell half
PS87/074-1	2816	Lomonosov Ridge (Makarov Basin)	36	dark brown (10 YR 3/3)	silty clay, sand admixture	water-saturated, mud clasts, sponges, gastropod shells, foraminifers
PS87/076-2	2763	Lomonosov Ridge (Makarov Basin)	37	dark greyish brown (10 YR 3/2)	silty clay, some sand	mud clasts, shells; surface and sediment core disturbed by coring
PS87/079-2	1359	Lomonosov Ridge (central)	43	dark brown (10 YR 3/3)	silty clay, some sand	mud clasts, shells, bivalve shells, polychaets, foraminifers, copepods, fragments of other shells up to 2 cm Ø
PS87/086-1	901	Lomonosov Ridge (central)	36	dark brown (10 YR 3/3)	silty clay, very small amount of sand	water-saturated, polychaets, Bivalvia (shell halves)
PS87/099-3	741	Lomonosov Ridge (Makarov Basin)	36,5	dark brown (10 YR 3/3)	silty clay, some sand	water-saturated, polychaets, shell fragments
PS87/100-1	951	Lomonosov Ridge (Makarov Basin)	39	dark brown (10 YR 3/3)	silty clay, some sand	Water-saturated, polychaets, shell up to 4 cm Ø
PS87/109-4	1303	Lomonosov Ridge (central)	37	dark brown (10 YR 3/3)	silty clay, some sand	Water-saturated, polychaets, shell halves

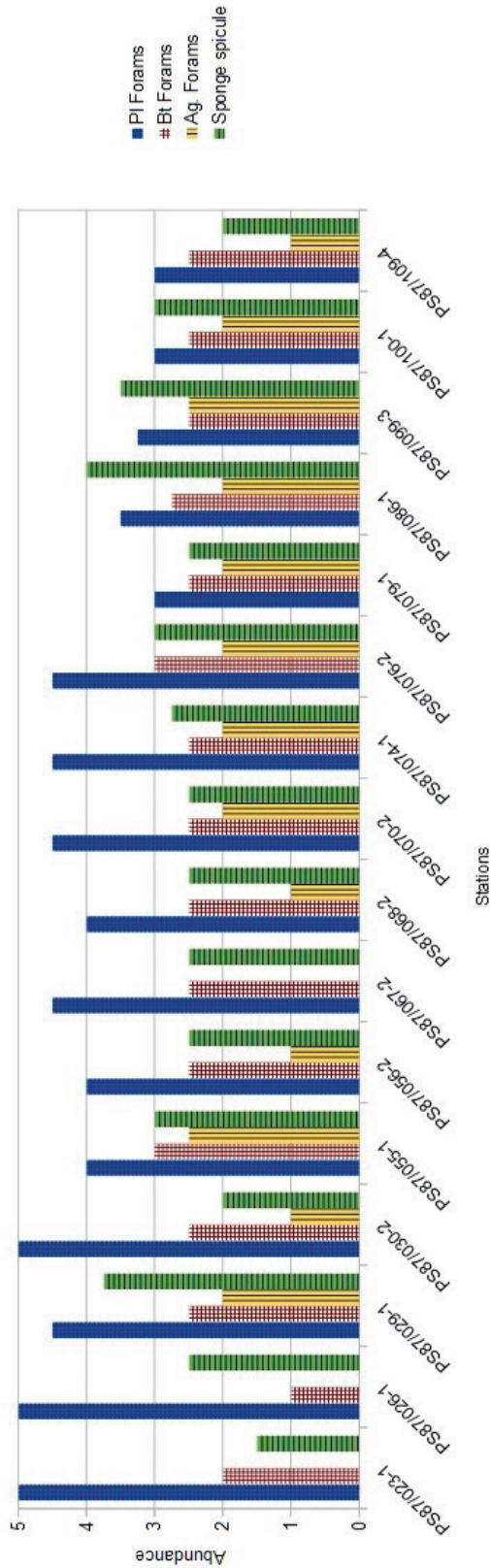


Fig. 10.5.1. Biogenic particles of processed GKG samples showing the abundance of planktic foraminifers (PI Forams), benthic foraminifers (Bt. Forams), agglutinated foraminifers (Ag Forams) and sponge spicules. Scale: 0=barren, 1=very rare, 2=rare, 3=common, 4= abundant, 5=dominant.

10.5 Characteristics of surface sediments

Tab. 10.5.2: Biogenic particles of processed GKG samples showing the abundance of planktic foraminifers (Pl Forams), benthic foraminifers (Bt. Forams), agglutinated foraminifers (Ag Forams) and sponge spicules. Scale: 0=barren, 1=very rare, 2=rare, 3=common, 4= abundant, 5=dominant. In addition, it shows the presence/absence of radiolarians, echinoderms, shells and bryozoa.

PS87 biogenic particles >63µm of GKG samples										
Station	Depth	Pl Forams	Bt Forams	Ag. Forams	Ostracodes	Sponge spicules	Radiolarians	Echinoderms	Shells	Bryozoa
PS87/023-1	2439	5	2	0	1	1,5			p	
PS87/026-1	3339	5	1	0	1	2,5				
PS87/029-1	2901	4,5	2,5	2	1	3,75				
PS87/030-2	1278	5	2,5	1	1	2			p	
PS87/055-1	730	4	3	2,5	2,5	3		p	p	p
PS87/056-2	836	4	2,5	1	1	2,5	p		p	
PS87/067-2	2857	4,5	2,5	0	0	2,5	p			
PS87/068-2	2711	4	2,5	1	1	2,5	p			
PS87/070-2	1340	4,5	2,5	2	1,5	2,5			p	
PS87/074-1	2816	4,5	2,5	2	0	2,75	p			
PS87/076-2	2763	4,5	3	2	0	3				
PS87/079-1	1359	3	2,5	2	1,5	2,5			p	
PS87/086-1	901	3,5	2,75	2	2	4	p	p	p	
PS87/099-3	741	3,25	2,5	2,5	1	3,5		p	p	
PS87/100-1	951	3	2,5	2	0	3		p	p	
PS87/109-4	1303	3	2,5	1	1	2		p	p	
p=present	0=absent	1=very rare	2=rare	3=common	4=abundant	5=dominant				

Tab. 10.5.3: Abiogenic particles of processed GKG samples showing the abundance of rock fragments (Rock Frag), mica, basalt, carbonate, heavy minerals (H. Mineral) and manganese nodules (M. Nodules). Scale: 0=barren, 1=very rare, 2=rare, 3=common, 4= abundant, 5=dominant.

PS87 abiogenic particles >63µm of GKG samples							
Station	Depth	Rock Frag	Mica	Basalt	Carbonate	H. mineral	M. nodules
PS87/023-1	2439	2	1	1	1	0	0
PS87/026-1	3339	0	0	0	0	0	0
PS87/029-1	2901	0	1	0	0	0	0
PS87/030-2	1278	2	1	0	2	0	0
PS87/055-1	730	2	1	0	2	0	0
PS87/056-2	836	1	1	0	1,5	1	0
PS87/067-2	2857	2	1	0	0	0	0
PS87/068-2	2711	2	1	0	0	1	1
PS87/070-2	1340	2	1	0	0	1	0
PS87/074-1	2816	2	2	0	0	2	0
PS87/076-2	2763	2	0	0	0	2	0
PS87/079-1	1359	2,5	1	0	0	2,5	0
PS87/086-1	901	2,5	1	1	0	2,5	0
PS87/099-3	741	2,75	1	2	2	2,5	0
PS87/100-1	951	2,5	1	1	0	2,75	0
PS87/109-4	1303	2,5	2	2	1	2,75	0
p=present	0=absent	1=very rare	2=rare	3=common	4=abundant	5=dominant	

The surface was always water-saturated and the >2mm benthic fauna often was dominated by polychaets and increased in diversity with the decrease of water depth. Other common organisms were bivalves, scaphopods and brachiopods. Shell fragments, gastropods and copepods also were reported. At station PS87/070-2, a sea cucumber was found on the surface. For a detailed analysis of organism assemblages see Chapter 10.8.

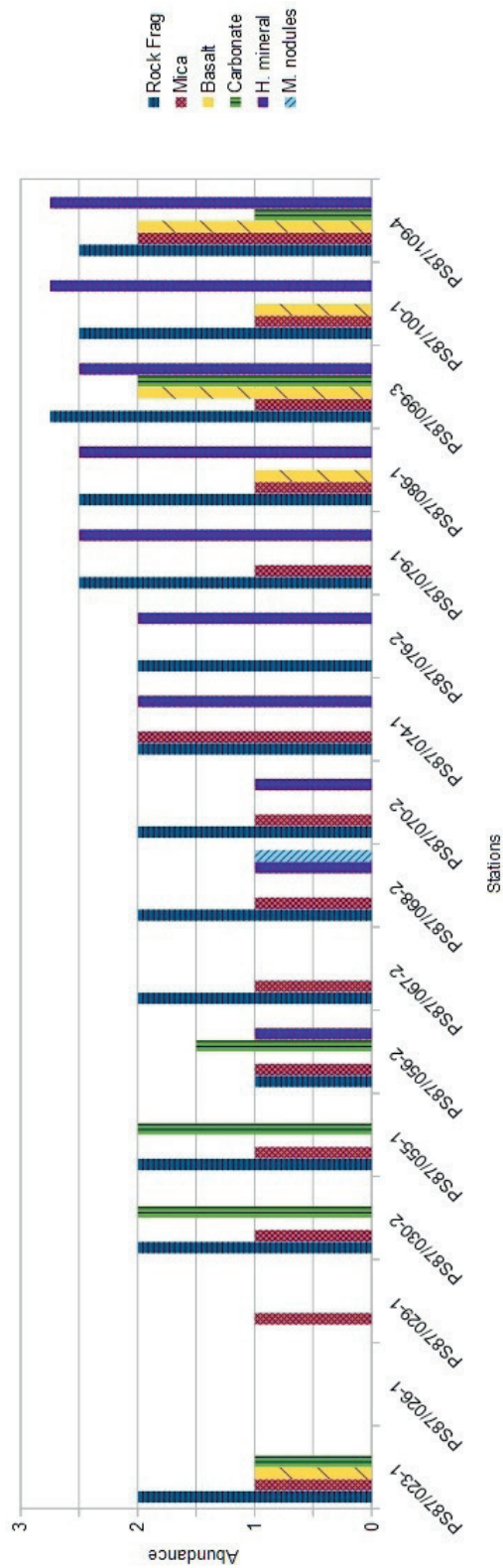


Fig. 10.5.2. Abiogenic particles of processed GKG samples showing the abundance of rock fragments (Rock Frag), mica, basalt, carbonate, heavy minerals (H. Mineral) and manganese nodules (M. Nodules). Scale: 0=barren, 1=very rare, 2=rare, 3=common, 4= abundant, 5=dominant.

The results of the analysis of the >63µm biogenic fraction are shown in Fig. 10.5.1 and Table 10.5.2). Planktic foraminifera are in general abundant but decrease in direction to the Siberian continental margin (PS87/079-1, PS87/086-1, PS87/099-3, PS87/100-1, PS87/109-4). Sponge spicules are rare to abundant with two maxima at PS87/029-1 and PS87/086-1. Benthic foraminifera are rare to common without a recognisable trend and have two maxima at stations PS87/055-1 and PS87/076-2. Agglutinated foraminifera were also found but their abundance is low (very rare to rare) with two maxima at PS87/055-1 and PS87/099-3. Ostracodes were also observed but only a semi-quantitative estimate was done which showed that they occur in every sample but in varying diversity.

The abiogenic fraction shows some distinctive changes (Fig. 10.5.2 and Tab. 10.5.3). Although in most samples rock fragments are rare, their amount slightly increases from station PS87/079-1 to PS87/109-4. The situation is similar concerning the heavy minerals which first occur in PS87/056-2 and continuously increase starting at PS87/074-1 (rare), reaching a maximum (almost common) at PS87/100-1 and PS87/109-4. Basalt fragments occur in rare amounts at stations PS87/023-1, PS87/086-1, PS87/100-1 and have two maxima at PS87/099-3 and PS87/109-4. Carbonate rock fragments are generally very rare or absent and found in rare amounts at stations PS87/030-2, PS87/055-1 and PS87/099-3.

Data management

All preliminary results of the coarse fraction analysis will be stored in the PANGAEA Data Publisher for Earth & Environmental Science. The sieved sand fractions will be stored at Department of Marine Geology and Paleontology of the AWI.

10.6 Main lithologies and lithostratigraphy of PS87 sediment cores

Rüdiger Stein ¹ , Evgenia Bazhenova ² ,	¹ AWI
Seung-il Nam ³ , Frank Niessen ¹ , Matthias	² UoStP
Forwick ⁵ , Anne de Vernal ⁶	³ KOPRI
	⁴ GEOMAR
	⁵ UoT
	⁶ GEOTOP

10.6.1 Results of smear-slide analysis

Evgenia Bazhenova ¹ , Anne de Vernal ²	¹ UoStP
	² GEOTOP

Objectives

Smear slides are used for preliminary investigation of grain-size and mineral composition of sediments as well as for examination of biogenic components. For preparation of smear slides, tooth-pick amounts are taken from selected fine-grained sediments avoiding coarse-grained layers. Therefore, the obtained results are discrete and should be used as complementary information to the lithological descriptions of the cores (see below).

Work at sea

During the PS87 (ARK-XXVIII/4) Expedition a set of smear slides was prepared following instructions described in details in the IODP Technical Note (2013). The optical adhesive used for mounting slides was Nordland 61, which has a refractive index $n=1.56$.

Smear-slides were studied using the petrographic microscope Leitz Laborlux 11 POL using the oculars of 10x magnification. Grain-size distribution was analyzed by rough estimating the sand ($> 63 \mu\text{m}$) and silt (2-63 μm) contents. Quantification was normally performed using the ocular scale at 10x, and when necessary at 25x and 63x magnification. The amount of clay was calculated by normalization to 100 %. Semi-quantitative estimations were made for abiogenic and biogenic components in the sand and silt fractions using standard comparator charts for sedimentary rocks. The biogenic components were also tentatively examined. For coccoliths, we used polarized light and high magnification (63x). The observation of other biogenic remains, which included foraminifers, diatoms and sponge spicules were made in transmitted light microscopy at magnification of 25x. However, presence of coccoliths should be verified by a specialist using higher magnification.

Preliminary (expected) results

Based on the smear-slide analysis, the main minerals in the sand and silt fraction are quartz, feldspars and mica. Fe-hydroxides are also often present. Terrigenous carbonates (mainly dolomite) are abundant only in specific layers, normally expressed in pinkish colour of sediments. Rock fragments often have siliceous composition (chert). The heavy minerals include hornblende, pyroxene, epidote, garnets, zircon, and black ores. The results of smear-slide description (generally representing summarized composition of sand and silt fractions, if not commented differently) are reported in Figs 10.6.1-10.6.6 and in the Appendix, Tables A5.2.1 – A5.2.8.

The sand size ($> 63 \mu\text{m}$) biogenic components of sediments from Kastenlot cores PS87/023-1, PS87/030-1, PS87/070-1 and PS87/079-1 were described in the *Micropaleontology and Biostratigraphy* chapter (Chapter 10.8). Therefore their distribution in smear slides will not be

10.6 Main lithologies and lithostratigraphy of PS87 sediment cores

discussed here, with exception of coccoliths which require high magnification and polarized microscopy due to their small size (2-10 μm).

36 smear slides were studied from core PS87/023-1 KAL. Results are summarized in Table A5.2.1 and Fig. 10.6.1. Sediments can be classified as silty clay. Carbonate-rich layers containing more than 5% terrigenous carbonates (mainly in the silt fraction) were observed at 92.5, 164, 281, 363, 381 and 598 cm core depth. Some smear slides contain coccoliths, mostly in the upper part of the core, but also in a few intervals downcore. Very rare and discontinuous occurrences are noted down to ~326 cm and common occurrences are noted at between 130 and 140 cm.

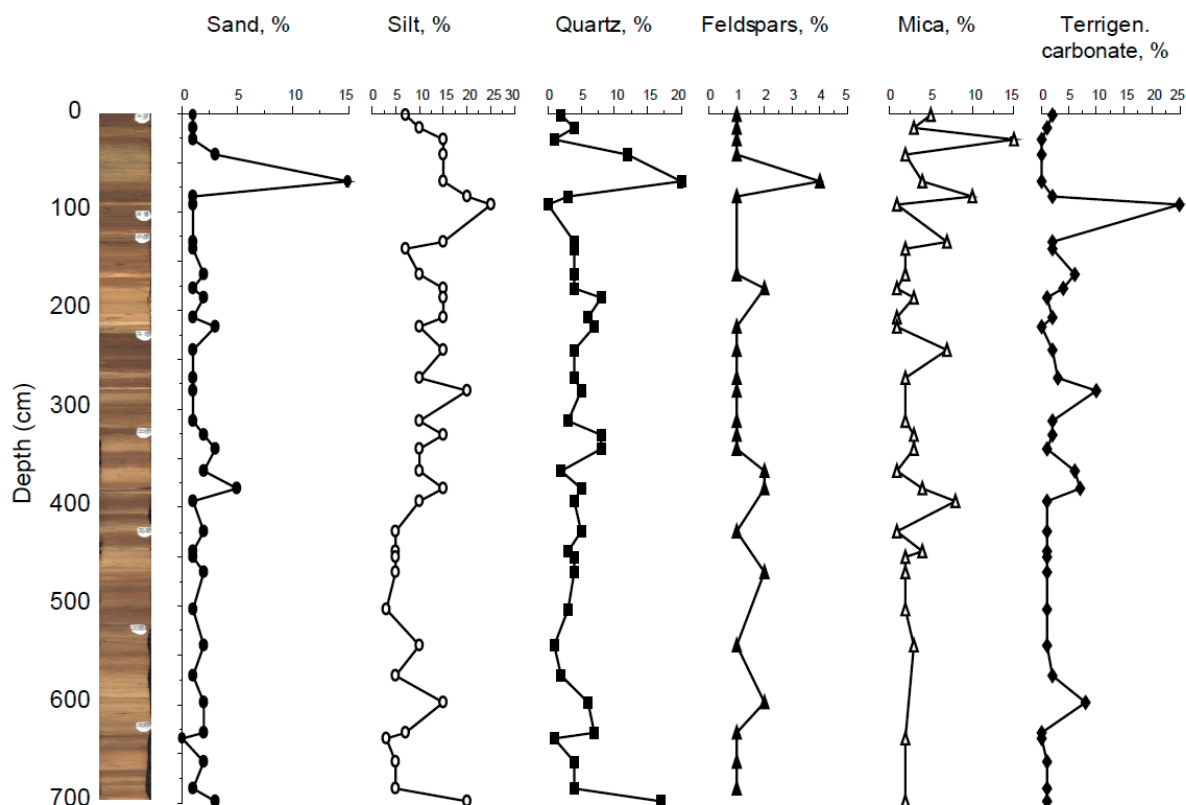


Fig. 10.6.1: Grain-size and major abiogenic components distribution in core PS87/023-1

29 smear slides were studied from core PS87/030-1 KAL. Results are summarized in Table A5.2.2 and Fig. 10.6.2. Carbonate-rich layers containing more than 5% terrigenous carbonates (mainly in the silt fraction) were observed at 90, 117, 216 and 222 cm core depth. Very rare and discontinuous occurrences of coccoliths are noted down to ~268 cm.

14 smear slides were studied from core PS87/040-1 KAL. Results are summarized in Table A5.2.3 and Fig. 10.6.3. Sediments can be classified as silty clay. Studied intervals contain very low amount of terrigenous carbonates. Remains of calcareous microfossils were observed at 13 (benthic foraminifers), 22 (benthic and planktic foraminifers and rare coccoliths) and 43 cm core depth.

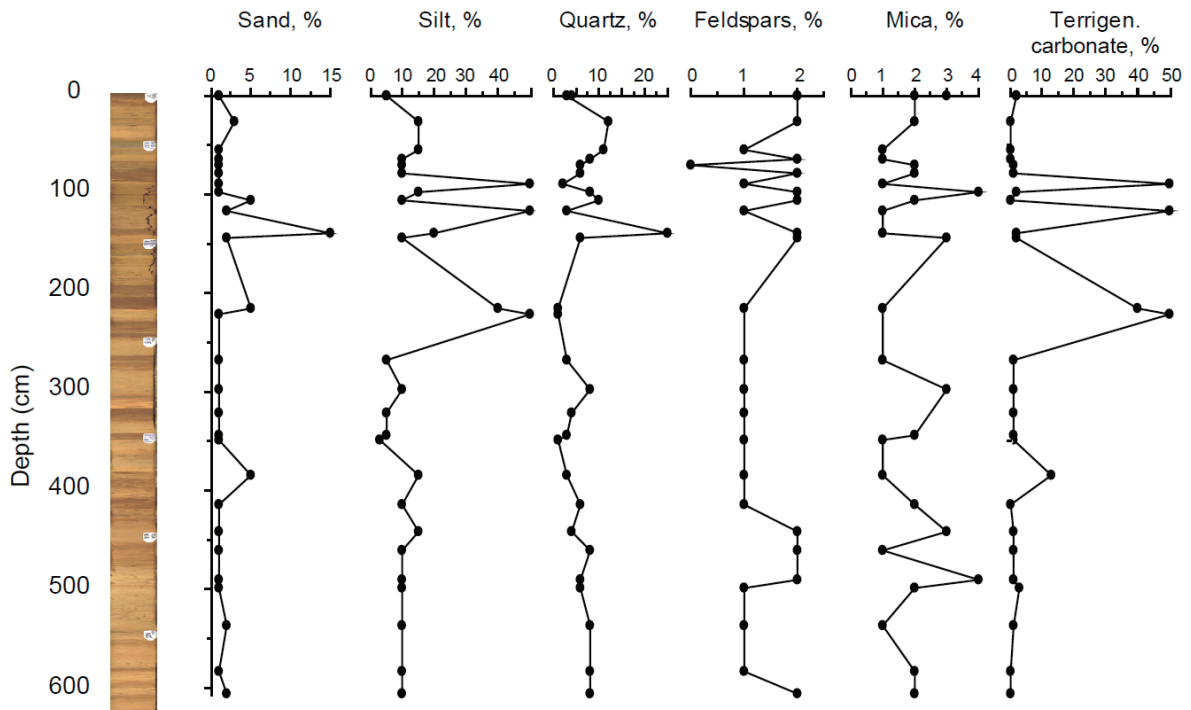


Fig. 10.6.2: Grain-size and major abiogenic components distribution in core PS87/030-1

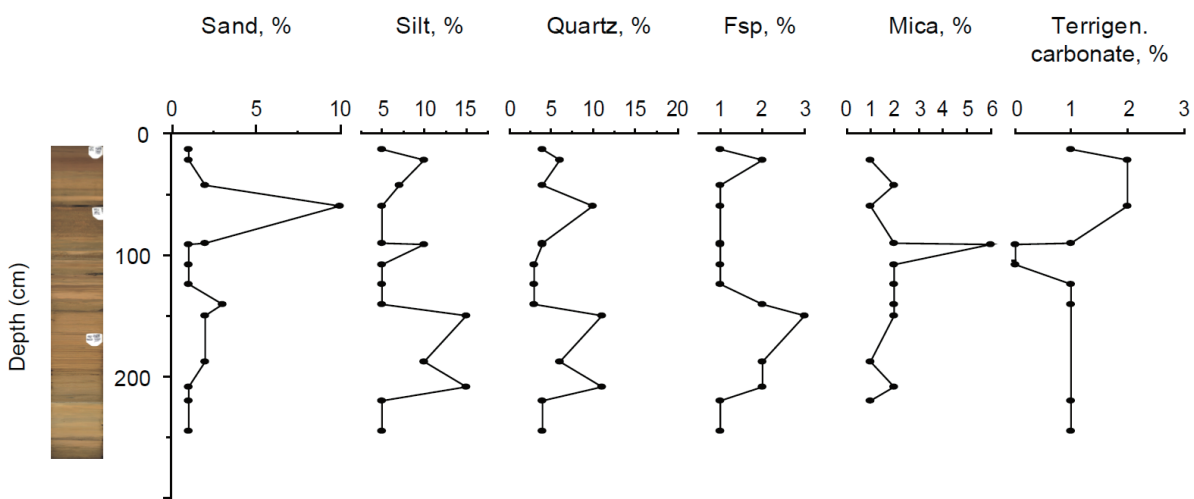


Fig. 10.6.3: Grain-size and major abiogenic components distribution in core PS87/040-1

14 smear slides were studied from core PS87/056-1 KAL. Results are summarized in Table A5.2.4 and Fig. 10.6.4. Sediments can be classified as silty clay. Studied intervals contain very low amount of terrigenous carbonates. Surface sediment from this site (sample from box core PS87/056-2) contains benthic and planktic foraminifers and very rare coccoliths.

10.6 Main lithologies and lithostratigraphy of PS87 sediment cores

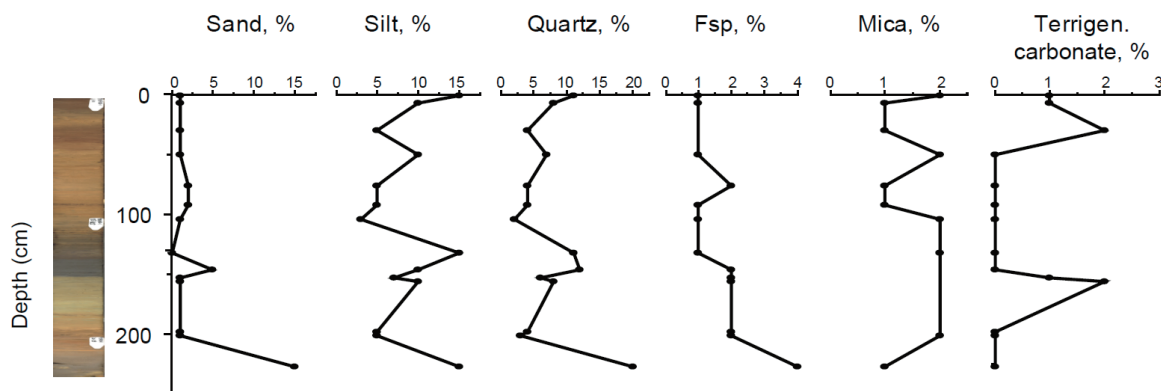


Fig. 10.6.4: Grain-size and major abiogenic components distribution in core PS87/056-1

29 smear slides were studied from core PS87/070-1 KAL. Results are summarized in Table A5.2.5 and Fig. 10.6.5. Sediments can be classified as silty clay. Studied intervals contain very low amount of terrigenous carbonates. At core depths of 375 and 410 cm rounded some well-rounded quartz grains were observed. Biogenic remains, including rare coccoliths, occur only in the uppermost sample.

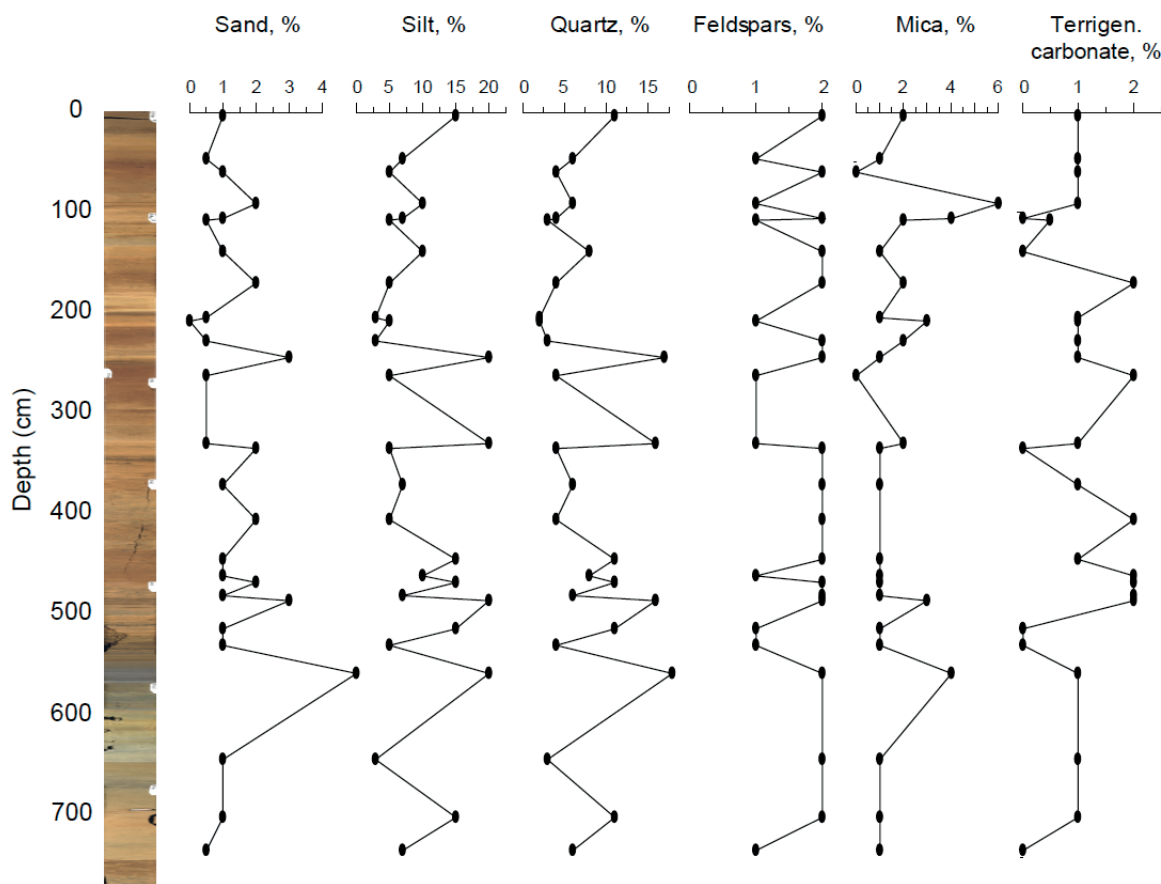


Fig. 10.6.5: Grain-size and major abiogenic components distribution in core PS87/070-1

26 smear slides were studied from core PS87/079-1 KAL. Results are summarized in Table A5.2.6 and Fig. 10.6.6. Sediments can be classified as silty clay. Few remains of calcareous shells were observed at 332 cm core depth.

Smear slides from gravity cores were checked in fewer details due to the shipboard working time constraints. 14 smear slides were studied from core PS87/003-1 SL taken at the Hovgaard Ridge (Fram Strait). Results (representing composition of sand fraction) are summarized in Table A5.2.7. Diverse microfossil remains (foraminifers, diatoms, radiolarians, sponge spicules, coccoliths) were found in the uppermost part (2 and 12 cm core depth) as well as at the 103 cm core depth (foraminifers).

Smear slides were scanned to check the presence of biogenic components in gravity cores PS87/051-1, PS87/080-3, PS87/080-4, PS87/088-1, PS87/089-1 and PS87/093-1. One single benthic foram was found in core PS87/080-3 at the depth of 251 cm. Slightly increased amount of terrigenous carbonates (up to 3%) was observed in core PS87/093-1 at the depth of 560 cm.

8 smear slides were studied from core PS87/095-1 SL. Results are summarized in Table A5.2.8. Studied intervals are composed of silty clay. Sample from 330 cm core depth contains zonal feldspar grains of sand size (similar to 51 cm core depth in PS87/093-1). No biogenic remains were observed in the smear slides.

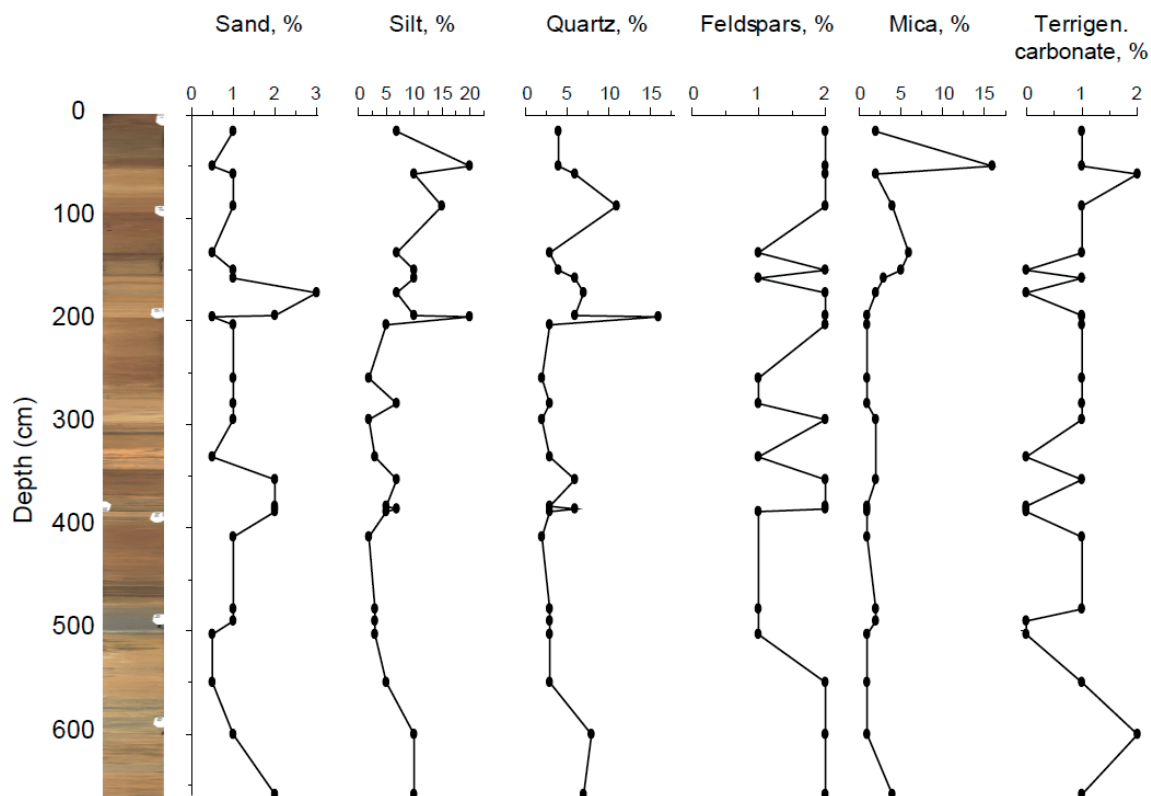


Fig. 10.6.6: Grain-size and major abiogenic components distribution in core PS87/079-1

Data management

All results of the smear-slide analysis will be stored in the PANGAEA Data Publisher for Earth & Environmental Science. The smear slides will be stored at Department of Marine Geology and Paleontology of the AWI.

10.6.2 Coarse fraction components of Lomonosov Ridge sediment cores

Seung-il Nam

KOPRI

Objectives

In the Arctic Ocean, variations in the sediment composition are generally related to sub/surface-water productivity, supply of terrigenous ice rafted-debris, and resuspended material transported by icebergs, sea-ice, and currents from the shallow coastal areas (Stein, 2008). During glacial periods with a relatively lower sea-level stand than the present, perennial sea-ice coverage, discharge of large amounts of icebergs, and extended continental ice sheets, the sediment transported to the deep-sea floor is dominated by non-biogenic material (e.g. Ruddiman & McIntyre 1976; Ruddiman 1977; Stein 2008). In contrast, during interglacial periods, reduced sea-ice coverage and/or open-water conditions coupled with a high sea-level stand have contributed not only to the reduced supply of terrigenous sediment from the surrounding lands, but also to an increase in sub/surface-water productivity resulting in enhanced flux-rates of biogenic material to the sea floor sediments (Gard & Backman 1990).

In general, biogenic components in marine sediments in the Arctic Ocean include carbonate, siliceous and organic-walled microfossils (e.g., de Vernal et al. 2013; see Chapter 10.8). The biogenic carbonate content (e.g. coccoliths, calcareous foraminifers and ostracodes) of marine sediments are generally related to water-mass properties, open water and/or sea-ice coverage and biological productivity (Wollenburg et al. 2004, 2007; Cronin et al. 2013; Polyak et al. 2013). Other factors such as water depth, sedimentation, preservation, and dissolution are also of major importance. Furthermore, it is known that authigenic compositions such as manganese nodules occurred during interglacials, interstadials and terminations in the Arctic marine sediments (Jokat 2009; Maerz et al. 2011). The main goal of this work is to roughly estimate sediment compositions (siliciclastic, biogenic and authigenic in origin) in the sand fraction (>63 μm) from the four sediment cores recovered with the Kastenlot (KAL) from the western and eastern part of Lomonosov Ridge.

Work at sea

In order to estimate the sediment components within the sand fractions (>63 μm) onboard *Polarstern*, about 30 cm³ of sediment were taken from the four Kastenlot cores recovered from the eastern and western profiles of the Lomonosov Ridge (see Chapter 10.1). The samples were wet-sieved with a mesh of 63 μm to separate the sand fraction (>63 μm) from the silt and clay fractions. The sand fraction was dried at 60°C, and then sand fractions were roughly estimated using a binocular microscope. The amounts of each component was simply expressed in the five criteria of 0 to 5 (0, barren; 1 very rare; 2, rare; 3, common; 4, abundant; 5, dominant) because the estimation of the sand fraction was carried out based on five simple criteria (0 to 5). This estimation is generally relevant to a scale ranging from 0 (absent) to 4 (abundant) done also in micropaleontology work (see Chapter 10.8).

Preliminary results

According to the semi-quantitative estimation, the sediment components of sand fraction (>63 μm) can be simply classified into siliciclastic (terrigenous), biogenic and authigenic components in origin. In general, the siliciclastic components are mainly composed of quartz, feldspar, rock fragment, mica, carbonate/dolomite, basalt and heavy minerals. The biogenic components consist mostly of planktic and benthic (calcareous and agglutinated) foraminifers, ostracodes, mollusca and biogenic opal such as radiolarian and sponge spicules (see Chapter 10.8). The authigenic component identified is mainly of micro-manganese nodules, whereas authigenic carbonate is also observed in some intervals of cores PS87/023-1 and PS87/030-1 only with very low amounts (Figs. 10.6.7 and 10.6.8).

Preliminary results from the western profile of the Lomonosov Ridge

The first preliminary results are shown in Figs 10.6.7 and 10.6.8 (data are listed in Tables A5.3.1 and A5.3.2 in the Appendix). In most sediment depths of the two cores PS87/023-1 and PS87/030-1 recovered from the western part of Lomonosov Ridge, the dominant siliciclastic components are quartz and feldspar, while rock fragments, detrital carbonate/ dolomite, basalt, mica and heavy minerals occurred in minor amounts throughout the sediment. In contrast, the biogenic components are mostly dominated by planktic foraminifers with a monospecific species of *N. pachyderma* sin.. *N. pachyderma* dex. (subpolar species) together with the other subpolar species like as *T. quinqueloba*, *G. bulloides* is also present, but with small amounts. Although subpolar species of planktic foraminifers occurred with low amounts, the most intervals with dominant amounts of both planktic and benthic foraminifera might be tentatively interpreted as interglacial/interstadial periods (e.g., MIS 11, 9, 7, 5.5 and Holocene).

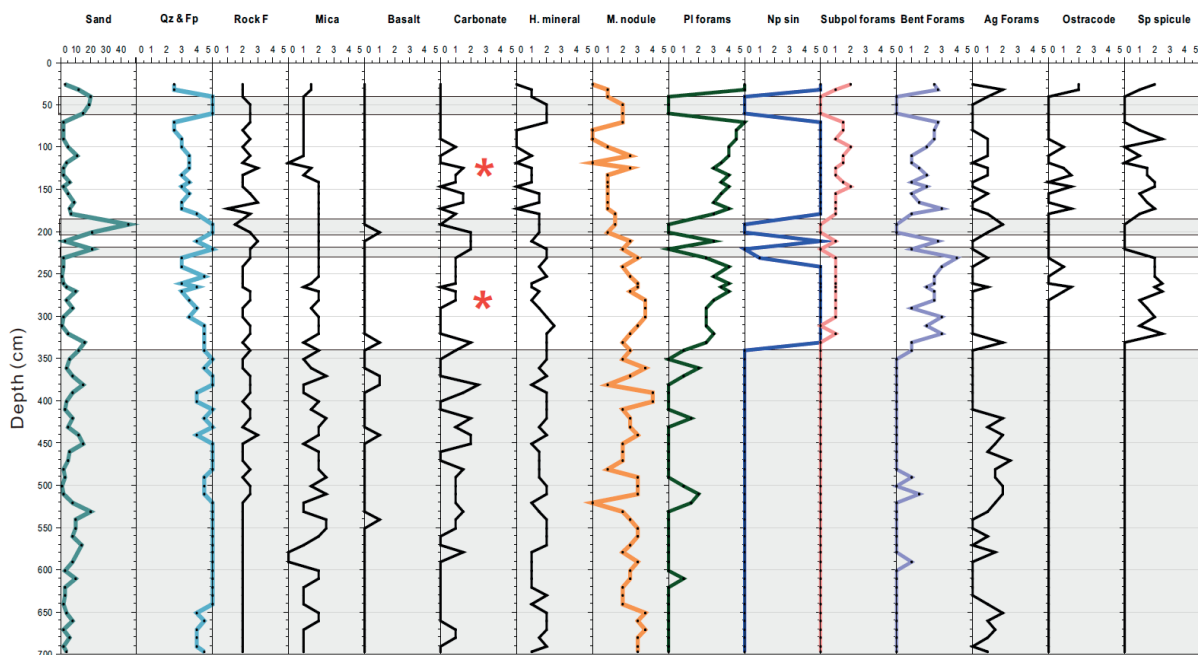


Fig. 10.6.7: Down-core variations in siliciclastic, biogenic and authigenic sediment components roughly estimated from the coarse sand fraction ($>63 \mu\text{m}$) of core PS87/023-1KAL recovered from the western part of the Lomonosov Ridge. Note that scales from 0 to 5 indicate relative abundance of each component (0, barren; 1, very rare; 2, rare; 3, common; 4, abundant; 5, dominant). Shadow area indicates intervals with high amounts of siliciclastic sediment components dominated by quartz and feldspar within the sediment cores, whereas biogenic origin sediments are of barren. Micro-manganese nodules occurred in common abundances throughout the cores. Red stars in carbonate indicate occurrence of authigenic carbonate in few amounts.

It is supposed that there might have been evidence of relatively reduced sea ice coverage, but it seemed to have been less advection of the North Atlantic Intermediate Water into the coring sites in the western part of Lomonosov Ridge mostly during the interglacial/interstadial periods. Further information on biogenic compositions (calcareous and agglutinated benthic foraminifera, ostracode and sponge spicules, etc.) are shown and explained in Chapter 10.8 in more details. The micro-manganese nodules mostly occurred in brown color layers with high variability of lack to predominance in both cores PS87/023-1 and PS87/030-1. However, the micro-manganese nodules decreased toward the upper part of sediment core with relatively low amounts.

10.6 Main lithologies and lithostratigraphy of PS87 sediment cores

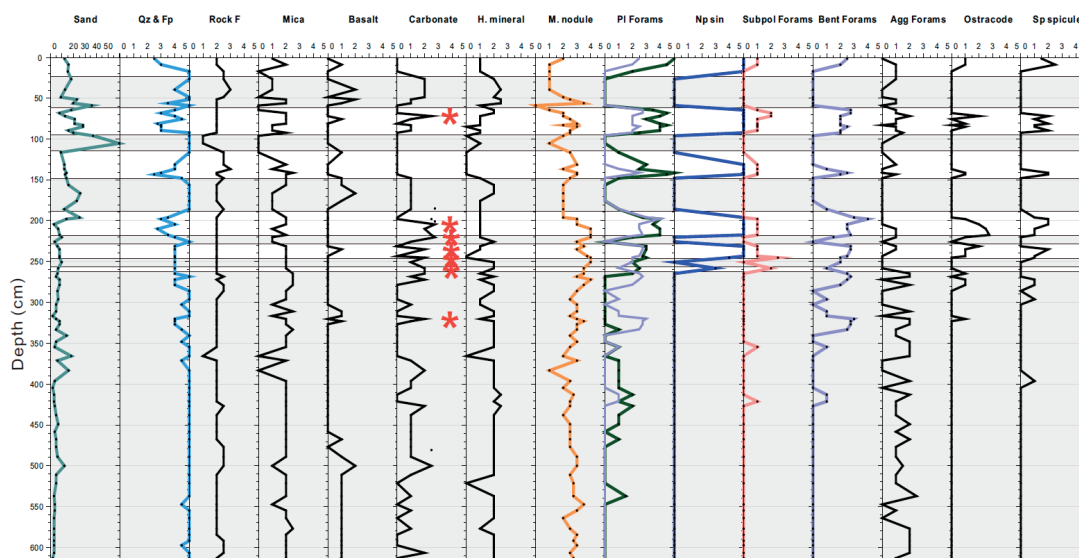


Fig. 10.6.8: Down-core variations in siliciclastic, biogenic and authigenic sediment components roughly estimated from the coarse sand fraction ($>63 \mu\text{m}$) of core PS87/030-1 recovered from the western part of the Lomonosov Ridge. Notice that scales from 0 to 5 indicate relative abundance of each component (0, barren; 1, very rare; 2, rare; 3, common; 4, abundant; 5, dominant). Shadow area indicates intervals with high amounts of siliciclastic sediment components dominated by quartz and feldspar within the sediment cores, whereas biogenic origin sediments are of barren. Micro-manganese nodules occurred in common to abundant amounts throughout the cores. Red stars in carbonate indicate occurrence of authigenic carbonate in few amounts.

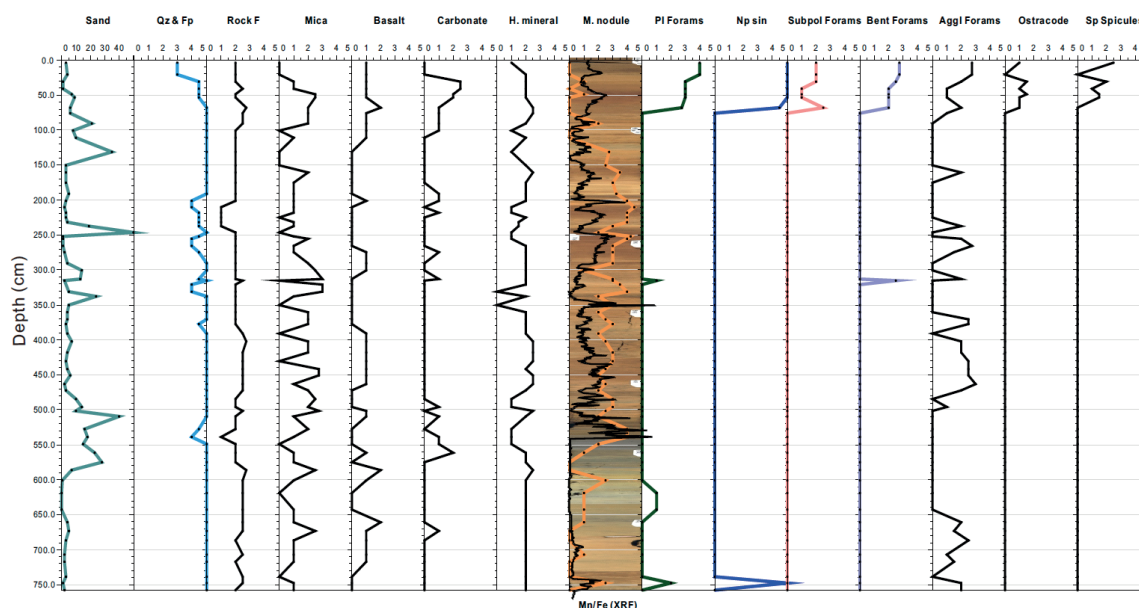


Fig. 10.6.9: Down-core variations in siliciclastic, biogenic and authigenic sediment components roughly estimated from the coarse sand fraction ($>63 \mu\text{m}$) of core PS87/070-1 recovered from the eastern part of the Lomonosov Ridge. Notice that scales from 0 to 5 indicate relative abundance of each component (0, barren; 1, very rare; 2, rare; 3, common; 4, abundant; 5, dominant). Note that high amounts of siliciclastic sediment components are dominated by quartz and feldspar throughout the sediment cores, whereas biogenic origin sediments occurred in the uppermost part (0-67 cm in core depth) dominated only by planktic foraminifer *N. pachyderma sin.*. Micro-Mn nodules (brown-color line) occurred in common to abundant amounts throughout the cores except for some barren zones. Mn/Fe ratios (black line) based on Avaatech XRF core scanner data (measured on board Polarstern by M. Forwick). Background image shown in the Mn nodule record is a linescan photography obtained by the 3-CCD (charge-coupled device) camera installed in XRF core scanner.

Preliminary results from the eastern profile of the Lomonosov Ridge

Except for the agglutinated foraminifers occurring with rare to common amounts throughout sediment cores, it is noticed that there are totally barren of biogenic components below 70 cm in core depth of PS87/070-1 and below 40 cm in core depth of PS87/079-1, respectively (Figs. 10.6.9 and 10.6.10; Tables A5.3.3 and A5.3.4 in the Appendix; see also Chapter 10.8). Extraordinary predominant terrigenous components in both cores PS87/070-1 and PS87/079-1 are mainly composed of quartz (including feldspar), and mica as well as minor amounts of rock fragments, carbonate, heavy minerals and basalt (Figs. 10.6.9 and 10.6.10). In contrast to the cores from the western profile of the Lomonosov Ridge, biogenic components occurred only in the uppermost part of core depth (>70 cm) of core PS87/070-1. Among them, the planktic foraminifer *N. pachyderma* sin. is mostly dominant biogenic component and calcareous benthic foraminifers also occurred with minor to common amounts (see Chapter 10.8). In core PS87/079-1, rare amounts of biogenic components occurred that are mostly dominated by the planktic foraminifer *N. pachyderma* sin. only in the uppermost part of core depth (>40 cm).

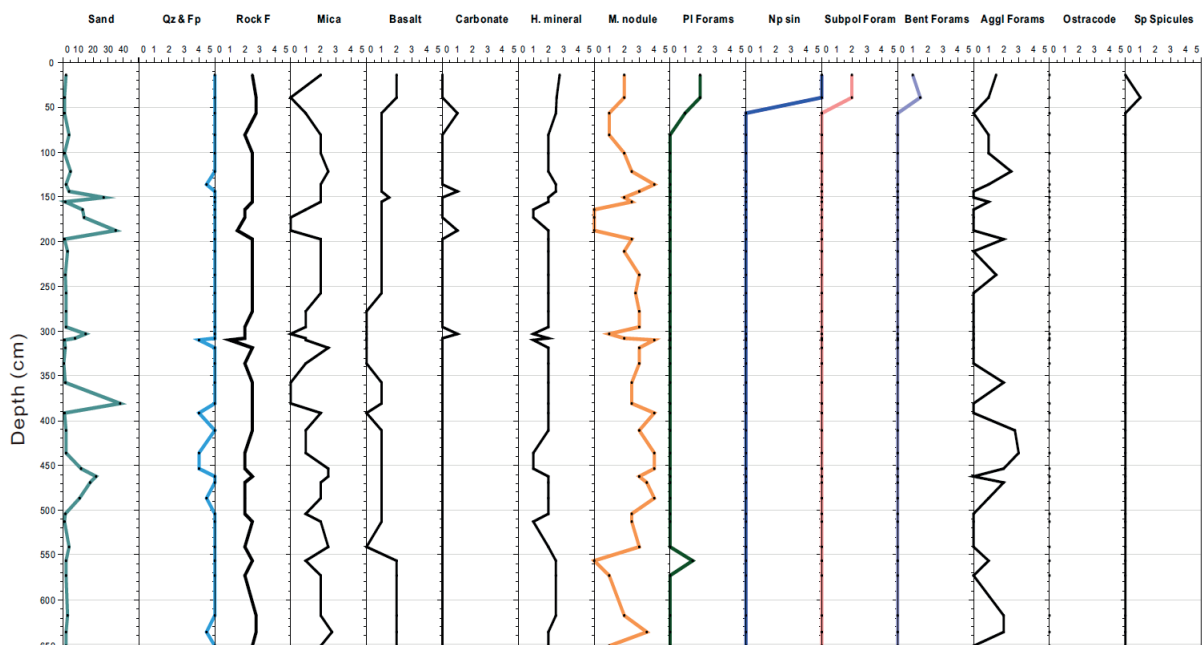


Fig. 10.6.10: Down-core variations in siliciclastic, biogenic and authigenic sediment components roughly estimated from the coarse sand fraction (>63 μm) of core PS87/079-1 recovered from the eastern part of the Lomonosov Ridge. Notice that scales from 0 to 5 indicate relative abundance of each component (0, barren; 1, very rare; 2, rare; 3, common; 4, abundant; 5, dominant). Noticed that high amounts of siliciclastic sediment components are dominated by quartz and feldspar throughout the sediment cores, whereas biogenic origin sediments occurred in the uppermost 67 cm in minor amounts, still dominated by planktic foraminifer *N. pachyderma* sin.. Micro-Mn nodules occurred in common to abundant amounts throughout the cores except for some barren zones.

In both cores PS87/070-1 and PS87/079-1, the micro-Mn nodules show high fluctuations varying from lack to abundant amounts. In core PS87/070-1, the occurrence pattern of micro-Mn nodules observed in the sand fraction seems to be relatively well correlated with Mn/Fe ratio analyzed with Avaatech XRF core scanner onboard *Polarstern* (Fig. 10.6.9).

Data management

All preliminary results of the coarse fraction analysis will be stored in the PANGAEA Data Publisher for Earth & Environmental Science. The sieved sand fractions will be stored at Department of Marine Geology and Paleontology of the AWI.

10.6.3 Lithostratigraphy and chronology of PS87 sediment cores

Rüdiger Stein¹, Matthias Forwick² ¹AWI
 Frank Niessen¹ ²UoT

Objectives

One of the main objectives of the shipboard studies of the PS87 sediment cores was the establishment of a preliminary lithostratigraphy and age model of these cores, based on correlation with dated sediment cores recovered across Lomonosov Ridge in 1995 (Rachor 1997) and in the Amerasian Basin in a transect across Mendeleev Ridge in 2008 (Jokat 2009) (Fig. 10.6.11). Some examples are presented and discussed below.

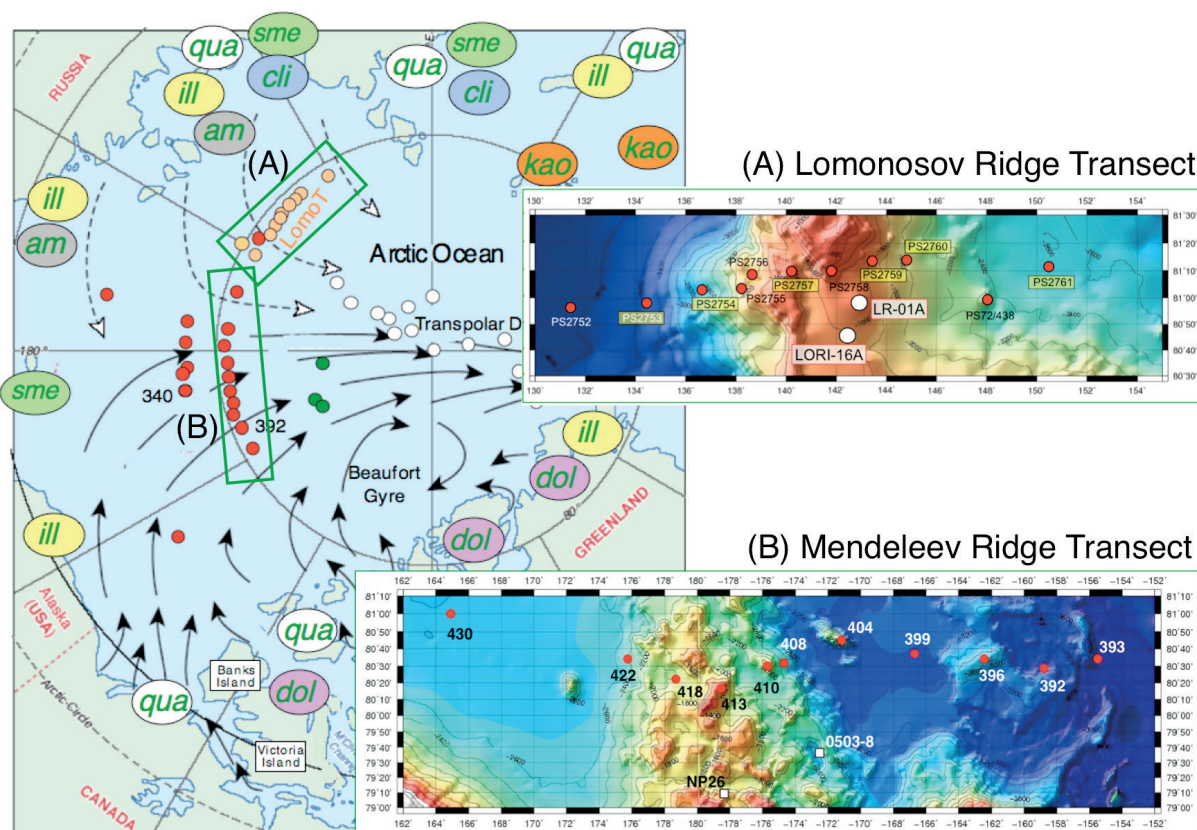


Fig. 10.6.11: Locations of sediment cores recovered during Expedition ARK-XIX (Lomonosov Ridge Transect) and during Expedition ARK-XXIII/3 (Mendeleev Ridge Transect), main surface water circulation systems (i.e., Transpolar Drift and Beaufort Gyre), and main minerals indicative for specific circum-Arctic Ocean source regions of terrigenous sediments (am amphibole, cli clinopyroxene, dol dolomite, ill illite, kao kaolinite, qua quartz, sme smectite) (Stein et al. 2010a and references therein).

For the Amerasian Basin, Clark et al. (1980) developed a widely applied standard lithostratigraphy based on a detailed sedimentological study of several hundreds of short sediment cores collected from Ice Island T-3 in the Amerasia Basin between 1952 and 1974. These authors established 13 lithostratigraphic units A to M, which include silty and arenaceous lutites, and

carbonate-rich, pinkish-white layers, with variable characteristic contents of quartz-feldspar, detrital carbonate grains, foraminifers, and Fe-Mn particles. The content of sand-sized material (enriched in units C, F, H, J, L, and parts of M) and the pink-white layers were considered to be the key sedimentary characteristic used for correlation of these lithostratigraphic units (Fig. 10.6.12; Stein et al. 2010a).

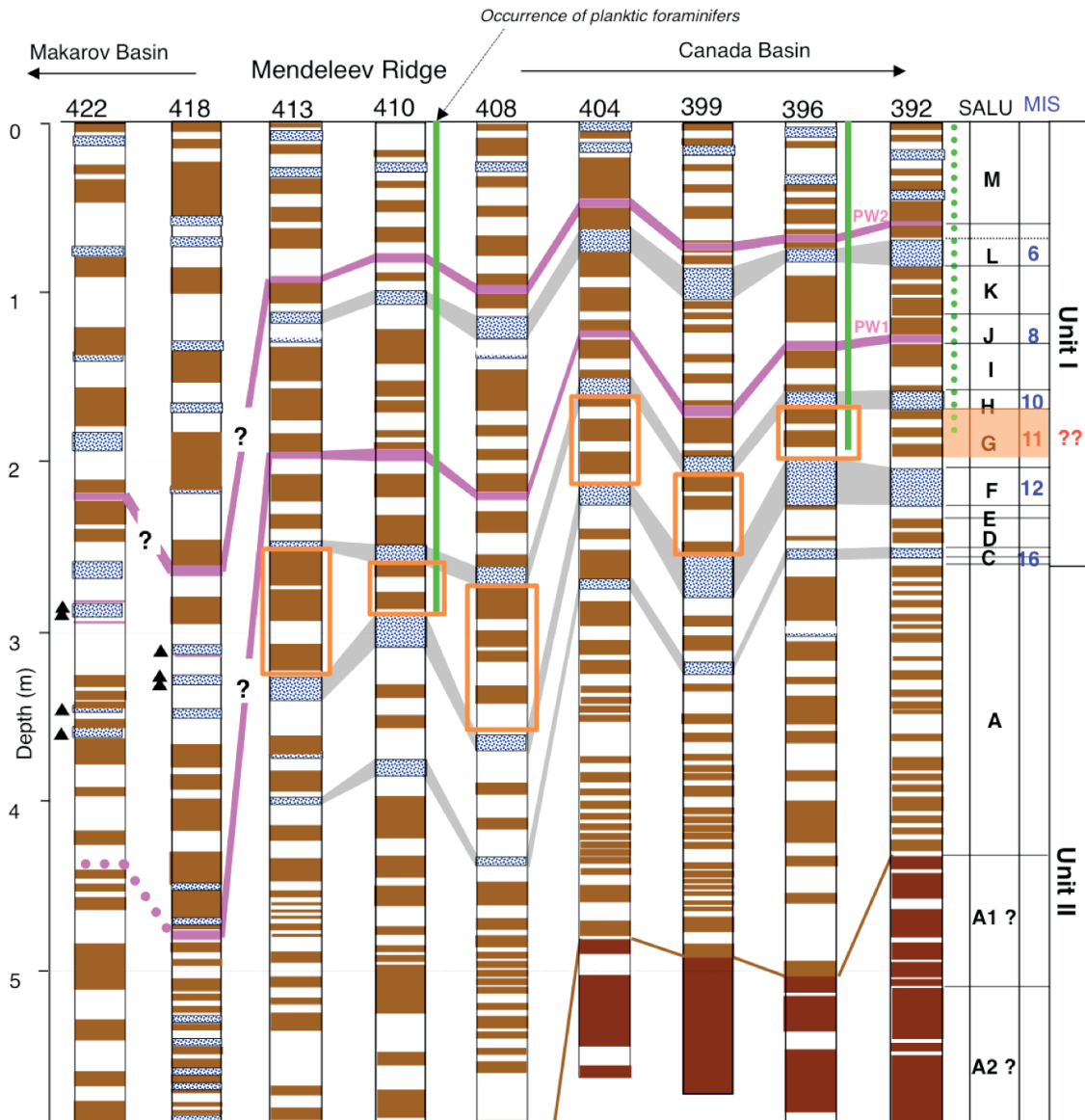


Fig. 10.6.12: Main lithologies (brown to dark brown and beige silty clays) of sediment cores recovered during Expedition ARK-XXIII/3 (Jokat 2009) across the central Mendeleev Ridge (for core location on transect see Fig. 10.6.11). Occurrence of brown intervals, pink layers and sandy intervals (light blue) are highlighted. Furthermore, standard lithological units A to M of Clark et al. (1980) and proposed chronology (Marine Isotope Stages MIS) are shown. Fig. from Stein et al. (2010a).

10.6 Main lithologies and lithostratigraphy of PS87 sediment cores

In addition, the dark brown horizons (cf., Jakobsson et al. 2000; Polyak et al. 2004) are key elements for a lithostratigraphic framework and related tentative age model developed by Stein et al. (2010a, 2010b) for the sediment cores recovered on the transect across the Mendeleev Ridge. Based on this approach, Marine Isotope Stage (MIS) 16 to MIS 1 are represented in these sediments (Fig. 10.6.12; for more details and background see Stein et al. 2010).

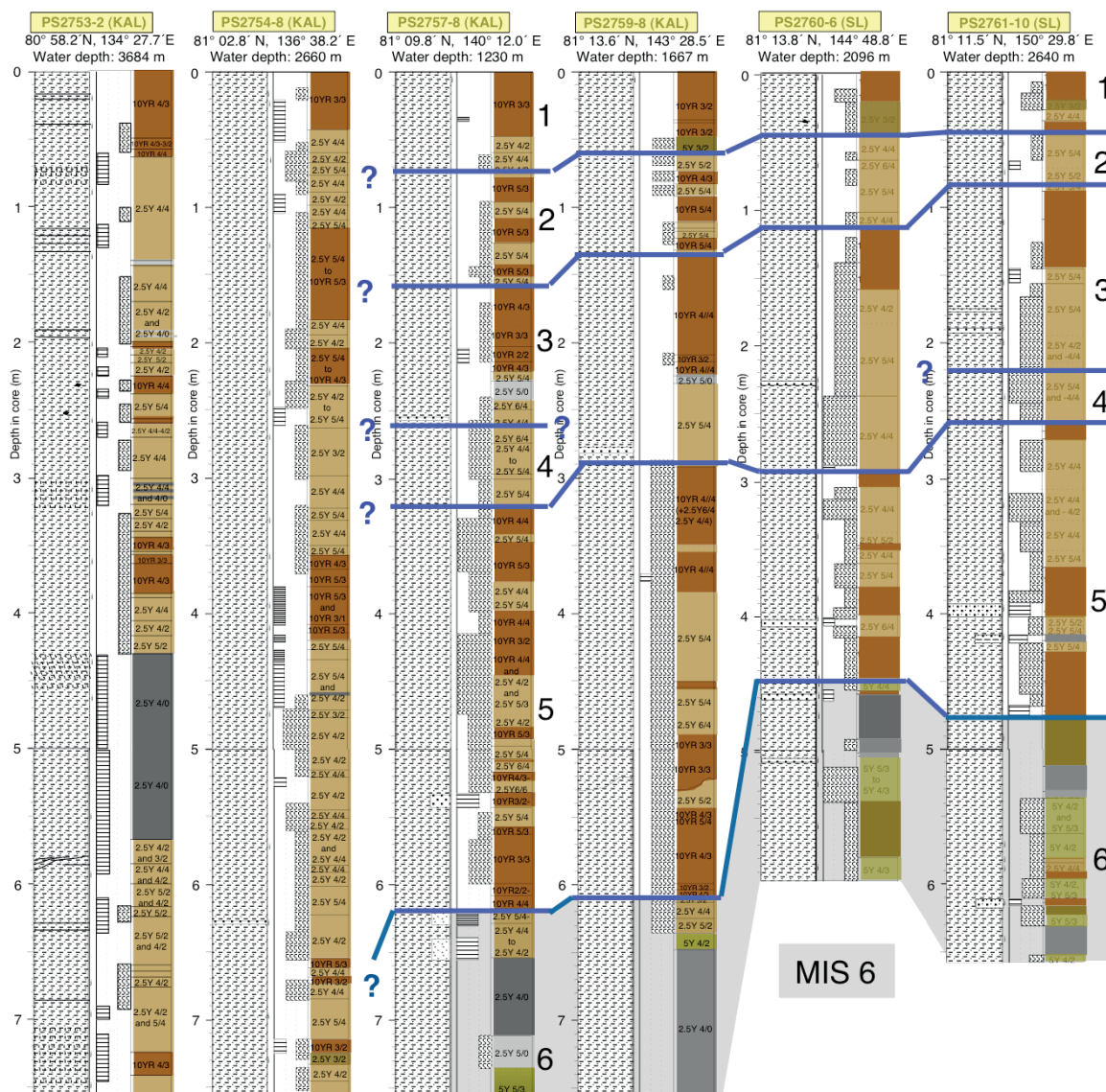


Fig. 10.6.13: Main lithologies (mainly brown to dark brown, beige and gray to dark gray silty clays with some more sandy intervals) of sediment cores recovered during Expedition XIX/1 in 1995 (Rachor 1997) across the southern Lomonosov Ridge (for core location on transect see Fig. 10.6.11). Intervals with brown, beige and dark gray sediment colours, intervals with lamination and different degrees of bioturbation as well as proposed chronology (Marine Isotope Stages MIS) are indicated. Figure from Stein et al. (1997, supplemented).

For sediment cores recovered in 1995 from the Siberian side of the Lomonosov Ridge (for core locations see Fig. 10.6.11), Stein et al. (1997) established a first lithostratigraphic framework based on a detailed visual core description (and supported by physical property data; Niessen

et al., 1997), and proposed an age model representing MIS 6 to 1 (Fig. 10.6.13). This tentative age model has later been further supported by a few AMS ^{14}C datings, magnetic stratigraphy, correlation with other dated sediment cores, etc. (see Stein 2008 details and references). The stratigraphic framework shown in Fig. 10.6.13 is still valid.

Work at sea

During the *Polarstern* Expedition PS87 (ARK-XXVIII/4), 43 long sediment cores were taken on Lomonosov Ridge (Figs. 10.1.2 and 10.1.3; Table 10.1.2). Already onboard *Polarstern*, a larger number of the sediment cores have already been studied onboard *Polarstern*, as outlined in more detail in the previous Chapters 10.2 – 10.5 and 10.7 – 10.9. In the following subchapters, main lithologies of the recovered sediments from selected areas are described, and a lithostratigraphic concept and preliminary age model as well as some preliminary interpretations are presented.

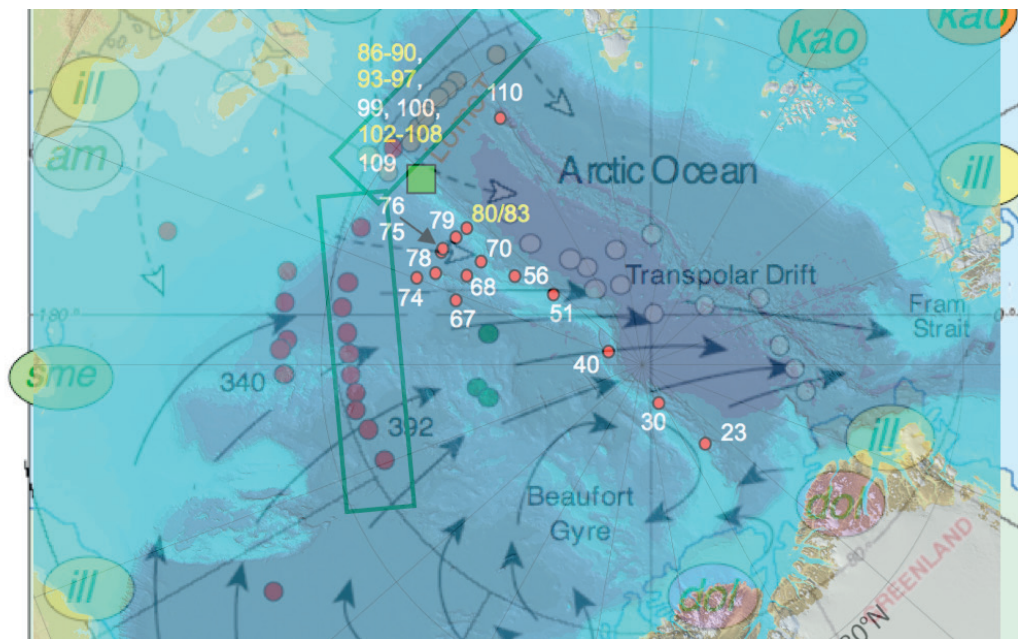


Fig. 10.6.14: Part of Fig. 10.6.11 showing main surface water circulation systems (i.e., Transpolar Drift and Beaufort Gyre), and main minerals indicative for specific circum-Arctic Ocean source regions of terrigenous sediments (for details see complete Fig. 10.6.11), overlain by a semi-transparent map with locations of PS87 sediment cores in white and yellow numbers (cf., Fig. 10.1.2)

Preliminary results

Lithostratigraphy and preliminary age model of Cores PS87/023-1 and PS87/030-1

Cores PS87/023-1 and PS87/030-1 recovered on the „Greenland/Canadian side“ of Lomonosov Ridge and thus influenced predominantly by the Beaufort Gyre System (Fig. 10.6.14), are mainly composed of brown to dark brown and beige silty clay, with a couple of intercalated more sandy intervals (Figs. 10.6.15 and 10.6.16). The more sandy intervals generally correlate with increased wet bulk density values. A few horizons with pink/pale layers and/or lenses occur in Core PS87/023-1 at 92-93, 177-179, and 260-270 cm and in Core PS87/030-1 at 87-92, 123-125, 171, and 216-218 cm. These horizons are characterized by detrital carbonate as determined in smear slides (Figs. 10.6.15 and 10.6.16; cf. Chapter 10.6.1), indicative for detrital sediment supply from the Canadian Arctic via the Beaufort Gyre System (Clark et al. 1980; Stein et al. 2010a, 2010b and references therein).

10.6 Main lithologies and lithostratigraphy of PS87 sediment cores

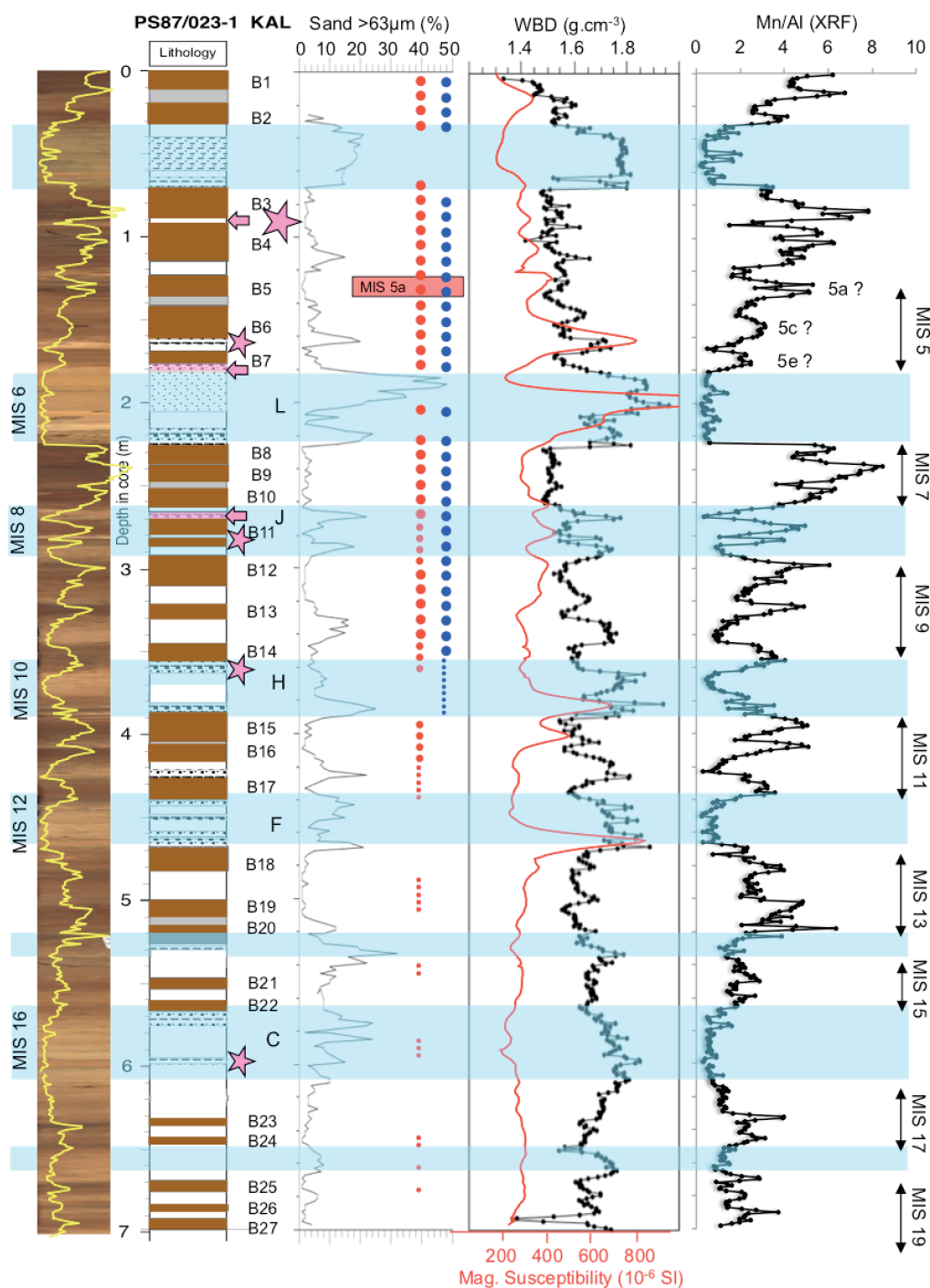


Fig. 10.6.15. Linescan image (with Mn/Al record in yellow) and summary of visual core description, indicating main lithologies (brown to dark brown silty clay horizons; B1-B27; sandy intervals; pink horizons and lenses = pink arrows) of sediment core PS87/023-1 (see Fig. 10.6.14 for location). Pink asterisks indicate detrital carbonate peaks in smear slides (cf. Fig. 10.6.1). Occurrence of sandy intervals are highlighted as light blue bars. Furthermore, standard lithological units L, J, H, F and C of Clark et al. (1980). In addition, the sand content and the occurrence of planktic foraminifers (red circles) and calcareous benthic foraminifers (blue circles) (adapted from Fig. 10.8.1), the wet bulk density and magnetic susceptibility (cf., Chapter 10.3 for MSCL background), and the preliminary XRF scanning record of Mn/Al (cf., Chapter 10.4 for XRF scanning background). Proposed MIS 5a based on benthic foraminifer data (see Chapter 10.8). Proposed MIS 5 to MIS 19 based on lithostratigraphy, MSCL data and Mn/Al record (cf., Stein et al. 2010a, 2010b; Alexanderson et al. 2013).

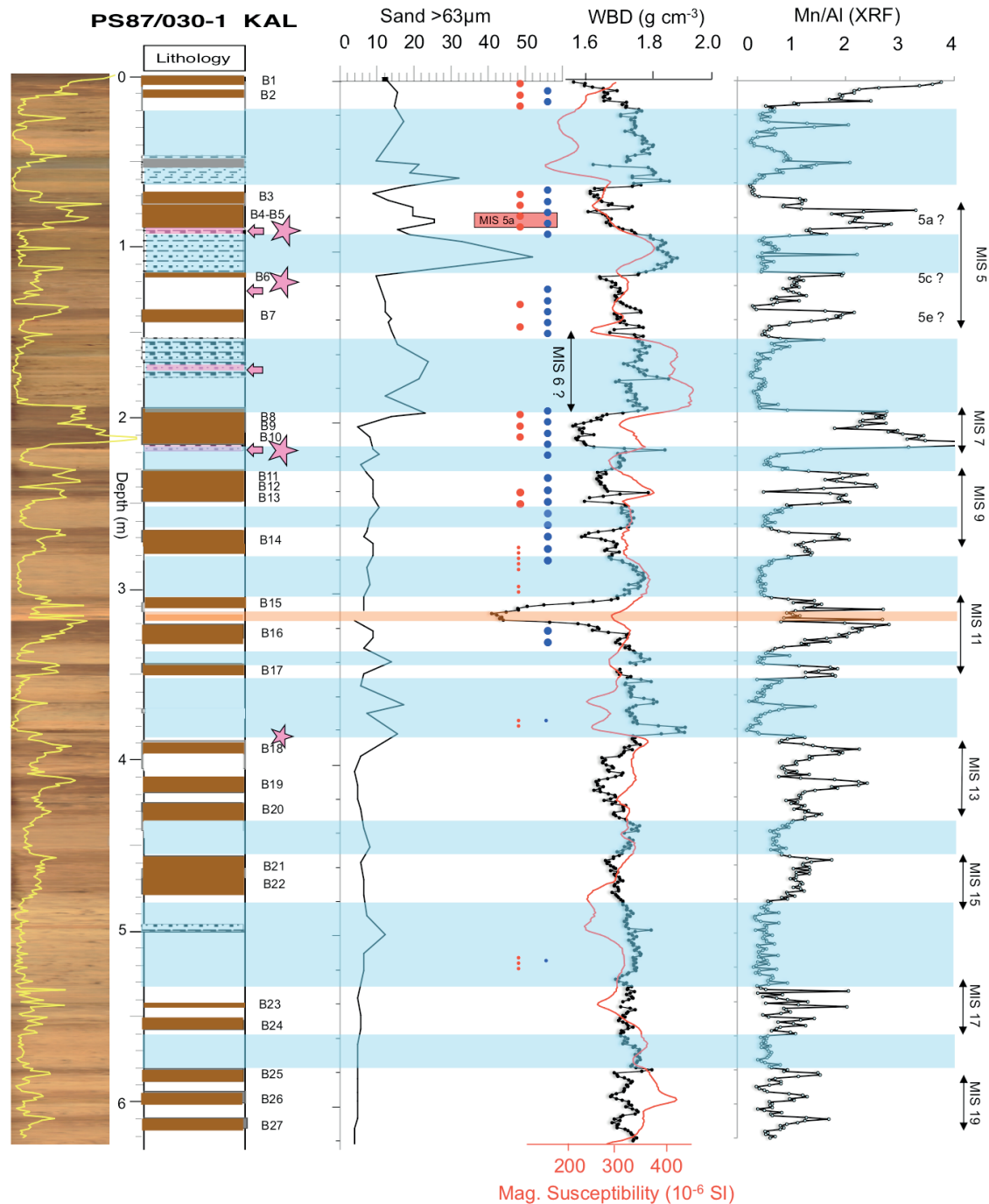


Fig. 10.6.16: Linescan image (with Mn/Al record in yellow) and summary of visual core description, indicating main lithologies (brown to dark brown silty clay horizons, B1-B27; sandy intervals; pink horizons and lenses = pink arrows) of sediment core PS87/030-1 KAL (see Fig. 10.6.14 for location). Pink asterisks indicate detrital carbonate peaks in smear slides (cf. Fig. 10.6.2). In addition, the sand content and the occurrence of planktic foraminifers (red circles) and calcareous benthic foraminifers (blue circles) (adapted from Fig. 10.8.2), the wet bulk density and magnetic susceptibility (cf., Chapter 10.3 for MSCL background), and the preliminary XRF scanning record of Mn/Al (cf., Chapter 10.4 for XRF scanning background) are shown. Orange bar indicates yellow (10YR7/6) clay layer characterized by a prominent WBD minimum („peach layer“?). Proposed MIS 5a based on benthic foraminifer data (see Chapter 10.8). Proposed MIS 5 to MIS 19 based on lithostratigraphy, MSCL data and Mn/Al record (cf., Stein et al. 2010a, 2010b; Alexanderson et al. 2013).

In order to get a first stratigraphic framework we tried to correlate cores PS87/023-1 and PS87/030-1 more influenced by the Beaufort Gyre System and detrital sediment input from the Canada (cf., Fig. 10.6.14), with the 2008 cores recovered along the transect across Mendeleev Ridge (Fig. 10.6.12). Especially for Core PS87/023-1, the brown layers and the occurrence of sandy intervals (lithological units L, J, H, F and C according to Clark et al. 1980) and pink, detrital-carbonate-rich layers seems to be very similar to those features identified in the cores from Mendeleev Ridge (Stein et al. 2010a, 2010b). In general, the dark brown layers B1 to B27 are characterized by minima in wet bulk density and maxima in Mn content (Fig. 10.6.15). The more coarse-grained lithological units L, J, H, F and C are interpreted as glacial intervals (i.e., probably MIS 6, 8, 10, 12, and 16) characterized by extended North American/Canadian ice sheets and increased input of ice-rafted debris (IRD) into the Arctic Ocean. The intervals composed of prominent (bundles of) dark brown and Mn-rich layers, on the other hand, probably represent more the interglacial intervals (cf., Jakobsson et al. 2000; Polyak et al. 2004; Stein et al. 2010a; Löwenmark et al. 2012, 2014; Alexanderson et al. 2013). The dark brown, Mn-rich intervals are more distinct at Core PS87/023-1 than at Core PS87/030-1, and 27 intervals (B1 to B27) were identified at the former, probably representing MIS 1 to MIS 19 (Fig. 10.6.15), i.e., the last about 800 ka. This tentative lithostratigraphic framework and age model has been transferred to Core PS87/030-1, probably representing the same time span of MIS 1 to MIS 19 (Fig. 10.6.16). In both cores, MIS5a was determined by the occurrence of specific benthic foraminifers, i.e., *O. tener*, *B. arctica* and/or *B. aculeata* (see Chapter 10.8 for details).

Lithostratigraphy and preliminary age model of sediment cores from the Siberian side of the Lomonosov Ridge

Based on the main lithologies, the new PS87 cores from the Siberian side of Lomonosov Ridge more influenced by the Transpolar Drift System (Fig. 10.6.14), can be correlated very well with the sediment cores recovered from this area in 1995 (Fig. 10.6.17; Stein et al. 1997). Main characteristics in grain size, structure and sediment colour were identified and allowed to transfer the age model of the 1995 cores to those recovered during Expedition PS87. Based on these data, a preliminary age model has been established, i.e., the sediment cores shown in Fig. 10.6.17 probably represent MIS 6 to MIS 1. The sediments of MIS 6 consists of very dark gray (sandy) silty clay, separated by more coarse-grained, partly laminated sediments (correlating with Termination II; TII) from the overlaying MIS 5 sediments. The latter are characterized by dominantly dark brown and beige silty clay. The warm interstadials MIS5e, 5c and 5e are represented by prominent dark brown intervals. The sediments of MIS 4 consist of mainly beige silty clay and more coarse-grained sandy intervals. In the upper MIS 4, a distinct gray clayey horizon occurs in most of the cores (Fig. 10.6.17). The upper part of the sediment sequences representing MIS 3 to 1, are composed of dark brown, brown and beige silty clay.

The correlation based on main lithologies and the obtained age model (cf., Stein et al. 1997) are supported by wet bulk density (WBD) and magnetic susceptibility (MS) records (cf., Niessen et al. 1997). Especially MIS 6 and TII, MIS5b/5c as well as MIS 4 display prominent WBD and MS signatures recorded in most of the studied cores from this area, that can be used for regional core correlation and age classification very well (Figs. 10.6.18 and 10.6.23). The dark gray sediments of MIS 6 (characterized by high content of terrigenous organic carbon; Stein et al., 2001) and the coarser-grained sediments of TII are characterized by very high WBD values with a prominent MS minimum just at the base of TII. MIS 4 shows very distinct maxima in WBD and MS values that correlate with the prominent coarse-grained layers (Fig. 10.6.18). Increased input of coarse-grained (IRD) sediments are related to extended continental ice sheets in western as well as eastern Eurasia (e.g., Arkhipov et al. 1986; Velitchko et al. 1997; Müller 1999; Stein et al. 2001; Niessen et al. 2013).

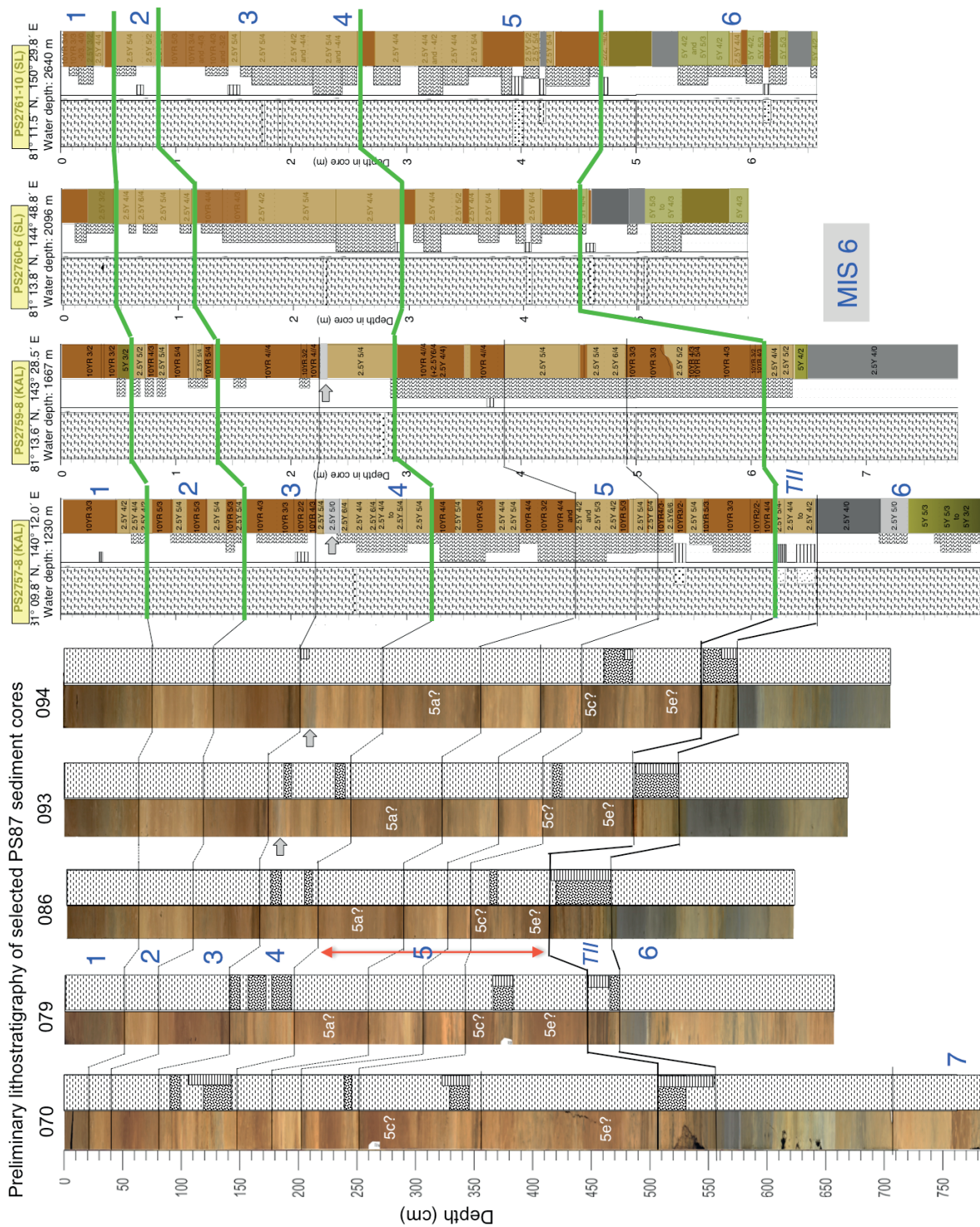


Fig. 10.6.17: Linescan image and summary of visual core description, indicating main lithologies (brown to dark brown, beige and gray silty clay horizons; sandy intervals) of sediment cores PS87/070, /079, /086, /093, and /094 recovered on the „Siberian side“ of Lomonosov Ridge (influenced predominantly by the Transpolar Drift System) and correlation with the lithologies of the 1995 cores (see Fig. 10.6.13 for details). Gray arrow marks prominent gray interval (upper MIS 4/boundary to MIS 3). Proposed preliminary chronology (Marine Isotope Stages - MIS - in blue numbers; 5a, 5c, 5d in white numbers) are shown (according to Stein et al. 1997).

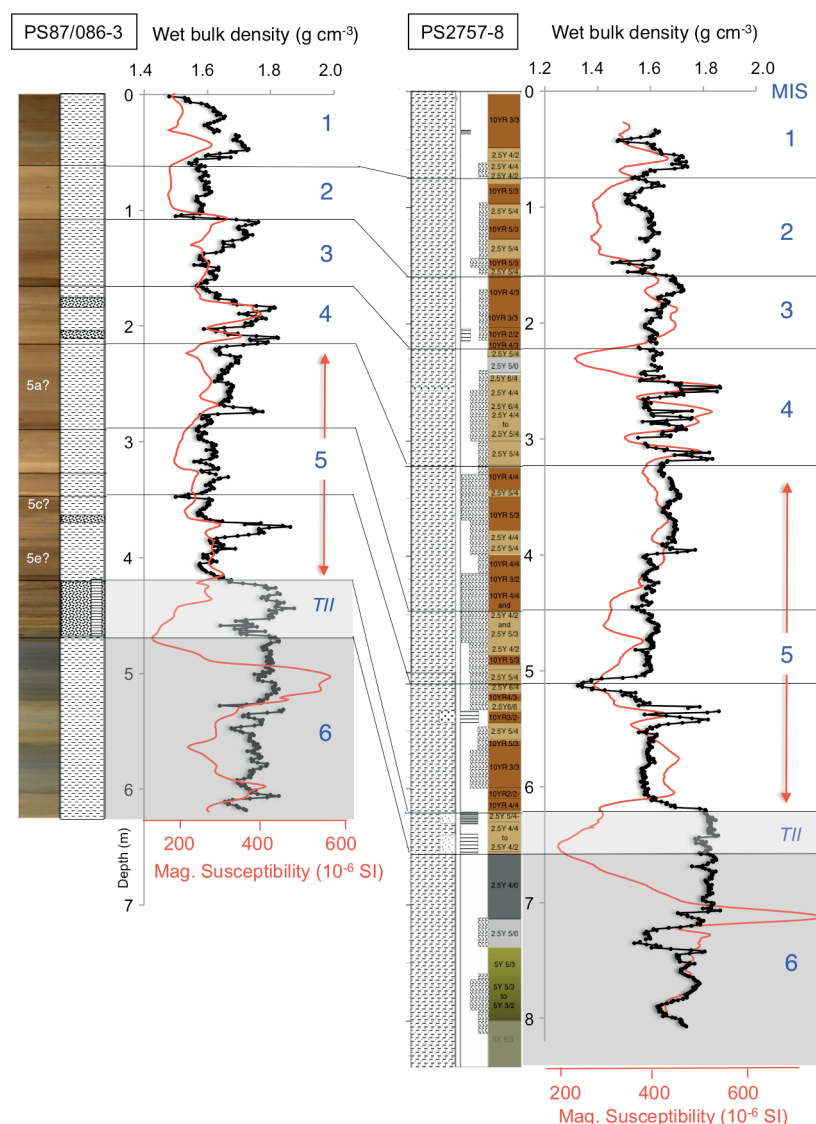


Fig. 10.6.18: Correlation of Core PS87/086-3 and Core PS2757-8, using lithology and MSCL (wet bulk density and magnetic susceptibility) data; MSCL data of Core PS2757-8 from Niessen et al. (1997). Proposed preliminary chronology (Marine Isotope Stages - MIS - in blue numbers) are shown (according to Stein et al. 1997; cf., Fig. 10.6.17)

Main lithologies of Core PS87/040 (central Lomonosov Ridge) and environmental significance

The sedimentary section of Core PS87/040 recovered in a prominent Intra-Basin on Lomonosov Ridge, can be divided into four lithological units (Fig. 10.6.19). Unit I (12.5 - 31 cm; 0-12.5 cm is lost) is composed of very dark grayish brown (10YR 3/2), dark brown (10YR 3/3) and brown (10YR 4/3) silty clay with strong bioturbation in the upper part. Unit II (31 - 216 cm) mainly contains grayish brown (2.5Y 5/2), light olive brown (2.5Y 5/4), yellowish brown (2.5Y 5/6) and olive gray (5Y 4/2) silty clays and sandy silty clays. Rhythmic alternations of silty clay and sandy silty clay with fining-upwards features and the occurrence of more sandy layers/laminae are characteristic for this Unit II. Unit III (216 - 251 cm) is composed of grayish brown (2.5Y 5/2) to olive gray (5Y 5/2) bioturbated (sandy) silty clay, intercalated by a very dark grayish brown (10YR 3/2) sandy silty clay at 242-246 cm. The bottom interval, Unit IV (251 - 260 cm) is a dark grayish brown (2.5Y 4/2) (silty) sand with fining-upwards structures.

Whereas the sediments of Units I and III probably represent normal pelagic sedimentation, the sediments of Units II and IV mainly represent turbidites and/or contourites. That means, these sediments are related to sediment redeposition and lateral transport by turbidity and contour currents, respectively. Some of the thicker turbidites display sharp (?erosional) contacts at their basis (e.g., at about 85, 103, 115, and 142 cm). These sediments have probably been controlled/influenced by bottom-water currents. Detailed grain-size measurements of this core may allow to reconstruct changes in bottom-water currents and exchange between the Makarov Basin and the Amundsen Basin (Fig. 10.6.19; see Björk et al. 2007 for modern oceanographic circulation patterns).

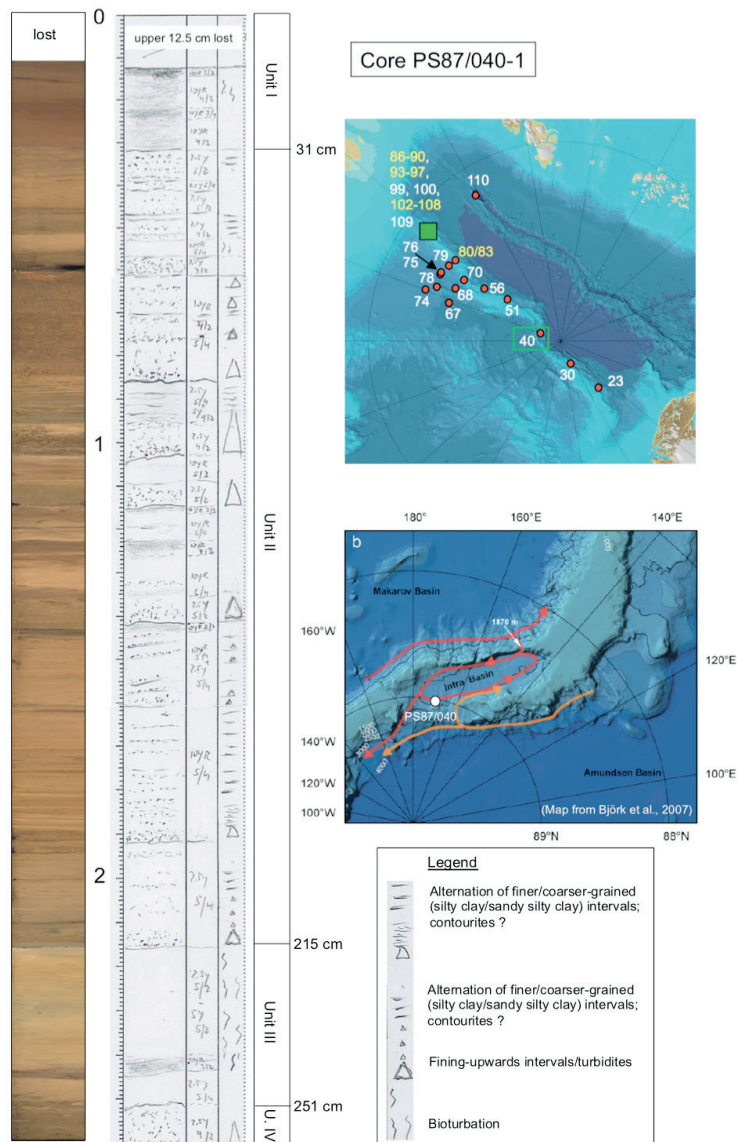


Fig. 10.6.19: Linescan image and summary of visual core description of Core PS87/040-1 KAL, recovered in a prominent Intra-Basin on Lomonosov Ridge (see Map b for location). The sediment sequence is characterized by numerous coarser-grained intervals representing turbidites and/or contourites, i.e., lithologies indicative for sediment redeposition and current-influence, respectively. In Map b, main current patterns are indicated in red (related to a Makarov-Basin source) and orange (related to a Amundsen-Basin source) (Björk et al. 2007).

Recovery of pre-Quaternary sediments on Lomonosov Ridge ?

As outlined in Chapter 10.1, one of the major goals of the marine-geological research programme was devoted to the long-term history of the Mesozoic and Cenozoic Arctic Ocean and its environmental evolution from a warm (Greenhouse) to an ice-covered polar (Icehouse) ocean. In areas such as the Alpha-Ridge, the original main target area of Expedition PS87, pre-Quaternary sediments are cropping out (Jackson et al. 1985; Clark et al. 1986; Thiede et al. 1990; Firth & Clark 1998), which could even be cored with coring gears aboard *Polarstern* and which would allow to study the early preglacial history of the Arctic Ocean. Unfortunately, too strong ice conditions did not allow to reach the Alpha Ridge area (see Chapter 1). Thus, the main target area of the expedition has been shifted to the Lomonosov Ridge where ice conditions just showed the opposite, i.e., minimum ice cover with widespread ice-free conditions on southern Lomonosov Ridge (see Fig. 1.1). These optimum sea-ice conditions allowed us to carry out an extended bathymetric Hydrosweep survey (cf. Chapter 8) as well as detailed multi-channel seismic profiling (cf. Chapter 9).

An important result of these surveys, i.e., a real highlight of the entire expedition, were the discovery and detailed Hydrosweep mapping of large-scale slide scars and mega-slides that occurred along the western slope of Lomonosov Ridge and exposed older in general more deeply buried sediments. Two areas where probably older sediments are cropping-out at the seafloor, were selected for gravity coring from *Polarstern* (Fig. 10.6.20, “Old Seds 1” and “Old Seds 2”). As the coring stations at this steep slope of Lomonosov Ridge are located very close to each other (i.e., about one ship’s length or even less!), a precise navigation and the use of a special acoustic pinger system (“Posidonia”) was needed to locate the ship and the gravity corer exactly on the spot (Fig. 10.6.21).

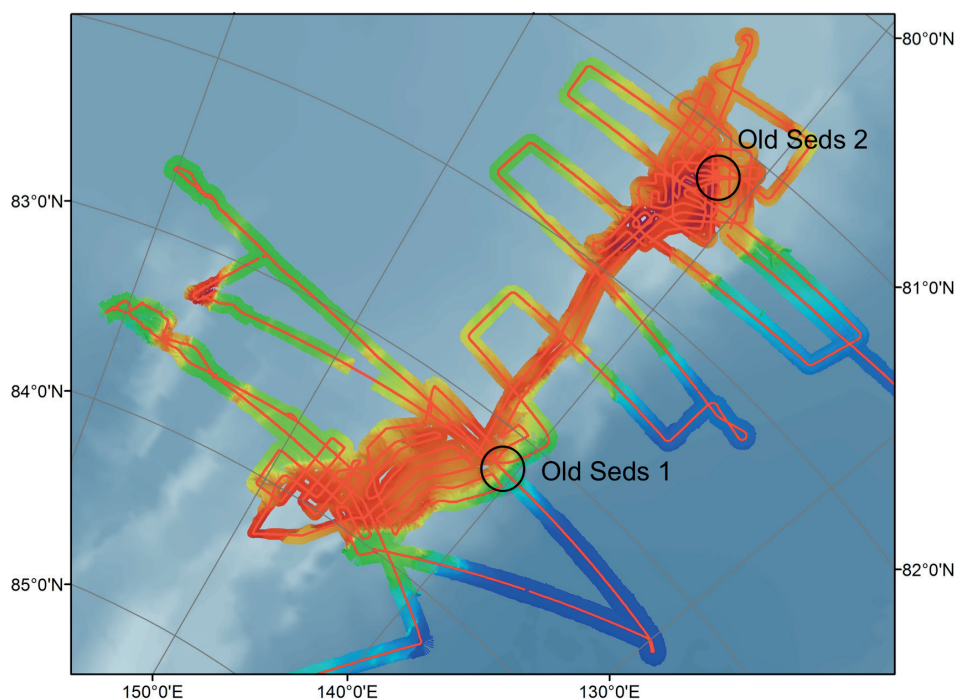


Fig. 10.6.20: Summary plot of Hydrosweep survey tracks carried out during Expedition 87 (see Chapter 8 for details), indicating the areas where probably old (pre-Quaternary) sediments are partly cropping out (Old Seds 1 and Old Seds 2).

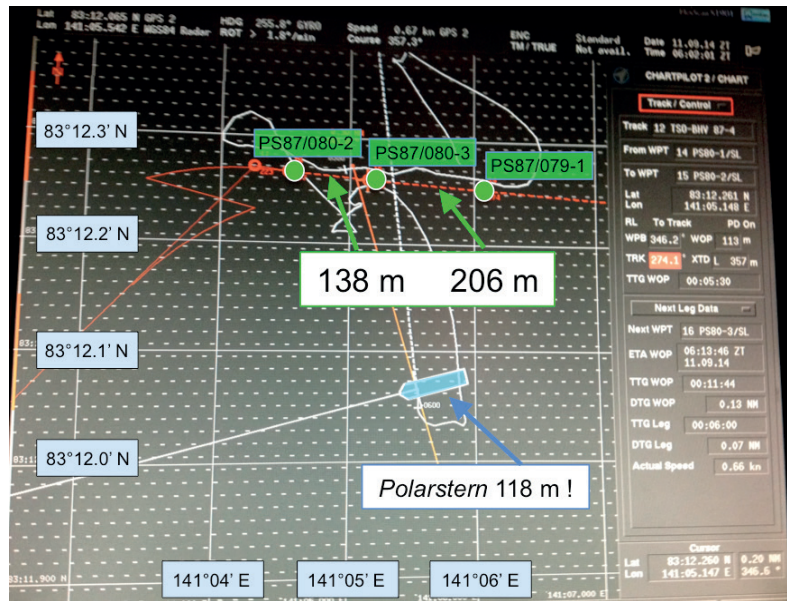


Fig. 10.6.21: Screen shot of navigation screen at the bridge with locations of the three selected coring stations. Distance between core locations and length of Polarstern is indicated.

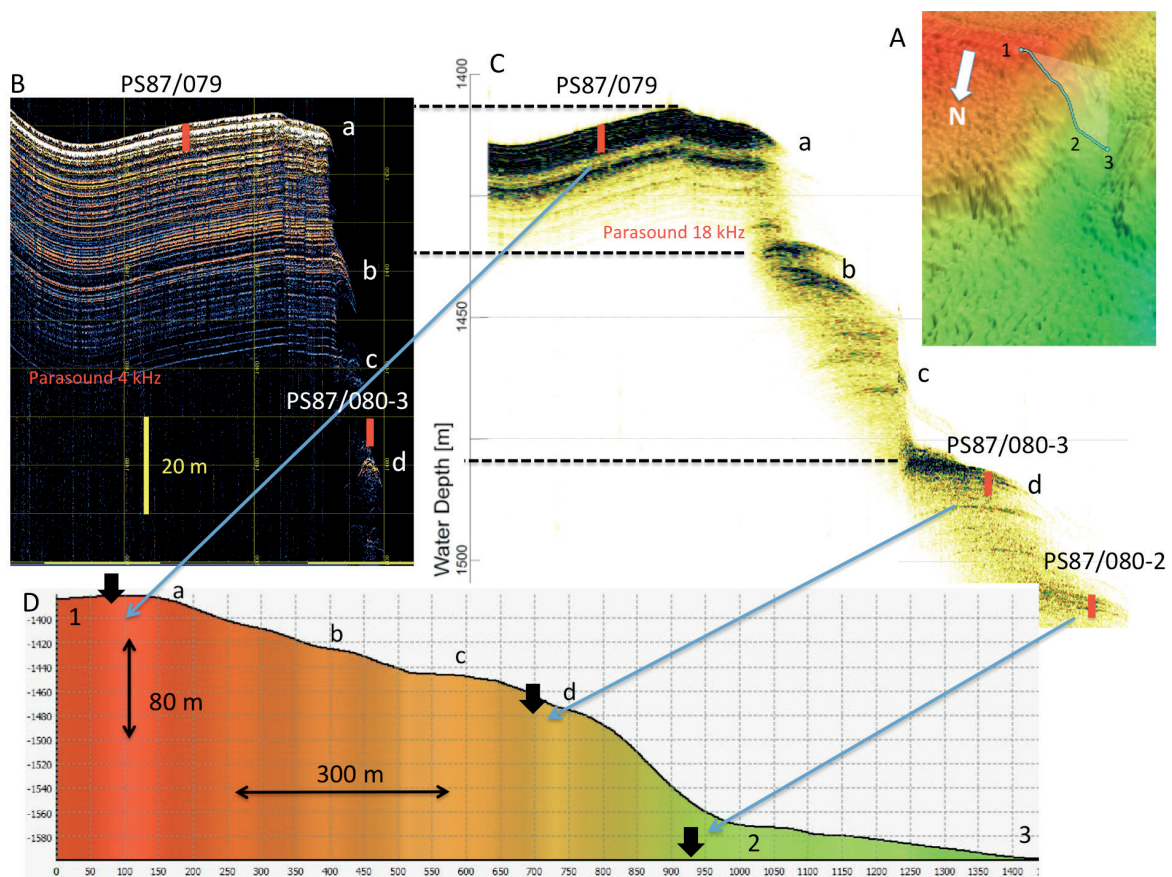


Fig. 10.6.22: Example from Area „Old Seds 1“. (A) Hydrosweep 3D Plot across the slope at Lomonosov Ridge, indicating the location of the Parasound profile of B to D. (B) and (C) Parasound profiles (B: 4 kHz and C: 18 kHz) with locations of Cores PS87/079-1, PS87/080-2 (PS87/080-4) and PS87/080-3 (PS87/080-1); and (D) bathymetric profile with core locations. Numbers 1-3 and letters a-d indicate sections on the profile.

10.6 Main lithologies and lithostratigraphy of PS87 sediment cores

In area "Old Seds 1" at about 83° 12.25' N / 141° E, four sediment cores were taken at the steep slope (Cores PS87/080-1 to PS87/080-4) where older sediments are probably cropping out as suggested from the Parasound profiling, and one reference core was taken on top of Lomonosov Ridge (PS87/079-1) characterized by undisturbed pelagic sedimentation (Fig. 10.6.22). Cores PS87/080-4 and PS87/080-1 were recovered at the same locations as cores PS87/080-2 and PS87/080-3 (shown in Fig. 10.6.22), respectively.

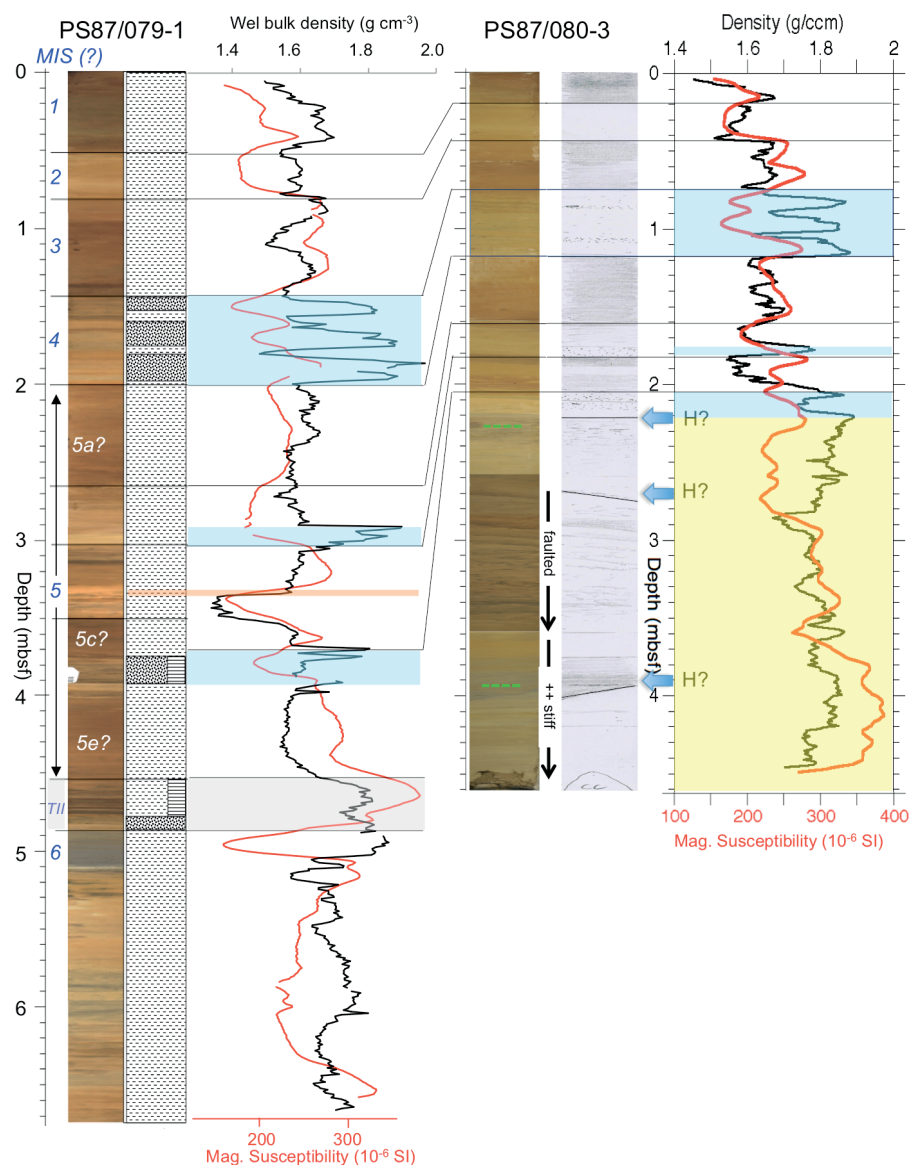


Fig. 10.6.23: Linescan images and summary of visual core descriptions, indicating main lithologies (brown to dark brown, beige and gray silty clay horizons; sandy intervals), and MSCL data (wet bulk density and magnetic susceptibility) of sediment cores PS87/079-1 and /080-3. In addition, depths of suggested hiatuses (H?) in Core PS87/080-3 are shown. Prominent intervals characterized by coarser grain size and WBD maxima and used for core correlation are marked in blue, yellow (10YR7/6) clay layer characterized by a prominent WBD minimum (see also Fig. 10.6.18) in orange („peach layer“?). Green stippled lines mark occurrence of semi-lithified horizon. Proposed chronology (MIS stages) according to Stein et al. (1997); see Fig. 10.6.17 for some more details. Based on this preliminary age model and correlation, the youngest hiatus (erosional/slide event) probably occurred during MIS 5d.

The reference core PD87/079-1 probably represent the time interval from MIS 6 (??) to MIS 1, as already described above (see Fig. 10.6.17). Based on the lithology as well as WBD and MS records, the upper 2 m of Core PS87/080-3 seem to correlate quite well with the upper about 3.7 m of reference core PS87/079-1 representing MIS 5c to MIS 1 (Fig. 10.6.23). Below 2 m, the sediments of Core PS87/080-3 are partly faulted, become more stiff, contain some sharp unconformities, and cannot be correlated with Core PS87/079-1 (Fig. 10.6.23). Based on the lithology, this lower part may contain several hiatuses highlighted by “H” in Fig. 10.6.23. According to the still preliminary age model, the youngest unconformity may coincide with stadial MIS 5d. This erosional event may have been triggered by an extended Siberian ice sheet during that time (cf., Stein et al. 2010a; Niessen et al. 2013). Based on the present data base, however, our first interpretation remains preliminary and further more detailed studies of these sediment cores, especially the chronology, are certainly needed before a more precise reconstruction of the environmental and glacial history is possible.

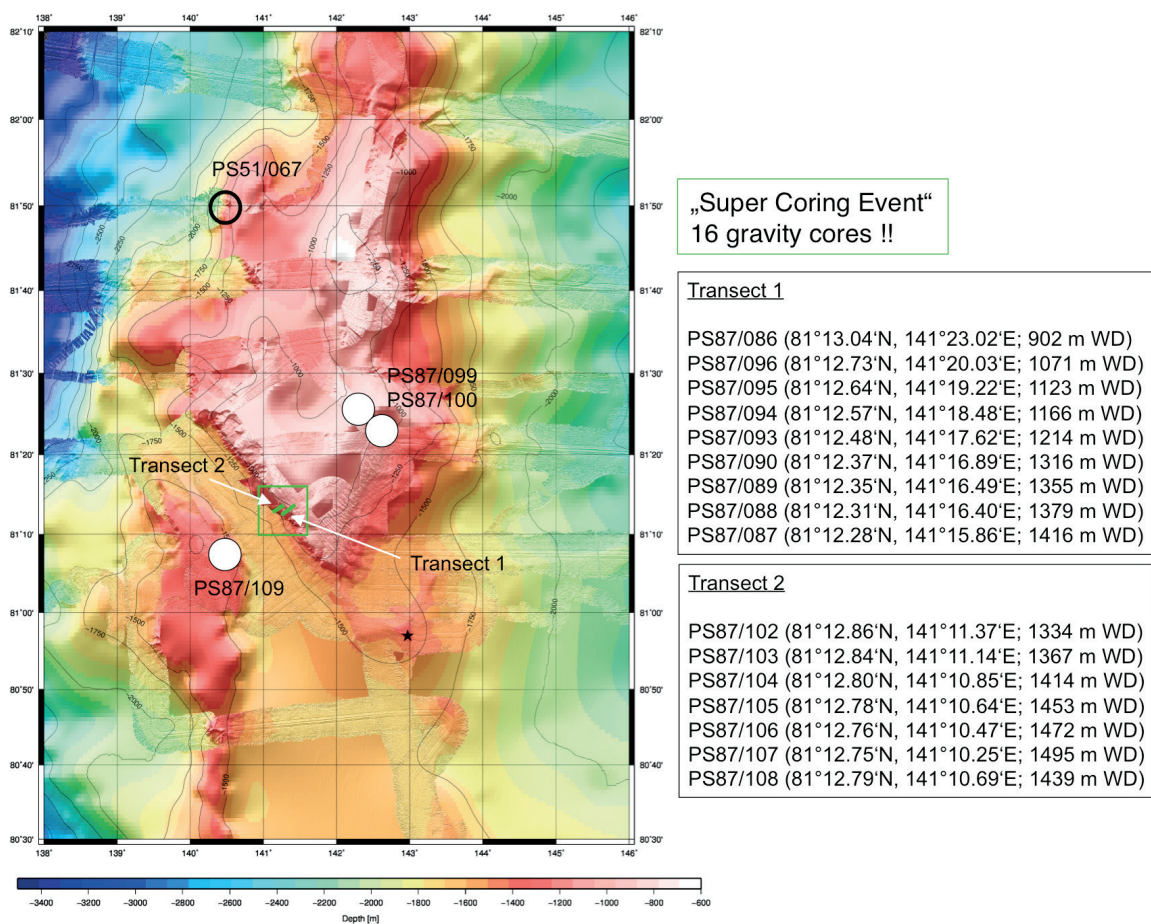


Fig. 10.6.24: Bathymetric map of southern part of Lomonosov Ridge. Cores in green box are those where probably old (pre-Quaternary) sediments are partly cropping out (“Old Seds 2”). Location of Core PS51/067 where also pre-Quaternary sediments are probably cropping out, are also shown (see Fig. 10.6.27).

10.6 Main lithologies and lithostratigraphy of PS87 sediment cores

In area “Old Seds 2” (Fig. 10.6.20), an area characterized by a very steep slope between 900 and >1,400 m of water depth, has been mapped in great detail between 81°25'N/140°E and 81°05'N/142°E (Fig. 10.6.24). That means, comprehensive data sets with Hydrosweep, Parasound and multi-channel seismic profiling data were obtained during Expedition PS87 and are available for future detailed studies. Based on these surveys, two main transects for comprehensive coring activities across the steep slope were selected, and a „super-coring event“ was carried out (Fig. 10.6.24). At Transect 1, eight cores (ie.e., PS87/96 to PS87/087) were recovered between 1071 and 1416 m of water depth (Fig. 10.6.25), at Transect 2 six cores (PS87/102 to PS87/108) were recovered between 1334 and 1439 m of water depth (Fig. 10.6.24). At Transect 1, a reference sediment core (PS87/086) was taken on top of Lomonosov Ridge in a water depth of 902 m, representing undisturbed pelagic sedimentation (Fig. 10.6.25).

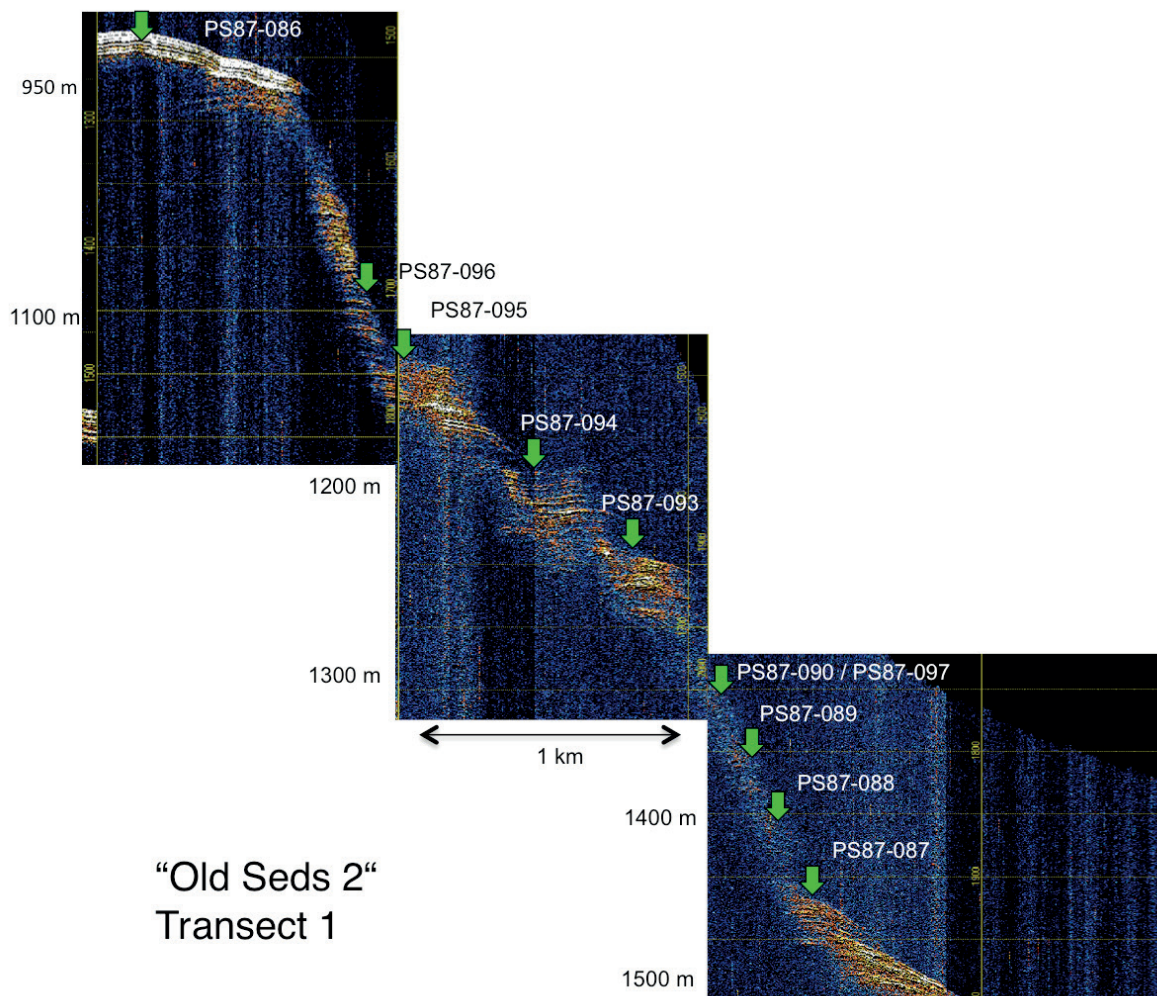


Fig. 10.6.25: Parasound profile across Transect 1 with location of sediment cores PS87/087 to PS87/096 recovered from the steep slope and reference core PS87/086 recovered from the top of Lomonosov Ridge. For location of transect see Fig. 10.6.24.

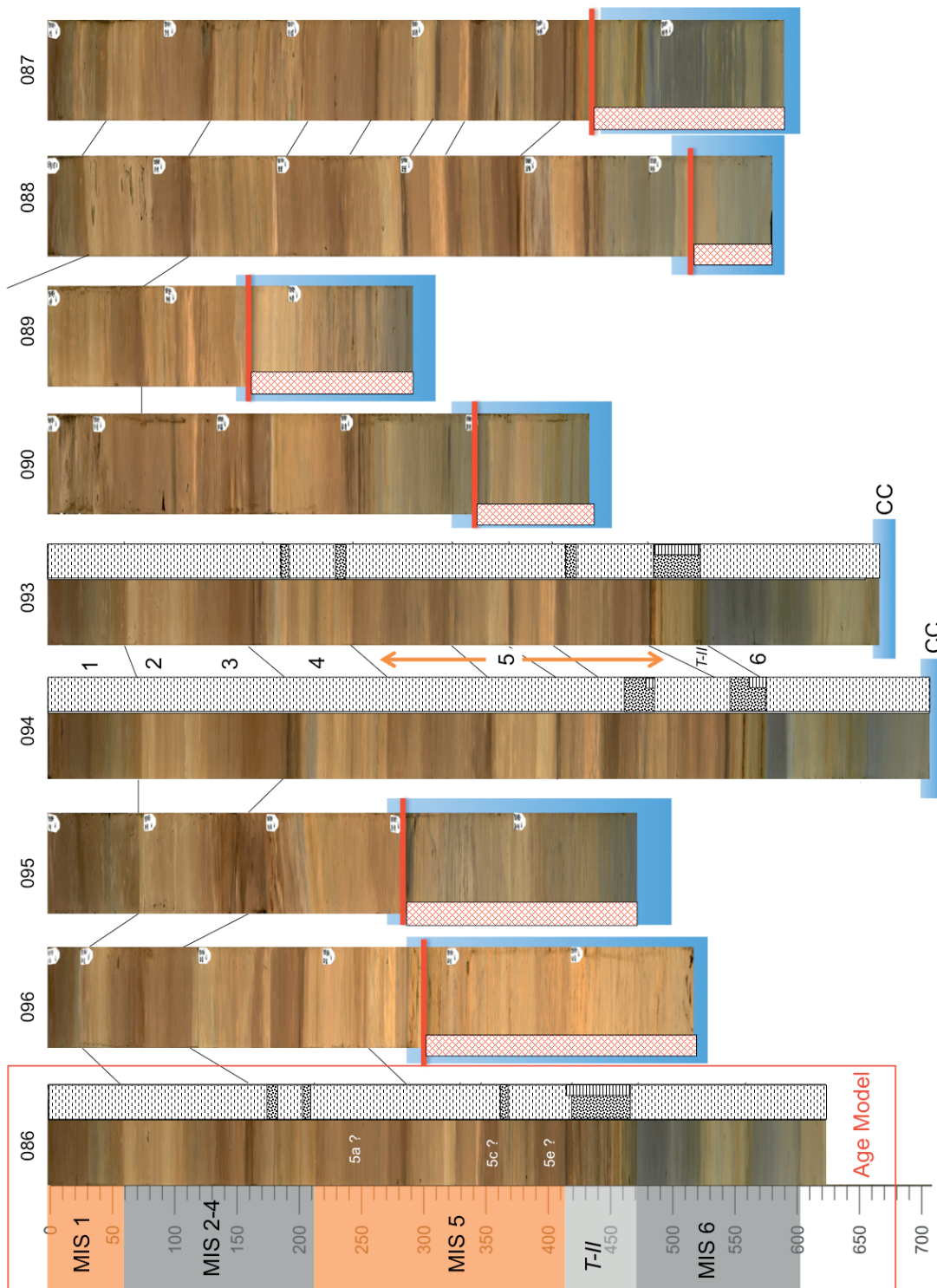


Fig. 10.6.26: Linescan images and summary of visual core descriptions, indicating main lithologies (brown to dark brown, beige and gray silty clay horizons; sandy intervals) of core PS87/086 (reference core of undisturbed section on top of Lomonosov Ridge, water depth 902 m) and cores PS87/096 (shallow) to PS87/087 (deep) from the slope of Lomonosov Ridge between 1071 and 1416 m of water depth. Proposed chronology (Marine Isotope Stages - MIS) according to Stein et al. (1997); see Fig. 10.6.14 for some more details. Below red bar, sediment are very firm suggesting „older“ (pre-Quaternary?) sediments. Core catchers (CC) of cores PS87/093 and PS87/094 contain late Miocene benthic foraminifers (see Chapter 10.8).

10.6 Main lithologies and lithostratigraphy of PS87 sediment cores

Based on the lithological core description, the linescan images and the correlation with the other sediment cores shown in Fig. 10.6.17, the pelagic reference core PS87/086 probably represents the time interval of MIS 6 to MIS 1 (Fig. 10.6.26). According to the still preliminary age model, MIS 6, MIS 5 (5e, 5c and 5a), MIS 4-2 and MIS 1 have been identified. In the cores recovered from the steepest parts of the slope, i.e., cores PS87/087 to PS87/090 as well as PS87/095 and PS87/096 (cf., Fig. 10.6.25), a break in the sedimentary sequence is obvious in the lower part, represented by a more or less abrupt increase in stiffness towards the base of the cores (Fig. 10.6.26). This break may represent a major unconformity, suggesting significantly older sediments may have been recovered in the lowermost part of the sedimentary sections. Based on core correlation, the break in sedimentation/erosional event seems to coincide with MIS 5d and/or MIS 6. How old the sediments below the unconformity really are, cannot be clearly stated so far. At least in the core catchers of cores PS87/093 and PS87/094 some agglutinated benthic foraminifers may point to a late Miocene age (see Chapter 10.8).

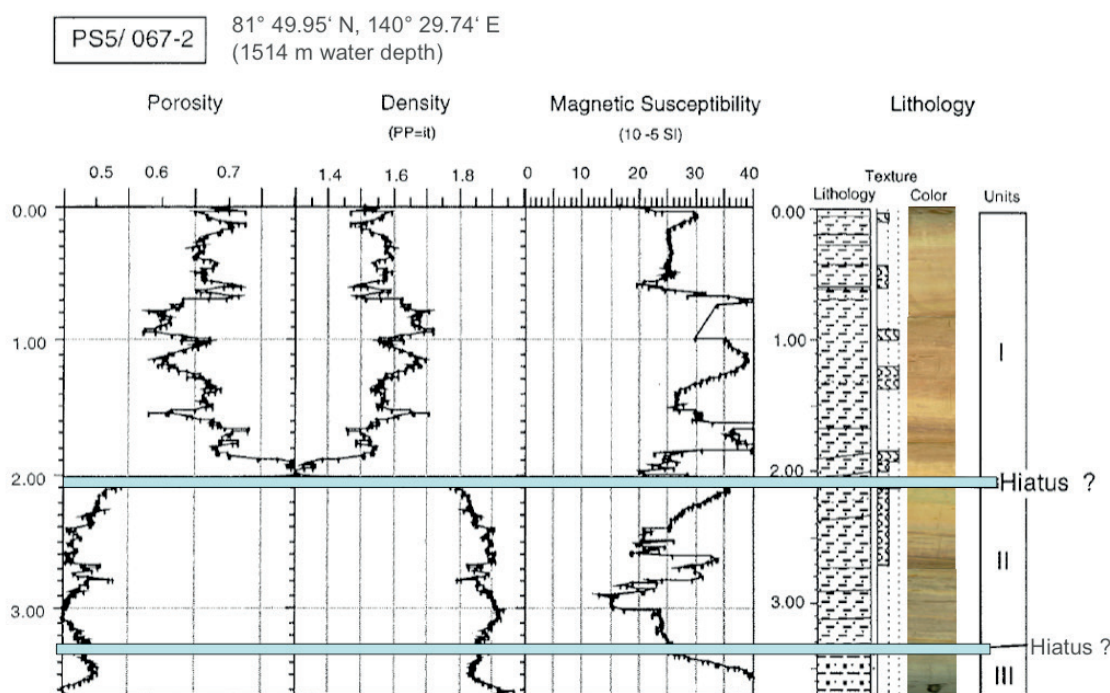


Fig. 10.6.27: Summary plot of MSCL data, main lithology, and sediment colour of Core PS51/067 (recovered during Polarstern Expedition ARK-XIV/1a (Jokat 1999). Position of proposed hiatuses are marked (from Stein et al. 1999).

A major break in sedimentation reflected in the lithology as well as physical property data, was also recorded at the nearby Core PS51/067-2 (for location see Fig. 10.6.24) and interpreted as major hiatus (Fig. 10.6.27; Stein et al., 1999). In his master thesis, Soltmann (2009) compared this record of Core PS51/067-2 with the ACEX drill core (Backman et al. 2006, 2008; Moran et al. 2006; for location of ACEX Site see Fig. 10.1.1) and proposed that the lowermost part of Core PS51/067-2 may be of late/middle Miocene age. Certainly more work has to be done on the PS87 sediment cores to get a better chronology of the sedimentary records. If new data will approve that some of the PS87 sediment cores recovered on Lomonosov Ridge really represent Neogene (or even older?) time intervals, however, this would give the unique chance to get information about the older (preglacial?) climate history of the Arctic Ocean.

References

- Alexanderson H, Backman J, Cronin TM, Funder S, Ingolfsson O, Jakobsson M, Landvik JY, Löwemark L, Mangerud J, März C, Möller P, O'Regan M, Spielhagen RF (2013) An Arctic perspective on dating Mid-Late Pleistocene environmental history. *Quat. Sci. Revs.*, 91, 1-23.
- Arkipov SA, Isayeva LL, Bepaly VG, and Glushkova OY (1986) Glaciation of Siberia and northeast USSR. *Quat. Sci. Rev.*, 5, 463-474.
- Backman J, Jakobsson M, Frank M, Sangiorgi F, Brinkhuis H, Stickley C, O'Regan M, Løvlie R, Pälike H, Spofforth D, Gattacecca J, Moran K, King J, Heil C (2008) Age Model and Core-Seismic Integration for the Cenozoic ACEX Sediments from the Lomonosov Ridge. *Paleoceanography*, doi:10.1029/2007PA001476.
- Backman J, Moran K, McInroy DB et al. (2006) Proceedings IODP, 302, College Station, Texas (Integrated Ocean Drilling Program Management International, Inc.). doi:10.2204/iodp.proc.302.104.2006.
- Björk G, Jakobsson M, Rudels B, Swift JH, Anderson L, Darby DA, Backman J, Coakley B, Winsor P, Polyak L, Edwards M (2007) Bathymetry and deep-water exchange across the central Lomonosov Ridge at 88-89°N. *Deep-Sea Res. I*, 54, 1197-1208.
- Clark DL, Byers CW and Pratt LM (1986) Cretaceous black mud from the central Arctic Ocean. *Paleoceanography*, 1, 265-271. Firth and Clark, 1998
- Clark DL, Whitman RR, Morgan KA, and Mackey SC (1980) Stratigraphy and glacial-marine sediments of the Amerasian Basin, central Arctic Ocean. *GSA Special Paper*, 181, 57 pp.
- Cronin T.M et al. (2013) A 600-ka Arctic sea-ice record from Mendeleev Ridge based on ostracodes. *Quaternary Science Reviews*, 79, 157-167.
- de Vernal A, Gersonde R, Goosse H, Seidenkrantz M-S, Wolff EW (2013) Sea ice in the paleoclimate system: the challenge of reconstructing sea ice from proxies - an introduction. *Quaternary Science Reviews*, 79, 1-8.
- Firth JV. and Clark, DL (1998) An early Maastrichtian organic-walled phytoplankton cyst assemblage from an organic-walled black mud in Core F1-533, Alpha Ridge: evidence for upwelling conditions in the Cretaceous Arctic Ocean. *Mar. Micropaleont.*, 34, 1-27.
- Gard G, Backman J (1990) Synthesis of Arctic and subarctic coccolith biochronology and history of North Atlantic Drift Water influx during the last 500,000 years. In: U. Bleil & J. Thiede (eds.), *Geological history of the polar oceans: Arctic versus Antarctic*. Dordrecht: Kluwer Academic Publishers, NATO ASI Series, C 308: 417-436.
- Jackson HR, Mudie PJ, and Blasco SM (1985) Initial geological report on CESAR - The Canadian Expedition to study the Alpha Ridge, Arctic Ocean. *Geol. Surv. Canada, Paper* 84-22, 177 pp.
- Jakobsson M, Løvlie R, Al-Hanbali H, Arnold E, Backman J, Mörrth M (2000) Manganese and color cycles in Arctic Ocean sediments constrain Pleistocene chronology. *Geology*, 28, 23-26.
- Jokat W (Ed.) (2009) The Expedition ARK-XIV/ 1a of RV *Polarstern* in 1998, *Rep. Pol. Mar. Res.*, 308, 159 pp.
- Jokat W (Ed.) (1999) Arctic '98: The Expedition of the Research Vessel *Polarstern* to the Arctic in 2008, *Rep. Pol. Res.*, 597, 221 pp.
- Löwemark L, März C, O'Regan M, Gyllencreutz R (2014) Arctic Ocean Mn-stratigraphy: genesis, synthesis and inter-basin correlation. *Quat. Sci. Revs.*, 92, 97-111.
- Löwemark L, O'Regan M, Hanebuth T, Jakobsson M (2012) Late Quaternary spatial and temporal variability in Arctic deep-sea bioturbation and its relation to Mn cycles. *Palaeogeogr., Palaeoclimatol. Palaeoecol.*, 365-366, 192-208.

10.6 Main lithologies and lithostratigraphy of PS87 sediment cores

- Marsaglia K, Milliken K, and Doran L (2013) IODP digital reference for smear slide analysis of marine mud. Part 1: Methodology and atlas of siliciclastic and volcanogenic components. IODP Technical Note 1. doi:10.2204/iodp.tn.1.2013
- März C, Stratmann A, Matthiessen J, Meinhardt AK, Ekert S, Schnetger B, Vogt C, Stein R, Brumsack HJ (2011) Manganese-rich brown layers in Arctic Ocean sediments: composition, formation mechanisms, and diagenetic overprint. *Geochim. Cosmochim. Acta*, 75, 7668-7687.
- Moran K, Backman J, Brinkhuis H, Clemens SC, Cronin T, Dickens GR, Eynaud F, Gattacceca J, Jakobsson M, Jordan RW., Kaminski M, King J, Koc N, Krylov A, Martinez N, Matthiessen J, McInroy D, Moore T.C, Onodera J, O'Regan AM, Pälike H, Rea B, Rio D, Sakamoto T., Smith DC, Stein R, St. John K, Suto I, Suzuki N., Takahashi K, Watanabe M, Yamamoto M, Frank M, Jokat W., Kristoffersen Y (2006) The Cenozoic palaeoenvironment of the Arctic Ocean. *Nature*, 441, 601-605.
- Müller C (1999) Rekonstruktion der Paläo-Umweltbedingungen am Laptev-See-Kontinentalrand während der beiden letzten Glazial-/Interglazial-Zyklen anhand sedimentologischer und mineralogischer Untersuchungen. *Reps. Pol. Res.*, 328, 146 pp.
- Niessen F, Hong JK, Hegewald A, Matthiessen J, Stein R, Kim H, Kim S, Jensen L, Jokat W, Nam S-I, Kang S-H (2013). Repeated Pleistocene glaciation of the East Siberian Continental Margin. *Nature Geoscience*, 11.08.2013 (DOI 10.1038/NNGEO1904). Polyak et al. 2004
- Niessen F, Nørgaard-Pedersen N, Musatov E (1997) Physical properties in marine sediments. In: Rachor, E (Ed.), Scientific cruise report of the Arctic Expedition ARK-XI/1 of RV "Polarstern" in 1995, *Rep. Pol. Res.* 226, pp. 133-143.
- Polyak L, Best KM, Crawford KA, Council EA, St-Onge G (2013) Quaternary history of sea ice in the western Arctic Ocean based on foraminifera. *Quaternary Science Reviews*, 79, 145-156.
- Polyak LV, Curry WB, Darby DA, Bischof J, Cronin TM (2004) Contrasting glacial/interglacial regimes in the western Arctic Ocean as exemplified by a sedimentary record from the Mendeleev Ridge. *Palaeogeogr., Palaeoclim., Palaeoecol.* 203, 73-93.
- Rachor E (Ed.) (1997) Scientific cruise report of the Arctic Expedition ARK-XI/1 of RV "Polarstern" in 1995. *Rep. Pol. Res.*, 226, 157 pp.
- Ruddiman WF (1977) North Atlantic Ice-Rafting: a major change at 75,000 years before the present. *Science*, 196, 1208-1211.
- Ruddiman WF, McIntyre A (1976) Northeast Atlantic paleoclimatic changes over the past 600,000 years. *Geol. SOC. Amer. Memoir*, 145; 1 11 -1 46.
- Soltmann Y (2009) Lithostratigraphie von Sedimentabfolgen vom Lomonosov-Rücken: Signifikanz für Paläoumweltrekonstruktionen des spätquartären Arktischen Ozeans. Unpubl. Diplomarbeit, Universität Bremen, 103 pp.
- Stein R (2008) Arctic Ocean Sediments: processes, proxies and paleoenvironment. Elsevier Verlag. 592 p.
- Stein R, Behrends M, Spielhagen RF (1997) Lithostratigraphy and sediment characteristics. In: Rachor, E (Ed.), Scientific cruise report of the Arctic Expedition ARK-XI/1 of RV "Polarstern" in 1995, *Rep. Pol. Res.* 226, pp. 143-153.
- Stein R, Boucsein B, Fahl K, Garcia de Oteyza T, Knies J, Niessen F (2001) Accumulation of particulate organic carbon at the Eurasian continental margin during late Quaternary times: Controlling mechanisms and paleoenvironmental significance. *Glob. Plan. Change*, 31/1-4: 87-102.
- Stein R, Kukina N, Matthiessen J, Müller C, Nørgaard-Pedersen N, Usbeck R (1999) Lithostratigraphy of Alpha Ridge sediments cores., in: Jokat, W. (Ed.), Arctic'98: The Expedition ARKXIV/ 1a of RV *Polarstern* in 1998, *Rep. Pol. Res.* 308, pp. 60-75

- Stein R, Matthiessen J, and Niessen F (2010b) Re-Coring at Ice Island T3 Site of Key Core FL-224 (Nautilus Basin, Amerasian Arctic): Sediment Characteristics and Stratigraphic Framework. *Polarforschung* 79 (2), 81-96.
- Stein R, Matthiessen J, Niessen F, Krylov R, Nam S and Bazhenova E, (2010a) Towards a Better (Litho-) Stratigraphy and Reconstruction of Quaternary Paleoenvironment in the Amerasian Basin (Arctic Ocean). *Polarforschung*, 79 (2), 97-121.
- Thiede J, Clark DL, Hermann Y (1990) Late Mesozoic and Cenozoic paleoceanography of the northern polar oceans, in: *The Geology of North America, Vol. L, The Arctic Ocean Region*, pp. 427-458.
- Velitchko A.A, Dolukhanov PM, Rutter N.W., and Catto N.R (Eds.) (1997) Quaternary of northern Eurasia: Late Pleistocene and Holocene landscapes, stratigraphy and environments. *Quaternary International*, 41/42, 1991 pp.
- Wollenburg JE, Knies J, Mackensen A (2004) High-resolution paleoproductivity fluctuations during the past 24 kyr as indicated by benthic foraminifera in the marginal Arctic Ocean. *Palaeogeography, Palaeoclimatology, Palaeoecology* 204, 209-238.
- Wollenburg JE, Mackensen A, Kuhnt W, (2007) Benthic foraminiferal biodiversity response to a changing Arctic palaeoclimate in the last 24,000 years. *Palaeogeography, Palaeoclimatology, Palaeoecology* , 255, 195-222.

10.7 Occurrences of dropstones

Evgenia Bazhenova¹, Anna Kudriavtseva¹
not onboard A. Krylov²

¹UoStP
²UoStP/VNIIO

Objectives

Identification of source areas for the material transported from the hinterland gives important information about the surface circulation patterns in the Arctic Ocean. Whereas today sea ice is the dominant sediment transport agent, during Pleistocene times icebergs from the continental ice sheets delivered coarse-grained ice-rafted debris to the Arctic Ocean. Based on the petrographical diversity and other characteristics of these rock clasts, information about both past circulation patterns as well as locations where ice sheet existed and calved into the Arctic Ocean, may be obtained (e.g. Bischof et al., 1996; Phillips & Grantz, 2001).

Work at sea

The collected dropstones were taken from box corers, gravity and Kastenlot cores. Sediments from box corers were wet sieved at 0.5 cm. The stones from gravity and Kastenlot cores were collected during description and sampling after opening of the cores. Before the description, every dropstone was washed, numbered and photographed. The sizes of the stones were measured along three perpendicular axes (A – the largest, B – medium, C – the smallest). Based on the length of the A axis, stones were divided into 4 classes following classification by Friedman and Sanders (1978). Preliminary petrographic classification was performed using hand lens observation. Additionally, samples were treated with HCl 1 N to check the presence of carbonate components. Rock clasts were classified based on the Arctic Ocean studies, reported by Bischof et al. (1996) and Phillips and Grantz (2001).

Preliminary results

During the expedition, 514 dropstones of size larger than 1 cm were collected from 17 stations. Information about these stones, including size and composition, is stored in the Appendix. 465 stones were collected from box corers at 16 stations, respective file with results can be located according to Table 10.7.1. Distribution of stones, including the size-based classification, is shown in Fig. 10.7.1. Stones are mainly represented by sandstones and quartzites. Closer to North America and Greenland, also carbonate rocks are abundant.

Tab. 10.7.1: Number of stones collected from giant box corer (GKG) stations and table numbers where detailed data are listed in the Appendix.

N	Station	n of stones > 1 cm	Appendix
1	PS87/003-1	77	Table A5.4.1
2	PS87/023-2	101	Table A5.4.2
3	PS87/026-1	13	Table A5.4.3
4	PS87/029-1	27	Table A5.4.4
5	PS87/030-2	62	Table A5.4.5
6	PS87/040-1	36	Table A5.4.6
7	PS87/055-1	17	Table A5.4.7
8	PS87/056-2	16	Table A5.4.8
9	PS87/067-2	29	Table A5.4.9
10	PS87/068-2	8	Table A5.4.10
11	PS87/070-2	16	Table A5.4.11
12	PS87/074-1	26	Table A5.4.12

N	Station	n of stones > 1 cm	Appendix
13	PS87/076-2	18	Table A5.4.13
14	PS87/079-2	5	Table A5.4.14
15	PS87/086-1	9	Table A5.4.15
16	PS87/109-4	5	Table A5.4.16

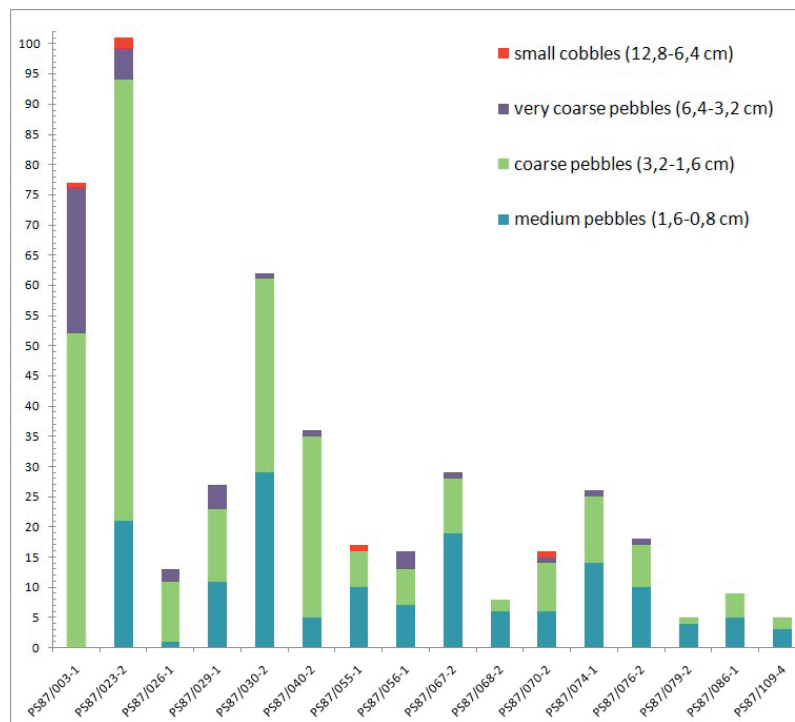


Fig. 10.7.1: Distribution of dropstones collected at the PS87 (ARK-XXVIII/4) giant box corer (GKG) stations and their size-based classification according to Friedman and Sanders (1978).

38 stones were collected from Kastenlot cores at 4 stations. 11 stones were collected from gravity cores at 8 stations. Results for stones from gravity and Kastenlot cores are summarized in Table 10.7.2.

Data Management

Additional provenance investigations will be carried out on the dropstones, including more precise petrographic determination of the rock composition, as well as geochemical and mineralogical analyses for comparison with potential source rocks. Morphological features of dropstones, including roundness, will be used for statistical comparison with the dropstones collected at the Mendeleev Ridge during the ARK-XXIII/3 *Polarstern* Expedition in 2008.

References

- Bischof J, Clark DL, Vincent J-S 1996. Origin of Ice-Rafted Debris: Pleistocene Paleoceanography in the Western Arctic Ocean. *Paleoceanography* 11, 743-756.
- Phillips RL, Grantz A 2001 Regional variations in provenance and abundance of ice-rafted clasts in Arctic Ocean sediments: implications for the configuration of late Quaternary oceanic and atmospheric circulation in the Arctic. *Marine Geology*, 172, 91-115.

10.7 Occurrences of dropstones

Tab. 10.7.2: Occurrence, size (three perpendicular axes: A – the largest, B – medium, C – the smallest), classification according to Friedman and Sanders (1978), and composition of large dropstones.

N	Stone ID	Station	Gear	Depth,	Size, cm			Classification after	
				cm	A	B	C	Friedman & Sanders	Composition
1	K-1	PS87/023-1	KAL	170	11,4	9,2	7,5	small cobbles	quarzite
2	K-2	PS87/023-1	KAL	175	6,7	5,9	4	small cobbles	sandstone
3	K-3	PS87/023-1	KAL	568	2,2	1,8	1,6	coarse pebbles	concretion
4	K-4	PS87/023-1	KAL	595	2,5	2,2	1,6	coarse pebbles	quarzite
5	K-5	PS87/023-1	KAL	460	5,5	3,7	2,6	very coarse pebbles	effusive
6	K-6	PS87/023-1	KAL	642	4,5	3,9	1,9	very coarse pebbles	sandstone
7	K-7	PS87/023-1	KAL	417	3,6	2,9	2,7	very coarse pebbles	sandstone
8	K-8	PS87/023-1	KAL	460	1,6	1,3	0,8	coarse pebbles	sandstone
9	K-9	PS87/023-1	KAL	593	3	2,3	1,5	coarse pebbles	granite
10	K-10	PS87/023-1	KAL		5,2	3	1,7	very coarse pebbles	sandstone carb.
11	K-11	PS87/023-1	KAL		2,4	2	1,7	coarse pebbles	quarzite
12	K-12	PS87/023-1	KAL		2	2	1,3	coarse pebbles	chert
13	K-13	PS87/023-1	KAL	383	5	4	3	very coarse pebbles	sandstone carb.
14	K-14	PS87/023-1	KAL	138	2,8	2,7	1,9	coarse pebbles	quarzite
15	K-15	PS87/023-1	KAL	464	5,1	3,6	3,3	very coarse pebbles	quarzite
16	K-16	PS87/023-1	KAL	379	2,7	1,6	1,3	coarse pebbles	quarzite
17	K-17	PS87/023-1	KAL	438	3,7	2,4	1,8	very coarse pebbles	quarzite
18	K-18	PS87/023-1	KAL	175	4	3,2	2,3	very coarse pebbles	quarzite
19	K-19	PS87/023-1	KAL	368	3,3	2,5	2	very coarse pebbles	volcanic
20	K-22	PS87/023-1	KAL	89	2,4	1,5	1,1	coarse pebbles	dolomite
21	K-23	PS87/023-1	KAL	288	2,2	1,7	1,3	coarse pebbles	quarzite
22	K-24	PS87/023-1	KAL	382	2,1	1,7	0,6	coarse pebbles	shale
23	K-25	PS87/023-1	KAL	154	2,1	1,3	0,6	coarse pebbles	quarzite
24	K-26	PS87/023-1	KAL	124	1,4	1,3	0,8	medium pebbles	sandstone
25	K-27	PS87/023-1	KAL	132	1,5	1,2	0,7	medium pebbles	sandstone met.
26	K-28	PS87/023-1	KAL	698	2	1,2	0,6	coarse pebbles	sandstone
27	K-29	PS87/023-1	KAL	532	1,4	1,1	0,8	medium pebbles	
28	K-30	PS87/023-1	KAL	514	1,4	0,6	0,4	medium pebbles	
29	K-31	PS87/023-1	KAL	148	1,1	0,8	0,8	medium pebbles	
30	K-32	PS87/023-1	KAL	124	1,1	1	0,8	medium pebbles	
31	K-33	PS87/023-1	KAL	534	1,1	0,9	0,3	medium pebbles	
32	K-34	PS87/023-1	KAL	536	1,4	1,1	0,7	medium pebbles	
33	K-35	PS87/023-1	KAL	596	1,1	0,8	0,7	medium pebbles	
34	K-43	PS87/040-1	KAL	41	6,1	4,1	3,3	very coarse pebbles	sandstone met.
35	K-37	PS87/051-1	SL	171	10	6,1	4,2	small cobbles	quarzite
36	K-40	PS87/056-1	KAL	172	2	1,5	1,3	coarse pebbles	quarzite
37	K-41	PS87/056-1	KAL	122	1,4	1,4	1	medium pebbles	sandstone
38	K-42	PS87/056-1	KAL	181	1,4	1,3	0,8	medium pebbles	undetermined
39	K-39	PS87/067-1	SL	227	7,3	6,4	3,6	small cobbles	quarzite
40	K-38	PS87/067-1	SL	236	7,2	5,4	2,2	small cobbles	sandstone met.
41	K-48	PS87/070-1	KAL		0,9	0,8	0,8	medium pebbles	
42	K-36	PS87/078-1	SL	104	3,1	2,5	1,8	coarse pebbles	sandstone
43	K-44	PS87/079-1	KAL	305	2,7	1,8	1	coarse pebbles	sandstone
44	K-20	PS87/083-3	SL	92	6,3	5,1	2,2	very coarse pebbles	sandstone
45	K-19	PS87/083-3	SL	330	3,6	2,5	1,8	very coarse pebbles	sandstone
46	K-21	PS87/090-1	SL	95	4,5	3,7	1,7	very coarse pebbles	sandstone
47	K-45	PS87/094-1	SL	364	1,8	1,4	0,8	coarse pebbles	sandstone
48	K-46	PS87/109-2	SL	487,5	2,2	1,8	1,3	coarse pebbles	granite
49	K-47	PS87/109-2	SL	27	1,4	1	0,7	medium pebbles	sandstone

10.8 Micropaleontology and biostratigraphy

Stefanie Kaboth¹, Mike Kaminski², Seung-il Nam³,
Mike Zwick⁴, Anne de Vernal⁵

¹AWI

²KFU

³KOPRI

⁴UoBr

⁵GEOTOP

Objectives

Micropaleontological examination of sediment samples was carried out on board in order to document the biogenic content of the sediment, to establish a biostratigraphic scheme, and to determine the age of the oldest sediments recovered in the long kastenlot and gravity cores. The occurrence, abundance, and taxonomic diversity of the microfossils preserved in sediment provide a picture of the pelagic fluxes and benthic productivity, but it also depends upon the preservation of calcium carbonate, opaline silica, and marine organic matter. The microfossils preserved in Arctic sediments thus form the basis for paleoecological and paleoceanographic interpretations. Moreover, the occurrence of key species may help to establish a biostratigraphical scheme and to propose correlations with the biostratigraphy of the Arctic Ocean in reference to previous studies, both for the Pleistocene (e.g. Ishman et al. 1996; Polyak et al. 2013; Alexandresson et al. 2014), and for older Neogene sediments (e.g. Kaminski et al. 2005, 2009).

Work at sea

Surface sediment samples collected with the giant box corer were examined to characterize their paleontological content. The macrofauna visible on the sediment surface was subsampled for further observation and identification. The uppermost 2 cm of the sediment were also subsampled and washed through a 63 µm mesh sieve for on-board observations. The observation of the >63 µm fraction was made on a tray of 9 X 5 cm and the volume examined corresponds to approximately one third of a cubic centimetre. The biogenic content is succinctly reported, and special attention was paid to ostracodes, planktic and benthic foraminifers, which dominate the microfaunal assemblages. Their occurrence is reported semi-quantitatively, from rare to abundant. The identification of common benthic foraminifer taxa was made at genera or species level. The identification of common benthic foraminifer taxa was made at generic or species level, mostly in reference to Herman (1973), Lagoe (1977), Wollenburg (1992, 1996) for the calcareous shells, and in reference to Verdenius and Van Hinte (1983) and Kaminski et al. (1990, 2005, 2009) for the agglutinated forms. The occurrence of ostracodes, sponge spicules and echinoderm spines were also noted downcore. The most distinctive ostracode taxa were identified after Joy and Clark (1977) and Stepanova et al. (2002).

The Kastenlot cores were subsampled on board for semi-quantitative micropaleontological analyses with the main objective of providing preliminary information about the downcore biogenic content and biostratigraphy. The samples analysed represent an initial volume of about 30 cm³, which were wet sieved at 63 µm. The sand contents (see Appendix, Tables A5.5.1, A5.5.2, A5.5.4, A5.5.5, and A5.5.7) refer to height (mm) of material in vials having a radius of 1 cm, thus corresponding to about 0.3 cm³ or about 1 % of the total volume processed. The abundance of foraminifers is given in reference to the number of specimens per tray. For planktic foraminifers, it corresponds to a scale ranging 0-4 as follows: 0 (none), 1 (rare < 5), 2 (frequent = 5-50), 3 (common = 50-500); 4 (abundant > 500). For benthic foraminifers, it corresponds to the following scale : 0 (none), 1 (rare < 5), 2 (frequent = 5-10), 3 (common = 10-50); 4 (abundant > 50). The tables also report the occurrence of a few diagnostic calcareous benthic foraminifer taxa (*Cassidulina*, *Oridorsalis tener*) in addition to ostracodes, sponge spicules and spines of echinoderms. No attempt of calibration for microfossil density was made and the results presented here only provide first order estimates of abundances. Semi-

quantitative analyses were performed, mostly from the >125 µm fraction. Special attention was paid to foraminifers, including planktic and benthic foraminifers, the latter being represented by agglutinated and/or calcareous taxa. The occurrence of foraminifers was reported in terms of abundance on a scale ranging from 0 (absent) to 4 (abundant).

Large-volume samples (about 100 – 250 cm³) were collected from the core-catchers of the gravity cores. In this study focussing on the agglutinated taxa, samples were gently sieved under a spray of water, without 'rubbing the sample through the sieve' and sample residues were dried at 60°C. The foraminifers were picked from the >125 µm fraction, and mounted onto cardboard microscope slides.

Preliminary results

Biogenic content of surface sediment samples

The examination of surface sediment samples collected from the surface of the giant box core from 17 sites indicates a very rich biogenic content. In most cores, macrofossils were observed at the surface. They include shells of bivalves, gastropods, remains of silicisponges and echinoderms, in addition to fish otoliths and calcareous tubes of polychaetes. It is of note, however, that none of the biological remain mentioned above was seen alive. The results of visual observations (macrofauna) and observation under microscope binocular (microfauna) of are reported in Table 10.8.1.

The >63 µm of the uppermost 2 cm consisted in biogenic ooze dominated by planktic foraminifers in most cases except samples PS87/086, PS87/099, PS87/100 and PS87/109, which were characterized by abundant (> 70%) small-size sand particles. Among planktic foraminifers, *Neogloboquadrina pachyderma* sinistral was dominant in all samples, with very rare occurrence of subpolar taxa such as *Turborotalita quinqueloba*, *Globigerina bulloides* and the dextral form of *Neogloboquadrina pachyderma*.

Benthic foraminifer assemblages include a large variety of calcareous taxa among which *Oridorsalis tener*, *Cibicidoides wuellerstorfi*, and *Triloculina* sp. often dominate. At the deeper sites (PS87/067 and PS87/068), *Cibicidoides* was noted to be particularly abundant with some specimens being poorly preserved and showing features of alteration.

Agglutinated foraminifers are present in all surface sediment samples, but their taxonomic diversity is variable. In addition to foraminiferal shells, calcareous remains include ostracodes, juvenile bivalve shells, spicules and plates of echinoderms, pteropods and unidentified shell fragments. Siliceous microfossils include sponge spicules, which occur in almost all samples. Radiolaria and diatoms were rarely seen. In general, higher taxonomical diversity characterized the biogenic assemblages of shallower sites.

Tab. 10.8.1: Paleontological and micropaleontological content of surface sediment recovered by giant box coring (GKG). The macrofauna refer to biogenic remains seen and collected at the surface of the box core before to sediment sampling. The microfauna refer to biogenic remains recovered in the > 63 µm fraction of the uppermost 2 cm in the giant box core. Occurrence is indicated by « X ». Among planktic foraminifer assemblages, the almost exclusive dominance of *Neogloboquadrina pachyderma* left-coiling is indicated by « D ».

Core number	023-2	026-1	029-1	030-2	040-2	055-1	056-2	067-2	068-2	070-1	074-1	076-2	079-2	086-1	099-3	100-1	109-4
Water depth (m)	2439	3339	2909	1275	2629	737	836	2857	2711	1340	2816	2763	1359	901	741	951	1303
MACROFAUNA (> 2 mm)																	
Bivalvia undifferentiated/fragments	X			X	X	X	X			X	X			X	X	X	X
<i>Yoldiella</i> sp.	X	X	X	X	X	X		X	X	X	X	X	X	X	X	X	X
cf. <i>Hyalopecten</i>			X	X	X	X		X	X	X		X					
<i>Hiatella arctica</i>										X				X			
<i>Mya</i>																	X
<i>Cuspidaria</i>						X									X		X
Bivalvia (unidentified)				X		X	X		X				X	X	X		X
Gastropod (type <i>Buccinum</i>)				X							X		X				
Gastropod (operculum)				X									X	X	X		X
Scaphopod				X		X	X			X			X	X	X		X
Fish otoliths	X			X		X	X							X	X		X
Sponges						X	X		X		X						
Calcareous tubes of polychaetes				X										X	X	X	X
Echinoderm plates										X				X	X		X
Bryozoa (on shells or tubes)															X		
MICROFOSSILS (> 63 µm)																	
Echinoderm spines				X		X	X			X				X	X	X	X
Echinoderm plates				X		X	X							X	X	X	X
Sponges spicules	X	X	X	X	X	X	X	X	X	X	X	X	X	X	X	XX	X
Gastropod (<i>Limecola helicina</i>)	X			X	X	X	X			X				X	X		X
Bivalvia (juvenile forms)			X	X	X	X	X			X				X	X	X	X
Bivalvia (shell fragments)	X		X	X	X	X	X		X		X			X	X	X	X
Brachiopods							X										
Radiolaria			X	X	X		X	X	X	X	X		X	X			
Diatoms	X			X						X							
Bryozoa						X											
Lignous fragment														X			X
Ostracods																	
<i>Cytheroïperon</i> spp. (alate forms)	X	X	X		X		X	X	X	X	X	X	X	X	X	X	X
cf. <i>Acetabulastroma arcticum</i>	X	X	X		X	X	X	X	X	X	X	X	X	X	X	X	X
cf. <i>Echinocythereis</i>			X	X	X			X	X	X	X	X				X	X
<i>Polycopse</i> spp.				X		X	X			X				X			
Valves with smooth ornamentation	X	X	X	X	X	X	X	X	X	X			X	X	X		X
cf. <i>Heterocypridis</i>						X	X										
Planktic foraminifers																	
<i>Neogloboquadrina pachyderma</i> l.	D	D	D	D	D	D	D	D	D	D	D	D	D	D	D	D	D
<i>Neogloboquadrina pachyderma</i> d.	X	X	X	X	X	X	X	X	X	X	X	X	X	X	X	X	X
<i>Globigerina bulloides</i>				X	X	X	X	X	X	X	X	X	X	X	X	X	X
<i>Turborotalia quinqueloba</i>	X	X	X	X	X	X	X	X	X	X	X	X	X	X	X	X	X
Calcareous benthic foraminifers																	
<i>Bolivina</i>														X			
<i>Bulinella</i>						X	X								X		
<i>Cassidulina</i>						X	X			X				X	X	X	X
<i>Ceratobullina</i>					X				X								
<i>Cibicides</i>	X	X	X	X	X	X	X	X	X	X	X	X	X	X	X		X
<i>Chilostomella</i>						X	X										
<i>Cyrtogira</i>	X																X
<i>Dentalina</i>							X					X					X
<i>Epistominella</i>											X			X			X
<i>Eponides</i>	X	X	X		X	X	X	X	X	X	X	X	X				X
<i>Fissurina</i>							X										X
<i>Favulina</i>						X											
<i>Fursenkoina</i>			X		X		X						X	X	X	X	X
<i>Haynesina</i>	X				X				X	X			X	X	X	X	X
<i>Legena</i>		X			X					X				X			X
<i>Melonis</i>																	X
<i>Nodosaria</i>									X								
<i>Nonionella</i>			X			X	X		X	X			X		X	X	X
<i>Onidorsalis</i>	X	X	X	X	X	X	X	X	X	X	X	X	X	X	X	X	X
<i>Parafussurina</i>					X							X		X	X	X	
<i>Patellina</i>							X										
<i>Polymorphina</i>								X									X
<i>Pullenia</i>						X											
<i>Pyrgo</i>	X		X		X	X	X						X	X	X		X
<i>Quinqueloculina</i>	X		X	X	X				X	X	X		X		X		X
<i>Reussoculina</i>	X	X	X					X			X						
<i>Stetsonia</i>	X	X	X		X	X	X	X	X	X	X	X	X	X	X		
<i>Triloculina</i>	X	X	X	X	X	X	X	X	X		X	X	X	X	X	X	X
Agglutinated benthic foraminifers																	
Agglutinated plates	F	R	F		R	C	C	F	C	C	C	C	A	A	A	A	A
<i>Alveophragmium</i>										X							
<i>Ammodiscus</i>			X		X			X	X								
<i>Archimerismus</i>														X	X	X	X
<i>Bathysiphon</i>					X									X	X	X	X
<i>Cribrostomoides</i>	X				X							X	X	X	X	X	X
<i>Cnithionina</i>																	X
<i>Eggerelloides</i>															X		
<i>Glomospira</i>			X						X								
<i>Hemisphaerammina</i>										X							X
<i>Hormosinelloides</i>														X	X	X	X
<i>Hyperammina</i>	X		X		X		X		X				X		X	X	X
<i>Jacutella</i>																	X
<i>Lagenammina</i>																	
<i>Placostilina</i>	X		X		X								X				
<i>Psammospaera</i>										X				X	X	X	X
<i>Pseudonodosinella</i>		X	X				X		X	X				X	X	X	
<i>Recurvoides</i>			X			X	X	X	X	X							
<i>Reophax</i>														X		X	X
<i>Rhizammina</i>						X	X			X				X		X	X
<i>Rhabdammina</i>								X	X					X	X	X	X
<i>Saccorhiza</i>															X		
<i>Tolypammina</i>														X			
<i>Trochammina</i>								X	X							X	
Remarks :																	
(1) signs of CaCO ₃ alteration; (2) Sand content ~30-50%; (3) Sand content > 70%			1			2		1	1		1	1	2	3	3	3	3

Biostratigraphy of Kastenlot cores: on board analyses and preliminary results

Core PS87/023-1-KAL

Core PS87/023-1-KAL was subsampled in continuous at 2-cm intervals for on board analyses of the micropaleontological content. The results of semi-quantitative observations are presented in Appendix Table A5.5.1 and schematically illustrated in Fig. 10.8.1.

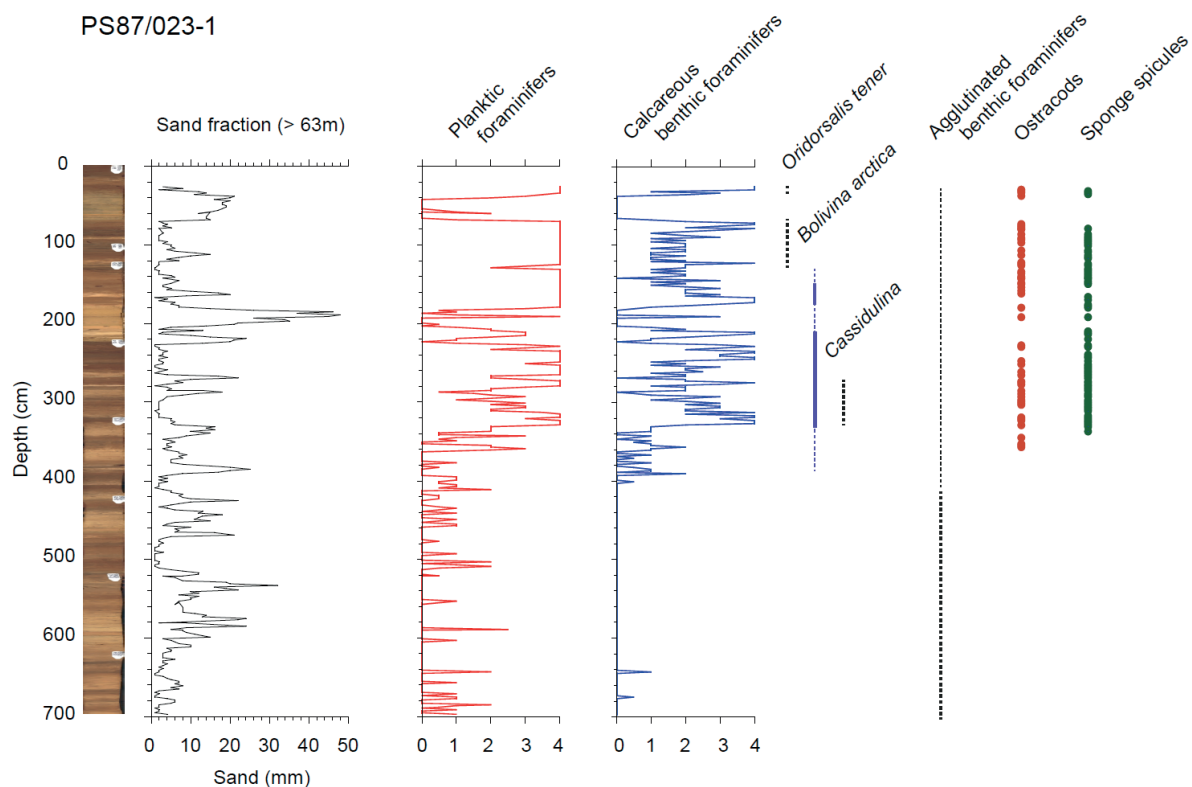


Fig. 10.8.1: Schematized stratigraphy of core PS87/023-1-KAL. From left to right, log of the cores from photographs, sand (> 63µm) content expressed in mm which corresponds to about 1% of the total volume processed, abundance of planktic foraminifers on a scale ranging from 0 (none) to 4 (abundant; i.e. > 500 specimens per tray), abundance of calcareous benthic foraminifers on a scale ranging from 0 (none) to 4 (abundant; i.e. > 50 specimens per tray), occurrence (dashed line) and acme (thick line) of key benthic foraminifer taxa, abundance of agglutinated benthic foraminifers on a scale ranging from 0 (none) to 4 (abundant; i.e. > 50 specimens per tray), occurrence of ostracodes and sponge spicules. See Appendix Table A5.5.1 for data.

In the upper ~400 cm of the core, the biogenic content of sediment is generally high and taxonomically diversified with dominant calcareous microfossils. Planktic foraminifers are abundant in most samples. The assemblages are largely dominated by *Neogloboquadrina pachyderma* leftcoiling, with dextral forms being a very minor component. Benthic foraminifers are often common and ostracodes and sponge spicules also occur in many samples down to about 360 cm.

The calcareous benthic foraminifer assemblages recovered downcore are showing a high diversity of species and are generally well-preserved. *Oridorsalis tener* is dominating the

assemblage between 69 to 130 cm with variable abundance of *Cibicoides* spp., *Triloculina frigida* and *Pyrgo* spp. *Bolivina arctica* dominates the assemblage from 144 to 330 cm with a remarkable abundance peak between 210 to 232 cm where the >63 μm size fraction consists quasi exclusively in *B. arctica* shells. A zonation may be developed from the occurrence of *B. arctica* and *O. tener*, allowing correlation with biostratigraphical scheme from the Northwind Ridge as defined by Ishman et al. (1996).

Throughout the core, rare agglutinated foraminifers were observed, most being poorly preserved. The dominant genera observed throughout the lower half of the core include *Reticulophragmium*, *Rhabdammina*, *Alveolophragmium*, *Psammosphaera* and *Trochammina*. Because of the fragmentary nature of the recovered specimens, the agglutinated foraminifers in this core were not studied in detail.

Core PS87/030-1-KAL

Core PS87/030-1-KAL was subsampled at 5-cm intervals for on board analyses of the micropaleontological content. The results of semi-quantitative observations are presented Table A5.5.2 (Appendix) and schematically illustrated in Fig. 10.8.2.

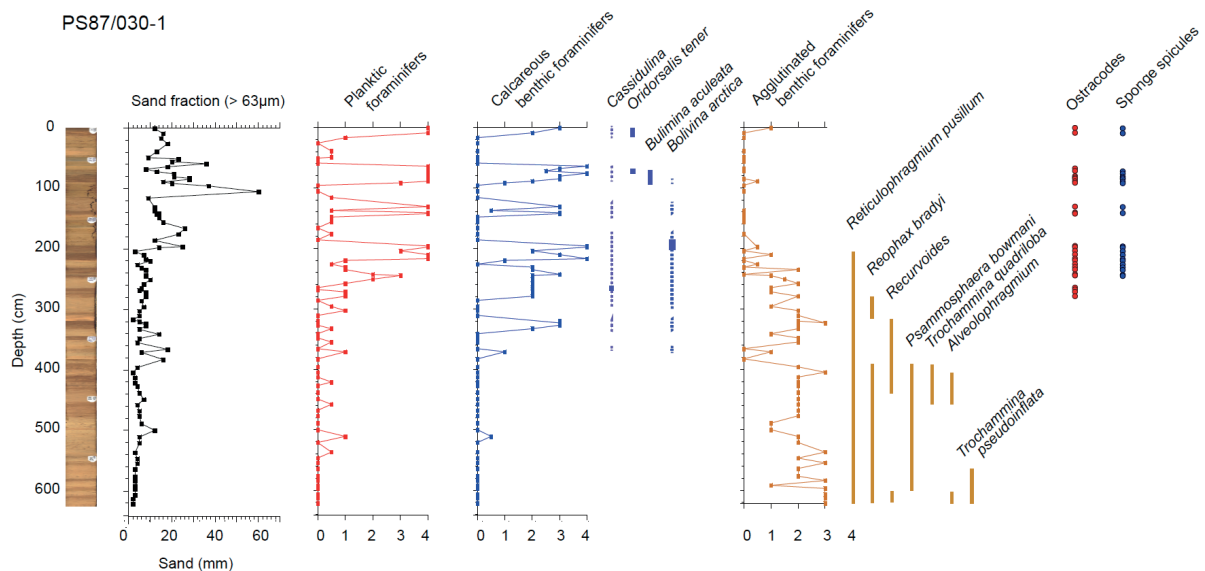


Fig. 10.8.2: Schematized stratigraphy of core PS87/030-1-KAL. From left to right, log of the cores from photographs, sand (> 63 μm) content expressed in mm which corresponds to about 1% of the total volume processed, abundance of planktic foraminifers on a scale ranging from 0 (none) to 4 (abundant; i.e. > 500 specimens per tray), abundance of calcareous benthic foraminifers on a scale ranging from 0 (none) to 4 (abundant; i.e. > 50 specimens per tray), occurrence (dashed line) and acme (thick line) of key benthic calcareous foraminifer taxa, abundance of agglutinated benthic foraminifers on a scale ranging from 0 (none) to 4 (abundant; i.e. > 50 specimens per tray), discontinuous occurrence (dashed line) and continuous occurrence (thick line) of agglutinated foraminifer taxa, occurrence of ostracodes and sponge spicules. See Appendix Tables A5.5.2 and A5.5.3 for data.

In the uppermost 350 cm, calcareous foraminifers including benthic and planktic taxa occur in relatively high number, with exception of a few layers. Calcareous benthic foraminifer assemblages show a very high diversity of species and a generally good preservation. Among the taxa recorded, some have a biostratigraphic value. Among those, *Oridorsalis tener* dominated the assemblage between 0 to 65 cm with *Cassidulina teretis*, *Cibicidoides* spp. and *Triloculina frigida*. Below 67 cm and down to 90 cm, *Bulimina acculeata* occurred as characteristic species. It should be noted that this is the only interval within all the studied cores where this taxon has been seen. From 71 to 372 cm, *Bolivina arctica* is common and is often associated with *C. teretis*. The remarkable abundance peak of *B. arctica* of Kastenlot core PS87/023-1 could not be identified in core PS87/030-1 probably due to the lower sample resolution and/or the shallower water depth of core PS87/030-1. Nevertheless, a zonation may be developed from the occurrence of *B. arctica*, *O. tener* and *B. aculeata*, allowing to propose correlations with biostratigraphical scheme from the Northwind Ridge as defined by Ishman et al. (1996) and Alexanderson et al. (2014) from other sectors of the Arctic Ocean.

In the lower part of the core, from 215 cm, agglutinated benthic foraminifers occur in relatively high numbers. They dominate the biogenic content of sediment below 350 cm. Given their abundance and their potential use for biostratigraphy, special attention has been paid in agglutinated foraminifer assemblages from 215 cm to 621 cm. In this interval, 25 samples were picked quantitatively into microscope slides and analysed to describe the agglutinated fauna (cf. Appendix Table A5.5.2). A total of 27 species were recorded among which many are reported for the first time to occur in modern or Pleistocene sediments in the Arctic Ocean (Evans and Kaminski, 1998). The agglutinated foraminifers have thus the potential to produce stratigraphically meaningful record. Moreover, overlaps with calcareous benthic foraminifers should enable cross-correlation between calcareous benthic and agglutinated assemblages.

The agglutinated faunal assemblage consists of a mixture of cosmopolitan species such as *Reticulophragmium pusillum* and Arctic endemics such as *Alveolophragmium polarensis*. The dominant species throughout the core are *Reticulophragmium pusillum*, *Trochammina lomonosovensis*, *Haplophragmoides* sp. 1, and *Psammosphaera fusca*. At 215 cm, the agglutinated assemblages are sparse and dominated by *R. pusillum*. Below, the diversity of agglutinated foraminifers progressively increases. The relative proportions of *Haplophragmoides* sp. 1 and *Trochammina lomonosovensis* also increase downcore, and species diversity reaches a maximum between 395 and 457 cm. Two intervals containing *Alveolophragmium polarensis* are observed: the upper one between 404 and 457 cm, and the one between 606 cm and the bottom of the core. The occurrence of *Trochammina quadriloba* and *Cribrostomoides subglobosus* in the core is restricted to the upper *A. polarensis* interval. The species *Psammosphaera bowmani* is fairly common between 395 and 583 cm. This species first described from the North Sea has not been previously reported from the Arctic. Because of its small dimensions it was most likely overlooked in previous studies. At 510 cm, the assemblage is dominated by *Haplophragmoides* sp. 1 and *Trochammina lomonosovensis*, with subordinate *R. pusillum* and *Psammosphaera*. The small, fragile tests of *Haplophragmoides* are common in the core, but this taxon has not been previously reported to occur in the Arctic. It most closely resembles the species *Haplophragmoides trullisatus*, but a detailed comparison and a differential description needs to be carried out. There appears to be two forms of this species always occurring together: a microspheric form that often has darker agglutinated grains along its sutures, and a larger, more lobate megalospheric variety with a visibly larger proloculus.

Core PS87/056-1-KAL

The section from 179 to 232 cm, which presented interesting sedimentary features was subsampled and analysed at about 10 cm intervals. All samples consisted mainly of quartz sand, with no biogenic remains except traces of agglutinated foraminifers (see Appendix, Table A5.5.4). A single specimen of *Trochammina lomonosoviensis* was observed at 188–190 cm. The sample at 195–197 contained rare specimens of *Psammospaera fusca* and *Placopsilinella aurantiaca*, the latter species attached to sand grains. Because of the low abundance of foraminifers in these samples, no further analysis was done.

Core PS87/070-1-KAL

Core PS87/070-1-KAL was subsampled and analysed at 10-cm to 20-cm intervals. With the exception of the upper ~70 cm that contain calcareous foraminifers, ostracodes and sponges spicules, the micropaleontological content of the core PS87/070-1 consists almost exclusively of agglutinated foraminifers (cf. Table A5.5.5 and Fig. 10.8.3).

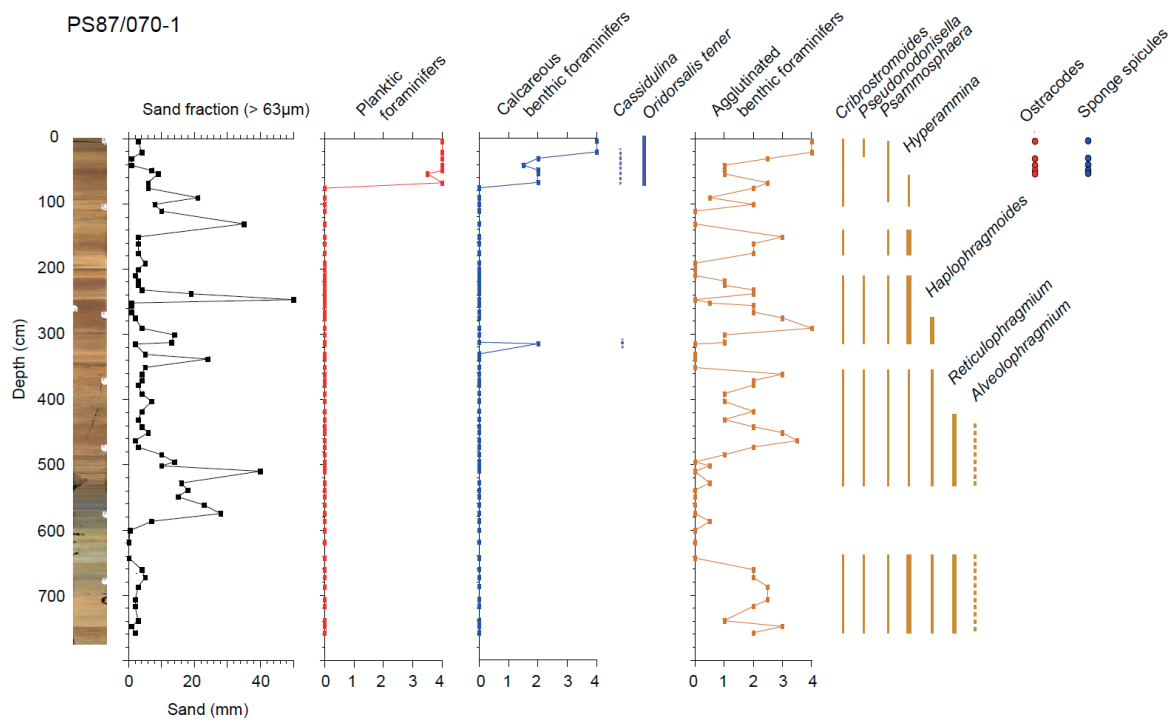


Fig. 10.8.3: Schematized stratigraphy of core PS87/070-1-KAL. From left to right, log of the cores from photographs, sand (> 63 μm) content expressed in mm which corresponds to about 1% of the total volume processed, abundance of planktic foraminifers on a scale ranging from 0 (none) to 4 (abundant; i.e. > 500 specimens per tray), abundance of calcareous benthic foraminifers on a scale ranging from 0 (none) to 4 (abundant; i.e. > 50 specimens per tray), occurrence (dashed line) and acme (thick line) of key benthic calcareous foraminifer taxa, abundance of agglutinated benthic foraminifers on a scale ranging from 0 (none) to 4 (abundant; i.e. > 50 specimens per tray), discontinuous occurrence (dashed line) and continuous occurrence (thick line) of agglutinated foraminifer taxa, occurrence of ostracodes and sponge spicules. See Appendix Table A5.5.5 and A5.5.6 for data.

The planktic foraminifer assemblages of the upper 70 cm are largely dominated by *Neogloboquadrina pachyderma* sinistral, with rare occurrences of its dextral form. Among calcareous benthic taxa with stratigraphical importance, only *Cassidulina* and *Oridorsalis tener* were identified. It should be noted that neither *Bulimina aculeata* nor *Bolivina arctica* were found in the samples examined.

Special attention was paid to agglutinated foraminifers, which were recovered throughout the core with exception of a few barren intervals (cf. Appendix Tables A5.5.5 and A5.5.6; Figure 10.8.3). In the upper 40 cm of the core, the assemblages mainly comprised of *Cribrostomoides subglobosus* accompanied by *Psammosphaera fusca* and *Pseudonodosinella nodulosa*. Below 48 cm, *Hyperammina rugosa* became a characteristic component of the assemblage. At ~ 150 cm the highest stratigraphic occurrences of *Gomospira* and *Rhabdammina* is recorded. The agglutinated foraminifers become more abundant below 265 cm, where the highest stratigraphic occurrence of *Verrucina arctica* is observed, mainly attached to fragments of *Psammosphaera fusca*. The highest occurrence of *Haplophragmoides* sp. 1 was found at ~290 cm. From ~ 360 to 432 cm, the assemblage consisted of *Haplophragmoides* sp. 1 with *Hyperammina*, *Rhabdammina*, *Glomospira*, *Pseudonodosinella*, and large agglutinated plates. Below, the abundance of agglutinated foraminifers increases with the highest stratigraphic occurrences of *Reticulophragmium pusillum* and *Evolutinella* sp. 1. From this level down to the base of the core, *R. pusillum* remained the dominant species. The highest occurrence of *Alveolophragmium polarensis* was found at ~ 462. The interval from ~ 484 to 644 cm is nearly barren or only contains a few specimens of *R. pusillum* in isolated samples. In the lower part of the core, below 660 cm, the agglutinated foraminifers increased in abundance and diversity with occurrence of *R. pusillum* and *Cribrostomoides*, *Alveolophragmium*, *Hyperammina rugosa*, *Rhabdammina*, *Psammosphaera*, *Haplophragmoides*, *Pseudonodosinella*, *Glomospira*, and *Placopsilinella*.

Core PS87/079-1-KAL

Core PS87/079-1-KAL was subsampled at ~20-cm intervals. The results of semi-quantitative observations are presented Appendix Tables A5.5.7 and A5.5.8 and schematically illustrated in Fig. 10.8.4. With the exception of the upper ~40 cm that contain few calcareous foraminifers, the micropaleontological content of core PS87/079-1 consists almost exclusively of agglutinated foraminifers. Hence, special attention has been paid to agglutinated taxa in order to develop a biostratigraphical scheme based on highest occurrences of the common taxa.

The agglutinated foraminiferal assemblage in the upper section of the core is sparse and comprised of only a few species. *Pseudonodosinella nodulosa* and *Glomospira gordialis* are present at 10–12 cm, and are observed sporadically throughout the core. Both species were also found in modern foraminiferal assemblages from box cores collected on the Lomonosov Ridge (cf. above). In the sample at 100–102 cm, agglutinated foraminifers are more common with highest occurrence of the coarsely-agglutinated *Hyperammina rugosa* and *Hemisphaerammina* sp. The highest occurrences of *Reticulophragmium pusillum* and *Cribrostomoides subglobosus* were observed at 120–122 cm, and the highest occurrence of *Trochammina lomonosovensis*, *Reophax* spp., were found at 143–145 cm. Below 196 cm, the agglutinated fauna records an increase in species diversity and includes *Hyperammina*, *Recurvoides*, *Glomospira*, *Rhabdammina*, and *Hemisphaerammina*. From 410 to 514 cm, *Hyperammina* and *Psammosphaera* occur in association with *Cribrostomoides*, *Verrucina*, and *Placopsilinella*. The interval from 540 cm to the base of the core contains a diverse assemblage with the finely-agglutinated species *Haplophragmoides* and *Rhabdammina*, in addition to *Reophax duplex* and *Glomospira*. Finally, the core-catcher sample yielded a total

of 13 species dominated by *R. pusillum*, with common *Haplophragmoides*, *Hyperammina* and *Psammosphaera*. The genera *Ammodiscus*, *Glomospira*, *Rhabdammina*, *Evolutinella*, *Pseudonodosinella* and *Alveolophragmium* were present in smaller proportions.

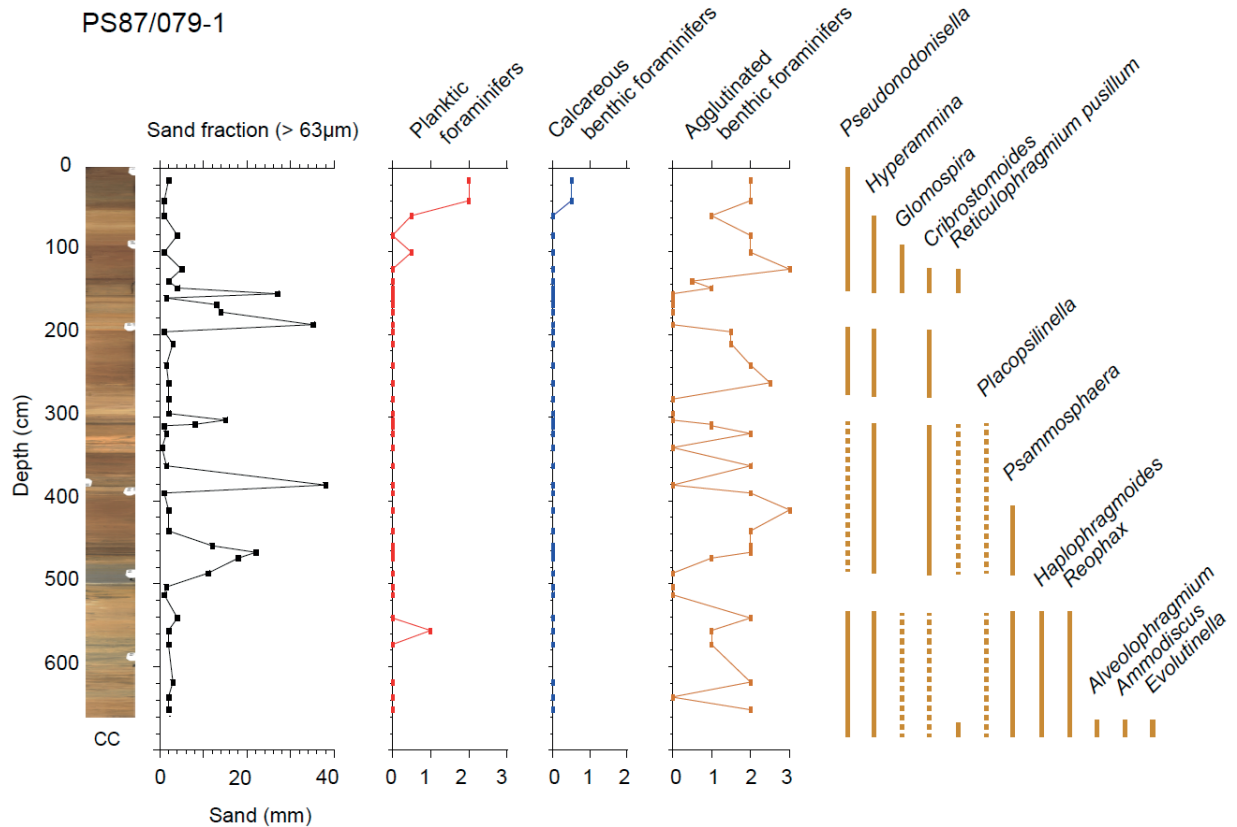


Fig. 10.8.4: Schematized stratigraphy of core PS87/079-1-KAL. From left to right, log of the cores from photographs, sand (> 63µm) content expressed in mm which corresponds to about 1% of the total volume processed, abundance of planktic foraminifers on a scale ranging from 0 (none) to 4 (abundant; i.e. > 500 specimens per tray), abundance of calcareous benthic foraminifers on a scale ranging from 0 (none) to 4 (abundant; i.e. > 50 specimens per tray), occurrence (dashed line) and acme (thick line) of key benthic calcareous foraminifer taxa, abundance of agglutinated benthic foraminifers on a scale ranging from 0 (none) to 4 (abundant; i.e. > 50 specimens per tray), discontinuous occurrence (dashed line) and continuous occurrence (thick line) of agglutinated foraminifer taxa, occurrence of ostracodes and sponge spicules. See Appendix Tables A5.5.7 and A5.5.8 for data.

Foraminifera from core catcher samples from Kastenlot and gravity core stations

No calcareous biogenic remains were observed in any of the samples, except in that of core PS87/086-3 that contained a few *N. pachyderma* specimens, which might represent contamination. Some samples were totally barren and others contained agglutinated foraminifers as summarized on Table 10.8.2.

10.8 Micropaleontology and biostratigraphy

From the 28 core-catcher samples studied on board a total of 35 species and other taxonomic groups of deep water agglutinated foraminifers were recorded (Table 10.8.2), which is nearly three times the number of taxa reported by Evans and Kaminski (1998) from the *Polarstern* cores collected in 1991.

Tab. 10.8.2: Occurrence of agglutinated benthic foraminifer taxa in core catcher samples of kastenlot and gravity cores. R = rare (<5 specimen), F = frequent (5-10), C = common (10-50), A = abundant (> 50). Gray columns correspond to samples barren in agglutinated foraminifers. Tentative age assignments are made in the last row of the table (see text for details).

Core number	PS87/023-1-KAL	PS87/030-1-KAL	PS87/068-1-GC	PS87/070-2-KAL	PS87/074-3-GC	PS87/079-1-KAL	PS87/080-3-GC	PS87/080-4-GC	PS87/086-3-GC	PS87/087-1-GC	PS87/088-1-GC	PS87/089-1-GC	PS87/090-1-GC	PS87/093-1-GC	PS87/094-1-GC	PS87/095-1-GC	PS87/096-1-GC	PS87/097-1-GC	PS87/099-2-GC	PS87/100-2-GC	PS87/102-1-GC	PS87/103-1-GC	PS87/104-1-GC	PS87/105-1-GC	PS87/106-1-GC	PS87/107-1-GC	PS87/108-1-GC	PS87/109-2-GC
Species																												
<i>Alveolophragmium polarensis</i>	F					R								R	C					F				R			R	F
<i>Ammodiscus catinus</i>					R	F																						
<i>Bathysiphon</i> sp.																		A										
<i>Capsamina</i> sp.																	A											
<i>Cribrostomoides subglobosus</i>							R	R									A											
<i>Evolutinella</i> sp. 1						F											A											
<i>Glomospira charoides</i>	R																											
<i>Glomospira gordialis</i>			F	F	F																							
<i>Glomospira irregularis</i>	R			F																								
<i>Haplophragmoides</i> sp. 1	R					C	F									A							R				R	
<i>Haplophragmoides</i> cf. <i>carinata</i>																A												
<i>Haplophragmoides sphaeriloculus</i>						F																						
<i>Hemisphaerammina</i> sp.	R		F			R					R														R			R
<i>Hormosinella distans</i>																	A											
<i>Hormosinelloides</i> cf. <i>guttifer</i>																A												
<i>Hyperammina rugosa</i>	R	F		F	F	C			R					R		A					R		R					A
<i>Karrerulina apicularis</i>						R																						
<i>Lagenammina arenulata</i>	R		R													A												
Large agglutinated plates	F	F		R		R	R	R								A								R				R
<i>Placopsilinella aurantiaca</i>																								R				
<i>Psammosphaera fusca</i>	F	F	R	R	R	F	F	R								A												R
<i>Psammosphaera bowmani</i>		F			F	R										A												R
<i>Psammosiphonella cylindrica</i>																A												
<i>Pseudonodosinella nodulosa</i>	R				R	F																						
<i>Recurvoides laevigatum</i>	R		F			C		R				R					A									R		
<i>Reophax bradyi</i>	F	F		F			R	R																				
<i>Reophax duplex</i>																	A											
<i>Reticulophragmium pusillum</i>	C	F	C	C	F	A	C	F	A							A	R		R		C		R				R	A
<i>Rhabdammina discreta</i>																A												
<i>Rhabdammina antarctica</i>	F		R					R																				
<i>Rhabdammina</i> sp. 1		F		R	C	F		R	R			R					A											
<i>Rhizammina</i> spp.																	A											
<i>Trochammina lomonosovensis</i>	F	F		F	C		R																					
<i>Trochammina quadrilobus</i>																	A											
<i>Verrucina arctica</i>	R																											
Probable age	P	P	P	P	P	P	P	P	P		EP			LM	LM		P	EP		LM		EP		EP			EP	EP
P= Pleistocene; EP = Early Pleistocene; LM = Late Miocene																												

The foraminifers found in the core-catcher samples are mostly extant species, which can be found in the modern Arctic Ocean and its marginal seas. The two species of *Haplophragmoides* reported here have not been previously illustrated from the modern Arctic Ocean, although *H. sphaeriloculus* is known to occur in the abyssal Pacific and in the Atlantic Ocean. The most common pre-Holocene species is *Reticulophragmium pusillum*, followed by *Psammosphaera fusca*. The “large agglutinated plates” may be fragments of large *Psammosphaera* specimens, and/or fragments of an unknown agglutinated protozoan. *Reticulophragmium pusillum* and the coarsely-agglutinated species *Hyperammina rugosa* have not been previously reported in the literature on modern Arctic foraminifers, but these species are well-known from the Cenozoic of the Norwegian Sea DSDP and IODP cores (Verdenius and Van Hinte, 1983; Kaminski et al., 1990, 2005), and both species were found in the Miocene of the ACEX cores drilled on the Lomonosov Ridge (Kaminski et al. 2009). The minute attached species *Verrucina arctica* is here reported for the first time since its initial discovery by Cushman (1948). It generally grows like a mushroom, attached to fragments of *Psammosphaera fusca*.

Assessing the age of the sediment recovered in the cores is difficult because most of the extant species of agglutinated foraminifers have long or unknown stratigraphic ranges. Fortunately, the preservation state of specimens from core catchers in comparison with those found in kastenlot cores PS87/030-1 and PS87/70-1 can provide useful indication of the sediment age. Because all agglutinated species build their shells out of quartz grains bound by organic cement, they are susceptible to degradation and decay after a period of time. Bacteria present in the sediment consume the organic cement used to bind the shell, which then becomes fragile and eventually disintegrates. Consequently, many delicate species found in the modern ocean either leave no fossil record, or are only preserved under exceptional circumstances. In the kastenlot cores studied on board, the modern and late Pleistocene assemblages are diverse, but the delicate species disappeared downcore. Therefore, we can use the preservation state of the fauna to provide a rough estimate of the sediment age. Younger assemblages should show better preservation and higher diversity, and contain more delicate species than older assemblages.

Studies of the ACEX cores (Kaminski et al., 2009) revealed low species diversity in the older Pleistocene to Pliocene assemblages and the occurrence of large robust forms such as *Reticulophragmium pusillum*, *Alveolophragmium polarensis*, and *Rhabdammina* sp. The Late Miocene assemblages recovered on the Lomonosov Ridge were dominated by the species *Alveolophragmium polarensis*. The older Middle Miocene assemblages in the ACEX cores were taxonomically diverse and showed relatively good preservation because of the presence of silica in pore waters. They also contained species that are known from the Oligocene and Miocene of the Norwegian Sea (see Kaminski et al. 2005).

Using the stratigraphy of the kastenlot cores as a guide together with information from ACEX cores, we may assess that the majority of core-catchers contained Late or Middle Pleistocene material, which is younger than ca. 1 Ma. However, the *R. pusillum*-dominated assemblages recovered at the base of cores PS87/088-1, PS87/97-1, PS87/103-1, PS87/109-2 are likely to be early Pleistocene or Pliocene. Core catchers PS87/105-1 and PS87/108-1 are probably older than the assemblages found in the Kastenlot cores, but still Pleistocene in age. Only three of the core-catcher samples analysed on board (PS87/93-1, PS87/94-1, and PS87/100-2) contain assemblages dominated by *Alveolophragmium polarensis*, and may be as old as late Miocene or latest middle Miocene. The very distinctive oldest Middle Miocene assemblage found in the ACEX cores was not recovered.

Preliminary conclusions

The examination of the micropaleontological content in 17 surface sediment samples from box cores, 544 samples from 5 kastenlot cores and of core catcher samples from 28 kastenlot and gravity cores permits some considerations about the biogenic content of sediments and biostratigraphy as summarized below:

The surface sediments all contained rich microfossil assemblages dominated by planktic foraminifers (mostly *N. pachyderma*), with benthic foraminifers, both agglutinated and calcareous, ostracodes, sponge spicules, echinoid and mollusc remains.

The microfossils recovered at the surface are mostly composed of calcium carbonate, which apparently preserves well under the present day conditions. The occurrence of pteropods (*Limacina helicina*) shells composed of aragonite is another sign of good calcium carbonate preservation. The only samples showing signs of CaCO₃ alteration are those collected below 2,700 m water depth.

The downcore observations indicate a generally high biogenic content, also dominated by calcareous remains, but only in the western part of the Lomonosov Ridge, down to about 350 and 250 cm in cores PS87/023-1 and PS87/030-1 respectively. In contrast, the calcareous biogenic content of the cores PS 87/070-1 and PS87/79-1 from the eastern Lomonosov Ridge is restricted to the uppermost 70 cm.

In cores PS87/023-1 and PS87/030-1 from western Lomonosov Ridge, the abundance of calcareous foraminifers and occurrence of a few benthic taxa (*Bolivina arctica*, *Bulimina aculeata* and *Oridorsalis tener*, notably) can be used to define a stratigraphical scheme. In particular, the lowest occurrence of *O. tener* coincides with the highest occurrence of *B. arctica* in both cores and the transition appears concomitant with the occurrence peak of *B. aculeata* in core PS87/030. Correlations with other biostratigraphic records from the Arctic Ocean can be proposed, notably based on the work of Ishman et al. (1996) and Alexanderson et al. (2014). Age assignments are not straightforward in the absence of absolute dating of Pleistocene Arctic sedimentary sequences. Nevertheless, the interval encompassing the lowest occurrence of *O. tener*, highest occurrence of *B. arctica* and the acme of *B. aculeata* in core PS87/030-1 probably belong the marine isotope stage 5a after regional correlations proposed by Adler et al. (2009) and Alexanderson et al. (2014) based on various geochronological approaches. Therefore, one may propose an age of ca. 80 ka at about 125 cm in core PS87/023-1, and between 67 and 90 cm in core PS87/030-1.

In the lower part of core PS87/030-1, below 250 cm and in the cores PS87/070-1 and PS87/79-1 from the eastern Lomonosov Ridge, agglutinated foraminifers dominate almost exclusively the microfaunal assemblages and appear characterized by a relatively high taxonomical diversity, increasing downcore. Thus, special attention should be paid to agglutinated foraminifers in the Arctic Ocean as a means to develop a biostratigraphical scheme for the early to middle Pleistocene. In most previous studies of the Arctic Pleistocene, the agglutinated foraminifers were treated as a group, with no attempt to identify the species. In the PS87 cores more than 35 species have been identified, which is much more than what was reported in any previous study from the Arctic Ocean. Hence, agglutinated foraminifers offer a great potential for biostratigraphical purposes. However, samples must be treated as gently as possible in order to avoid breaking delicate specimens. Whereas many taxa may have a local paleoecological significance, the observations made during Expedition PS87 suggest that some taxa such as *Alveolophragmium polarensis*, *Haplophragmoides sp. 1*, *Hyperammina rugosa* and *Reticulophragmium pusillum*, may be useful biostratigraphical markers.

The micropaleontological data collected during Expedition PS87 show a geographical gradient from west to east with a decrease in calcareous microfossil abundance to the east relative to the increased abundance of agglutinated taxa. A stratigraphical gradient seems to also characterize also the Lomonosov Ridge with a decrease in biogenic carbonate together with an increase in the taxonomic diversity of agglutinated foraminifers downcore. These gradients suggest large scale regionalism along the Lomonosov Ridge in relation with ocean circulation, water chemistry and productivity. They also indicate that a major change occurred in the paleoceanography of the Arctic Ocean during the Late Pleistocene. This change might have been time transgressive from the West to the East of the Lomonosov Ridge.

Micropaleontological studies of the core-catcher samples from the “older sediments” suggest that Pre-Pleistocene sediments were cored at three stations (PS87/93-1, PS87/94-1, and PS87/100-2). In the core catcher samples at these sites, agglutinated foraminiferal assemblages dominated by *Alveolophragmium polarensis* may be as old as late Miocene or latest middle Miocene. The *R. pusillum*-dominated assemblages recovered at the base of cores PS87/088-1, PS87/97-1, PS87/103-1, PS87/109-2 are likely to be early Pleistocene or Pliocene in age. Core catchers PS87/105-1 and PS87/108-1 are probably older than the assemblages found in the Kastenlot cores, but are still Pleistocene in age. Unfortunately the distinctive Middle Miocene assemblage documented from the ACEX core by Kaminski et al. (2009) was not observed.

Data management

All micropaleontological residues and microscope slides from the shipboard analyses will be stored in the collections of Micropaleontology Press (MicroPress Europe) at the AGH University of Science & Technology, Faculty of Geology, Geophysics, and Environmental Protection, in Kraków, Poland.

References

- Adler RE, Polyak L, Crawford KA, Grottoli AG, Ortiz JD, Kaufman DS, Channell JET, Xuan C, Sellen E (2009) Sediment record from the western Arctic Ocean with an improved Late Quaternary age resolution: HOTRAX core HLY0503-8JPC, Mendeleev Ridge. *Global and Planetary Change*, 68, 18-29.
- Alexanderson H, Backman J, Cronin TM, Funder S, Ingólfsson O, Jakobsson M, Landvik JY, Löwemark L, Mangerud J, März C, Möller P, O'Regan M, Spielhagen RF (2014) An Arctic perspective on dating Mid-Late Pleistocene environmental history. *Quaternary Science Reviews*, 92, 9-31
- Cushman JA (1920) Foraminifera from the Atlantic Ocean. Part 2. Lituolidae. *United States National Museum Bulletin*, 104, 111 pp.
- Cushman JA (1948) Arctic Foraminifera. Cushman Laboratory for Foraminiferal Research Special Publication, 23, 79 pp + 8 pls.
- Evans JR, Kaminski MA (1998) Pliocene and Pleistocene chronostratigraphy and palaeoenvironment of the Central Arctic Ocean, using deep water agglutinated foraminifera. *Micropaleontology*, 44, 109-130.
- Herman Y (1973) *Bolivina arctica*, a new benthonic foraminifera from Arctic Ocean sediments. *Journal of Foraminiferal Research*, 3, 137-141.
- Ishman SE, Polyak L, Poore RZ (1996) An expanded record of Pleistocene deep Arctic change: Canada basin, western Arctic Ocean. *Geology*, 24, 139-142.

10.8 Micropaleontology and biostratigraphy

- Joy JA, Clark DL (1977) The distribution, ecology and systematics of the benthic Ostracoda of the central Arctic Ocean. *Micropaleontology*, 23, 129-154.
- Kaminski MA, Gradstein FM, Goll RM, Grieg D (1990) Biostratigraphy and paleoecology of deep-water agglutinated foraminifera at ODP Site 643, Norwegian-Greenland Sea. In: Hemleben, C, Kaminski, M.A, Kuhnt, W. and Scott, D.B., (eds), *Paleoecology, Biostratigraphy, Paleoceanography and Taxonomy of Agglutinated Foraminifera*, NATO ASI Series, Kluwer Acad. Publ, 345-386.
- Kaminski MA, Silye L, Kender S (2005) Miocene deep-water agglutinated foraminifera from ODP Hole 909c: Implications for the paleoceanography of the Fram Strait Area, Greenland Sea. *Micropaleontology*, 51, 373-403.
- Kaminski MA, Silye L, Kender S (2009) Miocene deep-water agglutinated foraminifera from IODP Hole M0002a, Lomonosov Ridge: Faunal constraints for the timing of the opening of the Fram Strait. *Micropaleontology*, 55, 117-135.
- Lagoe MB (1977) Recent benthic foraminifera from the central Arctic Ocean. *Journal of Foraminiferal Research*, 7, 106-129.
- Polyak L, Best KM, Crawford KA, Council EA, St-Onge G (2013) Quaternary history of sea ice in the western Arctic Ocean based on foraminifera. *Quaternary Science Reviews*, 79, 145-156.
- Scott DB, Mudi, PJ, Baki V, MacKinnon KD, Cole FE (1989) Biostratigraphy and late Cenozoic paleoceanography of the Arctic Ocean: Foraminiferal, lithostratigraphic, and isotopic evidence. *Geological Society of America Bulletin*, 101, 260-277.
- Verdenius JG, Van Hinte JE (1983) Central Norwegian-Greenland Sea: Tertiary arenaceous foraminifera, biostratigraphy and environment. *Proceedings of the First Workshop Arenaceous Foraminifera*, 7-9 Sept. 1981. *Continental Shelf Institute Publication*, 108, 173-224.
- Wollenburg JE (1992) Zur Taxonomie von rezenten benthischen Foraminiferen aus dem Nansen-Becken, Arktischer Ozean. *Berichte zur Polarforschung*, 112, 137 pp.
- Wollenburg JE (1995) Benthic foraminiferal assemblages in the Arctic Ocean: indicators for water mass distribution, productivity, and sea-ice drift. *Berichte zur Polarforschung*, 179, 227pp.

10.9 Inorganic geochemistry: pore water & sediment

Jessica Volz,
not onboard: Sabine Kasten

AWI
AWI

Objectives

The goal of geochemical investigations of pore water and sediments during Leg 4 of PS87 ARK-XXVIII was to document biogeochemical processes. The main focus was the characterization of inorganic compounds related to the degradation of organic matter and early diagenesis in the sediment. Such information are useful for the interpretation of other data for the reconstruction of past changes in water masses and environmental conditions. In addition to shipboard analyses and storage of pore waters and sediment samples for detailed geochemical characterizations, the analysis of methane concentrations in the sediment aims at the characterization of potential methanogenesis.

Work at sea

Sampling

Immediately after sediment core recovery with different coring devices (GC: gravity corer, KAL: Kastenlot/box corer, MUC: multi-corer), interstitial water (pore water) sampling was performed. During the whole cruise, a total of 545 (Table 10.9.1) samples was retrieved in the areas of Hovgaard Ridge, Lomonosov Ridge and Gakkel Ridge.

Samples of 8 ml were usually generated for the chemical analysis of pore fluids. For this purpose, 5 cm long rhizons having a volume of 130 μl and a pore size of 0.2 μm (Seeberg et al. 2005) were attached to a 20 ml plastic pull-back syringe that remained in the sediment for a maximum of 5 hours (Fig. 10.9.1). The pore water got extracted out of the fresh sediment by applying a vacuum with the plastic pull-back syringe and blocking it with a wooden stick. After each use, the rhizons were rinsed and stored with distilled MilliQ water.

To avoid any geochemical alteration of the sediment, the shipboard activities including analyses and storage of pore water samples were carried out under anoxic conditions. Hence, the first ~ 0.5 ml of extracted pore water from each syringe was discarded since it got potentially oxidized by remaining oxygen in the syringes. In order to keep the conditions as natural as possible, pore water samples from gravity core segments and multi-corer tubes were taken prior to opening at *in-situ* temperatures of approximately 4°C in the cool lab. For box core sediments, pore fluid samples were retrieved immediately after opening in the wet lab ($>4^\circ\text{C}$). Depending on sediment porosity and permeability, the volume of all filtered extracted pore fluid samples ranged from 2 to 12 ml. Each pore water extract was subsequently split into five fractions: a subsample for dissolved iron (Fe^{2+}) and phosphate (PO_4^{3-}), one for dissolved inorganic carbon (DIC), one for ammonium (NH_4^+) and the determination of pH and Eh, one for element analyses (pore fluid acidified with HNO_3) and the last one for the storage of original pore water. After performing the pore water sampling, the sediment was subsampled for further analyses of the solid phase.

Sample processing

Immediately after core recovery, sequential pore water sampling was performed:

Fe^{2+} and PO_4^{3-}

In order to avoid further oxidation, subsamples for the analysis of Fe^{2+} and PO_4^{3-} were analyzed immediately after the extraction of 2 ml of pore water, which was usually done after ~ 2 hours. Following the spectrophotometrical method of Cline (1969), the concentrations were

immediately analyzed onboard using a Cecil CE 2021 photometer for the determination of Fe^{2+} and a Lange DR 2800 photometer for PO_4^{3-} .

DIC

After extraction, >2 ml were transferred into an amber vial sealed with a PTFE septum-bearing lid and stored at 4°C for further analyses of DIC.

NH₄⁺, pH and Eh

A 0.5 ml subsample was used to measure pH- and Eh-values and stored with 0.5 ml of MilliQ water, distilled by an onboard Millipore machine of the type MilliQ Gradient A10. These subsamples were filled into an amber vial and sealed with a PTFE septum-bearing lid and got stored at -20°C for the later quantification of NH_4^+ .

Original (and acidified) pore water samples

After 5 hours of extraction, all pore fluids were transferred from the syringes into Zinsser vials and stored at 4°C as original pore water samples for the later investigation of anions, cations and trace elements.

For samples from the Gakkel Ridge (Table 10.9.1), 2-3 ml of the total extracted pore fluid was acidified with HNO_3 and stored at 4°C.

Sediment samples

After the interstitial water sampling, sediment samples were taken in parallel using either 12 ml cut-off syringes or a plastic spatula. After transferring these sediment samples into plastic vials sealed with a plastic lid, they were stored in argon-flushed glass bottles (“Bonbongläser”) at -20°C until further analysis.

Multi-corer (MUC)

The multi-corer was equipped with 3 PVC tubes prepared for rhizon sampling. These tubes had holes of 3.75 mm at 1 cm intervals that were sealed with Tesa tape prior to deployment. Immediately after recovery, the tube with the highest sediment recovery was fixed in the cool lab, the tape got punctuated and rhizons were injected through the holes at 5 cm intervals (Fig. 10.9.1). After 5 hours of extracting the pore water, measuring Fe^{2+} and PO_4^{3-} and taking subsamples as described above, sediment samples were taken using a plastic spatula at the same depth as the pore water got extracted.

Gravity Corer (GC)

In gravity core, samples for methane (CH_4) analyses were taken. Immediately after recovery, the core was split into 1 m long sections and CH_4 -samples of ~3 ml sediment were usually taken at the bottom of each section. These were stored in 10 ml of a saturated NaCl-solution at 4°C. After splitting, sealing and labeling the sections in the wet lab, pore water sampling was performed at 4°C in the cool lab. For this purpose, 3.75 mm holes were drilled into PVC liners and rhizons were inserted at 20 cm intervals (Fig. 10.9.1). After 5 hours of extraction, the pore fluid volume was usually not enough to conduct the sampling processing as described above. Therefore, the pore water extraction of some gravity cores was extended to a maximum of 12 hours.

After extracting the pore fluid, measuring Fe^{2+} and PO_4^{3-} and taking subsamples as described above, no sediment samples were taken yet in order to store the sediments as archives. The sediment samples for the analyses of the solid-phase will be taken during a post-cruise sampling party.

Kastenlot/Box Corer (KAL)

The box corer was usually opened some hours after its recovery in the wet lab ($>4^{\circ}\text{C}$). Hereafter, pore water sampling was performed at 20 cm intervals. One box core with a sediment recovery of 625 cm (PS87/030-1) was sampled in high resolution – at 5 cm intervals. After 5 hours of extracting the pore fluid, measuring Fe^{2+} and PO_4^{3-} and taking subsamples as described above, sediment samples were taken in parallel using cut-off syringes at 20 cm intervals (Fig. 10.9.1).



Fig. 10.9.1: Pore water sampling; a: Multi-corer tube (5 cm intervals); b: Box core sediment (20 cm intervals); c: Gravity corer segments (20 cm intervals)

Preliminary results

Phosphate (PO_4^{3-})

The overall concentration of phosphate (PO_4^{3-}) in the pore water ranges from 0 ppm to 0.3 ppm in all cores for the uppermost 4-5 meters of sediment. This concentration is too low in order to define an interval of active degradation of organic matter. However, most profiles show a slight increase in the concentration of PO_4^{3-} with depth (Fig. 10.9.2). Some gravity cores show higher concentrations up to 0.65 ppm PO_4^{3-} below 4-5 meters of sediment (cores PS080-3, PS083-2, PS086-3, PS087-1, PS093-1).

Dissolved iron (Fe^{2+})

The dissolved iron (Fe^{2+}) concentration lies mostly below detection limit. However, in parallel with increasing PO_4^{3-} , some gravity cores show Fe^{2+} concentrations of up to 19 mg/l below 4-5 m in the sediment (Fig. 10.9.2; cores PS080-3, PS083-2, PS086-3, PS087-1, PS093-1).

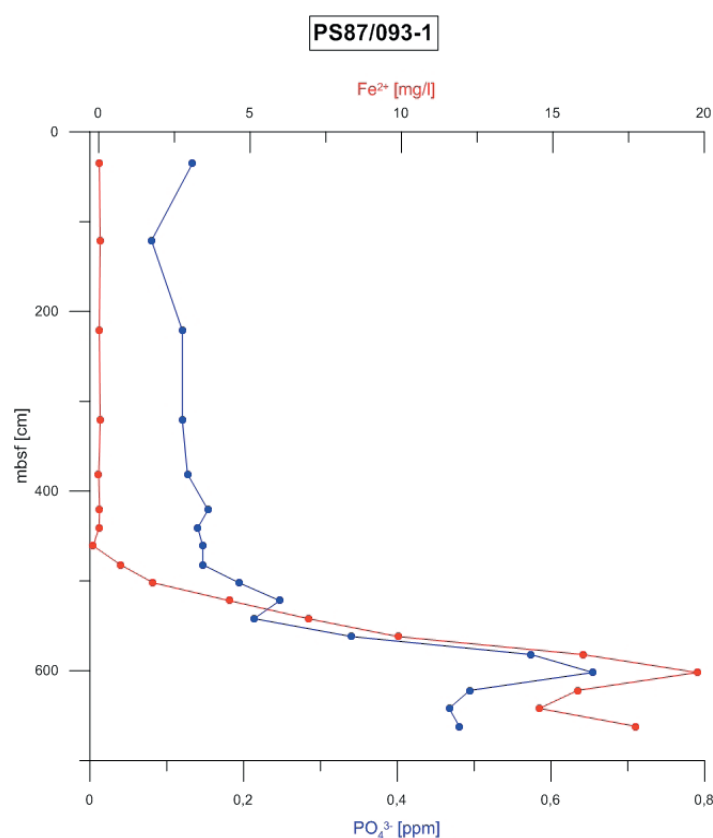


Fig. 10.9.2: PO_4^{3-} and Fe^{2+} concentrations of gravity core PS87/093-1 showing increasing PO_4^{3-} -values and high PO_4^{3-} and Fe^{2+} concentrations below 5 mbsf

pH & Eh

pH and Eh values provide additional information about the organic matter decay and are depending on the sediment types. They were determined using Hamilton (redox) electrodes. However, the pH and Eh values obtained were non-reproducible values, thus the measurements were only conducted for 3 sediment cores (see table 10.9.3).

Tab. 10.9.3: Sampling report of PS87 ARK-XXVIII/4

Date	Station	Gear	Fe	PO4	DIC	NH4	pH/ Eh	CH4	Original PW- samples	PW- samples in HNO3	Sediment samples
08.08.2014	PS87/003-2	GC	x	x	x				x		
18.08.2014	PS87/023-1	KAL	x	x	x	x			x		x
21.08.2014	PS87/029-3	MUC	x	x	x	x	x		x		x
23.08.2014	PS87/030-1	KAL	x	x	x	x	x		x		x
23.08.2014	PS87/030-3	MUC	x	x	x	x	x	x	x		x
26.08.2014	PS87/035-3	MUC	x	x	x	x			x		x
28.08.2014	PS87/040-1	KAL	x	x	x	x			x		x
28.08.2014	PS87/040-3	MUC	x	x	x	x			x		x
31.08.2014	PS87/051-1	GC	x	x	x	x		x	x		
02.09.2014	PS87/056-1	KAL	x	x	x	x			x		x
03.09.2014	PS87/067-1	GC	x	x	x	x		x	x		
03.09.2014	PS87/067-3	MUC	x	x	x	x			x		x
03.09.2014	PS87/068-1	GC	x	x	x			x	x		
06.09.2014	PS87/070-1	KAL	x	x	x	x			x		x
06.09.2014	PS87/070-3	MUC	x	x	x	x			x		x
09.09.2014	PS87/074-2	MUC	x	x	x	x			x		x
09.09.2014	PS87/074-3	GC	x	x	x	x			x		
09.09.2014	PS87/076-1	GC	x	x	x	x		x	x		
09.09.2014	PS87/076-3	MUC	x	x	x	x			x		x
10.09.2014	PS87/079-1	KAL	x	x	x	x			x		x
10.09.2014	PS87/079-4	MUC	x	x	x	x			x		x
11.09.2014	PS87/080-3	GC	x	x	x	x			x		
23.09.2014	PS87/083-2	GC	x	x	x	x		x	x		
23.09.2014	PS87/083-3	GC	x	x	x	x		x	x		
24.09.2014	PS87/086-2	MUC	x	x	x	x			x		x
24.09.2014	PS87/086-3	GC	x	x	x	x		x	x		
24.09.2014	PS87/087-1	GC	x	x	x	x		x	x		
25.09.2014	PS87/093-1	GC	x	x	x	x		x	x		
27.09.2014	PS87/110-1	GC	x	x				x	x	x	

Data management

As soon as all analyses are processed, the data will be accessible to other cruise participants and research partners on request.

References

- Cline JD (1969) Spectrophotometric Determination of Hydrogen Sulfide in Natural Waters Source. *Limnology and Oceanography*, Vol. 14, No. 3 (May, 1969), pp. 454-458.
- Seeberg-Elverfeldt, Schlüter M, Kölling M (2005) Rhizon sampling of porewaters near the sediment-water interface of aquatic systems. *Limnol. Oceanogr. Methods*, 3, 361-371.

APPENDIX

A1 Teilnehmende Institute / Participating Institutions

A2 Fahrtteilnehmer / Cruise Participants

A3 Schiffsbesatzung / Ship's Crew

A4 PS87 Station List

A5 Marine Geology

A5.1 Lithological description of Giant Box Corer (GKG) and Gravity Corer (SL) sections (E. Bazhenova, R. Stein)

Note: For SL cores, only the description of Core PS87/003-2 is included here. From the other cores (SL and KAL), core descriptions are available at the AWI (Contact: R. Stein)

A5.2 Tables with data of smear-slide analysis (E. Bazhenova)

A5.3 Tables with preliminary data of coarse-fraction analysis (S. Nam)

A5.4 Tables with data of dropstone analysis (E. Bazhenova)

A5.5 Tables with micropaleontological data (S. Kaboth, M. Kaminski, S. Nam, A. de Vernal, M. Zwick)

A1 TEILNEHMENDE INSTITUTE / PARTICIPATING INSTITUTIONS

	Address
AWI	Alfred-Wegener-Institut Helmholtz-Zentrum für Polar- und Meeresforschung Postfach 120161 27515 Bremerhaven Germany
DWD	Deutscher Wetterdienst Geschäftsbereich Wettervorhersage Seeschiffahrtsberatung Bernhard-Nocht-Str. 76 20359 Hamburg Germany
ESYS	ESYS GmbH Schwedterstr. 34a 10435 Berlin Germany
GEOMAR	Helmholtz-Zentrum für Ozeanforschung (GEOMAR) Wischhofstr. 1-3 24148 Kiel Germany
GEOTOP	Département des Sciences de la Terre Université du Québec à Montreal CP 8888 Montréal Québec, H3C 3P8 Canada
HeliService	HeliService International GmbH Am Luneort 15 27572 Bremerhaven Germany
KFU	Earth Sciences Department, King Fahd University of Petroleum and Minerals Dhahran 31261 Saudi Arabia
KOPRI	Korea Polar Research Institute 6 Songdomirae-ro, Yeonsu-gu 406-840 Incheon Korea

	Address
PoIE	Laboratory for Polar Ecology 502 chemin de Ribian 26130 Saint-REstitut France
SIOSOA	Second Institute of Oceanography, State Oceanic Administration 36 Baochubeilu Hangzhou 310012 China
UoAE	University of Alberta Edmonton Edmonton, Alberta, T6G 2E3 Canada
UoAF	Department of Geology and Geophysics, University of Alaska Fairbanks 903 Koyukuk Drive Fairbanks, Alaska 99775-7320 USA
UoB	Department of Earth Science, University of Bergen Allégaten 41 5007 Bergen Norway
UoBr	University of Bremen Bibliothekstraße 1 28359 Bremen Germany
UoH	University of Hamburg Mittelweg 177 20148 Hamburg Germany
UoK	Institute for Geosciences, University of Kiel Otto-Hahn-Platz 1 24118 Kiel Germany
UoM	Institute for Geology and Paleontology, University of Münster Corrensstr. 24 48149 Münster Germany

	Address
UoStP	University of St. Petersburg Universitetskaya 7-9 199034 St. Petersburg Russia
UoT	Institute of Geology, University of Tromsø Dramsveien 201 9037 Tromsø Norway
UoU	Department of Earth Science, University of Utrecht Budapestlaan 4, Kamer O.332 3584CD Utrecht The Netherlands
VNIIO	All-Russia Research Institute for Geology and Mineral Resources of the World Ocean, VNIIOkeangeologiya 1, Angliysky ave., 190121 St.Petersburg Russia
YUoT	York University of Toronto 4700 Keele Street Toronto, ON, M3J 1P3 Canada

A2 FAHRTTEILNEHMER / CRUISE PARTICIPANTS

No	Name	First name	Institute	Profession	Discipline
1	Bazhenova	Evgenia	UoStP	Scientist	Geology
2	Brauer	Jens	HeliService	Pilot/Technician	Pilot/Technician
3	Bublitz	Anne	YUoT	Scientist	Sea ice
4	Cahnbley	Mirjam	AWI	Student/HiWi	Bathymetry
5	Castro de la Guardia	Laura	UoAE	PhD student	Geology
6	Coakley	Bernard	UoAF	Scientist	Geophysics
7	de Vernal	Anne	GEOTOP	Scientist	Geology
8	Eagles	Graeme	AWI	Scientist	Geophysics
9	Eisermann	Hannes	UoH	Student/HiWi	Geophysics
10	Forwick	Matthias	UoT	Scientist	Geology
11	Fromm	Tanja	AWI	PhD student	Geophysics
12	Gebhardt	Catalina	AWI	Scientist	Geophysics
13	Geissler	Wolfram	AWI	Scientist	Geophysics
14	Gischler	Michael	HeliService	Pilot	Pilot
15	Heckmann	Hans	HeliService	Pilot/Technician	Pilot/Technician
16	Hörner	Tanja	AWI	PhD student	Geology
17	Jamar	Oria	PoIE	Scientist	Polar ecology
18	Jensen	Laura	AWI	Scientist	Bathymetry
19	Jin	Haiyan	SIOSOA	Scientist	Geology
20	Jokat	Wilfried	AWI	Scientist	Geophysics
21	Kaboth	Stefanie	UoU	PhD student	Geology
22	Kaminski	Mike	KFU	Scientist	Geology
23	Kimmel	Bastian	UoH	Student/HiWi	Geophysics
24	Kolling	Henriette	AWI	PhD student	Geology
25	Kopsch	Conrad	ESYS	Technician	Geophysics
26	Kremer	Anne	AWI	PhD student	Geology
27	Kristoffersen	Yngve	UoB	Scientist	Geophysics
28	Kudryavtseva	Anna	UoStP	Student/HiWi	Geology
29	Lensch	Norbert	AWI	Technician	Geology/ Geophysics
30	Matthiessen	Jens	AWI	Scientist	Geology
31	Möllendorf	Carsten	HeliService	Technician	Technician
32	Nachtsheim	Dominik	PoIE	PhD student	Polar ecology

No	Name	First name	Institute	Profession	Discipline
33	Nam	Seung-il	KOPRI	Scientist	Geology
34	Niessen	Frank	AWI	Scientist	Geophysics
35	Petersen	Florian	UoK	Student/HiWi	Geophysics
36	Prim	Anna Katharina	UoM	Student/HiWi	Geology
37	Rentsch	Harald	DWD	Scientist	Meteorologist
38	Riefstahl	Florian	UoBr	Student/HiWi	Geophysics
39	Ritter	Francois	AWI	Scientist	Glaciology
40	Roloff	Albrecht	AWI	Student/HiWi	Oceanography
41	Sauermilch	Isabel	UoBr	Student/HiWi	Geophysics
42	Schreck	Michael	KOPRI	Scientist	Geology
43	Sonnabend	Hartmut	DWD	Technician	Technician
44	Spielhagen	Robert	GEOMAR	Scientist	Geology
45	Stein	Ruediger	AWI	Scientist	Chief scientist/ Geology
46	Stolle	Clara	AWI	Student/HiWi	Bathymetry
47	Tholfsen	Audun	UoB	Scientist	Geophysics
48	Volz	Jessica	UoBr	Student/HiWi	Geology
49	Winkler	Maria	UoD	Student/HiWi	Sea ice
50	Zwick	Mike	UoBr	Student/HiWi	Geology

A3 SCHIFFSBESATZUNG / SHIP'S CREW

No.	Name	Rank
	Schwarze, Stefan	Master
	Grundmann, Uwe	1st Offc.
	Heuck, Hinnerk	Ch.Eng.
	Fallei, Holger	2nd Offc.
	Langhinrichs, Moritz .	2nd Offc
	Stolze, Henrik	2nd Offc.
	Pohl, Klaus	Doctor
	Fröb, Martin	Comm.Offc
	Grafe, Jens .	2nd Eng
	Minzlaff, Hans-Ulrich	2nd Eng.
	Holst, Wolfgang .	3rd Eng
	Scholz, Manfred .	ElecEng
	Christian, Boris	ELO
	Himmel, Frank	ELO
	Hüttebräucker, Olaf	ELO
	Nasis, Ilias	ELO
	Loidl, Reiner	Boatsw.
	Reise, Lutz	Carpenter
	Bäcker, Andreas	A.B.
	Brickmann, Peter	A.B.
	Brück, Sebastian .	A.B.
	Guse, Hartmut	A.B.
	Hagemann, Manfred	A.B.
	Scheel, Sebastian	A.B.
	Schmidt, Uwe .	A.B.
	Wende, Uwe	A.B.
	Winkler, Michael	A.B.
	Preußner, Jörg .	Storek
	Lamm, Gerd	Mot-man
	Pinske, Lutz	Mot-man
	Schonemann, Mario	Mot-man
	Schütt, Norbert	Mot-man
	Teichert, Uwe	Mot-man
	Müller-Homburg, R.-D	Cook
	Martens, Michael	Cooksmate
	Silinski, Frank	Cooksmate
	Czyborra, Barbel	1.Stwdess
	Wöckener, Martina	Stwdss/Kr
	Arendt, Rene	2.Steward

No.	Name	Rank
	Dibenau, Torsten	2.Steward
	Möller, Wolfgang	2.Steward
	Silinski, Carmen	2.Stwdess
	Sun, Yong Sheng	2.Steward
	Yu, Kwok Yuen .	Laundrym

A4 STATION LIST

Station	Date	Time	Gear	Action	PositionLat	PositionLon	Depth [m]
PS87/001-1	06.08.14	10:20	MTC	profile start	73°41.94'N	13°35.13'E	1579,2
PS87/001-1	06.08.14	11:36	MTC	on ground/ max depth	73°42.02'N	13°35.02'E	1579,5
PS87/001-1	06.08.14	11:36	MTC	action	73°42.02'N	13°35.02'E	1579,5
PS87/001-1	06.08.14	12:41	MTC	profile end	73°42.01'N	13°34.91'E	1546,4
PS87/002-1	07.08.14	16:49	XCTD	in the water	77°57.14'N	2°30.80'E	3043,5
PS87/002-1	07.08.14	16:49	XCTD	on ground/ max depth	77°57.14'N	2°30.80'E	3043,5
PS87/003-1	07.08.14	21:53	GBG	on ground/ max depth	78°24.12'N	1°2.88'E	1170,8
PS87/003-2	07.08.14	23:12	GC	on ground/ max depth	78°24.08'N	1°2.77'E	1173,2
PS87/004-1	09.08.14	07:45	ICE	on ground/ max depth	80°51.00'N	8°57.04'W	70,2
PS87/004-1	09.08.14	08:10	ICE	off ground	80°50.69'N	8°59.30'W	65,4
PS87/005-1	09.08.14	08:28	MTC	profile start	80°50.74'N	9°8.20'W	56,8
PS87/005-1	09.08.14	09:47	MTC	on ground/ max depth	80°51.49'N	9°8.48'W	70
PS87/006-1	11.08.14	00:04	XCTD	in the water	82°59.17'N	4°39.41'W	2557,8
PS87/006-1	11.08.14	00:10	XCTD	on ground/ max depth	82°59.38'N	4°38.95'W	2568,6
PS87/007-1	11.08.14	09:24	XCTD	in the water	83°24.16'N	3°23.90'W	3138,5
PS87/007-1	11.08.14	09:24	XCTD	on ground/ max depth	83°24.16'N	3°23.90'W	3138,5
PS87/008-1	11.08.14	21:35	XCTD	in the water	83°49.50'N	2°48.34'W	3334
PS87/008-1	11.08.14	21:40	XCTD	on ground/ max depth	83°49.52'N	2°48.33'W	3322,5
PS87/009-1	12.08.14	06:21	XCTD	in the water	84°12.97'N	3°39.49'W	2709,5
PS87/009-1	12.08.14	06:27	XCTD	on ground/ max depth	84°13.61'N	3°38.87'W	2748,3
PS87/010-1	12.08.14	13:30	XCTD	in the water	84°39.62'N	2°59.69'W	3527,2
PS87/010-1	12.08.14	13:35	XCTD	on ground/ max depth	84°39.63'N	2°59.82'W	3525,6
PS87/011-1	12.08.14	22:07	XCTD	in the water	85°3.60'N	2°50.69'W	4110,2
PS87/011-1	12.08.14	22:12	XCTD	on ground/ max depth	85°3.58'N	2°50.64'W	4095,4
PS87/012-1	13.08.14	06:24	XCTD	in the water	85°26.44'N	2°8.83'W	3549,2
PS87/012-1	13.08.14	06:30	XCTD	on ground/ max depth	85°26.91'N	2°7.27'W	3634,1
PS87/013-1	13.08.14	15:30	XCTD	on ground/ max depth	85°51.32'N	2°55.21'W	4152,9
PS87/013-1	13.08.14	15:35	XCTD	on ground/ max depth	85°51.37'N	2°57.16'W	4083,5
PS87/014-1	13.08.14	22:29	XCTD	in the water	86°11.86'N	5°33.21'W	4142
PS87/014-1	13.08.14	22:34	XCTD	on ground/ max depth	86°11.85'N	5°33.43'W	4142,8
PS87/015-1	14.08.14	12:24	XCTD	in the water	86°24.69'N	10°59.42'W	4191,8

Station	Date	Time	Gear	Action	PositionLat	PositionLon	Depth [m]
PS87/015-1	14.08.14	12:30	XCTD	on ground/ max depth	86°24.65'N	10°59.60'W	4193,7
PS87/016-1	14.08.14	21:17	XCTD	in the water	86°33.59'N	15°4.46'W	4207
PS87/016-1	14.08.14	21:24	XCTD	on ground/ max depth	86°33.65'N	15°5.87'W	4206,7
PS87/017-1	15.08.14	06:58	XCTD	in the water	86°52.54'N	19°32.43'W	4212
PS87/017-1	15.08.14	07:04	XCTD	on ground/ max depth	86°52.34'N	19°36.32'W	5313,2
PS87/018-1	15.08.14	15:08	XCTD	in the water	86°49.47'N	27°11.40'W	4103,5
PS87/018-1	15.08.14	15:13	XCTD	on ground/ max depth	86°49.52'N	27°11.55'W	4106
PS87/019-1	16.08.14	04:40	XCTD	in the water	86°44.84'N	34°37.64'W	3744,8
PS87/019-1	16.08.14	04:46	XCTD	on ground/ max depth	86°44.81'N	34°38.81'W	3740,9
PS87/020-1	16.08.14	16:16	XCTD	in the water	86°26.14'N	38°48.72'W	3351,7
PS87/020-1	16.08.14	16:21	XCTD	on ground/ max depth	86°26.13'N	38°48.70'W	3348,5
PS87/021-1	17.08.14	03:26	XCTD	in the water	86°7.66'N	42°46.78'W	3272,5
PS87/021-1	17.08.14	03:33	XCTD	on ground/ max depth	86°7.65'N	42°46.82'W	3271,8
PS87/022-1	18.08.14	09:14	XCTD	in the water	86°36.04'N	44°32.70'W	2374,4
PS87/022-1	18.08.14	09:21	XCTD	on ground/ max depth	86°36.45'N	44°35.47'W	2569,2
PS87/023-1	18.08.14	16:00	BC	on ground/ max depth	86°38.23'N	44°53.98'W	2444,8
PS87/023-2	18.08.14	17:44	GKG	on ground/ max depth	86°37.86'N	44°52.45'W	2439
PS87/024-1	19.08.14	14:56	XCTD	in the water	86°59.85'N	46°46.17'W	1833,6
PS87/024-1	19.08.14	15:00	XCTD	on ground/ max depth	86°59.84'N	46°45.91'W	1833,5
PS87/025-1	20.08.14	02:47	XCTD	in the water	87°23.46'N	46°26.40'W	3263
PS87/025-1	20.08.14	02:54	XCTD	on ground/ max depth	87°23.42'N	46°26.21'W	3263,6
PS87/026-1	20.08.14	07:54	GKG	on ground/ max depth	87°26.95'N	46°33.95'W	3339
PS87/027-1	20.08.14	22:53	XCTD	in the water	87°46.70'N	46°51.61'W	3305,8
PS87/027-1	20.08.14	23:00	XCTD	in the water	87°46.69'N	46°51.47'W	3312,8
PS87/027-1	20.08.14	23:05	XCTD	on ground/ max depth	87°46.69'N	46°51.32'W	3306,9
PS87/028-1	21.08.14	09:06	XCTD	in the water	88°9.50'N	46°50.70'W	2413,8
PS87/028-1	21.08.14	09:12	XCTD	on ground/ max depth	88°9.66'N	46°50.48'W	2410,6
PS87/029-1	21.08.14	14:59	GKG	on ground/ max depth	88°29.08'N	48°6.85'W	2901,4
PS87/029-1	21.08.14	15:41	GKG	on deck	88°29.01'N	48°5.81'W	2903
PS87/029-2	21.08.14	16:47	MUC	on ground/ max depth	88°28.91'N	48°4.55'W	2905,1
PS87/029-3	21.08.14	18:24	MUC	on ground/ max depth	88°28.73'N	48°2.88'W	2911,9

Station	Date	Time	Gear	Action	PositionLat	PositionLon	Depth [m]
PS87/030-1	23.08.14	01:09	KAL	on ground/ max depth	88°39.72'N	61°32.52'W	1276,8
PS87/030-2	23.08.14	02:11	GKG	on ground/ max depth	88°39.56'N	61°29.20'W	1278,4
PS87/030-3	23.08.14	03:30	MUC	on ground/ max depth	88°39.39'N	61°25.55'W	1277,8
PS87/030-4	23.08.14	04:26	XCTD	in the water	88°39.28'N	61°22.64'W	1278,8
PS87/030-4	23.08.14	04:32	XCTD	on ground/ max depth	88°39.26'N	61°21.92'W	1278,9
PS87/031-1	23.08.14	11:30	SEISREFL	in the water	88°30.75'N	52°47.50'W	2575,5
PS87/031-1	23.08.14	11:50	SEISREFL	profile start	88°31.77'N	52°29.54'W	2812
PS87/031-1	23.08.14	12:30	SEISREFL	profile end	88°32.11'N	52°14.19'W	2778,6
PS87/031-1	23.08.14	12:40	SEISREFL	on deck	88°32.05'N	52°15.31'W	2782,5
PS87/032-1	23.08.14	19:53	XCTD	in the water	88°49.06'N	44°44.66'W	4002,6
PS87/032-1	23.08.14	19:59	XCTD	on ground/ max depth	88°49.10'N	44°43.04'W	4002,6
PS87/033-1	24.08.14	19:08	XCTD	in the water	89°25.77'N	27°45.95'W	4125,5
PS87/033-1	24.08.14	19:14	XCTD	on ground/ max depth	89°25.76'N	27°42.43'W	4129,4
PS87/034-1	25.08.14	16:47	ICE	action	89°37.19'N	8°46.37'W	4176,9
PS87/034-1	25.08.14	16:52	ICE	on ground/ max depth	89°37.17'N	8°44.02'W	4177
PS87/034-1	25.08.14	17:00	ICE	on deck	89°37.15'N	8°40.28'W	4174,4
PS87/035-1	26.08.14	11:00	ICE	on ground/ max depth	89°59.24'N	2°38.91'E	4186,6
PS87/035-1	26.08.14	11:30	ICE	information	89°59.15'N	9°45.69'E	4185,4
PS87/035-1	26.08.14	11:32	ICE	action	89°59.15'N	10°10.72'E	4186,7
PS87/035-1	26.08.14	11:59	ICE	action	89°59.06'N	15°6.65'E	4186,9
PS87/035-2	26.08.14	12:16	GKG	on ground/ max depth	89°59.01'N	17°46.41'E	4186,6
PS87/035-2	26.08.14	12:22	GKG	on ground/ max depth	89°58.99'N	18°39.13'E	4184,3
PS87/035-2	26.08.14	12:28	GKG	on ground/ max depth	89°58.97'N	19°28.74'E	4183,1
PS87/035-3	26.08.14	14:24	MUC	on ground/ max depth	89°58.61'N	31°53.17'E	4184,9
PS87/035-4	26.08.14	15:17	XCTD	in the water	89°58.43'N	36°9.42'E	4185,3
PS87/035-4	26.08.14	15:23	XCTD	on ground/ max depth	89°58.41'N	36°33.80'E	4186,1
PS87/036-1	26.08.14	21:52	XCTD	in the water	89°36.94'N	138°57.63'E	4195,8
PS87/036-1	26.08.14	21:56	XCTD	on ground/ max depth	89°36.95'N	138°55.77'E	4196
PS87/037-1	27.08.14	06:37	ICE	information	89°28.69'N	167°17.10'E	4170,5
PS87/037-1	27.08.14	06:44	ICE	on ground/ max depth	89°28.68'N	167°15.20'E	4168,6
PS87/038-1	27.08.14	10:13	XCTD	in the water	89°26.86'N	179°1.56'W	4102,9
PS87/038-1	27.08.14	10:18	XCTD	on ground/ max depth	89°26.85'N	179°4.45'W	4112,2
PS87/039-1	27.08.14	19:26	XCTD	in the water	89°4.04'N	177°34.75'E	2259,5

Station	Date	Time	Gear	Action	PositionLat	PositionLon	Depth [m]
PS87/039-1	27.08.14	19:33	XCTD	on ground/ max depth	89°4.02'N	177°33.00'E	2259,4
PS87/040-1	27.08.14	23:10	KAL	on ground/ max depth	88°59.31'N	171°53.20'E	2614,1
PS87/040-2	28.08.14	00:45	GKG	on ground/ max depth	88°59.18'N	171°44.50'E	2618,4
PS87/040-3	28.08.14	02:25	MUC	on ground/ max depth	88°58.96'N	171°37.55'E	2621,4
PS87/041-1	28.08.14	07:07	XCTD	in the water	88°43.44'N	172°1.10'E	961,9
PS87/041-1	28.08.14	07:13	XCTD	on ground/ max depth	88°43.42'N	172°0.41'E	962,9
PS87/042-1	28.08.14	15:16	XCTD	in the water	88°19.64'N	165°11.40'E	3750,7
PS87/042-1	28.08.14	15:22	XCTD	on ground/ max depth	88°19.62'N	165°11.58'E	3752,6
PS87/043-1	29.08.14	01:33	XCTD	in the water	87°56.86'N	161°10.54'E	3915
PS87/043-1	29.08.14	01:38	XCTD	in the water	87°56.86'N	161°10.84'E	3915,9
PS87/043-1	29.08.14	01:44	XCTD	on ground/ max depth	87°56.86'N	161°11.09'E	3917,2
PS87/044-1	29.08.14	13:02	XCTD	in the water	87°32.78'N	158°45.62'E	3912,8
PS87/044-1	29.08.14	13:08	XCTD	on ground/ max depth	87°32.77'N	158°46.15'E	3915,4
PS87/045-1	29.08.14	17:19	ICE	action	87°26.07'N	158°14.85'E	3923,7
PS87/046-1	30.08.14	03:18	ICE	action	87°20.98'N	156°28.44'E	3907,6
PS87/046-1	30.08.14	06:38	ICE	information	87°21.07'N	156°47.62'E	3900,4
PS87/046-1	30.08.14	15:15	ICE	on ground/ max depth	87°21.79'N	157°35.30'E	3908,1
PS87/047-1	30.08.14	07:02	ICE	on ground/ max depth	87°21.10'N	156°49.61'E	3904,3
PS87/048-1	30.08.14	20:23	XCTD	in the water	87°11.70'N	151°53.95'E	2256,4
PS87/048-1	30.08.14	20:29	XCTD	on ground/ max depth	87°11.70'N	151°54.18'E	2248,8
PS87/049-1	31.08.14	02:32	XCTD	in the water	86°51.43'N	149°58.94'E	1162,2
PS87/049-1	31.08.14	02:35	XCTD	on ground/ max depth	86°51.44'N	149°59.00'E	1162,6
PS87/050-1	31.08.14	07:26	EF	on ground/ max depth	86°40.78'N	148°45.04'E	1104,8
PS87/051-1	31.08.14	13:08	GC	on ground/ max depth	86°26.98'N	147°20.31'E	1190,7
PS87/052-1	31.08.14	13:40	HS_PS	profile start	86°27.03'N	147°20.76'E	1192,4
PS87/052-1	31.08.14	16:00	HS_PS	alter course	86°29.94'N	144°2.51'E	864,9
PS87/052-1	31.08.14	17:10	HS_PS	alter course	86°27.14'N	143°1.85'E	963,3
PS87/052-1	01.09.14	08:56	HS_PS	alter course	85°38.76'N	149°9.50'E	710,8
PS87/052-1	01.09.14	09:31	HS_PS	alter course	85°38.07'N	148°49.30'E	756
PS87/052-1	01.09.14	14:25	HS_PS	alter course	85°59.72'N	146°2.07'E	955,1
PS87/052-1	01.09.14	14:51	HS_PS	alter course	85°58.13'N	145°36.24'E	1031,2
PS87/052-1	01.09.14	22:00	HS_PS	information	85°45.06'N	147°53.16'E	828,1
PS87/052-1	02.09.14	00:05	HS_PS	profile end	85°37.00'N	148°18.36'E	867,8
PS87/053-1	31.08.14	16:50	XCTD	in the water	86°27.26'N	143°6.31'E	950,7

Station	Date	Time	Gear	Action	PositionLat	PositionLon	Depth [m]
PS87/053-1	31.08.14	16:55	XCTD	on ground/ max depth	86°27.27'N	143°6.30'E	950,6
PS87/053-2	31.08.14	16:56	XCTD	in the water	86°27.27'N	143°6.30'E	950,8
PS87/053-2	31.08.14	17:01	XCTD	on ground/ max depth	86°27.28'N	143°6.32'E	949,4
PS87/054-1	01.09.14	02:46	XCTD	in the water	85°54.04'N	147°27.46'E	841
PS87/054-1	01.09.14	02:52	XCTD	on ground/ max depth	85°54.04'N	147°27.43'E	841,5
PS87/055-1	01.09.14	07:13	GKG	on ground/ max depth	85°41.47'N	148°59.47'E	730,7
PS87/056-1	01.09.14	20:31	KAL	on ground/ max depth	85°45.15'N	147°57.24'E	835,8
PS87/056-2	01.09.14	21:17	GKG	on ground/ max depth	85°45.07'N	147°55.85'E	836
PS87/057-1	02.09.14	05:05	XCTD	in the water	85°15.37'N	145°19.54'E	2571,6
PS87/057-1	02.09.14	05:10	XCTD	on ground/ max depth	85°15.34'N	145°19.35'E	2573
PS87/058-1	02.09.14	09:06	XCTD	in the water	84°44.22'N	141°24.79'E	3401,6
PS87/058-1	02.09.14	09:12	XCTD	on ground/ max depth	84°43.87'N	141°23.50'E	3412,1
PS87/059-1	02.09.14	11:56	XCTD	in the water	84°15.56'N	138°9.59'E	3804,6
PS87/059-1	02.09.14	12:01	XCTD	on ground/ max depth	84°15.21'N	138°7.22'E	3892,2
PS87/060-1	02.09.14	12:21	SEISREFL	in the water	84°13.17'N	138°2.10'E	4111,8
PS87/060-1	02.09.14	12:29	SEISREFL	in the water	84°12.99'N	138°6.45'E	4085,3
PS87/060-1	02.09.14	12:44	SEISREFL	in the water	84°12.57'N	138°15.15'E	4016,2
PS87/060-1	02.09.14	12:50	SEISREFL	profile start	84°12.32'N	138°19.22'E	3976,3
PS87/061-1	02.09.14	17:43	XCTD	in the water	84°0.09'N	141°50.90'E	2541,1
PS87/061-1	02.09.14	17:49	XCTD	on ground/ max depth	83°59.85'N	141°55.16'E	2523,7
PS87/060-1	02.09.14	22:15	SEISREFL	alter course	83°48.61'N	145°5.82'E	1195,3
PS87/062-1	02.09.14	23:14	XCTD	in the water	83°48.25'N	145°52.02'E	1329,9
PS87/062-1	02.09.14	23:21	XCTD	on ground/ max depth	83°48.20'N	145°57.60'E	1323,9
PS87/060-1	02.09.14	23:59	SEISREFL	alter course	83°48.03'N	146°27.88'E	1333,2
PS87/060-1	03.09.14	13:30	SEISREFL	alter course	83°35.04'N	156°46.03'E	2305,9
PS87/060-1	03.09.14	11:15	SEISREFL	alter course	83°37.17'N	155°7.13'E	2712,3
PS87/060-1	03.09.14	12:26	SEISREFL	alter course	83°37.14'N	156°2.05'E	2588,6
PS87/063-1	03.09.14	04:21	XCTD	in the water	83°43.85'N	149°48.96'E	2416,5
PS87/063-1	03.09.14	04:26	XCTD	on ground/ max depth	83°43.79'N	149°52.67'E	2412
PS87/064-1	03.09.14	08:25	XCTD	in the water	83°39.88'N	152°59.12'E	1982,8
PS87/064-1	03.09.14	08:32	XCTD	on ground/ max depth	83°39.77'N	153°4.74'E	1817,4
PS87/060-1	03.09.14	19:05	SEISREFL	profile end	83°29.80'N	160°40.62'E	2866,4
PS87/060-1	03.09.14	19:15	SEISREFL	hoisting	83°30.28'N	160°45.96'E	2848,9
PS87/060-1	03.09.14	19:39	SEISREFL	on deck	83°31.66'N	160°53.53'E	2705,7
PS87/060-1	03.09.14	19:50	SEISREFL	on deck	83°31.68'N	160°53.42'E	2708,9

Station	Date	Time	Gear	Action	PositionLat	PositionLon	Depth [m]
PS87/065-1	03.09.14	13:29	XCTD	in the water	83°35.08'N	156°45.40'E	2299,6
PS87/065-1	03.09.14	13:34	XCTD	on ground/ max depth	83°34.85'N	156°48.65'E	2326,8
PS87/066-1	03.09.14	18:58	XCTD	in the water	83°29.43'N	160°36.87'E	2783,2
PS87/066-1	03.09.14	19:04	XCTD	on ground/ max depth	83°29.75'N	160°40.00'E	2866,1
PS87/067-1	03.09.14	21:33	GC	on ground/ max depth	83°29.47'N	160°34.29'E	2862,3
PS87/067-2	03.09.14	23:09	GKG	on ground/ max depth	83°29.65'N	160°35.36'E	2857
PS87/067-3	04.09.14	00:54	MUC	on ground/ max depth	83°29.90'N	160°34.48'E	2867,1
PS87/068-1	04.09.14	13:08	GC	on ground/ max depth	83°37.89'N	154°46.50'E	2708,9
PS87/068-2	04.09.14	15:01	GKG	on ground/ max depth	83°37.70'N	154°46.87'E	2711
PS87/068-3	04.09.14	16:45	MUC	on ground/ max depth	83°37.41'N	154°45.27'E	2712,6
PS87/069-1	04.09.14	20:25	SEISREFL	action	83°37.99'N	150°4.57'E	2415,3
PS87/069-1	04.09.14	20:35	SEISREFL	in the water	83°37.60'N	150°10.60'E	2418,5
PS87/069-1	04.09.14	20:54	SEISREFL	in the water	83°37.17'N	150°20.98'E	2421,3
PS87/069-1	04.09.14	21:15	SEISREFL	action	83°37.28'N	150°36.44'E	2446
PS87/069-1	04.09.14	22:09	SEISREFL	profile start	83°38.26'N	150°1.33'E	2418,6
PS87/069-1	05.09.14	03:34	SEISREFL	alter course	83°42.92'N	145°48.01'E	1405,9
PS87/069-1	05.09.14	05:37	SEISREFL	alter course	83°53.23'N	145°53.05'E	1293,9
PS87/069-1	05.09.14	10:43	SEISREFL	alter course	83°49.19'N	150°1.55'E	2360,3
PS87/070-1	06.09.14	09:26	KAL	on ground/ max depth	83°48.17'N	146°7.01'E	1339,8
PS87/070-1	06.09.14	10:22	GKG	on ground/ max depth	83°48.16'N	146°6.77'E	1340,4
PS87/070-3	06.09.14	11:28	MUC	on ground/ max depth	83°48.18'N	146°7.04'E	1340,2
PS87/071-1	06.09.14	12:09	HS_PS	profile start	83°48.22'N	146°6.18'E	1340,5
PS87/071-1	06.09.14	13:51	HS_PS	alter course	83°56.47'N	143°42.83'E	2610,6
PS87/071-1	06.09.14	14:09	HS_PS	alter course	83°58.78'N	143°55.78'E	2665,9
PS87/071-1	06.09.14	15:20	HS_PS	alter course	83°53.61'N	145°34.58'E	1214,3
PS87/071-1	06.09.14	15:40	HS_PS	alter course	83°55.38'N	146°1.23'E	1247,4
PS87/071-1	06.09.14	17:24	HS_PS	profile end	84°4.21'N	143°38.76'E	2720,9
PS87/072-1	06.09.14	18:00	MTC	profile start	83°59.74'N	143°2.60'E	2593,5
PS87/072-1	06.09.14	18:35	MTC	on ground/ max depth	83°59.61'N	143°2.71'E	2589,5
PS87/072-1	06.09.14	19:10	MTC	profile end	83°59.63'N	143°2.55'E	2589,3
PS87/073-1	07.09.14	05:06	SEISREFL	action	83°19.85'N	129°39.28'E	4147,3
PS87/073-1	07.09.14	05:06	SEISREFL	in the water	83°19.85'N	129°39.28'E	4147,3
PS87/073-1	07.09.14	06:16	SEISREFL	profile start	83°18.11'N	129°58.39'E	4139,5
PS87/073-1	07.09.14	23:41	SEISREFL	alter course	83°11.40'N	142°43.68'E	1243,9
PS87/073-1	08.09.14	03:02	SEISREFL	information	83°10.10'N	145°0.14'E	1635,9
PS87/073-1	08.09.14	06:07	SEISREFL	in the water	83°9.90'N	144°23.48'E	1619,4

Station	Date	Time	Gear	Action	PositionLat	PositionLon	Depth [m]
PS87/073-1	08.09.14	06:12	SEISREFL	action	83°9.87'N	144°26.97'E	1608,6
PS87/073-1	08.09.14	06:25	SEISREFL	information	83°9.68'N	144°36.21'E	1608,6
PS87/074-1	09.09.14	08:11	GKG	on ground/ max depth	82°43.39'N	158°37.49'E	2816,5
PS87/074-2	09.09.14	09:49	MUC	on ground/ max depth	82°43.44'N	158°37.54'E	2815,7
PS87/074-3	09.09.14	11:15	GC	on ground/ max depth	82°43.12'N	158°36.88'E	2772
PS87/075-1	09.09.14	17:34	GC	on ground/ max depth	82°51.49'N	155°45.19'E	2711,5
PS87/076-1	09.09.14	19:43	GC	on ground/ max depth	82°53.80'N	154°57.93'E	2762,2
PS87/076-2	09.09.14	21:10	GKG	on ground/ max depth	82°53.81'N	154°57.88'E	2763
PS87/076-3	09.09.14	22:48	MUC	on ground/ max depth	82°53.78'N	154°57.79'E	2764,9
PS87/077-1	09.09.14	23:45	HS_PS	profile start	82°54.42'N	154°59.04'E	2761,5
PS87/077-1	10.09.14	02:54	HS_PS	alter course	83°15.68'N	157°17.86'E	1075,8
PS87/077-1	10.09.14	03:16	HS_PS	alter course	83°16.88'N	157°2.14'E	820,6
PS87/077-1	10.09.14	04:18	HS_PS	profile end	83°12.54'N	156°27.23'E	1144,3
PS87/077-1	10.09.14	04:18	HS_PS	on ground/ max depth	83°12.54'N	156°27.23'E	1144,3
PS87/078-1	10.09.14	05:39	GC	on ground/ max depth	83°15.14'N	156°48.17'E	784,2
PS87/079-1	10.09.14	17:26	BC	on ground/ max depth	83°12.06'N	141°22.77'E	1360,8
PS87/079-2	10.09.14	18:22	GKG	on ground/ max depth	83°12.09'N	141°22.92'E	1359,6
PS87/079-3	10.09.14	20:19	MUC	on ground/ max depth	83°12.09'N	141°22.54'E	1358,6
PS87/079-4	10.09.14	21:03	MUC	on ground/ max depth	83°12.09'N	141°22.48'E	1360,8
PS87/080-1	11.09.14	00:40	GC	on ground/ max depth	83°12.26'N	141°4.97'E	1471,8
PS87/080-2	11.09.14	02:23	GC	on ground/ max depth	83°12.28'N	141°4.41'E	1508,9
PS87/080-3	11.09.14	03:43	GC	on ground/ max depth	83°12.27'N	141°5.05'E	1468,8
PS87/080-4	11.09.14	05:01	GC	on ground/ max depth	83°12.30'N	141°4.45'E	1512,1
PS87/081-1	11.09.14	06:12	SEISREFL	action	83°11.39'N	140°52.70'E	1554,8
PS87/081-1	11.09.14	06:22	SEISREFL	in the water	83°10.85'N	140°47.28'E	1617,2
PS87/081-1	11.09.14	06:29	SEISREFL	in the water	83°10.58'N	140°44.56'E	1695,7
PS87/081-1	11.09.14	06:37	SEISREFL	in the water	83°10.19'N	140°40.73'E	1767,8
PS87/081-1	11.09.14	06:45	SEISREFL	in the water	83°9.73'N	140°36.87'E	1894,2
PS87/081-1	11.09.14	06:53	SEISREFL	in the water	83°9.28'N	140°33.22'E	2026,5
PS87/081-1	11.09.14	07:00	SEISREFL	in the water	83°8.84'N	140°30.44'E	2104
PS87/081-1	11.09.14	07:09	SEISREFL	in the water	83°8.24'N	140°27.14'E	2213,1
PS87/081-1	11.09.14	07:18	SEISREFL	in the water	83°7.47'N	140°23.01'E	2447,6

Station	Date	Time	Gear	Action	PositionLat	PositionLon	Depth [m]
PS87/081-1	11.09.14	07:27	SEISREFL	in the water	83°6.72'N	140°19.54'E	2607,5
PS87/081-1	11.09.14	07:37	SEISREFL	in the water	83°5.90'N	140°15.63'E	2748,6
PS87/081-1	11.09.14	07:50	SEISREFL	in the water	83°4.80'N	140°10.70'E	2817,7
PS87/081-1	11.09.14	08:02	SEISREFL	in the water	83°3.81'N	140°6.72'E	2893,7
PS87/081-1	11.09.14	08:23	SEISREFL	in the water	83°2.04'N	139°59.86'E	2924,5
PS87/081-1	11.09.14	08:49	SEISREFL	in the water	82°59.87'N	139°52.75'E	2827,1
PS87/081-1	11.09.14	08:52	SEISREFL	action	82°59.61'N	139°52.66'E	2852,3
PS87/081-1	11.09.14	10:02	SEISREFL	profile start	82°54.35'N	139°58.06'E	2515,9
PS87/081-1	11.09.14	18:06	SEISREFL	alter course	82°44.62'N	145°17.80'E	2048,6
PS87/081-1	11.09.14	22:09	SEISREFL	alter course	82°24.77'N	145°1.10'E	2076,6
PS87/081-1	12.09.14	11:49	SEISREFL	alter course	82°29.36'N	136°6.19'E	3955,7
PS87/081-1	12.09.14	11:59	SEISREFL	information	82°29.23'N	135°59.78'E	3950,9
PS87/081-1	12.09.14	12:07	SEISREFL	on deck	82°28.79'N	135°55.65'E	3947,6
PS87/081-1	12.09.14	15:30	SEISREFL	information	82°11.64'N	135°48.45'E	3855,6
PS87/081-1	12.09.14	18:40	SEISREFL	information	82°11.70'N	134°0.23'E	3905,9
PS87/081-1	12.09.14	19:22	SEISREFL	in the water	82°9.53'N	133°47.30'E	3897,7
PS87/081-1	12.09.14	19:25	SEISREFL	action	82°9.32'N	133°48.31'E	3895,1
PS87/081-1	13.09.14	14:32	SEISREFL	alter course	81°58.19'N	145°33.53'E	2083
PS87/081-1	13.09.14	18:32	SEISREFL	alter course	81°54.10'N	147°59.80'E	2571,2
PS87/081-1	13.09.14	21:25	SEISREFL	alter course	81°40.20'N	147°43.35'E	2560,9
PS87/081-1	14.09.14	07:11	SEISREFL	alter course	81°42.30'N	142°10.25'E	774,8
PS87/081-1	14.09.14	20:27	SEISREFL	alter course	81°38.37'N	134°10.91'E	3770,2
PS87/081-1	15.09.14	00:08	SEISREFL	alter course	81°20.58'N	133°32.45'E	3762,3
PS87/081-1	15.09.14	08:12	SEISREFL	alter course	81°19.39'N	137°56.65'E	2699,5
PS87/081-1	15.09.14	16:00	SEISREFL	alter course	81°21.84'N	142°26.52'E	861,4
PS87/081-1	16.09.14	00:43	SEISREFL	alter course	81°19.65'N	147°20.05'E	2386
PS87/081-1	16.09.14	02:57	SEISREFL	alter course	81°8.59'N	147°24.63'E	2385,9
PS87/081-1	16.09.14	17:31	SEISREFL	alter course	81°7.42'N	139°23.66'E	1692,2
PS87/081-1	16.09.14	21:52	SEISREFL	alter course	80°45.37'N	139°28.29'E	2002,2
PS87/081-1	17.09.14	04:07	SEISREFL	alter course	80°46.79'N	142°46.34'E	1750,1
PS87/081-1	17.09.14	05:16	SEISREFL	alter course	80°46.92'N	143°22.32'E	1554,1
PS87/081-1	17.09.14	06:30	SEISREFL	profile end	80°42.14'N	143°20.94'E	1752,7
PS87/081-1	17.09.14	06:41	SEISREFL	on deck	80°41.32'N	143°17.25'E	1753,7
PS87/081-1	17.09.14	10:15	SEISREFL	in the water	80°31.57'N	143°29.99'E	1567,1
PS87/081-1	17.09.14	10:20	SEISREFL	profile start	80°31.36'N	143°28.33'E	1576,7
PS87/081-1	17.09.14	13:32	SEISREFL	alter course	80°44.91'N	142°51.79'E	1749,8
PS87/081-1	17.09.14	13:53	SEISREFL	alter course	80°46.65'N	142°47.26'E	1751,2
PS87/081-1	17.09.14	16:14	SEISREFL	alter course	80°58.52'N	142°28.11'E	1464,2
PS87/081-1	17.09.14	20:26	SEISREFL	alter course	81°20.04'N	142°28.59'E	924,1
PS87/081-1	18.09.14	00:13	SEISREFL	alter course	81°18.79'N	140°27.02'E	1646,6
PS87/081-1	18.09.14	05:22	SEISREFL	alter course	80°59.57'N	141°47.09'E	1649,9
PS87/081-1	18.09.14	05:32	SEISREFL	alter course	80°59.05'N	141°50.65'E	1637,6
PS87/081-1	18.09.14	06:42	SEISREFL	alter course	80°58.22'N	142°27.92'E	1457,5
PS87/081-1	18.09.14	07:40	SEISREFL	alter course	80°56.98'N	142°58.80'E	1400,5

Station	Date	Time	Gear	Action	PositionLat	PositionLon	Depth [m]
PS87/081-1	18.09.14	09:30	SEISREFL	alter course	80°58.80'N	143°54.39'E	1643,4
PS87/081-1	18.09.14	10:02	SEISREFL	alter course	81°1.46'N	143°55.81'E	1716,7
PS87/081-1	18.09.14	13:16	SEISREFL	alter course	81°3.26'N	142°15.99'E	1519
PS87/081-1	18.09.14	15:38	SEISREFL	alter course	81°14.58'N	142°4.97'E	884,9
PS87/081-1	18.09.14	19:53	SEISREFL	alter course	81°5.35'N	140°11.94'E	1276,1
PS87/081-1	18.09.14	20:31	SEISREFL	alter course	81°2.62'N	140°12.70'E	1356
PS87/081-1	19.09.14	02:00	SEISREFL	alter course	81°16.87'N	142°46.32'E	1200,2
PS87/081-1	19.09.14	05:16	SEISREFL	alter course	81°31.64'N	141°42.02'E	1152,3
PS87/081-1	19.09.14	10:00	SEISREFL	alter course	81°19.39'N	139°33.59'E	1652,5
PS87/081-1	19.09.14	14:33	SEISREFL	alter course	80°59.98'N	140°50.29'E	1701,4
PS87/081-1	19.09.14	16:48	SEISREFL	alter course	81°5.24'N	141°53.99'E	1429,3
PS87/081-1	19.09.14	18:38	SEISREFL	alter course	81°13.44'N	141°25.92'E	894,7
PS87/081-1	19.09.14	22:34	SEISREFL	alter course	81°29.42'N	140°5.73'E	1225,6
PS87/081-1	20.09.14	02:31	SEISREFL	alter course	81°34.41'N	142°6.70'E	867,8
PS87/081-1	20.09.14	04:07	SEISREFL	information	81°41.74'N	142°26.17'E	790,9
PS87/081-1	20.09.14	05:24	SEISREFL	information	81°38.16'N	142°40.62'E	782,9
PS87/081-1	20.09.14	07:25	SEISREFL	alter course	81°42.08'N	142°19.93'E	781,5
PS87/081-1	20.09.14	11:22	SEISREFL	alter course	82°1.55'N	142°46.42'E	1336,1
PS87/081-1	20.09.14	16:00	SEISREFL	alter course	82°25.12'N	142°17.87'E	1443,1
PS87/081-1	20.09.14	20:38	SEISREFL	alter course	82°49.36'N	142°27.95'E	1243,2
PS87/081-1	21.09.14	01:06	SEISREFL	alter course	83°12.72'N	141°58.92'E	1327,7
PS87/081-1	21.09.14	05:03	SEISREFL	alter course	83°29.08'N	143°49.37'E	1399,8
PS87/081-1	21.09.14	09:22	SEISREFL	alter course	83°50.64'N	144°27.48'E	1164,1
PS87/081-1	21.09.14	14:08	SEISREFL	profile end	84°9.75'N	146°46.80'E	1812
PS87/081-1	21.09.14	14:23	SEISREFL	information	84°10.40'N	146°57.62'E	1821,6
PS87/081-1	21.09.14	14:28	SEISREFL	information	84°10.56'N	147°0.32'E	1826,6
PS87/081-1	21.09.14	15:04	SEISREFL	information	84°11.88'N	147°23.16'E	1508,4
PS87/081-1	21.09.14	15:20	SEISREFL	information	84°12.43'N	147°32.35'E	1261,9
PS87/081-1	21.09.14	15:44	SEISREFL	information	84°13.22'N	147°45.59'E	1170,7
PS87/081-1	21.09.14	16:03	SEISREFL	information	84°13.82'N	147°56.25'E	1187,3
PS87/081-1	21.09.14	16:20	SEISREFL	information	84°14.35'N	148°5.42'E	1185,6
PS87/081-1	21.09.14	16:45	SEISREFL	information	84°15.16'N	148°19.43'E	1083,7
PS87/081-1	21.09.14	17:01	SEISREFL	information	84°15.61'N	148°26.89'E	1004,5
PS87/081-1	21.09.14	17:14	SEISREFL	information	84°15.94'N	148°32.88'E	934,8
PS87/081-1	21.09.14	17:28	SEISREFL	information	84°16.31'N	148°39.22'E	891
PS87/081-1	21.09.14	17:41	SEISREFL	information	84°16.64'N	148°45.19'E	885,8
PS87/081-1	21.09.14	17:52	SEISREFL	information	84°16.93'N	148°50.25'E	885,6
PS87/081-1	21.09.14	17:57	SEISREFL	information	84°17.07'N	148°52.54'E	889,2
PS87/081-1	21.09.14	18:02	SEISREFL	on deck	84°17.21'N	148°54.92'E	899,1
PS87/081-1	21.09.14	18:08	SEISREFL	on deck	84°17.38'N	148°57.82'E	908,4
PS87/082-1	21.09.14	19:58	HS_PS	profile start	83°59.93'N	149°22.55'E	1468,1
PS87/082-1	21.09.14	20:23	HS_PS	alter course	83°55.77'N	149°16.56'E	1958,4
PS87/082-1	21.09.14	21:40	HS_PS	alter course	83°56.36'N	147°11.73'E	983,6
PS87/082-1	21.09.14	22:49	HS_PS	alter course	83°45.23'N	146°59.22'E	1576,5

Station	Date	Time	Gear	Action	PositionLat	PositionLon	Depth [m]
PS87/082-1	21.09.14	23:46	HS_PS	alter course	83°38.90'N	145°53.21'E	1407,4
PS87/082-1	22.09.14	00:59	HS_PS	alter course	83°26.81'N	145°26.58'E	1806,9
PS87/082-1	22.09.14	02:23	HS_PS	alter course	83°16.16'N	144°4.82'E	1235,1
PS87/082-1	22.09.14	03:55	HS_PS	alter course	83°26.76'N	144°58.59'E	1629
PS87/082-1	22.09.14	05:40	HS_PS	alter course	83°45.01'N	145°17.59'E	1267,7
PS87/082-1	22.09.14	05:58	HS_PS	information	83°46.97'N	144°57.59'E	1043,3
PS87/082-1	22.09.14	22:54	HS_PS	alter course	83°51.82'N	142°43.40'E	2304,9
PS87/082-1	23.09.14	00:32	HS_PS	alter course	83°43.11'N	144°55.40'E	1016,1
PS87/082-1	23.09.14	01:49	HS_PS	alter course	83°33.76'N	146°22.27'E	1745,7
PS87/082-1	23.09.14	07:36	HS_PS	profile end	83°8.34'N	141°36.52'E	1405,5
PS87/083-1	23.09.14	09:11	GC	on ground/ max depth	83°12.26'N	141°5.55'E	1448,6
PS87/083-2	23.09.14	10:30	GC	on ground/ max depth	83°12.23'N	141°4.72'E	1486,9
PS87/083-3	23.09.14	11:56	GC	on ground/ max depth	83°12.24'N	141°4.18'E	1537,8
PS87/084-1	23.09.14	13:23	HS_PS	profile start	83°5.75'N	141°4.40'E	1600,3
PS87/084-1	23.09.14	14:11	HS_PS	alter course	82°58.31'N	140°38.53'E	2090,2
PS87/084-1	23.09.14	14:39	HS_PS	alter course	82°57.50'N	141°17.53'E	1785,1
PS87/084-1	23.09.14	15:22	HS_PS	alter course	83°4.13'N	141°37.09'E	1426,9
PS87/084-1	23.09.14	16:40	HS_PS	alter course	82°50.49'N	141°56.11'E	1755,1
PS87/084-1	23.09.14	17:55	HS_PS	alter course	82°32.39'N	141°54.33'E	1118,7
PS87/084-1	23.09.14	18:24	HS_PS	alter course	82°25.70'N	141°41.96'E	1648,4
PS87/085-1	23.09.14	19:09	XCTD	in the water	82°15.67'N	141°57.79'E	1445,2
PS87/085-1	23.09.14	19:15	XCTD	on ground/ max depth	82°15.15'N	141°59.05'E	1440,4
PS87/084-1	23.09.14	20:09	HS_PS	alter course	82°2.56'N	142°18.99'E	1368,9
PS87/084-1	23.09.14	21:00	HS_PS	alter course	81°50.27'N	142°12.46'E	1166,2
PS87/084-1	23.09.14	21:59	HS_PS	alter course	81°36.27'N	141°56.42'E	1018,9
PS87/084-1	23.09.14	22:34	HS_PS	alter course	81°29.12'N	141°31.28'E	1127,2
PS87/084-1	23.09.14	23:21	HS_PS	alter course	81°23.75'N	140°30.23'E	928
PS87/084-1	23.09.14	23:53	HS_PS	alter course	81°17.31'N	140°45.86'E	1563,9
PS87/084-1	24.09.14	00:16	HS_PS	alter course	81°14.47'N	141°2.61'E	1007,9
PS87/084-1	24.09.14	00:36	HS_PS	profile end	81°13.06'N	141°22.78'E	903
PS87/086-1	24.09.14	02:43	GBG	on ground/ max depth	81°13.04'N	141°22.99'E	901,8
PS87/086-2	24.09.14	03:35	MUC	on ground/ max depth	81°13.04'N	141°22.98'E	901,7
PS87/086-3	24.09.14	04:28	GC	on ground/ max depth	81°13.04'N	141°23.02'E	901
PS87/087-1	24.09.14	05:55	GC	on ground/ max depth	81°12.29'N	141°15.92'E	1407,6
PS87/088-1	24.09.14	07:22	GC	on ground/ max depth	81°12.31'N	141°16.40'E	1378,2
PS87/089-1	24.09.14	08:44	GC	on ground/ max depth	81°12.35'N	141°16.47'E	1364,8

Station	Date	Time	Gear	Action	PositionLat	PositionLon	Depth [m]
PS87/090-1	24.09.14	10:01	GC	on ground/ max depth	81°12.37'N	141°16.87'E	1313
PS87/091-1	24.09.14	11:25	HS_PS	profile start	81°12.55'N	141°18.31'E	1179,8
PS87/091-1	24.09.14	11:44	HS_PS	alter course	81°12.69'N	141°40.89'E	874
PS87/091-1	24.09.14	12:22	HS_PS	alter course	81°16.67'N	142°11.64'E	887,2
PS87/091-1	24.09.14	13:01	HS_PS	alter course	81°14.14'N	142°51.39'E	1344,6
PS87/091-1	24.09.14	14:17	HS_PS	alter course	81°0.55'N	142°57.47'E	1509,3
PS87/091-1	24.09.14	15:11	HS_PS	alter course	80°50.97'N	143°11.27'E	1517,1
PS87/091-1	24.09.14	15:43	HS_PS	alter course	80°50.82'N	143°38.93'E	1516,5
PS87/091-1	24.09.14	16:38	HS_PS	alter course	80°59.98'N	143°23.81'E	1546,6
PS87/091-1	24.09.14	18:12	HS_PS	alter course	81°17.19'N	143°14.95'E	1443
PS87/091-1	24.09.14	18:59	HS_PS	alter course	81°24.38'N	142°44.16'E	1035,5
PS87/091-1	24.09.14	19:20	HS_PS	alter course	81°26.78'N	142°26.46'E	852,5
PS87/091-1	24.09.14	19:41	HS_PS	alter course	81°29.68'N	142°13.10'E	825,5
PS87/091-1	24.09.14	19:58	HS_PS	alter course	81°30.94'N	142°24.07'E	916,2
PS87/091-1	24.09.14	20:20	HS_PS	alter course	81°28.53'N	142°37.67'E	1159,8
PS87/091-1	24.09.14	20:36	HS_PS	alter course	81°29.51'N	142°49.07'E	1287,5
PS87/091-1	24.09.14	21:07	HS_PS	alter course	81°33.67'N	142°34.86'E	1093,7
PS87/091-1	24.09.14	21:38	HS_PS	alter course	81°31.75'N	142°6.06'E	810,2
PS87/091-1	24.09.14	22:14	HS_PS	alter course	81°26.49'N	141°42.24'E	1045,3
PS87/091-1	24.09.14	23:00	HS_PS	alter course	81°23.65'N	140°56.38'E	812,9
PS87/091-1	24.09.14	23:51	HS_PS	alter course	81°16.69'N	141°27.43'E	877,7
PS87/091-1	25.09.14	00:15	HS_PS	profile end	81°13.04'N	141°23.34'E	900,2
PS87/092-1	25.09.14	00:25	MTC	profile start	81°12.03'N	141°22.76'E	1131,9
PS87/092-1	25.09.14	01:42	MTC	on ground/ max depth	81°11.46'N	141°23.76'E	1268,5
PS87/092-1	25.09.14	01:42	MTC	profile end	81°11.46'N	141°23.76'E	1268,5
PS87/093-1	25.09.14	02:57	GC	on ground/ max depth	81°12.48'N	141°17.62'E	1215,7
PS87/094-1	25.09.14	04:16	GC	on ground/ max depth	81°12.57'N	141°18.49'E	1167,6
PS87/095-1	25.09.14	05:42	GC	on ground/ max depth	81°12.64'N	141°19.21'E	1125,9
PS87/096-1	25.09.14	06:51	GC	on ground/ max depth	81°12.73'N	141°20.04'E	1071,4
PS87/097-1	25.09.14	08:03	GC	on ground/ max depth	81°12.37'N	141°16.88'E	1327,8
PS87/098-1	25.09.14	08:42	HS_PS	profile start	81°12.56'N	141°17.73'E	1209,4
PS87/098-1	25.09.14	09:22	HS_PS	alter course	81°18.15'N	141°44.27'E	848,9
PS87/098-1	25.09.14	09:48	HS_PS	alter course	81°18.92'N	142°11.31'E	818,4
PS87/098-1	25.09.14	10:09	HS_PS	alter course	81°22.03'N	142°13.58'E	748,8
PS87/098-1	25.09.14	10:32	HS_PS	alter course	81°25.21'N	141°57.82'E	756
PS87/098-1	25.09.14	10:38	HS_PS	alter course	81°25.93'N	141°56.84'E	762,8
PS87/098-1	25.09.14	10:58	HS_PS	profile end	81°25.61'N	142°12.69'E	740,8
PS87/099-1	25.09.14	11:34	GC	on ground/ max depth	81°25.50'N	142°14.43'E	740,4

Station	Date	Time	Gear	Action	PositionLat	PositionLon	Depth [m]
PS87/099-2	25.09.14	12:21	GC	on ground/ max depth	81°25.49'N	142°14.24'E	739,5
PS87/099-3	25.09.14	13:05	GKG	on ground/ max depth	81°25.48'N	142°14.49'E	741,3
PS87/099-4	25.09.14	14:01	MUC	on ground/ max depth	81°25.50'N	142°14.33'E	741,2
PS87/100-1	25.09.14	15:52	GKG	on ground/ max depth	81°21.42'N	142°35.46'E	951
PS87/100-2	25.09.14	16:42	GC	on ground/ max depth	81°21.41'N	142°35.56'E	951,1
PS87/101-1	25.09.14	17:10	HS_PS	profile start	81°21.58'N	142°39.14'E	991,4
PS87/101-1	25.09.14	17:45	HS_PS	alter course	81°24.66'N	143°10.09'E	1176,8
PS87/101-1	25.09.14	18:00	HS_PS	alter course	81°26.27'N	142°56.36'E	1106,4
PS87/101-1	25.09.14	18:32	HS_PS	alter course	81°29.18'N	143°19.31'E	1414,3
PS87/101-1	25.09.14	18:45	HS_PS	alter course	81°31.21'N	143°20.62'E	1637,1
PS87/101-1	25.09.14	19:18	HS_PS	alter course	81°35.39'N	142°55.11'E	1311,4
PS87/101-1	25.09.14	20:43	HS_PS	alter course	81°50.08'N	143°4.84'E	1101,6
PS87/101-1	25.09.14	21:20	HS_PS	alter course	81°54.94'N	143°29.04'E	1586,6
PS87/101-1	25.09.14	21:44	HS_PS	alter course	81°56.89'N	143°8.21'E	1290,6
PS87/101-1	25.09.14	22:08	HS_PS	alter course	81°53.88'N	142°55.73'E	1129,5
PS87/101-1	25.09.14	22:28	HS_PS	alter course	81°50.66'N	142°48.64'E	776,7
PS87/101-1	25.09.14	23:01	HS_PS	alter course	81°45.21'N	142°42.66'E	957,5
PS87/101-1	25.09.14	23:44	HS_PS	alter course	81°45.46'N	141°49.68'E	1177,9
PS87/101-1	26.09.14	00:40	HS_PS	alter course	81°37.11'N	141°32.69'E	1169,1
PS87/101-1	26.09.14	01:23	HS_PS	alter course	81°32.01'N	141°0.23'E	868,3
PS87/101-1	26.09.14	01:51	HS_PS	alter course	81°29.51'N	140°34.77'E	972,1
PS87/101-1	26.09.14	02:52	HS_PS	alter course	81°22.96'N	141°5.21'E	848,4
PS87/101-1	26.09.14	04:51	HS_PS	profile end	81°13.71'N	141°10.83'E	1041,5
PS87/102-1	26.09.14	05:47	GC	on ground/ max depth	81°12.86'N	141°11.38'E	1330,6
PS87/103-1	26.09.14	07:00	GC	on ground/ max depth	81°12.84'N	141°11.12'E	1369,7
PS87/104-1	26.09.14	09:05	GC	on ground/ max depth	81°12.80'N	141°10.85'E	1417,8
PS87/105-1	26.09.14	10:16	GC	on ground/ max depth	81°12.78'N	141°10.65'E	1448,3
PS87/106-1	26.09.14	11:23	GC	on ground/ max depth	81°12.76'N	141°10.47'E	1471,8
PS87/107-1	26.09.14	12:53	GC	on ground/ max depth	81°12.74'N	141°10.25'E	1496,3
PS87/108-1	26.09.14	14:26	GC	on ground/ max depth	81°12.79'N	141°10.70'E	1439,6
PS87/109-1	26.09.14	15:47	CTD/RO	in the water	81°7.63'N	140°35.16'E	1308
PS87/109-1	26.09.14	15:47	CTD/RO	lowering	81°7.63'N	140°35.16'E	1308
PS87/109-1	26.09.14	15:50	CTD/RO	hoisting	81°7.64'N	140°35.09'E	1307,1
PS87/109-1	26.09.14	15:51	CTD/RO	lowering	81°7.65'N	140°35.08'E	1306,9
PS87/109-1	26.09.14	16:18	CTD/RO	on ground/ max depth	81°7.72'N	140°35.04'E	1307,1

Station	Date	Time	Gear	Action	PositionLat	PositionLon	Depth [m]
PS87/109-1	26.09.14	16:18	CTD/RO	hoisting	81°7.72'N	140°35.04'E	1307,1
PS87/109-1	26.09.14	16:55	CTD/RO	at surface	81°7.71'N	140°35.04'E	1306,8
PS87/109-1	26.09.14	16:56	CTD/RO	on deck	81°7.71'N	140°35.06'E	1309,5
PS87/109-2	26.09.14	17:24	GC	on ground/ max depth	81°7.70'N	140°34.99'E	1306,9
PS87/109-3	26.09.14	18:19	MUC	on ground/ max depth	81°7.67'N	140°34.91'E	1303,1
PS87/109-4	26.09.14	19:42	GKG	on ground/ max depth	81°7.69'N	140°34.95'E	1303,3
PS87/109-5	26.09.14	20:35	MUC	on ground/ max depth	81°7.69'N	140°34.94'E	1302,6
PS87/109-6	26.09.14	21:58	MUC	on ground/ max depth	81°7.67'N	140°35.13'E	1304,6
PS87/110-1	27.09.14	13:08	GC	on ground/ max depth	81°21.02'N	120°31.47'E	5071,9
PS87/110-2	27.09.14	15:43	GBG	on ground/ max depth	81°21.03'N	120°31.48'E	5129,5
PS87/111-1	27.09.14	17:04	HS_PS	profile start	81°20.85'N	120°32.38'E	5117,9
PS87/111-1	27.09.14	17:35	HS_PS	alter course	81°16.57'N	120°27.77'E	5161,4
PS87/111-1	27.09.14	18:37	HS_PS	alter course	81°24.12'N	120°59.34'E	4893
PS87/111-1	27.09.14	21:48	HS_PS	alter course	81°56.40'N	120°8.28'E	2778,7
PS87/111-1	27.09.14	22:38	HS_PS	alter course	81°58.28'N	119°12.58'E	3330,2
PS87/111-1	28.09.14	00:22	HS_PS	alter course	81°40.74'N	119°33.33'E	4596,5
PS87/111-1	28.09.14	06:18	HS_PS	profile end	81°20.02'N	114°43.74'E	3601,5

A5 MARINE GEOLOGY

A5.1 Lithological description of Giant Box Corer (GKG) and Gravity Corer (SL) sections (E. Bazhenova, R. Stein)

Note: For SL cores, only the description of Core PS87/003-2 is included here. From the other cores (SL and KAL), core descriptions are available at the AWI (Contact: R. Stein)

A5.2 Tables with data of smear-slide analysis (E. Bazhenova)

A5.3 Tables with preliminary data of coarse-fraction analysis (S. Nam)

A5.4 Tables with data of dropstone analysis (E. Bazhenova)

A5.5 Tables with micropaleontological data (S. Kaboth, M. Kaminski, S. Nam, A. de Vernal, M. Zwick)

A5.1 Lithological description of Giant Box Corer (GKG) and Gravity

Corer (SL) sections (E. Bazhenova, R. Stein)

Note: For SL cores, only the description of Core PS87/003-2 is included here. From the other cores (SL and KAL), core descriptions are available at the AWI (Contact: R. Stein)

PS 87/ 003-1 (GKG)

Hovgaard Ridge

ARK- XXVIII/4 (Arctic 14)

Recovery: 34 cm

78°24,12'N 1°02,88'W

Water depth: 1170 m

Lithology	Colour	Texture	Description
Surface: 0-1 cm, dark greyish brown (10 YR 4/2), silty clay, gravel, polychets, sea star			
0			
	10 YR 3/2		0-13 cm very dark grayish brown (10 YR 3/2) silty clay, sand admixture
10			
	10 YR 4/2	SS	13-17.5 cm dark grayish brown (10 YR 4/2) silty clay, sand admixture, black mottles up to 0.5 cm Ø
		SSS	17.5-34 cm dark grayish brown (10 YR 4/2) sandy silty clay, black mottles
20			
	10 YR 4/2		
30			
40			
50			

PS87/003-2 SL
Recovery: 1.78m

Hovgaard Ridge
78° 24.08' N, 01° 2.77' W

PS87 (ARK-XXVIII/4)
Water depth: 1174 m

Depth in core (m)	Lithology	Texture Color		Description
0		10YR 3/2		0-8 cm very dark grayish brown (10YR 3/2) silts clay with some sand
		10YR 4/2 to 10YR 4/3		8-25 cm dark brown (10YR 4/2) to brown (10YR 4/3) sandy silty clay
		10YR 5/3		25-33 cm dark brown (10YR 4/2) to brown (10YR 4/3) sandy silty clay with several dropstones (0.5 to 2 cm in diameter; 1 coal) = diamicton
		10YR 4/2 + 2.5Y 3/2 + 2.5Y 4/2		
		2.5Y 3/2		
		N4		
		2.5Y 4/2		33-47 cm dark brown to brown (10YR 4/2 to 4/3) sandy silty clay (more sandy at 43-47 cm); dropstones (0.5-1.5 cm) at 41, 43, and 46 cm
		N4		
1		2.5Y 5/1		
		10YR 5/2		47-52 cm brown (10YR 5/3) sandy silty clay
		5Y 4/2		52-73 cm alternation of thin more silty brown layers and dark more clayey layers; black spots
		5Y 3/2 to 5Y 4/2		73-76 cm very dark grayish brown silty clay
		10YR 5/3		76-81 cm dark gray (N4) silty clay
		2.5Y 4/4		81-83 cm olive gray (5Y 4/2) clayey sand silt
		N4		83-89 cm dark grayish brown (2.5YR 4/2) sandy silty clay
				89-94 cm dark gray (N4) silty clay
2				94-106 cm gray (2.5Y 5/1) silty sand (foaminifers), strong winnowing?); large dropstone (3cm in diameter) at 103-106 cm
				106-114 cm grayish brown (10YR 5/2) silty clay, bioturbated
				114-121 cm olive gray (5Y 4/2) (silty) clay
				121-151 cm dark olive gray to olive gray (5Y 3/2 to 4/2) (silty) clay, bioturbated; sandy layer at 141 and 150-152 cm
				151-156 cm brown (10YR/5/3) silty clay; sharp basis
				156-159 cm gray (2.5Y 4/1) silty clayey sand (winnowing?)
				159-165 cm olive brown (2.5Y 4/4) to dark grayish brown (2.5Y 4/2) sandy silty clay
3				165-178 cm dark gray (N4) silty clay; middle part some dark olive gray (5Y 3/2) sediments; coring disturbance
4				
5				

PS 87/ 023-2 (GKG)

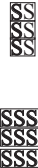
Lomonosov Ridge

ARK- XXVIII/4 (Arctic 14)

Recovery: 36 cm

86°37,86'N 44°52,45'W

Water depth: 2439 m

Lithology	Colour	Texture	Description
Surface: dark brown (10 YR 3/3) silty clay, sand admixture, dropstones up to 12 cm Ø, shell half, organisms living on stones			
0			
	10 YR 3/3		0-9.5 cm dark brown (10 YR 3/3) silty clay, stones 2 and 2.7 cm Ø
10	10 YR 4/3		9.5-13 cm dark brown (10 YR 4/3) silty clay, dropstone 2.5 cm Ø at 11-12 cm
	10 YR 6/3		13-15 cm pale brown (10 YR 6/3) silty clay, sandy admixture, dropstone 4 cm Ø
	10 YR 4/3		15-22 cm dark brown (10 YR 4/3) silty clay, sandy admixture, very soft
20			
	10 YR 3/4 and 2.5 Y 4/2		22-30 cm dark yellowish brown (10 YR 3/4) silty clay, sandy admixture, bioturbation increases towards the lower contact, mottles at the contact (2.5 Y 4/2 silty clay)
30			
	2.5 Y 4/2 and 10 YR 3/4		30-36 cm dark greyish brown (2.5 Y 4/2) silty clay, sandy admixture, bioturbation increases towards the lower contact, black mottling, clasts of unit (10 YR 3/4) dropstone 8 cm Ø at the bottom of the push core
40			
50			

PS 87/ 026-1 (GKG)

Lomonosov Ridge

ARK- XXVIII/4 (Arctic 14)

Recovery: 40 cm

87°26,95'N 46°33,95'W

Water depth: 3339 m

Lithology	Colour	Texture	Description
Surface: brown mud, sandy admixture, very water-saturated, half of Bivalvia shell			
0-13 cm	10 YR 3/2		0-13 cm very dark greyish brown (10 YR 3/2) silty clay, very soft
13-24 cm	10 YR 4/2 to 10 YR 4/3		13-24 cm dark greyish brown (10 YR 4/2) silty clay to dark brown (10 YR 4/3) silty clay, some sand, black mottling
24-29 cm	10 YR 4/3		24-29 cm dark brown (10 YR 4/3) silty clay, white clasts up to 4 mm Ø
29-40 cm	10 YR 3/4		29-40 cm dark yellowish brown (10 YR 3/4) silty clay, bioturbated (dark brown 10 YR 4/3)
40-50 cm			

PS 87/ 029-1 (GKG)

Lomonosov Ridge

ARK- XXVIII/4 (Arctic 14)

Recovery: 41 cm

88°29,08'N 48°6,85'W

Water depth: 2901 m

Lithology	Colour	Texture	Description
Surface: dark brown mud, sand admixture, fragment of calcareous shell			
0	10 YR 3/2 to 2.5 Y 5/2		0-18 cm dark brown (10 YR 3/2) to gray (10 YR 5/1) silty clay, more sandy in the upper part, very soft, small pinkish dots in the lowermost part
10			
20			
21			
22			
23			
24			
25			
26			
27			
28			
29			
30			
31			
32			
33			
34			
35			
36	2.5 Y 3/2		21-23 cm very dark greyish brown (2.5 Y 3/2) silty clay and greyish brown (2.5 Y 5/2) silty clay from the upper unit
37	2.5 Y 3/2 to 2.5 Y 4/2		23-28 cm very dark greyish brown (2.5 Y 3/2) to dark greyish brown (2.5 Y 4/2) silty clay, sand admixture, very soft, small pink spots
38	2.5 Y 5/2		28-30 cm greyish brown (2.5 Y 5/2) silty clay, very dark greyish brown (2.5 Y 3/2) mottling, several grey (2.5 Y 5) spots
39	2.5 Y 4/2		30-35 cm dark greyish brown (2.5 Y 4/2) silty clay, sand admixture, whitish spots up to 0.5 cm
40	10 YR 3/3		35-41 cm dark brown (10 YR 3/3) silty clay, very soft, dark greyish brown (2.5 Y 4/2) mottling
50			

PS 87/ 030-2 (GKG)

Lomonosov Ridge

ARK- XXVIII/4 (Arctic 14)

Recovery: 36 cm

88°39,56'N 61°29,20'W

Water depth: 1278 m

Lithology	Colour	Texture	Description
Surface: brown mud, very water-saturated, sand admixture, polychets, Bivalvia shells (halves), Gastropoda shell, dropstones with remains of organisms on the surface, dropstones up to 6 cm Ø, <u>clasts of biogenic ooze?</u>			
0	10 YR 3/3		0-3 cm dark brown (10 YR 3/3) silty clay, sand admixture
	10 YR 3/3 and 10 YR 4/3		3-10 cm dark brown (10 YR 3/3) silty clay and dark brown (10 YR 4/3) sandy silty clay, lower contact wavy
	10 YR 3/3, 10 YR 4/3 and 2.5 Y 5/2		10-13 cm dark brown (10 YR 3/3) silty clay, dark brown (10 YR 4/3) and greyish brown (2.5 Y 5/2) sandy silty clay, intensively bioturbated, brown (10 YR 5/3) mottling (dry silty clay with sand)
10	2.5 Y 5/2		13-15 cm greyish brown (2.5 Y 5/2) sandy silty clay, gravel, dark brown mottling
	2.5 Y 5/4		15-20 cm light olive brown (2.5 Y 5/4) silty clay, sand admixture, soft, dark brown mottling
20	2.5 Y 4/2 and 2.5 Y 5/4		20-26 cm dark greyish brown (2.5 Y 4/2) and light olive brown (2.5 Y 5/4) silty clay, bioturbated
	2.5 Y 4/2		26-29 cm dark greyish brown (2.5 Y 4/2) silty clay, some sand, sharp contact at the base
30	2.5 Y 5/4		29-31.5 cm light olive brown (2.5 Y 5/4) silty clay, sand admixture
40			
50			

PS 87/ 040-2 (GKG)

Lomonosov Ridge

ARK- XXVIII/4 (Arctic 14)

Recovery: 37 cm

88°59,18'N 171°44,50'E

Water depth: 2618 m

Lithology	Colour	Texture	Description
Surface: brown mud, very water-saturated, some sand, fragments of shells			
0-10 cm	10 YR 3/3		0-10 cm dark brown (10 YR 3/3) silty clay, some sand, small white spots through, coarser in the upper part
10-13 cm	2.5 Y 4/2 to 3/2		10-13 cm dark greyish brown (2.5 Y 4/2) to very dark greyish brown (2.5 Y 3/2) silty clay, rather dry
13-20 cm	2.5 Y 5/4 to darker (2.5 Y 5/3?)		13-20 cm light olive brown (2.5 Y 5/4) to darker (2.5 Y 5/3 ?) silty clay, coarser to the bottom, very dark greyish brown (2.5 Y 3/2) mottling, small pinkish and whitish spots
20-30 cm	10 YR 4/3 to 10 YR 4/2		20-30 cm dark brown (10 YR 4/3) to dark greyish brown (10 YR 4/2) silty clay, very soft, dark mottling in the top part, light olive brown (2.5 Y 5/4) mottling (two spots of 1-2 cm Ø) in the mid, sharp contact at the base
30-36 cm	2.5 Y 5/4		30-36 cm light olive brown (2.5 Y 5/4) sandy silty clay, rather dry, dark greyish brown (10 YR 4/2) mottling
40-50 cm			

PS 87/ 055-1 (GKG)

Lomonosov Ridge

ARK- XXVIII/4 (Arctic 14)

Recovery: 39 cm

85°41,47'N 148°59,47'E

Water depth: 730 m

	Lithology	Colour	Texture	Description
	Surface: brown mud, sandy silty clay, polychets, shell halves (Bivalvia, Brachiopoda)			
0		10 YR 3/3		0-3 cm dark brown (10 YR 3/3) silty clay
		2.5 Y 4/2		3-7.5 cm dark greyish brown (2.5 Y 4/2) silty clay, small pinkish spots at the lower contact, dark brown (10 YR 3/3) mottling
		10 YR 4/2		7.5-9.5 cm dark greyish brown (10 YR 4/2) silty clay, dark greyish brown (2.5 Y 4/2) mottling
10		2.5 Y 4/2 and 10 YR 3/2		9.5-15 cm dark greyish brown (2.5 Y 4/2) silty clay, very soft, very dark greyish brown (10 YR 3/2) mottling, intensively bioturbated, pinkish spot at 14 cm core depth
		2.5 Y 5/2 and 2.5 Y 5/4		15-18 cm greyish brown (2.5 Y 5/2) and light olive brown (2.5 Y 5/4) silty clay
20		2.5 Y 4/4		18-20.5 cm olive brown (2.5 Y 4/4) silty clay, some sand
		2.5 Y 4/2		20.5-22 cm dark greyish brown (2.5 Y 4/2) sandy silt
		10 YR 4/2		22-25 cm dark greyish brown (10 YR 4/2) silty clay, some sand, pinkish spots at the upper contact, greyish brown (2.5 Y 5/2) spot of 2 cm Ø
		10 YR 4/2, 10 YR 4/3, 10 YR 3/3		25-35 cm dark greyish brown (10 YR 4/2), dark brown (10 YR 4/3 and 3/3) silty clay, intensively bioturbated
30		10 YR 4/3		35-39 cm dark brown (10 YR 4/3) silty clay, soft
40				
50				

PS 87/ 056-2 (GKG)

Lomonosov Ridge

ARK- XXVIII/4 (Arctic 14)

Recovery: 40 cm

85°45,07'N 147°55,85'E

Water depth: 836 m

Lithology	Colour	Texture	Description
Surface: brown mud, sandy silty clay, rich fauna: polychets, Bivalvia, Gastropoda, Scaphepoda. In the box: half of Brachiopoda shell			
0	10 YR 3/3 to 10 YR 3/2		0-8 cm dark brown (10 YR 3/3) silty clay to very dark greyish brown (10 YR 3/2) silty clay with some sand, small white spots in the lower part
10	10 YR 4/2		8-12 cm dark greyish brown (10 YR 4/2) silty clay, very soft, some white spots
	10 YR 3/2		12-14 cm very dark greyish brown (10 YR 3/2) silty clay, very soft, dark greyish brown (10 YR 4/2) mottling
20	2.5 Y 4/2 to 2.5 Y 4/4		14-24 cm dark greyish brown (2.5 Y 4/2) to olive brown (2.5 Y 4/4) silty clay, intensively bioturbated, pinkish spot Ø 0.5 cm at 20 cm core depth, very soft, denser at the bottom
30	10 YR 4/2		24-30 cm dark greyish brown (10 YR 4/2) silty clay
	10 YR 4/2 and 10 YR 3/2		30-40.5 cm dark greyish brown (10 YR 4/2) and very dark greyish brown (10 YR 3/2) silty clay, intensively bioturbated, small pinkish spots
40			
50			

PS 87/ 067-2 (GKG)

Makarov Basin

ARK- XXVIII/4 (Arctic 14)

Recovery: 37 cm

83°29,65'N 160°35,36'E

Water depth: 2857 m

Lithology	Colour	Texture	Description
Surface: brown mud, very soft, some sand, half of Bivalvia shell, Foraminifera, bioturbated (warm tracers, clasts)			
0			
	10 YR 3/3		0-6 cm dark brown (10 YR 3/3) silty clay, coarser in the upper part, soft in the lower part
	10 YR 3/2		6-10 cm very dark greyish brown (10 YR 3/2) silty clay, very soft
10	10 YR 4/2		10-14 cm dark greyish brown (10 YR 4/2) silty clay, intensively bioturbated: transition to dark greyish brown (2.5 Y 4/2) silty clay, greyish brown (2.5 Y 5/2) spot at 10 cm core depth, small pinkish spots at the lower contact
	2.5 Y 4/2		14-16 cm dark greyish brown (2.5 Y 4/2) silty clay, dark brown (10 YR 3/3) spot at 14 cm core depth
	10 YR 4/2		16-19 cm dark greyish brown (10 YR 4/2) silty clay, very soft, light olive brown (2.5 Y 5/4) mottling
20	2.5 Y 5/4		19-23.5 cm light olive brown (2.5 Y 5/4) silty clay, very soft, dark greyish brown (10 YR 4/2) mottling, dark brown (10 YR 3/3) and very dark greyish brown (2.5 Y 3/2) spots, small pinkish spots at 19-21 cm core depth (related to brown spots), pinkish spots up to 0.5 cm Ø at the lower contact
	10 YR 5/3		23.5-26.5 cm brown (10 YR 5/3) silty clay, very soft, very dark greyish brown (2.5 Y 3/2) spots
	10 YR 5/3		26.5-27 cm light olive brown (2.5 Y 5/4) silty clay, very soft
	10 YR 5/3		27-29 cm brown (10 YR 5/3) silty clay, some sand
30	10 YR 4/3		29-33 cm brown (10 YR 4/3) silty clay, very soft, several pinkish spots
	10 YR 4/3 to 3/3		33-37 cm brown (10 YR 4/3) to dark brown (10 YR 3/3) silty clay, some sand
40			
50			

PS 87/ 068-2 (GKG)

Makarov Basin

ARK- XXVIII/4 (Arctic 14)

Recovery: 23 cm

83°37,70'N 154°46,87'E

Water depth: 2711 m

Lithology	Colour	Texture	Description
Surface: brown mud (silty clay, some sand), water-saturated, mud clasts. Fauna: Bivalvia (half of shell, up to 1.5 cm Ø), polychets.			
0			Section collapsed after opening of the BC side wall. Therefore, real thickness of layers was not measured.
	10 YR 3/3		0-7 cm dark brown (10 YR 3/3) sandy silty clay
	2.5 Y 4/2		7-9 cm dark greyish brown (2.5 Y 4/2) silty clay, some sand, dark brown (10 YR 3/3) mottling
10	2.5 Y 5/6		9-20.5 cm light olive brown (2.5 Y 5/6) mud, <u>very soft</u> , dark brown (10 YR 3/3) and dark greyish brown (2.5 Y 4/2) mottling in the upper part
20	2.5 Y 4/4		20.5-23 cm olive brown (2.5 Y 4/4) sandy silt
30			
40			
50			

PS 87/ 070-2 (GKG)

Lomonosov Ridge

ARK- XXVIII/4 (Arctic 14)

Recovery: 42 cm

83°48,16'N 146°6,77'E

Water depth: 1340 m

Lithology	Colour	Texture	Description
Surface: brown mud (silty clay, some sand), very water-saturated, living fauna: sea cucumber; shell half			
0-11 cm	10 YR 3/3		0-11 cm dark brown (10 YR 3/3) silty clay, very soft in the upper part, some sand
11-18 cm	10 YR 3/4 to 2.5 Y 4/2		11-18 cm dark yellowish brown (10 YR 3/4) to dark greyish brown (2.5 Y 4/2) silty clay, dark brown (10 YR 3/3) mottling
18-26 cm	10 YR 3/4 and 2.5 Y 4/2		18-26 cm dark yellowish brown (10 YR 3/4) and dark greyish brown (2.5 Y 4/2) silty clay, intensively bioturbated
26-27 cm	2.5 Y 3/2		26-27 cm very dark greyish brown (2.5 Y 3/2) silty clay, very soft, dark yellowish brown (10 YR 3/4) mottling
27-31 cm	10 YR 3/2		27-31 cm very dark greyish brown (10 YR 3/2) silty clay, very soft, dark brown (10 YR 3/3) and dark yellowish brown (10 YR 3/4) mottling
31-39 cm	2.5 Y 5/4		31-39 cm light olive brown (2.5 Y 5/4) silty clay, very soft, very dark greyish brown (2.5 Y 3/2) mottling
39-42 cm	2.5 Y 6/4		39-42 cm light yellowish brown (2.5 Y 6/4) silty clay, very soft, light olive brown (2.5 Y 5/4) mottling
42-50 cm			

PS 87/ 074-1 (GKG)

Makarov Basin

ARK- XXVIII/4 (Arctic 14)

Recovery: 36 cm

82°43,39'N 158°37,49'E

Water depth: 2816 m

Lithology	Colour	Texture	Description
Surface: brown mud (silty clay, some sand), very water-saturated, mud clasts; fauna: sponge, Gastropoda shell, forams			
0	10 YR 3/3		0-4 cm dark brown (10 YR 3/3) silty clay, sand admixture
	2.5 Y 4/2 to 2.5 Y 5/4		4-10 cm dark greyish brown (2.5 Y 4/2) to light olive brown (2.5 Y 5/4) silty clay, intensively bioturbated, dark brown (10 YR 3/3) mottling
10	2.5 Y 4/2 and 2.5 Y 5/4		10-12.5 cm dark greyish brown (2.5 Y 4/2) and light olive brown (2.5 Y 5/4) silty clay, intensively mixed
	10 YR 4/2 to 2.5 Y 6/4		12.5-15 cm dark greyish brown (10 YR 4/2) to light yellowish brown (2.5 Y 6/4) silty clay, very soft
	10 YR 4/2 and 2.5 Y 6/4		15-17 cm dark greyish brown (10 YR 4/2) and light yellowish brown (2.5 Y 6/4) silty clay, very dark greyish brown (2.5 Y 3/2) mottling
	2.5 Y 6/4		17-18 cm light yellowish brown (2.5 Y 6/4) silty clay, very dark greyish brown (2.5 Y 3/2) mottling
20	10 YR 5/3		18-19.5 cm brown (10 YR 5/3) silty clay, very soft, very dark greyish brown (2.5 Y 3/2) and dark greyish brown (10 YR 4/2) mottling
	2.5 Y 6/4		19.5-21 cm light yellowish brown (2.5 Y 6/4) silty clay, very soft
	10 YR 5/3 and 2.5 Y 5/2 and 10 YR 5/3		21-22 cm brown (10 YR 5/3) silty clay, very soft, very dark greyish brown (2.5 Y 3/2) mottling, pink spots
	10 YR 4/3		22-23.5 cm greyish brown (2.5 Y 5/2) and brown (10 YR 5/3) silty clay, very soft, very dark greyish brown (2.5 Y 3/2) mottling, pink spots
30	10 YR 4/2		23.5-27 cm brown (10 YR 4/3) silty clay, very soft, dark brown (10 YR 3/3) mottling
	10 YR 4/2		27-33 cm dark greyish brown (10 YR 4/2) silty clay, some sand, small pink spots
	10 YR 3/2 and 4/2		33-36 cm very dark greyish brown (10 YR 3/2) and dark greyish brown (10 YR 4/2) silty clay, some sand
40			
50			

PS 87/ 076-2 (GKG)

Makarov Basin

ARK- XXVIII/4 (Arctic 14)

Recovery: 37 cm

82°53,81'N 154°57,88'E

Water depth: 2763 m

Lithology	Colour	Texture	Description
Surface: dark brown mud (silty clay, some sand), mud clasts; shells. Surface and sediment core disturbed by coring.			
0	10 YR 3/2		0-3 cm very dark greyish brown (10 YR 3/2) silty clay, soft, some sand
	2.5 Y 4/2		3-11 cm dark greyish brown (2.5 Y 4/2) silty clay, intensively bioturbated, dark brown (10 YR 3/3) mottling
10	2.5 Y 3/2 to 2.5 Y 5/4		11-17.5 cm very dark greyish brown (2.5 Y 3/2) to light olive brown (2.5 Y 5/4) silty clay, very soft, intensively bioturbated
	10 YR 3/2		17.5-20 cm very dark greyish brown (10 YR 3/2) silty clay, very soft, very dark greyish brown (2.5 Y 3/2) mottling
20	2.5 Y 5/4 and 10 YR 5/3		20-24 cm light olive brown (2.5 Y 5/4) and brown (10 YR 3/3) silty clay, very soft, very dark greyish brown (2.5 Y 3/2) mottling 24-26 cm brown (10 YR 4/3) silty clay, very soft, very dark greyish brown (2.5 Y 3/2) mottling, small pink spots
	10 YR 4/3		26-28 cm light olive brown (2.5 Y 5/4) and brown (10 YR 3/3) silty clay, very soft, very dark greyish brown (2.5 Y 3/2) mottling
	2.5 Y 5/4 and 10 YR 5/3		28-29.5 cm brown (10 YR 4/3) silty clay, very soft, small pink spots
30	10 YR 4/3		29.5-31 cm greyish brown (2.5 Y 5/2) and dark greyish brown (2.5 Y 4/2) silty clay, very soft, pink spots
	2.5 Y 5/2 and 2.5 Y 4/2		
	10 YR 3/3 and 4/3		31-32 cm brown (10 YR 4/3), greyish brown (2.5 Y 5/2) and dark brown (10 YR 3/3) silty clay, small pink spot at the base
	10 YR 4/3		32-34 cm dark brown (10 YR 3/3) and brown (10 YR 4/3) silty clay, very soft
			34-37 cm brown (10 YR 4/3) silty clay, very soft
40			
50			

PS 87/ 079-2 (GKG)

Lomonosov Ridge

ARK- XXVIII/4 (Arctic 14)

Recovery: 43 cm

83°12,09'N 141°22,92'E

Water depth: 1359 m

Lithology	Colour	Texture	Description
Surface: brown mud (silty clay, some sand), mud clasts; shells. Fauna: Bivalvia (half of shell), polychets, forams, copepode, fragments of other shells up to 2 cm Ø.			
0-15 cm	10 YR 3/3		0-15 cm dark brown (10 YR 3/3) silty clay, very soft, shell remains in the upper part
15-25 cm	10 YR 4/3 and 2.5 Y 3/2		15-25 cm dark brown (10 YR 4/3) and very dark greyish brown (2.5 Y 3/2) silty clay, mixed
25-32 cm	2.5 Y 3/2 and 10 YR 4/3		25-32 cm very dark greyish brown (2.5 Y 3/2) and dark brown (10 YR 4/3) silty clay
32-36 cm	10 YR 4/2 and 2.5 Y 4/0		32-36 cm dark greyish brown (10 YR 4/2) and dark grey (2.5 Y 4/0) silty clay, contact at the base not straight, dark yellowish brown (10 YR 3/4) mottling
36-39 cm	2.5 Y 5/4		36-39 cm light olive brown (2.5 Y 5/4) silty clay, contacts at the base and at the top not straight
39-43 cm	10 YR 3/4		39-43 cm dark yellowish brown (10 YR 3/4) silty clay, very soft, light olive brown (2.5 Y 5/4) mottling
43-50 cm			

PS 87/ 086-1 (GKG)

Lomonosov Ridge

ARK- XXVIII/4 (Arctic 14)

Recovery: 36 cm

81°13,04'N 141°22,92'E

Water depth: 901 m

	Lithology	Colour	Texture	Description
0				Surface: brown mud (silty clay, very small amount of sand), very water-saturated. Fauna: polychets, Bivalvia (shell halves).
0-7		10 YR 3/3		0-7 cm dark brown (10 YR 3/3) mud, silty clay, very soft, very water saturated at 0-3 cm core depth
7-16		10 YR 4/2 and 2.5 Y 3/2		7-16 cm dark greyish brown (10 YR 4/2) and very dark greyish brown (2.5 Y 3/2) silty clay, bioturbated
16-29		10 YR 4/2 and 2.5 Y 4/2		16-29 cm dark greyish brown (10 YR 4/2) and dark greyish brown (2.5 Y 4/2) silty clay, intensively bioturbated, very soft in the lower part - dark greyish brown (10 YR 4/2)
29-31		10 YR 3/2		29-31 cm dark greyish brown (10 YR 4/2) and very dark greyish brown (10 YR 3/2) silty clay, rather dry
31-36		10 YR 4/2 and 2.5 Y 4/2		31-36 cm dark greyish brown (10 YR 4/2) and dark greyish brown (2.5 Y 4/2) silty clay, rather dense, softer to the base
36-50				

PS 87/ 099-3 (GKG)

Lomonosov Ridge

ARK- XXVIII/4 (Arctic 14)

Recovery: 36.5 cm

81°25,48'N 142°14,49'E

Water depth: 741 m

Lithology	Colour	Texture	Description
Surface: brown mud (silty clay, some sand), water-saturated, polychets.			
0-7 cm	10 YR 3/3		0-7 cm dark brown (10 YR 3/3) silty clay, some sand, rather water-saturated, shell fragments
7-15 cm	10 YR 4/3		7-15 cm dark brown (10 YR 4/3) silty clay, rather dense, very dark greyish brown (2.5 Y 3/2) mottling
15-25 cm	2.5 Y 3/2 to 10 YR 5/3		15-25 cm very dark greyish brown (2.5 Y 3/2) to brown (10 YR 5/3) silty clay, rather dense, some greyish brown (2.5 Y 5/2) mottling - softer silty clay
25-33 cm	10 YR 3/2 and 10 YR 5/3		25-33 cm very dark greyish brown (10 YR 3/2) and brown (10 YR 5/3) silty clay, interlayering
33-36.5 cm	10 YR 5/3		33-36.5 cm brown (10 YR 5/3) silty clay
40-50 cm			

PS 87/ 100-1 (GKG)

Lomonosov Ridge

ARK- XXVIII/4 (Arctic 14)

Recovery: 39 cm

81°21,42'N 142°35,46'E

Water depth: 951 m

Lithology	Colour	Texture	Description
Surface: brown mud (silty clay, some sand), water-saturated. Polychets, shell up to 4 cm Ø.			
0-6 cm	10 YR 3/3		0-6 cm dark brown (10 YR 3/3) silty clay, some sand in the upper part, soft
6-19 cm	10 YR 4/3 and 2.5 Y 3/2		6-19 cm dark brown (10 YR 4/3) silty clay and very dark greyish brown (2.5 Y 3/2) to dark greyish brown (2.5 Y 4/2) silty clay
19-28 cm	10 YR 5/3		19-28 cm bioturbated unit: brown (10 YR 5/3) silty clay brown (10 YR 4/3) and dark greyish brown (2.5 Y 4/2) silty clay
28-30 cm	10 YR 3/2 and 4/3		28-30 cm very dark greyish brown (10 YR 3/2) and brown (10 YR 4/3) silty clay, thin interlayering
30-39 cm	10 YR 4/3		30-39 cm brown (10 YR 4/3) silty clay, dark greyish brown (2.5 Y 4/2) and greyish brown (2.5 Y 5/2) mottling
40-50 cm			

PS 87/ 104-9 (GKG)

Lomonosov Ridge

ARK- XXVIII/4 (Arctic 14)

Recovery: 37 cm

81°7,69'N 140°34,95'E

Water depth: 1303 m

Lithology	Colour	Texture	Description
Surface: brown mud (silty clay, some sand), water-saturated. Surface bioturbated, polychets, shell halves.			
0-5 cm	10 YR 3/3		0-5 cm dark brown (10 YR 3/3) silty clay, water-saturated
5-12.5 cm	10 YR 4/2		5-12.5 cm dark greyish brown (10 YR 4/2) silty clay
12.5-18.5 cm	2.5 Y 4/2 and 10 YR 4/2		12.5-18.5 cm dark greyish brown (2.5 Y 4/2) silty clay, rather dense, dark greyish brown (10 YR 4/2) mottling
18.5-21.5 cm	10 YR 3/2		18.5-21.5 cm very dark greyish brown (10 YR 3/2), dark greyish brown (10 YR 4/2) to very dark greyish brown (2.5 Y 3/2) silty clay
21.5-24.5 cm	10 YR 3/2 and 2.5 Y 4/2		21.5-24.5 cm very dark greyish brown (10 YR 3/2) and dark greyish brown (2.5 Y 4/2) silty clay
24.5-28 cm	2.5 Y 4/2 and 10 YR 4/2		24.5-28 cm dark greyish brown (2.5 Y 4/2) and dark greyish brown (10 YR 4/2) silty clay
28-37 cm	10 YR 3/2		28-37 cm interlayering: very dark greyish brown (10 YR 3/2) silty clay -dark layers; dark greyish brown (10 YR 4/2) and dark greyish brown (2.5 Y 4/2) silty clay, more bioturbated - lighter units
37-40 cm	10 YR 4/2 and 2.5 Y 4/2		
40-45 cm	10 YR 3/2		
45-50 cm	10 YR 4/2 and 2.5 Y 4/2		

A5.2 Tables with data of smear-slide analysis

(E. Bazhenova)

Smear Slide Description

Tab. A5.2.1 Results of smear-slide analysis of core PS87/023-1

Depth cmbsf	Sand %	Silt %	Clay %	Quartz	Feldspars	Rock fragments	Mica	Terregen. carbonate	Glaukonite	Zeolithe	Heavy minerals	Calcar. fragments	Foraminifers	Coccoliths	Diatoms	Sponge spicules	Sediment	Comments
2.0	1	7	92	2	1		5	2		1	1	2	1	1		1	silty clay	
14.5	1	10	89	4	1		3	1	1				1	1			silty clay	
26.0	1	15	84	1	1		15	0				1	1	1			silty clay	
42.0	3	15	82	12	1		2	0			1						silty clay	
68.5	15	15	70	20	4	1	4	0			1						sandy silty clay	
84.0	1	20	79	3	1		10	2			2		1				silty clay	
92.5	1	25	74	0		1	1	25					1				silty clay	carbonate-rich micrite
131.0	1	15	84	4		1	7	2			1		1	1			silty clay	
138.0	1	7	92	4			2	2			1		2	2			silty clay	
164.0	2	10	89	4	1		2	6			2		1				silty clay	coarse sand, carbonate-rich micrite
178.0	1	15	84	4	2		1	4					1				silty clay	
187.0	2	15	83	8			3	1			1						silty clay	
207.0	1	15	84	6		1	1	2		1	1	1		1			silty clay	carbonate-rich micrite
217.0	3	10	87	7	1		1	0			1						silty clay	
240.0	1	15	84	4	1		7	2					1	1			silty clay	
269.0	1	10	89	4	1		2	3			1			1			silty clay	
281.0	1	20	79	5	1	1		10		1	1		1				silty clay	carbonate-rich micrite
312.0	1	10	89	3	1	1	2	2			1	1	1			1	silty clay	
326.0	2	15	83	8	1	1	3	2		1	2		2	1			silty clay	
340.0	3	10	87	8	1	1	3	1			1						silty clay	
363.0	2	10	88	2	2	2	1	6			1						silty clay	
381.0	5	15	80	5	2	1	4	7			2						silty clay	coarse sand
394.0	1	10	89	4			8	1		1							silty clay	
424.0	2	5	93	5	1		1	1									silty clay	
445.0	1	5	94	3			4	1									silty clay	
450.0	1	5	94	4		1	2	1									silty clay	
466.0	2	5	93	4	2		2	1			1						silty clay	
504.0	1	3	96	3			2	1		1							silty clay	
540.0	2	10	88	1	1		3	1		1	2						silty clay	
571.0	1	5	94	2				2									silty clay	
598.0	2	15	83	6	2	1		8									silty clay	
629.0	2	7	91	7	1			0									silty clay	
635.0	0	3	97	1			2	0		1							silty clay	
658.0	2	5	93	4	1	1		1									silty clay	
685.0	1	5	94	4	1			1									silty clay	
698.0	3	20	77	17			2	1			1						silty clay	

Tab. A5.2.2 Results of smear-side analysis of core PS87/030-1

Depth cmbfsf	Sand %	Silt %	Clay %	Quartz	Feldspars	Rock fragments	Mica	Terrigen. carbonate	Glaukonite	Zeolithe	Heavy minerals	Calcar. fragments	Foraminifers	Coccoliths	Diatoms	Sponge spicules	Sediment	Comments
0,0	1	5	94	4	2	1	3	2				1	1	1			silty clay	
1,0	1	5	94	3	2	1	2	2				1	2	1			silty clay	
27,0	3	15	82	12	2	1	2	0			1						silty clay	coarse sand
55,0	1	15	84	11	1	1	1	0		1	2						silty clay	
64,5	1	10	89	8	2	1	1	0			2						silty clay	
71,0	1	10	89	6	0	1	2	1		1	2	1					silty clay	
79,0	1	10	89	6	2	1	2	1			2	2	1	1			silty clay	
90,0	1	50	49	2	1		1	50			0		1	1			silty clay	carbonate-rich micrite
98,0	1	15	84	8	2	2	4	2			1	2	1	1			silty clay	
106,0	5	10	85	10	2	0	2	0			2						silty clay	
117,0	2	50	48	3	1		1	50			2						silty clay	carbonate-rich micrite
140,0	15	20	65	25	2	1	1	2			2	1	1	1			"sandy" silty clay	coarse sand
144,0	2	10	88	6	2		3	2			2	1	1	0			silty clay	
216,0	5	40	59	1	1	1	1	40			1		1				silty clay	carbonate-rich micrite
222,0	1	50	49	1				50									silty clay	carbonate-rich micrite
268,0	1	5	94	3	1	1	1	1			1			1			silty clay	
298,0	1	10	89	8	1	1	3	1			1						silty clay	
322,0	1	5	94	4	1	1		1					1				silty clay	
344,0	1	5	94	3		1	2	1			1						silty clay	
349,0	1	3	96	1	1		1	1									silty clay	
384,0	5	15	80	3	1		1	13			1						silty clay	
414,0	1	10	89	6	1	1	2	0									silty clay	
442,0	1	15	89	4	2	2	3	1		1							silty clay	
460,0	1	10	89	8	2	1	1	1			2						silty clay	
490,0	1	10	89	6	2		4	1			1						silty clay	
499,0	1	10	89	6	1	1	2	3			1						silty clay	
536,0	2	10	88	8	1		1	1			2						silty clay	
583,0	1	10	89	8	1		2	0			1						silty clay	
606,0	2	10	88	8	2		2	0			1						silty clay	

Tab. A5.2.3 Results of smear-side analysis of core PS87/040-1

Depth cmbsf	Sand %	Silt %	Clay %	Quartz	Feldspars	Rock fragments	Mica	Terrigen. carbonate	Glaukonite	Zeolithe	Heavy minerals	Calcar. fragments	Foraminifers	Coccoliths	Diatoms	Sponge spicules	Sediment
13,0	1	5	94	4	1			1			1	1	1				silty clay
22,0	1	10	89	6	2		1	2			1	1	1	1			silty clay
43,0	2	7	91	4	1	1	2				1	1					silty clay
60,0	10	5		10	1	1	1	2									sandy silty clay
90,5	2	5	93	4	1	1	2	1			2						silty clay
91,5	1	10	89	4	1		6	0			1						silty clay
108,0	1	5	94	3	1		2	0			1						silty clay
124,0	1	5	94	3	1		2	1						?			silty clay
141,0	3	5	92	3	2	1	2	1			1						silty clay
150,0	2	15	83	11	3	2	2				1						silty clay
188,0	2	10	88	6	2		1				1						silty clay
209,0	1	15	84	11	2		2				1						silty clay
220,0	1	5	94	4	1	1	1	1									silty clay
245,0	1	5	94	4	1	1		1			1						silty clay

Tab. A5.2.4 Results of smear-slide analysis of core PS87/056-1

Depth cmbsf	Sand %	Silt %	Clay %	Quartz	Feldspars	Rock fragments	Mica	Terrigen. carbonate	Glaukonite	Zeolithe	Heavy minerals	Calcar. fragments	Foraminifers	Coccoliths	Diatoms	Sponge spicules	Sediment	Comments
1,0	1	15	84	11	1		2	1			1	1	1	1			silty clay	
7,0	1	10	89	8	1		1	1			1						silty clay	
30,0	1	5	84	4			1	2			2	1	1				silty clay	
50,0	1	10	89	7	1		2	0			2						silty clay	
76,0	2	5	93	4	2		1	0			1						silty clay	coarse sand
92,0	2	5	93	4	1	1	1	0			1						silty clay	coarse sand
104,0	1	3	96	2	1		2	0			1						silty clay	
132,0	0	15	84	11	1		2	0			1						silty clay	
146,0	5	10	85	12	2	1		0									silty clay	coarse sand
153,0	1	7	92	6	2			1			1						silty clay	
156,0	1	10	89	8	2			2			1						silty clay	

Tab. A5.2.5 Results of smear-slide analysis of core PS87/070-1

Depth cmbsf	Sand %	Silt %	Clay %	Quartz	Feldspars	Rock fragments	Mica	Terrigen. carbonate	Glaukonite	Zeolithe	Heavy minerals	Calcar. fragments	foraminifer	Coccoliths	Diatoms	Sponge spicules	Sediment	Comments
4,0	1	15	84	11	2		2	1			1	1	1	1			silty clay	
47,0	0,5	7	92	6	1		1	1			1						silty clay	
60,0	1	5	94	4	2		0	1			1	1	1				silty clay	
93,0	2	10	88	6	1	1	6	1									silty clay	
107,0	1	7	92	4	2	1	4	0			2						silty clay	
109,0	0,5	5	94	3	1		2	0,5			1						silty clay	
140,0	1	10	89	8	2	1	1	0									silty clay	
172,0	2	5	93	4	2	1	2	2			1						silty clay	
207,0	0,5	3	96	2		1	1	1									silty clay	
210,0	0	5	97	2	1		3	1									silty clay	
230,0	0,5	3	96	3	2		2	1									silty clay	
247,0	3	20	78	17	2	1	1	1			2						silty clay	coarse sand
265,0	0,5	5	94	4	1		0	2			1						silty clay	
334,5	0,5	20	79	16	1		2	1			1						silty clay	
339,0	2	5	93	4	2		1	0			2						silty clay	coarse sand
375,0	1	7	92	6	2		1	1			1						silty clay	
410,0	2	5	83	4	2			2			1						silty clay	
450,0	1	15	84	11	2		1	1			1						silty clay	
468,0	1	10	89	8	1	1	1	2			1						silty clay	
474,0	2	15	83	11	2		1	2			1						silty clay	coarse sand
488,0	1	7	92	6	2		1	2			1						silty clay	
489,0	3	20	77	16	2		3	2			2						silty clay	coarse sand
493,0	2	20	78	16	2		2	1			2						silty clay	coarse sand
520,0	1	15	84	11	1		1	0			1						silty clay	
537,0	1	5	94	4	1		1	0									silty clay	
566,0	5	20	75	18	2		4	1			2						silty clay	coarse sand
652,0	1	3	96	3	2	1	1	1			2						silty clay	
710,0	1	15	84	11	2		1	1			1						silty clay	
744,0	0,5	7	92	6	1		1	0			1						silty clay	

Tab. A5.2.6 Results of smear-slide analysis of core PS87/079-1

Depth cmbfsf	Sand %	Silt %	Clay %	Quartz	Feldspars	Rock fragments	Mica	Terrigen. carbonate	Glaukonite	Zeolithe	Heavy minerals	Calcar. fragments	Foraminifer	Coccoliths	Diatoms	Sponge spicules	Sediment	Comments
16,0	1	7	94	4	2		2	1			2						silty clay	
50,0	0,5	20	80	4	2		16	1									silty clay	
58,0	1	10	89	6	2		2	2		1	2						silty clay	
88,0	1	15	84	11	2		4	1			1						silty clay	
134,0	0,5	7	92	3	1		6	1									silty clay	
151,0	1	10	89	4	2		5	0			2						silty clay	
159,0	1	10	89	6	1		3	1			2						silty clay	
173,0	3	7	20	7	2		2	0			1						silty clay	coarse sand
194,0	2	10	88	6	2	1	1	1			2						silty clay	coarse sand
196,0	0,5	20	80	16				1			1						silty clay	
204,0	1	5	94	3	2	1	1	1		1							silty clay	
255,0	1	2	97	2	1		1	1									silty clay	
280,0	1	7	92	3	1	1	1	1									silty clay	
295,0	1	2	97	2	2		2	1									silty clay	
332,0	0,5	3	96	3	1			0				0,5					silty clay	
353,0	2	7	91	6	2		2	1			1						silty clay	
379,0	2	5	93	3	2	1	1	0									silty clay	
382,0	2	7	91	6	2		1	0			1						silty clay	
384,0	2	5	93	3	1		1	0			1						silty clay	coarse sand
409,0	1	2	97	2			1	1			1						silty clay	
479,0	1	3	96	3	1		2	1			2						silty clay	
491,0	1	3	96	3			2	0			1						silty clay	
503,0	0,5	3	97	3	1		1	0			1						silty clay	
550,0	0,5	5	95	3	2	1	1	1									silty clay	
600,0	1	10	89	8	2		1	2			1						silty clay	
658,0	2	10	88	7	2	1	4	1			2						silty clay	

Tab. A5.2.7 Results of smear-slide analysis of core PS87/003-2

Depth cmbsf	Sand %	Silt %	Clay %	Quartz	Feldspars	Rock fragments	Mica	Terrigen. carbonate	Glaukonite	Zeolithe	Heavy minerals	Calcar. fragments	foraminifer	Coccoliths	Diatoms	Sponge spicules	Sediment
2	25	35	40	5	1	2	1						1		1	1	sandy silty clay
12	30	40	30	10	2	1	1				1		1	1	1		sandy silty clay
46	30			3	5	5	2			1	1						sandy silty clay
65,5	10	20	70	3	5	1	25	1		1	1						silty clay
69	15	10	75	5				1			1						silty clay
80	10							1		1	1						silty clay
81	5			2	1		2				1						silty clay
91	7	10	83	3	1		3		1		1						silty clay
92	3	15	82	5	1	1	5	2	1		1						silty clay
103	10			3	1		1	1			1		5				silty clay
124,5	10	15	75	5	1	1	5	2			1						silty clay
151,5	5	7	88	5	3		2	1			1						silty clay
157	5	5	90	5	2		3				1						silty clay
169	3				1		5		1		1						silty clay

Tab. A5.2.8 Results of smear-slide analysis of core PS87/095-1

Depth cmbsf	Sand %	Silt %	Clay %	Quartz	Feldspars	Rock fragments	Mica	Terrigen. carbonate	Glaukonite	Zeolithe	Heavy minerals	Calcar. fragments	Foraminifer	Coccoliths	Diatoms	Sponge spicules	Sediment
298,0	1	5	94	4	1	1	2				1						silty clay
305,0	1	7	92	6	1	1	1				1						silty clay
330,0	2	15	83	11	2	1	2				2						silty clay
350,0	1	7	92	6	1		1				1						silty clay
370,0	1	15	84	11	1		1				2	?					silty clay
403,0	1	10	89	8	1		2				2	?					silty clay
442,0	1	10	89	8	1	1	1				1						silty clay
474,0	1	5	94	4	1		1		1		2	?					silty clay

A5.3 Tables with preliminary data of coarse-fraction analysis

(S. Nam)

Tab. A5.3.1 :Results of coarse fraction analysis of core PS87/023-1 KAL

Depth (cm)	Sand	Qz/Fp	Rock F	Mica	Basalt	Carbo-nate	H. mineral	M. nodule	PI forams	Np sin	Np dex	Benthic Forams	Ag Forams	Ostra-code	Sp spicule
26	3	2,5	2	1,5	0	0	0	0	5	5	2	2,5	0	2	2
32	12	2,5	2	1,5	0	0	1	1	5	5	1	2,75	2	2	1
40	20	5	2	1	0	0	1	1	0	0	0	0	1	0	0
50	19	5	2,5	1	0	0	2	2	0	0	0	0	0	0	0
60	15	5	2,5	1	0	0	2	2	0	0	0	0	0	0	0
70	2	2,5	2,5	1	0	0	2	2	5	5	1,5	2,75	0	0	0
80	2	2,5	2	1	0	0	0	0	4,5	5	1,5	2,5	0	0	1
90	2	3	2,5	1	0	0	0	0	4,5	5	1	2,5	1	0	2,5
92	2														
100	5	3	2	1	0	1	0	1	4	5	2	2	1	1	0
110	11	3,5	2,5	1	0	0	1	2,5	4	5	1,5	1	1	0	1
118	4	3,5	2	0	0	0	0	0	3,5	5	1,5	1	0	0	0
125	2	3,5	3	1,5	0	1,5	1	2,5	3	5	1	1,5	1	1	1,5
133	2	3	2	1	0	1	1	1	4	5	1	2	1	1,5	1,5
141	6	3,5	2	2	0	1	1	1	3,5	5	1,5	1	0	0	2
147	6	3	2	2	0	0	0	1	4	5	2	2	0	1,5	2
155	5	3,5	2,5	2	0	1,5	1,5	1	3,5	5	1	1	1	0	1
161	17	3	3	2	0	1,5	1,5	1	3	5	1	1,5	0	0	1,5
165	9														
173	6	3	1	2	0	0	0	1	4	5	1	3	0	1,5	2
179	7	4	2,5	2	0	1	1,5	1,5	3	5	1	1	1	0	1
191	45	5	1,5	2	0	0	1,5	1,5	0	0	0	0	2	0	0
201	21	5	2,5	2	1	2	1,5	1	0	0	0	0	1	0	0
211	3	4	3	2	0	2	1	2,5	3	5	1	2,75	0	0	0
221	21	5	2,5	2	0	2	2	2	0	0	0	1	0	0	0
231	1	3	2,5	2	0	1	2	3	2,5	1	1	4	1	0	2
241	2	3	2	2	0	1	1,5	2	4	5	1	3	0	1	2
253	1	4,5	2	2	0	1	2	2,5	3	5	1	2,5	0	0	2
261	2	3	2	1,5	0	1	1	3	4	5	1	2,5	0	0	2,5
265	4	4	2	1	0	0	1	3	3,5	5	1	2	1	1,5	2

Depth (cm)	Sand	Qz/Fp	Rock F	Mica	Basalt	Carbo-nate	H. mineral	M. nodule	PI forams	Np sin	Np dex	Benthic Forams	Ag Forams	Ostra-code	Sp spicule
271	6	3	2,5	2	0	1	1,5	2,5	4	5	1	2,5	0	1	2,5
281	4	3,5	2,5	2	0	1	1	3,5	3	5	1	2,5	0	0	1
291	8	4	2	1,5	0	0	1,5	3,5	2,5	5	1	1	0	0	1,5
301	2	3,5	2	2	0	0	2	3,5	2,5	5	1	3	0	0	2
311	1	4,5	2,5	2	0	0	2,5	3	2,5	5	0	2	0	0	1
321	5	4,5	2,5	2	0	0	2	2,5	3	5	1	3	0	0	2,5
331	16	4,5	2	1	1	2	2	2	2,5	5	0	1	2	0	0
341	12	4,5	2,5	2	0	1	2	2,5	1	0	0	1	0	0	0
351	6	5	2	1	0	0	2	2	0	0	0	0	0	0	0
361	4	4,5	2	1,5	0	0	1,5	3,5	2	0	0	0	0	0	0
371	8	5	2,5	2,5	1	0	2	2,5	1	0	0	0	0	0	0
381	15	5	2,5	1	1	2,5	1	1	0	0	0	0	0	0	0
391	8	4	2,5	1	0	1,5	2	4	0	0	0	0	0	0	0
401	4	4	2	2	0	0	2	4	0	0	0	0	0	0	0
411	3	5	2,5	1,5	0	0	2	2	0	0	0	0	0	0	0
421	8	4,5	2,5	2,5	0	2	2	2,5	1,5	0	0	0	2	0	0
431	5	5	2	2	0	1	1,5	2,5	0	0	0	0	1	0	0
441	12	4	3	2	1	2	2	3	0	0	0	0	2	0	0
451	15	5	2	1	0	2	1	2	0	0	0	0	1,5	0	0
461	6	5	2	2	0	0	1,5	2	0	0	0	0	1	0	0
471	5	5	2	2	0	0	1,5	2	0	0	0	0	2,5	0	0
481	2	5	2,5	2	0	1,5	1,5	1	0	0	0	0	1,5	0	0
491	3	4,5	2	2,5	0	1	1,5	3	0	0	0	1	1,5	0	0
501	1	4,5	2,5	1,5	0	1	2	3	1	0	0	0	2	0	0
511	2	4,5	2,5	2,5	0	1	2	3	2	0	0	1,5	2	0	0
521	8	5	2	1	0	1	1	0	1,5	0	0	0	1,5	0	0
531	20	5	2	1	0	1,5	1,5	2	0	0	0	0	1	0	0
541	10	5	2	2,5	1	1	2	2,5	0	0	0	0	0	0	0
551	10	5	2	2,5	0	1	2	3	0	0	0	0	0	0	0
561	8	5	2	2	0	0	2	3	0	0	0	0	1	0	0

Depth (cm)	Sand	Qz/Fp	Rock F	Mica	Basalt	Carbo-nate	H. mineral	M. nodule	PI forams	Np sin	Np dex	Benthic Forams	Ag Forams	Ostra-code	Sp spicule
571	14	5	2	1	0	0	2	2,5	0	0	0	0	0	0	0
579		5	2	0	0	1,5	1	2	0	0	0	0	1,5	0	0
591	8	5	2	0	0	0	1	3	0	0	0	1	0	0	0
599	15														
601	3	5	2	2	0	0	1	2,5	0	0	0	0	0	0	0
611	10	5	2	2	0	0	1	2,5	1	0	0	0	0	0	0
621	3	5	2	1	0	0	1	2	0	0	0	0	0	0	0
631	3	5	2	1	0	0	2	2	0	0	0	0	0	0	0
641	2	5	2	1	0	0	1	2	0	0	0	0	1	0	0
651	4	4	2	2	0	0	2	3,5	0	0	0	0	2	0	0
661	8	4,5	2	2	0	0	2	3	0	0	0	0	1	0	0
671	2	4	2	1	0	1	2	3,5	0	0	0	0	1,5	0	0
681	6	4	2	1	0	1	1,5	3	0	0	0	0	1	0	0
691	2	4	2	1	0	0	2	3	0	0	0	0	0	0	0
697	4	4,5	2	1	0	0	1	3	0	0	0	0	1	0	0

Tab. A5.3.2 Results of coarse fraction analysis of core PS87/030-1 KAL

Mid-depth (cm)	Sand	Qz/Fp	Rock F	Mica	Basalt	Carbo-nate	H. mineral	M. nodule	PI Forams	Np sin	Np dex	B Forams	Agg Forams	Ostra-code	Sp spicule
1	12	2,5	2	1	0	0	1	2	5	5	1	2,5	0	1	1,5
9	16	3	2	2	1	0	1	1	4,5	5	1	2	1	1	2,5
17	15	5	2,5	0	0	0	1	1	2	5	0	0	1	0	0
26	18	5	2,5	1	0	2	2	1	0	0	0	0	1	0	0
39	13	4	3	1	2	2	2,5	1	0	0	0	0	0	0	0
49	9	5	2,5	0	0	2	2	2	0	0	0	0	0	0	0
51	23	5	2	2	2	1	2,5	2,5	0	0	0	0	1	0	0
56	20	3,5	2	2	1	1	2,5	3,5	0	0	0	0	1	0	0
59	36	5	2	0	0	0	1	0	0	0	0	0	0	0	0
64	18	4	2	0	0	0	2	1	3,5	5	1	2,75	1	0	0
68	8	3	2	2	0	0	2	2	4,5	5	2	2,75	1	0	0
72	13	4	2	2	0	2,5	1	2	4	5	2	2	2	2	2
76	21	4,5	2	2	1	1	1	2,5	3	5	1	2	1	0	1
81	21	2,75	2	2	0	0	1	3	4	5	1	2	1	1	2
83	28	3	2	1	0	1	1	2	4,5	5	1	2	0	0	1
85	28	3	2	1	0	1	0	3	4	5	1	2,5	1	1	1
89	16	3	2	1	0	1	1	2,5	4	5	1	2	1	0	2
92	20	5	2	2	0	0	1	2,5	2,5	5	0	2	1,5	0	0
96	37	5	1	0	0	0	0	2	0	0	0	0	1	0	0
105	60	5	1	0	0	0	1	1	0	0	0	0	0	0	0
116	9	5	2,5	0	1	0	0	2,5	1	0	0	0	0	0	0
131	12	4	2,5	2	0	0	0	3	3	5	1	0	1	0	0
137	12	4	3	1	0	0	0	2	2,5	5	1	1	0	0	0
141	14	3	2	2,5	0	0	0	3	5	5	1	2,5	0	1	2
143	13	2,5	2	2	0	0	0	3	4,5	5	1	2	1	1	2
148	14	4,5	2,5	2	1	1	1	2,5	1	0	0	0	0	0	0
156	16	5	2	2	1	1	2	2	0	0	0	0	0	0	0
166	26	5	2	1	2	1	2	2	0	0	0	0	0	0	0
176	23	5	2	1	1	1	1	2	0	0	0	0	0	0	0

Mid-depth (cm)	Sand	Qz/Fp	Rock F	Mica	Basalt	Carbo-nate	H. mineral	M. nodule	PI Forams	Np sin	Np dex	B Forams	Agg Forams	Ostra-code	Sp spicule
186	12	5	2,5	1	0	1	1	2	1	0	0	1	0	0	0
196	25	3,5	2	2	0	0	1	2	2,75	5	0	3	0	0	1
198	14	3	2	2	0	0	1	3	4	5	1	4	0	1	2
204	3	4	2	2	0	2,75	1	3	3,5	5	1	2,5	0	2	2
210	7	2,75	2	1	0	2	1	4	4	5	1	2,5	1	2,5	1
217	8	3,5	2	2	0	2,5	1	4	4	5	1	2,75	1	2,75	1
220	10	4	2	1	0	2,75	1	4	2	0	0	1,5	1	1	0
226	4	5	2	1	0	1	2	3	0	0	0	0	0	0	0
231	6	4	2	2	0	0	1	3,5	3	5	1	2,75	1	2	0
235	8	4	2	2	1	2	1	3	3	5	1	2,75	1	1	2
243	8	4	2	2	0	0	0	3,75	2,75	5	1	2,5	0	1	1
245	8	4	2	2	0	2	0	4	3	4	2,5	2	0	0	1
251	10	4	2	2	0	1	2	4	2	0	0	2	0	0	0
258	7	4	2	2	0	2	2	3,5	2,5	3	2	1	0	0	0
265	6	4	2	2,5	0	2	1	3,5	2	0	0	2,5	2	1	0
268	5	5	2,5	2,5	0	1	2	3	0	0	0	2,75	2	0	0
272	8	4	2	2,5	0	2	1	4	0	0	0	2,5	0	1	1
279	8	4	2,5	2,5	0	0	2	3,5	0	0	0	2	2	1	1
286	6	5	2,5	2	0	0	2	3	0	0	0	0	0	0	0
296	7	5	2	2	0	0	1	2,5	0	0	0	1	0	0	1
303	5	4,5	2	1	0	1	1	3	0	0	0	0	0	0	0
311	5	5	2	2,5	1	0	2	3	0	0	0	1	2	0	0
315														0	0
317	2	5	2	1	1	0	2	2,5	0	0	0	1	0	0	0
320	5	4	2	2	0	2	1	3	0	0	0	3	2	1	0
323	8	4	2	2	1	1	2	3,5	0	0	0	2,75	2	0	0
327	8	4	2	2	0	0	2	3	0	0	0	2,75	2	0	0
333	5	4,5	2	2,5	0	0	2	3	1	0	0	2,5	1	0	0
341	14	5	2	2	0	0	2	2,5	0	0	0	0	1	0	0

Mid-depth depth (cm)	Sand	Qz/ Fp	Rock F	Mica	Basalt	Carbo- nate	H. mineral	M. nodule	PI Forams	Np sin	Np dex	B Forams	Agg Forams	Ostra- code	Sp spicule
348	5	4,5	2	2	0	0	2	3	0	0	0	0	2	0	0
355	4	5	2	2	0	0	2	2,5	1	0	1	1	2	0	0
366	18	5	1	0	0	0	0	2	0	0	0	0	2	0	0
371	6	4,5	2	2	0	1	2	3	1	0	0	0	0	0	0
383	16	5	2	0	0	2	2	1	1	0	0	0	0	0	0
396	4	5	2	2	0	1	2	2,5	1	0	0	0	2	0	1
405	2	5	2	2	0	1	2	2	1	0	0	0	0	0	0
413	3	5	2	2	0	0	2,5	2,75	2	0	0	1	2	0	0
421	3	5	2	2	0	0	2	2,5	1	0	1	1	1	0	0
427	4	5	2,5	2	0	2	2,5	2,5	2	0	0	0	1	0	0
438	5	5	2	2	0	1	2	2	1	0	0	0	1	0	0
449	7	5	2	2	0	1	2	2,5	1	0	0	0	2	0	0
458	4	5	2	2	0	1	2	2,5	0	0	0	0	1	0	0
468	5	5	2	2	1	1	2	2,5	1	0	0	0	2	0	0
477	5	5	2,5	2	0	1	2	2,5	0	0	0	0	1	0	0
489	6	5	2,5	2	1	1	2	3	0	0	0	0	1	0	0
500	12	5	2,5	1	2	2,5	2	3	0	0	0	0	1,5	0	0
511	5	5	2	2	1	1	2	2,5	0	0	0	0	1	0	0
521	5	5	2	2	1	0	0	2,75	0	0	0	0	1	0	0
537	3	5	2	2	1	1	2	2,75	1,5	0	0	0	2,5	0	0
547	4	4,5	2	1	1	0	2	3,5	0	0	0	0	0	0	0
555	4	5	2	2	1	1	2	3	0	0	0	0	1	0	0
564	3	5	2	2	1	0	2	2	0	0	0	0	0	0	0
577	3	5	2	2,5	1	1	1	2,5	0	0	0	0	2	0	0
584	3	5	2	2	1	0	2	3	0	0	0	0	2	0	0
592	3	5	2,5	2	1	0	2	2,75	0	0	0	0	2	0	0
597	3	4,5	2,5	2	1	0	2	3	0	0	0	0	2	0	0
607	3	5	2,5	2	1	2	2	2,5	0	0	0	0	2	0	0
613	2	5	2	2	1	0	2	2,75	0	0	0	0	1	0	0
622	2	5	2	2	0	0	2	2,5	0	0	0	0	1,5	0	0

Tab. A5.3.3 Results of coarse fraction analysis of core PS87/070-1 KAL

Depth (cm)	Sand	Qz/Fp	Rock F	Mica	Basalt	Carbo-nate	H. mineral	M. nodule	PI Forams	Np sin	Np dex/ subpol	Betn Forams	Aggl Forams	Ostracode	Sp Spicules
4	3	3	2	0	1	0	1	0	4	5	2	2,75	2,75	1	2,5
21	4	3	2	0	1	0	2	0	4	5	2	2,75	2,75	0	0
31	1	4,5	2	1	1	2,5	2	1	3	5	2	2,5	2	1,5	2
41	1	4,5	2,5	1	1	2,5	2	0	3	5	1	2	1	1	1
49	7	4,5	2	2,5	1	2	2	1	3	5	1	2	1	1,5	1,5
54	9	4,5	2	2,5	1	2	2	0	3	5	1	2	1	1	1,5
68	6	5	2,75	2	2	1	2,5	0	2,75	4,5	2,5	2	2	1	0
76	6	5	2,5	2	1	1	2,5	0	0	0	0	0	1	0	0
91	21	5	2,5	2	1	1	2	2	0	0	0	0	0	0	0
101	8	5	2	0	1	1	1	0	0	0	0	0	0	0	0
111	10	5	2	1	1	0	2	0	0	0	0	0	0	0	0
131	35	5	2	0	0	0	1	2,75	0	0	0	0	0	0	0
151	3	5	2	0	0	0	2	2,5	0	0	0	0	0	0	0
161	3	5	2	2	0	0	2,5	3,5	0	0	0	0	2	0	0
176	3	5	2	1	0	0	2	3	0	0	0	0	0	0	0
191	5	5	2	1	0	1	2	3,25	0	0	0	0	0	0	0
201	3	4	2	1	1	1	2	4	0	0	0	0	0	0	0
210	2	4	1	1	0	0	1	4,5	0	0	0	0	0	0	0
218	3	4,5	1	1	0	1	1	4	0	0	0	0	0	0	0
225	3	4,5	1	0	0	0	2	4	0	0	0	0	0	0	0
232	4	4,5	1	1	0	0	1,5	4	0	0	0	0	1	0	0
238	19	4,5	1	1	0	0	1,5	3	0	0	0	0	2	0	0
247	50	5	2	0	0	0	1	2	0	0	0	0	0	0	0
252	1	4,5	2	1	0	0	1	4,25	0	0	0	0	0	0	0
256	1	4	2	2	0	0	1	4	0	0	0	0	2	0	0
266	1	4	2	1	0	0	2	3	0	0	0	0	2,75	0	0
275	2	4,5	2	1	1	1	2	3	0	0	0	0	1,5	0	0
291	4	5	2	2	1	0	2	3	0	0	0	0	0	0	0

301	14	5	2	2,5	1	0	2	1	0	0	0	0	0	0	0	0	0	0	0
313	13	4,5	2	3	0	1	2	3	0	0	0	0	0	0	0	0	0	0	0
315	2	5	2,5	0	0	0	2	3	1	0	0	0	2,5	0	0	0	0	0	0
321		4	2	3	0	0	2	3,5	0	0	0	0	0	0	0	0	0	0	0
331	5	4	2	3	0	0	0	4	0	0	0	0	0	0	0	0	0	0	0
338	24	5	2	1	0	0	2	2	0	0	0	0	0	0	0	0	0	0	0
351	5	5	2	0	0	0	0	3	0	0	0	0	0	0	0	0	0	0	0
361	4	5	2	2	0	0	2	2	0	0	0	0	0	0	0	0	0	0	0
371	4	5	2	2	0	0	2	2,5	0	0	0	0	0	0	0	2,5	0	0	0
378	3	4,5	2	2	0	0	2	3	0	0	0	0	0	0	2,5	0	0	0	0
391	4	5	2,5	0	1	0	2	2	0	0	0	0	0	0	0	0	0	0	0
403	7	5	2,75	2	1	0	2,5	2,5	0	0	0	0	0	0	2	0	0	0	0
418	4	5	2,5	2	1	0	2,5	3	0	0	0	0	0	0	2	0	0	0	0
431	3	5	2,5	0	1	0	2,5	3	0	0	0	0	0	0	2,5	0	0	0	0
442	4	5	2,5	2,75	1	0	2	2,5	0	0	0	0	0	0	2,5	0	0	0	0
451	6	5	2,5	2,75	1	0	2,5	2	0	0	0	0	0	0	2,5	0	0	0	0
463	2	5	2,5	1	1	0	2,5	2,5	0	0	0	0	0	0	3	0	0	0	0
473	3	5	2,5	2	0	0	2	2	0	0	0	0	0	0	2	0	0	0	0
485	10	5	2	2,5	0	0	1	3	0	0	0	0	0	0	0	0	0	0	0
496	14	5	2	2	0	1	1	3	0	0	0	0	0	0	1	0	0	0	0
502	10	5	2,5	2,75	1	0	2,5	2,5	0	0	0	0	0	0	0	0	0	0	0
510	40	5	2	1	1	1	2	2	0	0	0	0	0	0	0	0	0	0	0
528	16	4,5	2	2	0	0	1	4	0	0	0	0	0	0	0	0	0	0	0
539	18	4	1	1	0	1	1	4	0	0	0	0	0	0	0	0	0	0	0
549	15	5	2	0	0	1	1	2	0	0	0	0	0	0	0	0	0	0	0
562	23	5	2	1	1	2	2	1	0	0	0	0	0	0	0	0	0	0	0
575	28	5	2	1	0	0	2	0	0	0	0	0	0	0	0	0	0	0	0
587	7	5	2,75	2,5	2	0	2,5	0	0	0	0	0	0	0	0	0	0	0	0
601	0,5	5	2,5	1	1	0	2	2,5	0	0	0	0	0	0	0	0	0	0	0
619	0,2	5	2,5	0	0	0	2	1	1	0	0	0	0	0	0	0	0	0	0
643	0,2	5	2,5	1	0	0	2	1	1	0	0	0	0	0	0	0	0	0	0
661	4	5	2,5	1	2	0	2	1	0	0	0	0	0	0	2	0	0	0	0

673	5	5	2,5	2,5	1	1	2	0	0	0	0	0	0	0	0	0	0	0	0
687	3	5	2	1	1	0	2	0	0	0	0	0	0	0	2,5	0	0	0	0
707	2	5	2,5	1	1	0	2	1	0	0	0	0	0	0	1	0	0	0	0
717	2	5	2	1	1	0	2	0	0	0	0	0	0	0	1,5	0	0	0	0
739	3	5	2,5	0	0	0	2	0	0	0	0	0	0	0	0	0	0	0	0
748	1	5	2,5	1	0	0	2	2,5	2	5	0	0	0	0	2	0	0	0	0
757,5	2	5	2	1	0	0	2	0	0	0	0	0	0	0	2	0	0	0	0

Tab. A5.3.4 Results of coarse fraction analysis of core PS87/079-1 KAL

Depth (cm)	Sand	Qz/Fp	Rock F	Mica	Basalt	Carbonate	H. mineral	M. nodule	PI Forams	Np sin	Np dex/subpol	Betn Forams	Aggl Forams	Ostracode	Sp Spicules
14,5	2	5	2,5	2	2	0	2,75	2	2	5	2	1	1,5	0	0
39	1	5	2,75	0	2	0	2,55	2	2	5	2	1,5	1	0	1
57	1	5	2,75	1	1	1	2,5	1	1	0	0	0	0	0	0
81	4	5	2	2	1	0	2	1	0	0	0	0	1	0	0
101	1	5	2,5	2	1	0	2	2	0	0	0	0	1	0	0
121,5	5	5	2,5	2,5	1	0	2	2,5	0	0	0	0	2,5	0	0
136	2	4,5	2,5	2	1	0	2,5	4	0	0	0	0	1	0	0
144	4	5	2,5	2	1	1	2,5	3	0	0	0	0	0	0	0
151	27	5	2,5	2	1,5	0	2	2	0	0	0	0	0	0	0
156	1,5	5	2,5	2	1	0	2	2,5	0	0	0	0	1	0	0
164	13	5	2	1	1	0	1	0	0	0	0	0	0	0	0
173	14	5	2	0	1	0	1	0	0	0	0	0	0	0	0
188	35	5	1,5	0	1	1	2	0	0	0	0	0	0	0	0
197	1	5	2,5	2	1	0	2	2,5	0	0	0	0	2	0	0
211	3	5	2,5	2	1	0	2	2	0	0	0	0	0	0	0
237	1,5	5	2,5	2	1	0	2	3	0	0	0	0	1,5	0	0
258	2	5	2,5	2	1	0	2	2,75	0	0	0	0	0	0	0
278	2	5	2,5	1	0	0	2	3	0	0	0	0	0	0	0
295	2	5	2	1	0	0	2	3	0	0	0	0	0	0	0
303	15	5	2	0	0	1	1	1	0	0	0	0	0	0	0
308	8	5	2	1	0	0	2	2	0	0	0	0	0	0	0
310	1	4	1	1	0	0	1	4	0	0	0	0	0	0	0
319	1,5	5	2,5	2,5	0	0	2	3	0	0	0	0	0	0	0
336	0,5	5	2	1	0	0	2	3	0	0	0	0	0	0	0
358	1,5	5	2,5	0	1	0	2	2,5	0	0	0	0	2	0	0
381	38	5	2,5	0	1	0	2	2,5	0	0	0	0	0	0	0
391	1	4	2,5	2	0	0	2	4	0	0	0	0	0	0	0
411	2	5	2,5	1	1	0	2	3	0	0	0	0	2,75	0	0
436	2	4	2	1	1	0	1	4	0	0	0	0	3	0	0

Depth (cm)	Sand	Qz/ Fp	Rock F	Mica	Basalt	Carbo- nate	H. mineral	M. nodule	PI Forams	Np sin	Np dex/ subpol	Betn Forams	Aggl Forams	Ostracode	Sp Spicules
454	12	4	2	2,5	1	0	1	4	0	0	0	0	2	0	0
462	22	5	2,5	2,5	1	0	2	3	0	0	0	0	0	0	0
469	18	5	2	2	1	0	2	3,5	0	0	0	0	2	0	0
487	11	4,5	2	2	1	0	2	4	0	0	0	0	1	0	0
504	1,5	5	2	1	1	0	2	2,5	0	0	0	0	0	0	0
513	1	5	2,5	2	1	0	1	2,5	0	0	0	0	0	0	0
541	4	5	2	2,5	0	0	2	3	0	0	0	0	0	0	0
556	2	5	2,5	1	2	0	2,5	0	1,5	0	0	0	1	0	0
573	2	5	2	2	2	0	2,5	1	0	0	0	0	0	0	0
618	3	5	2,75	2	2	0	2,5	2	0	0	0	0	2	0	0
636	2	4,5	2,75	2,75	2	0	2	3,5	0	0	0	0	2	0	0
651	2	5	2,5	2	2	0	2	1	0	0	0	0	0	0	0

A5.4 Tables with data of dropstone analyses

(E. Bazhenova)

Tab. A5.4.1: Occurrence, size (A largest, B medium, C smallest axes), classification, and composition of dropstones >1 cm in Core PS87/003-1.

N	Stone ID	Station	Size, cm			Classification after Friedman & Sanders	Composition
			A	B	C		
1	B1	PS87/003-1	9,5	4,8	3,3	small cobbles	undetermined
2	B2	PS87/003-1	6,1	4,1	2,3	very coarse pebbles	quartzite
3	B10	PS87/003-1	3,6	2,6	2	very coarse pebbles	sandstone
4	B11	PS87/003-1	3,3	2,7	1,3	very coarse pebbles	gneiss
5	B12	PS87/003-1	5,3	3,7	1,8	very coarse pebbles	shale
6	B13	PS87/003-1	3,9	3,1	2,9	very coarse pebbles	sandstone
7	B14	PS87/003-1	5,1	2,7	0,5	very coarse pebbles	sandstone
8	B15	PS87/003-1	3,9	3,1	1,8	very coarse pebbles	sandstone
9	B16	PS87/003-1	3,8	2,9	1,4	very coarse pebbles	undetermined
10	B17	PS87/003-1	2,7	2,2	1,2	coarse pebbles	shale
11	B18	PS87/003-1	3,3	2,4	1,6	very coarse pebbles	undetermined
12	B19	PS87/003-1	4,2	2,7	1,6	very coarse pebbles	limestone
13	B20	PS87/003-1	2,9	2,2	1,1	coarse pebbles	sandstone
14	B21	PS87/003-1	5,1	3,3	0,5	very coarse pebbles	shale
15	B22	PS87/003-1	4,5	2,1	1,7	very coarse pebbles	undetermined
16	B23	PS87/003-1	2,8	2,6	0,8	coarse pebbles	sandstone
17	B24	PS87/003-1	3	2,4	1,8	coarse pebbles	gneiss
18	B25	PS87/003-1	3,4	1,9	1,4	very coarse pebbles	undetermined
19	B26	PS87/003-1	3,8	2,5	1,6	very coarse pebbles	undetermined
20	B27	PS87/003-1	3,8	2	1,6	very coarse pebbles	undetermined
21	B28	PS87/003-1	2,9	1,8	0,9	coarse pebbles	shale
22	B29	PS87/003-1	2,3	2	1,1	coarse pebbles	quartzite
23	B3	PS87/003-1	5	3,3	2,8	very coarse pebbles	sandstone
24	B30	PS87/003-1	2,6	2	0,3	coarse pebbles	sandstone
25	B31	PS87/003-1	3,9	1,7	0,8	very coarse pebbles	limestone
26	B32	PS87/003-1	2,8	1,7	0,7	coarse pebbles	shale
27	B33	PS87/003-1	4,5	1,5	1,2	very coarse pebbles	quartzite
28	B34	PS87/003-1	2,6	2,2	1,3	coarse pebbles	sandstone carb.
29	B35	PS87/003-1	3	1,3	1,2	coarse pebbles	gneiss
30	B36	PS87/003-1	2,5	2	1,8	coarse pebbles	quartzite
31	B37	PS87/003-1	2,6	2	1,1	coarse pebbles	granitoid
32	B38	PS87/003-1	2,7	1,8	0,9	coarse pebbles	sandstone carb.
33	B39	PS87/003-1	2,8	2	1,8	coarse pebbles	sandstone
34	B4	PS87/003-1	4,8	3,1	2,8	very coarse pebbles	granite
35	B40	PS87/003-1	2,9	1,9	0,7	coarse pebbles	shale
36	B41	PS87/003-1	2,7	1,9	1,2	coarse pebbles	undetermined
37	B42	PS87/003-1	2,1	1,6	1,2	coarse pebbles	diorite
38	B43	PS87/003-1	2,3	2	1,2	coarse pebbles	sandstone
39	B44	PS87/003-1	2,3	1,8	1,5	coarse pebbles	flintstone
40	B45	PS87/003-1	2,7	1,9	0,5	coarse pebbles	sandstone
41	B46	PS87/003-1	2,4	2,2	1,7	coarse pebbles	sandstone
42	B47	PS87/003-1	3	2,5	1,4	coarse pebbles	sandstone
43	B48	PS87/003-1	2,6	1,8	1,7	coarse pebbles	undetermined

44	B49	PS87/003-1	3	2,1	0,9	coarse pebbles	shale
45	B5	PS87/003-1	5,3	3,1	1,9	very coarse pebbles	granite
46	B50	PS87/003-1	2,4	1,3	0,7	coarse pebbles	gneiss
47	B51	PS87/003-1	2,7	1,9	1	coarse pebbles	shale
48	B52	PS87/003-1	2,5	1,8	1,4	coarse pebbles	sandstone
49	B53	PS87/003-1	2,5	2,2	1,2	coarse pebbles	sandstone carb.
50	B54	PS87/003-1	2,8	1,8	1,6	coarse pebbles	quartzite
51	B55	PS87/003-1	2,7	1,5	1	coarse pebbles	gneiss
52	B56	PS87/003-1	2,2	1,9	1,7	coarse pebbles	quartzite
53	B57	PS87/003-1	2,8	1,7	1,3	coarse pebbles	shale
54	B58	PS87/003-1	2,6	1,7	0,8	coarse pebbles	granitoid
55	B59	PS87/003-1	2,5	1,5	1,2	coarse pebbles	quartzite
56	B6	PS87/003-1	5,7	3,5	2,9	very coarse pebbles	sandstone
57	B60	PS87/003-1	2,3	1,7	0,7	coarse pebbles	gneiss
58	B61	PS87/003-1	2,2	2	1,9	coarse pebbles	dolomite
59	B62	PS87/003-1	2,6	1,6	1,3	coarse pebbles	sandstone
60	B63	PS87/003-1	2,4	1,5	1,2	coarse pebbles	undetermined
61	B64	PS87/003-1	2,1	1,8	0,9	coarse pebbles	conglomerate carb.
62	B65	PS87/003-1	2,4	1,5	1	coarse pebbles	undetermined
63	B66	PS87/003-1	2	1,2	1,1	coarse pebbles	quartz
64	B67	PS87/003-1	2,1	1,8	1,4	coarse pebbles	sandstone carb.
65	B68	PS87/003-1	2,9	1,4	1	coarse pebbles	shale
66	B69	PS87/003-1	2,7	1,4	0,3	coarse pebbles	undetermined
67	B7	PS87/003-1	4,2	3,6	2,8	very coarse pebbles	limestone
68	B70	PS87/003-1	2,5	1,5	1,1	coarse pebbles	shale with Qu layers
69	B71	PS87/003-1	1,9	1,5	1,1	coarse pebbles	quartzite
70	B72	PS87/003-1	2,6	1,5	0,7	coarse pebbles	shale
71	B73	PS87/003-1	2,3	2	1,1	coarse pebbles	granitoid
72	B74	PS87/003-1	2,3	1,6	0,7	coarse pebbles	shale
73	B75	PS87/003-1	2,3	2,2	1,7	coarse pebbles	undetermined
74	B76	PS87/003-1	2	1,3	0,6	coarse pebbles	undetermined
75	B77	PS87/003-1	2,1	1,6	0,6	coarse pebbles	sandstone carb.
76	B8	PS87/003-1	4,2	3,4	1,9	very coarse pebbles	sandstone
77	B9	PS87/003-1	5	3,2	1,6	very coarse pebbles	shale

Tab. A5.4.2: Occurrence, size (A largest, B medium, C smallest axes), classification, and composition of dropstones >1 cm in Core PS87/023-2.

N	Stone ID	Station	Size, cm			Classification after Friedman & Sanders	Composition
			A	B	C		
1	B-78	PS87/023-2	5,5	5,3	3,6	very coarse pebbles	sandstone carb.
2	B-79	PS87/023-2	5,3	5,2	2,3	very coarse pebbles	sandstone carb.
3	B-80	PS87/023-2	4,3	2,9	1,9	very coarse pebbles	quartzite
4	B-81	PS87/023-2	2,8	2,4	1,6	coarse pebbles	quartzite
5	B-82	PS87/023-2	4,8	3,5	1,1	very coarse pebbles	sandstone carb.
6	B-83	PS87/023-2	12,7	12	6,5	small cobbles	sandstone carb.
7	B-84	PS87/023-2	9	7,5	6	small cobbles	quartzite
8	B-85	PS87/023-2	3	2,6	1,6	coarse pebbles	quartzite
9	B-86	PS87/023-2	2,9	2,6	1,6	coarse pebbles	quartzite
10	B-87	PS87/023-2	2,4	1,9	0,7	coarse pebbles	dolomite
11	B-88	PS87/023-2	1,9	1,1	0,8	coarse pebbles	
12	B-89	PS87/023-2	2,7	1,7	0,9	coarse pebbles	sandstone carb.
13	B-90	PS87/023-2	3	2,3	1,8	coarse pebbles	dolomite
14	B-91	PS87/023-2	2,9	2,3	1,2	coarse pebbles	quartzite
15	B-92	PS87/023-2	2,7	2	1,5	coarse pebbles	sandstone met.
16	B-93	PS87/023-2	2,4	1,2	1,2	coarse pebbles	
17	B-94	PS87/023-2	2,9	2,4	1,5	coarse pebbles	quartzite
18	B-95	PS87/023-2	1,7	1,6	1,4	coarse pebbles	quartzite
19	B-96	PS87/023-2	2	1,8	0,9	coarse pebbles	shale
20	B-97	PS87/023-2	2,2	1,6	0,7	coarse pebbles	dolomite
21	B-98	PS87/023-2	2,1	1,6	0,9	coarse pebbles	sandstone carb.
22	B-99	PS87/023-2	2,2	1,7	0,7	coarse pebbles	
23	B-100	PS87/023-2	1,8	1,4	0,8	coarse pebbles	
24	B-101	PS87/023-2	1,8	1,2	1	coarse pebbles	
25	B-102	PS87/023-2	1,7	1,4	0,9	coarse pebbles	
26	B-103	PS87/023-2	2,2	1,5	0,4	coarse pebbles	
27	B-104	PS87/023-2	2,2	1,7	1,2	coarse pebbles	sandstone carb.
28	B-105	PS87/023-2	3	1,4	1,3	coarse pebbles	limestone
29	B-106	PS87/023-2	2	1,7	1,2	coarse pebbles	quartzite
30	B-107	PS87/023-2	2,1	1,9	0,6	coarse pebbles	
31	B-108	PS87/023-2	1,9	1,5	0,9	coarse pebbles	
32	B-109	PS87/023-2	2,3	1,5	0,9	coarse pebbles	
33	B-110	PS87/023-2	2,1	1,1	1	coarse pebbles	volcanic
34	B-111	PS87/023-2	2,1	0,9	0,6	coarse pebbles	
35	B-112	PS87/023-2	2,1	1,3	0,7	coarse pebbles	
36	B-113	PS87/023-2	1,8	1,2	1,2	coarse pebbles	
37	B-114	PS87/023-2	2,1	1,1	0,7	coarse pebbles	
38	B-115	PS87/023-2	2,4	1,8	1,3	coarse pebbles	limestone
39	B-116	PS87/023-2	2,4	1,5	1,2	coarse pebbles	sandstone met.
40	B-117	PS87/023-2	1,9	0,9	0,8	coarse pebbles	
41	B-118	PS87/023-2	2,2	1,7	0,6	coarse pebbles	
42	B-119	PS87/023-2	2,6	1,2	1,1	coarse pebbles	limestone
43	B-120	PS87/023-2	2,5	1,5	1,1	coarse pebbles	
44	B-121	PS87/023-2	1,9	1,8	0,7	coarse pebbles	

45	B-122	PS87/023-2	2,1	0,9	0,6	coarse pebbles	
46	B-123	PS87/023-2	2,2	1,3	0,4	coarse pebbles	
47	B-124	PS87/023-2	1,6	1,2	0,4	medium pebbles	
48	B-125	PS87/023-2	2,2	1,9	0,9	coarse pebbles	
49	B-126	PS87/023-2	2,4	1,4	0,9	coarse pebbles	quartzite
50	B-127	PS87/023-2	2,4	1,4	0,7	coarse pebbles	
51	B-128	PS87/023-2	2	1,6	1,1	coarse pebbles	
52	B-129	PS87/023-2	2,1	1,3	0,4	coarse pebbles	
53	B-130	PS87/023-2	2,3	1,5	1	coarse pebbles	sandstone met.
54	B-131	PS87/023-2	2,4	1,6	1,2	coarse pebbles	
55	B-132	PS87/023-2	2,2	1	0,7	coarse pebbles	
56	B-133	PS87/023-2	1,9	1,2	0,7	coarse pebbles	
57	B-134	PS87/023-2	2,3	1,4	0,8	coarse pebbles	
58	B-135	PS87/023-2	2,1	1,7	0,6	coarse pebbles	
59	B-136	PS87/023-2	2	1	0,9	coarse pebbles	
60	B-137	PS87/023-2	4,1	3,2	2,4	very coarse pebbles	
61	B-138	PS87/023-2	3,1	1,9	0,9	coarse pebbles	
62	B-139	PS87/023-2	1,9	1,1	0,4	coarse pebbles	
63	B-140	PS87/023-2	2,3	1,3	1,1	coarse pebbles	
64	B-141	PS87/023-2	1,6	1,4	0,4	medium pebbles	
65	B-142	PS87/023-2	1,5	1,3	0,6	medium pebbles	
66	B-143	PS87/023-2	1,7	1,3	0,7	coarse pebbles	
67	B-144	PS87/023-2	1,8	1,3	1	coarse pebbles	
68	B-145	PS87/023-2	1,7	1,1	0,5	coarse pebbles	
69	B-146	PS87/023-2	1,7	1,2	0,8	coarse pebbles	
70	B-147	PS87/023-2	1,6	1	0,6	medium pebbles	
71	B-148	PS87/023-2	2	1,1	0,6	coarse pebbles	
72	B-149	PS87/023-2	1,4	1,3	0,9	medium pebbles	
73	B-150	PS87/023-2	1,6	1,1	1	medium pebbles	
74	B-151	PS87/023-2	1,6	1,1	0,7	medium pebbles	
75	B-152	PS87/023-2	1,6	1	0,8	medium pebbles	
76	B-153	PS87/023-2	1,7	1,3	0,6	coarse pebbles	
77	B-154	PS87/023-2	2,1	1,4	0,2	coarse pebbles	
78	B-155	PS87/023-2	1,9	0,8	0,8	coarse pebbles	
79	B-156	PS87/023-2	2	0,9	0,3	coarse pebbles	
80	B-157	PS87/023-2	1,9	1,1	0,6	coarse pebbles	
81	B-158	PS87/023-2	2,2	1,3	0,5	coarse pebbles	
82	B-159	PS87/023-2	1,7	1,1	0,5	coarse pebbles	
83	B-160	PS87/023-2	1,8	1,1	0,3	coarse pebbles	
84	B-161	PS87/023-2	1,7	0,9	0,5	coarse pebbles	
85	B-162	PS87/023-2	1,7	1,1	0,2	coarse pebbles	
86	B-163	PS87/023-2	1,6	1	0,5	medium pebbles	
87	B-164	PS87/023-2	1,8	1,1	0,9	coarse pebbles	
88	B-165	PS87/023-2	1,3	1	0,8	medium pebbles	
89	B-166	PS87/023-2	1,7	0,8	0,5	coarse pebbles	
90	B-167	PS87/023-2	1,4	1,3	0,5	medium pebbles	
91	B-168	PS87/023-2	1,6	1	0,9	medium pebbles	
92	B-169	PS87/023-2	1,4	1,3	1	medium pebbles	

PS87 (ARK-XXVIII/4)

93	B-170	PS87/023-2	1,4	1,1	0,7	medium pebbles	
94	B-171	PS87/023-2	1,5	1,2	0,1	medium pebbles	
95	B-172	PS87/023-2	1,1	0,8	0,7	medium pebbles	calcite
96	B-173	PS87/023-2	1,6	1,1	0,6	medium pebbles	
97	B-174	PS87/023-2	1,8	1,3	0,6	coarse pebbles	
98	B-175	PS87/023-2	1,5	1,2	1	medium pebbles	
99	B-176	PS87/023-2	1,4	1,1	1,1	medium pebbles	
100	B-177	PS87/023-2	1,4	1,1	0,7	medium pebbles	
101	B-178	PS87/023-2	1,6	1,2	0,7	medium pebbles	

Tab. A5.4.3. Occurrence, size (A largest, B medium, C smallest axes), classification, and composition of dropstones >1 cm in Core PS87/026-1.

N	Stone ID	Station	Size, cm			Classification after Friedman & Sanders	Composition
			A	B	C		
1	B-179	PS87/026-1	4,1	3,7	1,9	very coarse pebbles	sandstone carb
2	B-180	PS87/026-1	5,3	4,1	1,4	very coarse pebbles	sandstone
3	B-181	PS87/026-1	2,5	2,1	1,5	coarse pebbles	quartzite
4	B-182	PS87/026-1	1,9	1,9	0,9	coarse pebbles	quartzite
5	B-183	PS87/026-1	2,3	0,7	0,6	coarse pebbles	sandstone
6	B-184	PS87/026-1	2,2	1,8	0,4	coarse pebbles	sandstone
7	B-185	PS87/026-1	2,1	1,9	0,7	coarse pebbles	sandstone carb
8	B-186	PS87/026-1	2,5	1,4	0,4	coarse pebbles	sandstone
9	B-187	PS87/026-1	1,8	1,6	0,3	coarse pebbles	sandstone carb
10	B-188	PS87/026-1	1,6	1	0,7	medium pebbles	sandstone carb
11	B-189	PS87/026-1	1,8	0,6	0,6	coarse pebbles	sandstone met.
12	B-190	PS87/026-1	1,7	0,9	0,9	coarse pebbles	quartzite
13	B-191	PS87/026-1	1,7	1,1	0,6	coarse pebbles	sandstone

Tab. A5.4.4. Occurrence, size (A largest, B medium, C smallest axes), classification, and composition of dropstones >1 cm in Core PS87/029-1.

N	Stone ID	Station	Size, cm			Classification after Friedman & Sanders	Composition
			A	B	C		
1	B-192	PS87/029-1	4,3	1,6	1	very coarse pebbles	undetermined
2	B-193	PS87/029-1	6,4	5,9	3,7	very coarse pebbles	gneiss
3	B-194	PS87/029-1	4,4	3,4	1,8	very coarse pebbles	sandstone met.
4	B-195	PS87/029-1	3,3	2,2	0,5	very coarse pebbles	sandstone carb.
5	B-196	PS87/029-1	3,2	2,7	1,4	coarse pebbles	sandstone carb.
6	B-197	PS87/029-1	2,9	2,6	0,8	coarse pebbles	sandstone met.
7	B-198	PS87/029-1	2,4	1,9	1,8	coarse pebbles	sandstone met.
8	B-199	PS87/029-1	2,5	1,5	1,1	coarse pebbles	sandstone carb.
9	B-200	PS87/029-1	1,7	1,3	0,6	coarse pebbles	sandstone carb.
10	B-201	PS87/029-1	2,7	1,2	0,7	coarse pebbles	sandstone carb.
11	B-202	PS87/029-1	1,5	1,2	0,6	medium pebbles	sandstone carb.
12	B-203	PS87/029-1	1,9	1,3	1,2	coarse pebbles	shale
13	B-204	PS87/029-1	2	1,3	0,6	coarse pebbles	sandstone carb.
14	B-205	PS87/029-1	1,6	1,3	0,9	medium pebbles	quartzite
15	B-206	PS87/029-1	1,6	1,1	0,5	medium pebbles	sandstone met.
16	B-207	PS87/029-1	1,7	1	0,8	coarse pebbles	sandstone
17	B-208	PS87/029-1	1,5	1,3	0,9	medium pebbles	quartzite
18	B-209	PS87/029-1	1,6	1,4	0,8	medium pebbles	dolomite
19	B-210	PS87/029-1	2	1	0,8	coarse pebbles	quartzite
20	B-211	PS87/029-1	1,8	1,1	0,7	coarse pebbles	shale
21	B-212	PS87/029-1	1,4	1,2	0,5	medium pebbles	sandstone
22	B-213	PS87/029-1	1,8	1,2	0,8	coarse pebbles	sandstone met.
23	B-214	PS87/029-1	1,5	1,3	1,3	medium pebbles	quartzite
24	B-215	PS87/029-1	1,2	0,9	0,7	medium pebbles	sandstone carb.
25	B-216	PS87/029-1	1,6	1,1	0,6	medium pebbles	dolomite
26	B-217	PS87/029-1	1,5	1,4	0,9	medium pebbles	sandstone met.
27	B-218	PS87/029-1	1,6	1,4	1,2	medium pebbles	quartzite

Tab. A5.4.5: Occurrence, size (A largest, B medium, C smallest axes), classification, and composition of dropstones >1 cm in Core PS87/030-2.

N	Stone ID	Station	Size, cm			Classification after Friedman & Sanders	Composition
			A	B	C		
1	B-219	PS87/030-2	3,1	2,2	1,5	coarse pebbles	quartzite
2	B-220	PS87/030-2	3,1	2,2	1,7	coarse pebbles	undetermined
3	B-221	PS87/030-2	2,3	1,9	1,3	coarse pebbles	sandstone met.
4	B-222	PS87/030-2	2,4	1,3	1,3	coarse pebbles	sandstone met.
5	B-223	PS87/030-2	1,8	1,6	1,1	coarse pebbles	undetermined
6	B-224	PS87/030-2	2	1,6	1,1	coarse pebbles	sandstone met.
7	B-225	PS87/030-2	1,8	1	0,6	coarse pebbles	sandstone met.
8	B-226	PS87/030-2	1,9	1,2	1	coarse pebbles	sandstone met.
9	B-227	PS87/030-2	1,9	1,3	0,9	coarse pebbles	sandstone met.
10	B-228	PS87/030-2	2,1	1,1	0,7	coarse pebbles	
11	B-229	PS87/030-2	1,6	1,2	0,5	medium pebbles	
12	B-230	PS87/030-2	1,7	1,3	0,9	coarse pebbles	
13	B-231	PS87/030-2	2,3	1,7	0,9	coarse pebbles	
14	B-232	PS87/030-2	1,6	1,6	0,7	medium pebbles	
15	B-233	PS87/030-2	2,2	1,4	1,1	coarse pebbles	quartzite
16	B-234	PS87/030-2	1,5	1,3	0,6	medium pebbles	
17	B-235	PS87/030-2	1,7	1,3	0,7	coarse pebbles	
18	B-236	PS87/030-2	1,8	1,2	0,5	coarse pebbles	sandstone met.
19	B-237	PS87/030-2	1,8	1,4	0,5	coarse pebbles	quartzite
20	B-238	PS87/030-2	1,9	1,9	0,9	coarse pebbles	undetermined
21	B-239	PS87/030-2	2	1,5	0,7	coarse pebbles	undetermined
22	B-240	PS87/030-2	2,2	1,3	0,8	coarse pebbles	quartzite
23	B-241	PS87/030-2	2,2	1,4	0,9	coarse pebbles	sandstone met.
24	B-242	PS87/030-2	1,8	0,9	0,7	coarse pebbles	shale
25	B-243	PS87/030-2	1,8	1	0,8	coarse pebbles	
26	B-244	PS87/030-2	1,7	1,1	1,1	coarse pebbles	sandstone
27	B-245	PS87/030-2	1,4	1,1	0,8	medium pebbles	
28	B-246	PS87/030-2	2,1	1,1	0,6	coarse pebbles	sandstone met.
29	B-247	PS87/030-2	1,7	1,5	0,7	coarse pebbles	
30	B-248	PS87/030-2	1,8	1,1	0,6	coarse pebbles	
31	B-249	PS87/030-2	1,6	1,2	0,8	medium pebbles	
32	B-250	PS87/030-2	1,5	1,3	0,7	medium pebbles	
33	B-251	PS87/030-2	1,3	1	0,8	medium pebbles	
34	B-252	PS87/030-2	1,9	1,1	0,5	coarse pebbles	
35	B-253	PS87/030-2	1,6	1,5	1,1	medium pebbles	
36	B-254	PS87/030-2	1,9	1,4	0,7	coarse pebbles	
37	B-255	PS87/030-2	1,8	1,2	1	coarse pebbles	undetermined
38	B-256	PS87/030-2	1,6	0,9	0,7	medium pebbles	
39	B-257	PS87/030-2	1,2	0,8	0,5	medium pebbles	
40	B-258	PS87/030-2	1,3	1,3	0,5	medium pebbles	
41	B-259	PS87/030-2	1,5	1	0,9	medium pebbles	
42	B-260	PS87/030-2	1,6	1,2	1,1	medium pebbles	
43	B-261	PS87/030-2	1,4	1	0,9	medium pebbles	
44	B-262	PS87/030-2	1,5	0,9	0,5	medium pebbles	

PS87 (ARK-XXVIII/4)

45	B-263	PS87/030-2	1,5	1,1	0,8	medium pebbles	
46	B-264	PS87/030-2	1,5	1,2	0,7	medium pebbles	
47	B-265	PS87/030-2	1,2	0,9	0,5	medium pebbles	
48	B-266	PS87/030-2	1,2	1	0,8	medium pebbles	
49	B-267	PS87/030-2	1,2	1,2	1,1	medium pebbles	
50	B-268	PS87/030-2	1,6	1	0,2	medium pebbles	
51	B-269	PS87/030-2	1,5	1,3	0,5	medium pebbles	
52	B-270	PS87/030-2	1,4	1	0,9	medium pebbles	
53	B-271	PS87/030-2	1,3	1,1	0,6	medium pebbles	
54	B-272	PS87/030-2	1,4	1,3	0,9	medium pebbles	
55	B-273	PS87/030-2	1,4	0,9	0,8	medium pebbles	
56	B-274	PS87/030-2	1,2	0,9	0,9	medium pebbles	
57	B-275	PS87/030-2	1,5	0,9	0,8	medium pebbles	
58	B-276	PS87/030-2	1,5	1,3	0,7	medium pebbles	
59	B-452	PS87/030-2	5,5	3,2	3	very coarse pebbles	
60	B-453	PS87/030-2	3,1	2,7	1,2	coarse pebbles	
61	B-454	PS87/030-2	2,3	1,7	1,5	coarse pebbles	
62	B-455	PS87/030-2	1,9	1,8	1,2	coarse pebbles	

Tab. A5.4.6. Occurrence, size (A largest, B medium, C smallest axes), classification, and composition of dropstones >1 cm in Core PS87/040-2.

N	Stone ID	Station	Size, cm			Classification after Friedman & Sanders	Composition
			A	B	C		
1	B-277	PS87/040-2	4,5	3,6	1,1	very coarse pebbles	quarzite
2	B-278	PS87/040-2	2,9	2,3	1,2	coarse pebbles	sandstone
3	B-279	PS87/040-2	3,2	2,4	1,3	coarse pebbles	sandstone
4	B-280	PS87/040-2	3,1	1,7	1,4	coarse pebbles	sandstone
5	B-281	PS87/040-2	2,9	2,4	1,6	coarse pebbles	quarzite
6	B-282	PS87/040-2	3,7	2,1	1,2	coarse pebbles	sandstone carb.
7	B-283	PS87/040-2	3,7	1,1	1	coarse pebbles	sandstone met.
8	B-284	PS87/040-2	2,8	2	1,3	coarse pebbles	sandstone carb.
9	B-285	PS87/040-2	2,9	1,4	0,6	coarse pebbles	sandstone met.
10	B-286	PS87/040-2	2,3	2	1,4	coarse pebbles	sandstone met.
11	B-287	PS87/040-2	2,5	1,4	1,2	coarse pebbles	quarzite+Qu vein
12	B-288	PS87/040-2	2,5	1,1	0,6	coarse pebbles	shale
13	B-289	PS87/040-2	2,1	1,5	0,6	coarse pebbles	shale
14	B-290	PS87/040-2	2,1	1,7	0,9	coarse pebbles	sandstone
15	B-291	PS87/040-2	1,9	1,3	0,6	coarse pebbles	sandstone
16	B-292	PS87/040-2	2,1	1,8	1,1	coarse pebbles	sandstone
17	B-293	PS87/040-2	2,6	1,4	0,8	coarse pebbles	quarzite
18	B-294	PS87/040-2	2,8	1,3	0,1	coarse pebbles	sandstone
19	B-295	PS87/040-2	2,2	1,8	0,9	coarse pebbles	shale
20	B-296	PS87/040-2	1,9	1,1	0,5	coarse pebbles	sandstone
21	B-297	PS87/040-2	2	1,6	0,9	coarse pebbles	sandstone
22	B-298	PS87/040-2	2	1,2	0,6	coarse pebbles	sandstone
23	B-299	PS87/040-2	2	1,6	0,7	coarse pebbles	tuff
24	B-300	PS87/040-2	1,9	1,3	0,5	coarse pebbles	sandstone
25	B-301	PS87/040-2	2,1	1,8	0,9	coarse pebbles	sandstone
26	B-302	PS87/040-2	1,8	1,5	1	coarse pebbles	dolomite
27	B-303	PS87/040-2	2	1,6	1,1	coarse pebbles	quarzite
28	B-304	PS87/040-2	1,5	1,1	0,9	medium pebbles	sandstone
29	B-305	PS87/040-2	1,9	1,2	0,8	coarse pebbles	sandstone met.
30	B-306	PS87/040-2	1,8	1,4	0,7	coarse pebbles	gneiss
31	B-307	PS87/040-2	1,5	1	0,5	medium pebbles	quarzite
32	B-308	PS87/040-2	1,6	1,3	0,8	medium pebbles	Qu vein
33	B-309	PS87/040-2	1,7	1	0,2	coarse pebbles	sandstone met.
34	B-310	PS87/040-2	1,6	1	0,4	medium pebbles	sandstone met.
35	B-311	PS87/040-2	1,8	0,9	0,9	coarse pebbles	undetermined
36	B-312	PS87/040-2	1,6	0,8	0,7	medium pebbles	sandstone

Tab. A5.4.7. Occurrence, size (A largest, B medium, C smallest axes), classification, and composition of dropstones >1 cm in Core PS87/055-1.

N	Stone ID	Station	Size, cm			Classification after Friedman & Sanders	Composition
			A	B	C		
1	B-313	PS87/055-1	10	5,2	4,6	small cobbles	sandstone
2	B-314	PS87/055-1	2,4	1,7	1,5	coarse pebbles	sandstone
3	B-315	PS87/055-1	2,5	1,7	1,6	coarse pebbles	sandstone
4	B-316	PS87/055-1	2,6	1,6	0,7	coarse pebbles	sandstone
5	B-317	PS87/055-1	2,4	1,4	1,3	coarse pebbles	quartzite
6	B-318	PS87/055-1	1,4	1,3	1,1	medium pebbles	quartzite+Qu vein
7	B-319	PS87/055-1	1,9	1,1	0,7	coarse pebbles	undetermined
8	B-320	PS87/055-1	1,5	1,3	1	medium pebbles	sandstone met.
9	B-321	PS87/055-1	1,5	1,3	0,9	medium pebbles	sandstone met.
10	B-322	PS87/055-1	1,6	1,3	0,8	medium pebbles	shale
11	B-323	PS87/055-1	1,4	0,8	0,6	medium pebbles	sandstone
12	B-324	PS87/055-1	1,9	1,3	0,9	coarse pebbles	sandstone met.
13	B-325	PS87/055-1	1,3	1,1	0,5	medium pebbles	quartzite
14	B-326	PS87/055-1	1,6	0,9	0,5	medium pebbles	sandstone
15	B-327	PS87/055-1	1,6	0,9	0,6	medium pebbles	sandstone
16	B-328	PS87/055-1	1,4	1	0,5	medium pebbles	quartzite
17	B-329	PS87/055-1	1,1	0,6	0,6	medium pebbles	quartz

Tab. A5.4.8. Occurrence, size (A largest, B medium, C smallest axes), classification, and composition of dropstones >1 cm in Core PS87/056-1.

N	Stone ID	Station	Size, cm			Classification after Friedman & Sanders	Composition
			A	B	C		
1	B-330	PS87/056-1	4,1	3,6	1,6	very coarse pebbles	quartzite
2	B-331	PS87/056-1	3,5	3,2	1,9	very coarse pebbles	sandstone
3	B-332	PS87/056-1	5,3	3,4	1,1	very coarse pebbles	undetermined
4	B-333	PS87/056-1	2,4	2,2	1,1	coarse pebbles	sandstone
5	B-334	PS87/056-1	2,9	2,3	1,2	coarse pebbles	sandstone
6	B-335	PS87/056-1	2,4	1,3	1	coarse pebbles	sandstone
7	B-336	PS87/056-1	2,3	1,9	0,9	coarse pebbles	sandstone
8	B-337	PS87/056-1	2,1	1,7	1,1	coarse pebbles	quartzite
9	B-338	PS87/056-1	1,9	1,5	1	coarse pebbles	undetermined
10	B-339	PS87/056-1	1,4	1,4	0,8	medium pebbles	sandstone
11	B-340	PS87/056-1	1,4	1,3	1	medium pebbles	quartzite
12	B-341	PS87/056-1	1,6	1,3	0,8	medium pebbles	sandstone
13	B-342	PS87/056-1	1,6	1,1	0,9	medium pebbles	sandstone met.
14	B-343	PS87/056-1	1,6	1,4	1,1	medium pebbles	sandstone met.
15	B-344	PS87/056-1	1,5	1,4	0,7	medium pebbles	sandstone
16	B-345	PS87/056-1	1,6	1,1	0,8	medium pebbles	dolomite

Tab. A5.4.9. Occurrence, size (A largest, B medium, C smallest axes), classification, and composition of dropstones >1 cm in Core PS87/067-2.

N	Stone ID	Station	Size, cm			Classification after Friedman & Sanders	Composition
			A	B	C		
1	B-346	PS87/067-2	3,2	2	1,5	very coarse pebbles	sandstone met.
2	B-347	PS87/067-2	2,5	1,4	1,2	coarse pebbles	sandstone met.
3	B-348	PS87/067-2	2,2	1,3	0,8	coarse pebbles	sandstone
4	B-349	PS87/067-2	2	1,8	1,2	coarse pebbles	quarzite
5	B-350	PS87/067-2	2,2	1	0,8	coarse pebbles	quarzite
6	B-351	PS87/067-2	2,7	1,4	0,8	coarse pebbles	sandstone
7	B-352	PS87/067-2	2	1,3	0,7	coarse pebbles	quarzite
8	B-353	PS87/067-2	1,6	1,5	0,8	medium pebbles	sandstone met.
9	B-354	PS87/067-2	1,9	1,4	1	coarse pebbles	undetermined
10	B-355	PS87/067-2	2	1,1	0,6	coarse pebbles	sandstone
11	B-356	PS87/067-2	1,6	1,5	0,9	medium pebbles	quarzite
12	B-357	PS87/067-2	1,5	1,3	0,9	medium pebbles	quarzite
13	B-358	PS87/067-2	1,7	1,5	0,7	coarse pebbles	flintstone
14	B-359	PS87/067-2	1,5	1,2	1	medium pebbles	sandstone met.
15	B-360	PS87/067-2	1,6	1,2	0,8	medium pebbles	quarzite
16	B-361	PS87/067-2	1,6	1,3	0,6	medium pebbles	
17	B-362	PS87/067-2	1,5	1,2	1,1	medium pebbles	granitoid
18	B-363	PS87/067-2	1,4	0,9	0,9	medium pebbles	
19	B-364	PS87/067-2	1,3	1,2	1	medium pebbles	
20	B-365	PS87/067-2	1,3	1,2	0,9	medium pebbles	
21	B-366	PS87/067-2	1,4	1	0,7	medium pebbles	
22	B-367	PS87/067-2	1,4	1,2	1	medium pebbles	
23	B-368	PS87/067-2	1,2	1	0,9	medium pebbles	
24	B-369	PS87/067-2	1,4	1,1	0,5	medium pebbles	
25	B-370	PS87/067-2	1,3	0,9	0,7	medium pebbles	
26	B-371	PS87/067-2	1,4	1,2	0,6	medium pebbles	
27	B-372	PS87/067-2	1,2	0,8	0,6	medium pebbles	
28	B-373	PS87/067-2	1,4	1,2	0,3	medium pebbles	
29	B-374	PS87/067-2	1,2	1,1	0,5	medium pebbles	

Tab. A5.4.10. Occurrence, size (A largest, B medium, C smallest axes), classification, and composition of dropstones >1 cm in Core PS87/068-2.

N	Stone ID	Station	Size, cm			Classification after Friedman & Sanders	Composition
			A	B	C		
1	B-375	PS87/068-2	2,1	1,1	0,8	coarse pebbles	sandstone
2	B-376	PS87/068-2	1,8	1,5	0,3	coarse pebbles	sandstone
3	B-377	PS87/068-2	1,6	0,9	0,5	medium pebbles	sandstone met.
4	B-378	PS87/068-2	1,3	1	0,7	medium pebbles	quartzite
5	B-379	PS87/068-2	1,2	0,9	0,4	medium pebbles	
6	B-380	PS87/068-2	1,1	1	0,4	medium pebbles	
7	B-381	PS87/068-2	1,2	0,9	0,6	medium pebbles	
8	B-382	PS87/068-2	1,1	0,9	0,5	medium pebbles	

Tab. A5.4.11. Occurrence, size (A largest, B medium, C smallest axes), classification, and composition of dropstones >1 cm in Core PS87/070-2.

N	Stone ID	Station	Size, cm			Classification after Friedman & Sanders	Composition
			A	B	C		
1	B-383	PS87/070-2	7,6	4,8	2,8	small cobbles	undetermined
2	B-384	PS87/070-2	3,9	3,2	1,5	very coarse pebbles	sandstone
3	B-385	PS87/070-2	2,3	1,6	0,7	coarse pebbles	sandstone
4	B-386	PS87/070-2	2,1	0,8	0,8	coarse pebbles	quartzite
5	B-387	PS87/070-2	1,9	1,3	0,8	coarse pebbles	sandstone
6	B-388	PS87/070-2	2,1	1,4	0,6	coarse pebbles	quartzite
7	B-389	PS87/070-2	1,7	1,1	0,8	coarse pebbles	sandstone
8	B-390	PS87/070-2	2,2	1,2	0,8	coarse pebbles	quartzite
9	B-391	PS87/070-2	1,5	1,1	0,7	medium pebbles	sandstone
10	B-392	PS87/070-2	1,5	0,9	0,5	medium pebbles	sandstone met.
11	B-393	PS87/070-2	1,7	0,9	0,7	coarse pebbles	quartzite
12	B-394	PS87/070-2	1,9	0,8	0,3	coarse pebbles	sandstone
13	B-395	PS87/070-2	1,2	1	0,8	medium pebbles	quartzite
14	B-396	PS87/070-2	1,4	1,2	0,3	medium pebbles	quartzite
15	B-397	PS87/070-2	1,3	1	0,7	medium pebbles	quartzite
16	B-398	PS87/070-2	1	0,9	0,3	medium pebbles	quartzite

Tab. A5.4.12. Occurrence, size (A largest, B medium, C smallest axes), classification, and composition of dropstones >1 cm in Core PS87/074-1.

N	Stone ID	Station	Size, cm			Classification after Friedman & Sanders	Composition
			A	B	C		
1	B-399	PS87/074-1	3,3	1,8	1,6	very coarse pebbles	quartzite
2	B-400	PS87/074-1	2,9	2,2	2	coarse pebbles	sandstone met.
3	B-401	PS87/074-1	2,7	1,9	1,1	coarse pebbles	quartzite+Qu vein
4	B-402	PS87/074-1	2,4	2	0,7	coarse pebbles	sandstone
5	B-403	PS87/074-1	2,4	2	0,7	coarse pebbles	sandstone
6	B-404	PS87/074-1	1,9	1,5	1,4	coarse pebbles	sandstone
7	B-405	PS87/074-1	2	1,3	1	coarse pebbles	sandstone
8	B-406	PS87/074-1	2,1	1,5	0,9	coarse pebbles	quartzite
9	B-407	PS87/074-1	1,9	1,1	0,9	coarse pebbles	dolomite
10	B-408	PS87/074-1	1,6	1,3	1	medium pebbles	sandstone
11	B-409	PS87/074-1	1,6	1,2	1	medium pebbles	dolomite
12	B-410	PS87/074-1	1,4	1,3	0,9	medium pebbles	
13	B-411	PS87/074-1	2,5	0,9	0,8	coarse pebbles	sandstone met.
14	B-412	PS87/074-1	1,7	1,3	0,4	coarse pebbles	
15	B-413	PS87/074-1	1,5	1,1	0,9	medium pebbles	
16	B-414	PS87/074-1	1,6	1,4	0,8	medium pebbles	
17	B-415	PS87/074-1	1,3	1	0,7	medium pebbles	
18	B-416	PS87/074-1	1,4	1,1	0,9	medium pebbles	
19	B-417	PS87/074-1	1,4	1,1	0,7	medium pebbles	
20	B-418	PS87/074-1	1,5	1	0,8	medium pebbles	
21	B-419	PS87/074-1	1,4	1,1	0,6	medium pebbles	
22	B-420	PS87/074-1	1,6	1	0,4	medium pebbles	
23	B-421	PS87/074-1	1,4	1	0,6	medium pebbles	
24	B-422	PS87/074-1	1,5	0,8	0,7	medium pebbles	
25	B-423	PS87/074-1	1,2	1,1	0,7	medium pebbles	
26	B-424	PS87/074-1	1,8	0,9	0,3	coarse pebbles	

Tab. A5.4.13. Occurrence, size (A largest, B medium, C smallest axes), classification, and composition of dropstones >1 cm in Core PS87/076-2.

N	Stone ID	Station	Size, cm			Classification after Friedman & Sanders	Composition
			A	B	C		
1	B-425	PS87/076-2	3,4	3	2,4	very coarse pebbles	quartzite
2	B-426	PS87/076-2	2,7	2,6	1,5	coarse pebbles	sandstone
3	B-427	PS87/076-2	2,3	2,2	0,8	coarse pebbles	quartzite
4	B-428	PS87/076-2	2,2	1,8	0,8	coarse pebbles	dolomite
5	B-429	PS87/076-2	2,1	1,6	0,9	coarse pebbles	sandstone/conglomerate
6	B-430	PS87/076-2	1,9	1,5	1,4	coarse pebbles	gneiss
7	B-431	PS87/076-2	2	1,8	1,1	coarse pebbles	granitoid/pegmatite
8	B-432	PS87/076-2	2,1	1,4	0,8	coarse pebbles	sandstone/conglomerate
9	B-433	PS87/076-2	1,5	1,3	1,1	medium pebbles	quartzite
10	B-434	PS87/076-2	1,5	1	0,8	medium pebbles	undetermined
11	B-435	PS87/076-2	1,5	1,2	0,9	medium pebbles	sandstone
12	B-436	PS87/076-2	1,5	1	0,9	medium pebbles	sandstone
13	B-437	PS87/076-2	1,5	1,1	0,6	medium pebbles	undetermined
14	B-438	PS87/076-2	1,4	1,3	0,7	medium pebbles	sandstone met.
15	B-440	PS87/076-2	1,3	0,9	0,8	medium pebbles	quartzite
16	B-441	PS87/076-2	1,6	0,8	0,8	medium pebbles	quartzite
17	B-442	PS87/076-2	1,1	0,9	0,8	medium pebbles	quartzite
18	B-443	PS87/076-2	1,4	0,7	0,6	medium pebbles	Qu vein

Tab. A5.4.14. Occurrence, size (A largest, B medium, C smallest axes), classification, and composition of dropstones >1 cm in Core PS87/079-2.

N	Stone ID	Station	Size, cm			Classification after Friedman & Sanders
			A	B	C	
1	B-447	PS87/079-2	1,6	1	0,6	coarse pebbles
2	B-448	PS87/079-2	1,2	1,2	0,8	medium pebbles
3	B-449	PS87/079-2	1,2	0,8	0,6	medium pebbles
4	B-450	PS87/079-2	1	0,8	0,6	medium pebbles
5	B-451	PS87/079-2	1,1	0,7	0,5	medium pebbles

Tab. A5.4.51. Occurrence, size (A largest, B medium, C smallest axes), classification, and composition of dropstones >1 cm in Core PS87/086-1.

N	Stone ID	Station	Size, cm			Classification after Friedman & Sanders	Composition
			A	B	C		
1	B-456	PS87/086-1	2,4	1,5	1,3	coarse pebbles	
2	B-457	PS87/086-1	1,9	1,3	1	coarse pebbles	
3	B-458	PS87/086-1	1,8	1,2	0,5	coarse pebbles	
4	B-459	PS87/086-1	1,7	1,4	0,5	coarse pebbles	
5	B-460	PS87/086-1	1,4	1,2	0,5	medium pebbles	
6	B-461	PS87/086-1	1,4	1	0,7	medium pebbles	
7	B-462	PS87/086-1	1	0,9	0,6	medium pebbles	
8	B-463	PS87/086-1	1,1	0,8	0,6	medium pebbles	
9	B-464	PS87/086-1	1,3	0,8	0,4	medium pebbles	

A5.5 Tables with micropaleontological data

(S. Kaboth, M. Kaminski, S. Nam, A. de Vernal, M. Zwick)

Tab. A5.5.1: Summarized content of the > 63 µm fraction in core PS87/023-1.
For further details (scale ranging, calculation of sand content, etc.) see text.

PS87/023 KAL (Depth in cmbsf)										
	Sand particles (mm height in vials; ~ % of volume)	Planktic foraminifers (<i>N. pachyderma</i> l.)	Calcareous benthic foraminifers	<i>Oridorsalis tener</i>	<i>Bolivina arctica</i>	<i>Cassidulina</i>	Agglutinated benthic foraminifers	Ostracodes	Sponge spicules	echinoderm spines
25-27	3	4	4				0	X		
27-29	8	4	4				0	X		
29-31	2	4	4				3	X	X	
31-33	12	4	1				0	X	X	
33-35	14	4	3				0		X	
35-37	11	4	2				0	X		
37-39	21	3	0				0			
39-41	20	2	0				0			
41-43	16	0	0				0			
43-45	20	0	0				1			
45-47	18	0	0				0			
47-49	18	0	0				0			
49-51	19	0	0				0			
51-53	19	0	0				0			
53-55	18	0	0				0			
55-57	17	1	0				0			
57-59	15	1	0				0			
61-63	12	2	0				0			
59-61	15	0	0				1			
63-65	14	0	0				1			
65-67	14	0	0				0			
67-69	15	1	1			X	1			
69-71	2	4	2	X			1			
71-73	3	4	4	X			0	X		
73-75	4	4	4	X			0	X		
75-77	3	4	3	X			0	X		
77-79	5	4	2	X			0	X	X	
79-81	2	4	4				0	X	X	
84-87	3	4	1	X			1	X	X	
87-89	2	4	2				0		X	
89-91	2	4	3				0	X	X	

91-93	2	4	1	X			0	X	X	
93-95	2	4	2				1		X	
95-97	4	4	1				1	X	X	
97-99	3	4	2	X			0		X	
99-101	5	4	2	X			0		X	
101-103	5	4	2	X			0			
103-105	6	4	1				0			
105-107	4	4	2	X			1	X	X	
107-109	6	4	2	X			0		X	
109-111	11	4	1	X			1			
111-113	15	4	1				1	X	X	
113-115	10	4	2	X			0		X	X
115-117	7	4	1				1		X	
117-119	4	4	1				0			
119-121	7	4	2	X			0			
121-122	2	4	1	X			0	X		X
122-124	2	4	4	X	X	X	0	X	X	
124-126	2	4	2				0	X	X	
126-128	2	4	2				0	X	X	
128-130	1	2	2	X			0		X	
130-132	1	4	1				1		X	
132-134	2	4	2				0	X	X	
134-136	2	4	1				0	X	X	
136-138	2	4	2				1		X	
138-140	5	4	2				0	X	X	
140-142	6	4	1			X	0	X	X	
140-142bis	3	4	0				0	X	X	
144-146	7	4	3		X		0		X	
146-148	6	4	1		X		0	X	X	
148-150	5	4	2		X		0	X	X	
150-152	3	4	1		X		0			
152-154	3	4	2		X		0	X		
154-156	5	4	3		X		0			
156-158	4	4	2	X	X		0	X		
158-160	10	4	2		X		0			
160-162	17	4	2				0	X		
162-164	20	4	3		X	X	0			
164-166	9	4	2		X		0		X	
166-168	1	4	4		X		0		X	
168-170	4	4	4		X		0		X	
170-172	2	4	4		X		0		X	X
172-174	6	4	4		X		0			
174-176	5	4	3		X		0		X	X
176-178	7	4	2		X		0		X	X
178-180	7	4	1				0	X	X	X
180-182	15	3	1				0			X
182-184	26	1	0				1			
184-186	46	1	0				0			
186-188	37	0	0				1			
188-190	48	1	0				1			
190-192	45	4	3		X		0	X	X	
192-194	26	0	0				0			

194-196	34	0	0				0			
196-198	35	0	0				1			
198-200	22	0	0				1			
200-202	21	1	0				1			
202-204	14	0	0				2			
204-206	5	1	1				0			
206-208	2	2	2				0			
208-210	13	2	1				0		X	
210-212	3	3	4		X		0		X	
212-214	2	3	4		X		0		X	
214-216	10	3	3		X		0			
216-218	15	2	2		X	X	0			
218-220	24	1	1		X		1		X	
220-222	21	1	1		X		0			
222-224	20	0	0				0			
224-226	13	1	1	X			0			
226-228	1	3	3		X		0	X	X	
228-230	1	4	4		X		0	X	X	X
230-232	2	3	3		X		1			
232-234	2	2	2		X		0			X
234-236	4	4	4	X	X		1			
236-238	3	4	4		X		0			
238-240	3	4	3		X		1		X	X
240-242	2	4	3		X		0		X	
242-244	4	4	4		X		0		X	
246-248	2	4	4		X		0			
246-248	2	4	2		X	X	2	X	X	x
248-250	3	4	1		X		0		X	
250-252	3	3	2		X		0	X	X	
252-254	1	4	1		X		0		X	
254-256	1	4	3		X	X	0		X	
256-258	2	4	2		X		0		X	
258-260	4	4	2		X		0		X	
260-262	2	4	3		X		0	X	X	
262-264	1	4	1		X		1		X	
264-266	4	4	2		X		0	X	X	
266-268	17	2	2			X	1		X	
268-270	22	2	0				1		X	
270-272	10	3	2		X		0			
272-274	6	4	2		X		0	X	X	
274-276	8	4	4		X		0	X	X	X
276-278	4	4	3		X		1	X	X	X
278-280	1	4	1		X		0		X	
280-282	4	3	2		X		0		X	
282-284	5	2	2		X	X	0		X	X
284-286	4	2	2			X	0	X	X	
286-288	13	2	2		X	X	0	X	X	
286-288	18	1	0				0			
288-290	12	2	1				1	X	X	
290-292	8	2	1				0		X	
292-294	4	3	3		X		1	X	X	
296-298	3	1	1			X	1	X	X	

298-300	2	2	2		X	X	0	X	X	X
300-302	2	3	3		X		0	X	X	X
302-304	2	2	2			X	0	X	X	
304-306	2	3	3			X	0		X	X
306-308	2	3	3		X		0		X	
308-310	2	2	2			X	1		X	X
310-312	1	2	2		X	X	0		X	
312-314		4	4		X	X	0			X
314-316	2	4	2		X	X	0			
316-318	2	4	4		X	X	0		X	X
318-320	2	4	4		X	X	0	X	X	X
320-322	5	3	3		X	X	0	X	X	
322-324	5	4	4		X	X	0	X	X	X
324-326	6	4	4		X	X	0		X	
326-328	5	4	4		X	X	0		X	
328-330	6	4	2		X		1	X	X	
330-332	16	2	1				1		X	
332-334	14	2	1				1			
334-336	16	2	1				1			
336-338	10	2	1			X	1		X	
338-340	15	1	0				0			
340-342	12	1	0				1			X
342-344	9	3	1				0			
344-346	7	1	1				0	X		
346-348	3	1	0				0			
348-350	5	1	1				0			
350-352	6	0	1			X	0			
352-354	4	0	1				1	X		
354-356	4	2	1		X		1	X		
356-358	5	2	2		X		0	X		
358-360	3	3	1				0			
360-362	4	2	1				1			
362-364	7	0	0				0			
364-366	7	0	0				0			
366-368	9	0	1				0			
368-370	7	0	0				1			
370-372	8	0	1			X	0			
372-374	5	0	0				0			
374-376	5	0	0				0			
376-378	5	1	1				1			
378-380	8	0	0				0			
380-382	15	0	0				0			
382-384	20	1	1				0			
384-386	25	0	1		X		0			
386-388	20	0	1				0			
388-390	17	0	0				0			
390-392	8	0	2		X		1			
392-394	4	0	0				1			
394-396	2	1	0				1			
396-398	4	1	0				0			
398-400	2	1	0				0			
400-403	4	1	1				1			

402-404	2	1	0			0			
404-406	2	1	0			0			
406-408	2	1	0			1			
408-412	1	1	0			1			
410-412	3	2	0			0			X
412-414	5	0	0			1			
414-416	5	0	0			1			
416-418	8	0	0			2			
418-420	7	1	0			2			
420-422	8	1	0			1			
422-424	10	1	0			0			
424-426	22	0	0			1			
426-428	10	0	0			1			
428-430	7	0	0			0			
430-432	5	0	0			1			
432-434	2	1	0			0			
434-436	4	1	0			0			
436-438	6	1	0			2			
438-440	13	0	0			2			
440-442	12	1	0			0			
442-444	18	0	0			1			
444-446	13	0	0			1			
446-448	12	0	0			0			
448-450	11	1	0			1			
450-452	15	1	0			0			
452-454	6	0	0			1			
454-456	4	1	0			1			
456-458	3	1	0			1			
458-460	10	0	0			1			
460-462	6	0	0			1			
462-464	7	0	0			1			
464-466	6	0	0			1			
466-468	16	0	0			1			
468-470	21	0	0			0			
470-472	5	0	0			1			
472-474	3	0	0			0			
474-476	2	0	0			1			
476-478	2	1	0			1			
478-480	3	0	0			1			
480-482	2	0	0			0			
482-484	2	0	0			0			
484-486	1	0	0			0			
486-488	1	0	0			1			
488-490	1	0	0			1			
490-492	3	0	0			1			
492-494	1	1	0			1			
494-496	1	0	0			1			
496-498	1	0	0			1			
500-502	1	0	0			0			
502-504	2	2	0			1			
504-506	2	0	0			0			
506-508	1	1	0			1			

508-510	1	2	0				1			
510-512	2	1	0				1			
512-514	5	0	0				0			
514-516	8	0	0				1			
516-518	12	0	0				1			
518-520	12	0	0				1			
520-522	8	1	0				1			
522-524	3	0	0				0			
524-526	6	0	0				1			
526-528	8	0	0				0			
528-530	19	0	0				2			
530-532	20	0	0				1			
532-534	32	0	0				1			
534-536	16	0	0				2			
536-538	19	0	0				1			
538-540	22	0	0				1			
540-542	10	0	0				0			
542-544	12	0	0				1			
544-546	7	0	0				1			
546-548	12	0	0				0			
548-550	10	0	0				1			
550-552	10	0	0				1			
552-554	7	1	0				1			
556-558	6	0	0				1			
554-556	7	0	0				1			
560-562	8	0	0				1			
562-564	8	0	0				1			
564-566	8	0	0				0			
566-568	8	0	0				1			
568-570	11	0	0				1			
570-572	14	0	0				1			
572-574	13	0	0				1			
574-576	24	0	0				1			
576-578	22	0	0				1			
580-582	2	0	0				0			
582-584	9	0	0				0			
584-586	24	0	0				1			
586-588	9	0	0				1			
588-590	5	3	0				1			
588-590bis	8	0	0				1			
590-592	8	0	0				0			
592-594	9	0	0				1			
594-596	11	0	0				1			
596-598	13	0	0				0			
598-600	15	0	0				0			
600-602	3	0	0				0			
602-604	5	1	0				0			
604-606	6	0	0				1			
606-608	7	0	0				0			
608-610	10	0	0				0			
610-612	10	0	0				0			
612-614	4	0	0				1			

614-616	5	0	0			0			
616-618	5	0	0			1			
618-620	3	0	0			1			
620-622	3	0	0			1			
622-624	3	0	0			1			
624-626	3	0	0			0			
626-628	6	0	0			1			
628-630	3	0	0			1			
630-632	3	0	0			0			
632-634	4	0	0			1			
634-636	3	0	0			1			
636-638	2	0	0			1			
638-640	3	0	0			1			
640-642	2	0	0			1			
642-644	2	2	1			1			
644-646	1	0	0			1			
646-648	1	0	0			0			
648-650	3	0	0			1			
650-652	4	0	0			1			
652-654	5	0	0			1			
654-656	7	0	0			0			
656-658	7	1	0			0			
656-658bis	6	0	0			1			
660-662	8	0	0			0			
662-664	5	0	0			0			
664-666	7	0	0			0			
666-668	2	0	0			0			
668-680	1	0	0			1			
670-672	2	1	0			1			
672-674	1	0	0			0			
674-676	1	1	1			0			
676-678	4	1	0			1			
678-680	6	0	0			0			
680-682	6	0	0			1			
682-684	5	0	0			1			
684-686	2	2	0			0			
684-686bis	2	1	0			0			
686-688	2	1	0			1			
688-690	1	0	0			1			
690-692	2	1	0			0			
692-694	2	0	0			1			
694-696	1	0	0			1			
696-698	4	1	0			1			

Tab. A5.5.2: Summarized content of the > 63 µm fraction in core PS87/030-1.
For further details (scale ranging, calculation of sand content, etc.) see text.

PS87/030 KAL (Depth in cmbsf)	Sand particles (mm height in vials; ~ % of volume)	Planktic foraminifers (<i>N. pachyderma</i> l.)	Subpolar planktic foraminifers (mostly <i>N. pachyderma</i> d.)	Calcareous benthic foraminifers	<i>Cassidulina</i>	<i>Oridorsalis tener</i>	<i>Bolivina arctica</i>	<i>Bulimina aculeata</i>	Agglutinated benthic foraminifers	Ostracodes	Sponge spicules	echinoderm spines
0-2	12	4	X	3	X	X			1	X	X	X
8-10	16	4	X	2	X	X			0	X	X	X
16-18	15	1		0					0			
25-27	18	0		0					1			
38-40	13	0,5		0					0			
48-50	9	0,5		0					0			
50-52	23	0		0					0			
55-57	20	0		0					0			
58-60	36	0		0					0			
63-65	18	4	X	4	X	X			0			
67-69	8	4	X	3	X			X	0	X		X
71-73	13	4	X	2,5	X	X	X	X	0	X	X	X
75-77	21	4	X	4	X		X	X	0		X	
80-82	21	4	X	3		X	X	X	1	X	X	X
82-84	28	4	X	3	X		X	X	0	X	X	X
84-86	28	4	X	3	X		X	X	0	X	X	X
88-90	16	4	X	2	X		X	X	0,5	X	X	X
91-93	20	3		1	X				0	X	X	X
95-97	37	0		0					0			
104-106	60	0		0					0			
115-117	9	0,5		0					1			
130-132	12	4	X	3	X		X		1	X	X	
136-138	12	0,5	X	0,5	X				0			
140-142	14	4	X	3	X		X		2	X	X	X
142-144	13	4	X	3	X		X		0	X	X	X
147-148	14	0,5		0					0			
155-157	16	0,5		0					0			

165-167	26	0		0				0,5			
175-177	23	0,5		0				0			
185-187	12	0		0				1			
195-197	25	4		4	X		X	2	X	X	
197-199	14	4	X	4	X		X	0,5	X	X	X
203-205	3	3	X	2	X		X	0	X	X	X
209-211	7	4	X	3	X		X	1	X	X	X
215-219	8	4	X	4	X		X	0	X	X	
219-222	10	1		1	X			0	X	X	X
225-227	4	0,5		0				0,5	X	X	X
230-232	6	1	X	2	X		X	0	X	X	X
234-236	8	1	X	2	X		X	2	X	X	X
242-246	8	2	X	3	X		X	0	X	X	X
244-246	8	3		2	X		X	1	X	X	X
250-252	10	2	X	2	X			1,5			
257-259	7	1		2	X			2			X
264-266	6	0		2	X		X	1	X		
267-269	5	1		3	X		X	2	X		X
271-273	8	1		2	X			1	X		X
278-280	8	1		2	X		X	2	X		
285-287	6	0		0				0,5			
295-297	7	0,5		0				1			
302-304	5	1		0				2			
310-312	5	0		0				2			
322-324	8	0		3	X		X	3			
319-321	5	0		3	X		X	2			
326-328	8	0		3	X		X	2			X
332-334	5	0,5		2	X		X	2			X
340-342	14	0		0				1			
347-349	5	0		0				2			
354-356	4	0,5	X	0				2			
365-367	18	0		0				0			
370-372	6	1		1	X		X	1			
382-384	16	0		0				0			
395-397	4	0		0				2			
404-406	2	0		0				3			
412-414	3	0		0				2			
420-422	3	0,5	X	0				2			
426-428	4	0		0				2			
437-439	5	0		0				2			
448-450	7	0		0				2			
457-459	4	0,5		0				2			
467-469	5	0		0				2			
476-478	5	0		0				2			
488-490	6	0		0				1			
499-501	12	0		0				1			
510-512	5	1		0,5				2			
520-522	5	0		0				2			
536-538	3	0,5		0				3			

546-548	4	0		0					2			
554-556	4	0		0					3			
563-565	3	0		0					2			
576-578	3	0		0					2			
583-585	3	0		0					3			
591-593	3	0		0					1			
596-598	3	0		0					3			
606-608	3	0		0					3			
612-614	2	0		0					3			
621-623	2	0		0					3			

Tab. A5.5.3: Occurrence of agglutinated benthic foraminifer taxa in core PS87/030-1.

R = rare (<5 specimen), F = frequent (5-10), C = common (10-50), A = abundant (> 50).

PS87/30 KAL (Depth in cmbsf)	<i>Reticulophragmium pusillum</i>	<i>Rhabdammina</i>	<i>Haplophragmoides</i> sp. 1	<i>Glomospira gordialis</i>	<i>Trochammina Lomonosovensis</i>	<i>Psammosphaera fusca</i>	<i>Hemisphaerammina</i> sp.	<i>Placopsiella aurantiaca</i>	<i>Verrucina arctica</i>	<i>Pseudonodosinella nodulosa</i>	<i>Hyperammina rugosa</i>	<i>Reophax duplex</i>	<i>Reophax bradyi</i>	<i>Glomospira irregularis</i>	large agglutinated plates	<i>Reophax scoriurus</i>	<i>Capsammina</i> sp.	<i>Recurvoides</i> sp.	<i>Psammosphaera bowmani</i>	<i>Trochammina quadriloba</i>	<i>Haplophragmoides sphaeriloculus</i>	<i>Cribrostomoides subglobosus</i>	<i>Alveolophragmium polarensis</i>	<i>Reophax arcticus</i>	<i>Jaculella</i> sp.	<i>Trochammina Pseudoinfiata</i>	<i>Ammodiscus catinus</i>	
215-219	F	R	R	R	R																							
225-227	C	F	F		C	?R	R	R																				
234-236	C	R	R	F	C			R	R	R																		
257-259	A	F	C	R	R	F	F		R		R	R																
278-280	C	R	C	R	F	F	F	R	F				R	R	F													
302-304	C	C	A		C	F	F		F				F		F	R	R											
322-324	A	F	A	R	A	R	R	F			R				F		R	R	F									
332-334	F			R	F	R	F	R			R				F													
354-356	F		R			R									R													
370-372	F		R															R										
395-397	A	F	A	R	C	C	C		F	F	F	R	F		C	R		R	F	C	F	R						
404-406	C	F	C	R	C	F	C	R	C	R	C	R			F			R	F	C	R		F	R	R			
437-439	C	F	A	F	C	F	F	R				R	F		F			R	R			R	F	R				
457-459	C	F	C	R	C	F	C	F	R	R		F			F		F		C	R			F	R				
476-478	C	F	C	F	A	C			R	R					C	R	R		R									
499-501	F	R	R		F	F	R		R						R													
510-512	F	F	C		C	F	R			R			F		R					R								
520-522	C	F	A		C	F	F			R	R	F	F		R					R								
536-538	C	F	A		A	F	F	R	F	R	R	R	C		F		R		C				F	R				
546-548	C	R	F	R	C	R	R		R	R		R	F		R				F									
563-565	C	C	A	F	C	C	F	R	F	R	R	R	F		F				F					R		R		
583-585	A	F	C	R	A	R	R	R	R	R			F		F		R		C								R	
591-593	C	F	C	F	C			R			R	R	R	F										R				R
606-608	C	F	F		F	F	F			R			F		F			R					R					
612-614	A	F	C	F	F	C	F						C		C								F				R	
621-623	C	F	F	F	F		R						F					R					F					
Zipfel- mutze	C	F	F		F		R			R		R	F		F				R									

Tab. A5.5.4: Summarized content of the > 63 µm fraction in core PS87/056-1.

For further details (scale ranging, calculation of sand content, etc.) see text..

PS87/056 KAL (Depth in cmbsf)	Sand particles (mm height in vials; ~ % of volume)	Planktic foraminifers	Calcareous benthic foraminifers	Agglutinated benthic foraminifers
179,5-180,5	3	0	0	2
186,5-187,5	4	0	0	2
188,5-189,5	5	0	0	2
195,5-196,5	14	0	0	1
198,5-199,5	18	0	0	0
202,5-203,5	13	0	0	1
205-206	18	0	0	0
207-208	15	0	0	1
209,5-210,5	25	0	0	1
213-214	13	0	0	0
215,5-216,5	22	0	0	1
218-219	20	0	0	0
221-222	20	0	0	0
223,5-224,5	20	0	0	0
226-227	19	0	0	0
230,5-231,5	16	0	0	0

Tab. A5.5.5: Summarized content of the >63 µm fraction in core PS87/070-1.

For further details (scale ranging, calculation of sand content, etc.) see text.

PS87/070 KAL (Depth in cmbsf)	Sand particles (mm height in vials; ~ % of volume)	Planktic foraminifers (<i>N. pachyderma</i> l.)	Subpolar planktic foraminifers (<i>N. pachyderma</i> d.)	Calcareous benthic foraminifers	<i>Oridorsalis tener</i>	<i>Cassidulina</i>	Agglutinated benthic foraminifers	Ostracodes	Sponge spicules	echinoderm spines
3-5	3	4	X	4	X		4	X	X	X
20-22	4	4	X	4	X	X	4			
30-32	1	4	X	2	X		2,5	X	X	X
40-42	1	4	X	1,5		X	1	X	X	X
48-50	7	4	X	2	X		1	X	X	X
53-55	9	3,5	X	2	X		1	X	X	X
67-69	6	4	X	2	X	X	2,5			
75-77	6	0		0			2			
90-92	21	0		0			0,5			
100-102	8	0		0			2			
110-112	10	0		0			0			
130-132	35	0		0			0			
150-152	3	0		0			3			
160-162	3	0		0			2			
175-177	3	0		0			2			
190-192	5	0		0			0			
200-202	3	0		0			0			
209-211	2	0		0			0			
217-219	3	0		0			1			
224-226	3	0		0			1			
231-233	4	0		0			2			
237-239	19	0		0			2			
246-248	50	0		0			0			
251-253	1	0		0			0,5			
255-257	1	0		0			2			

265-267	1	0		0		2			
274-276	2	0		0		3			
290-292	4	0		0		4			
300-302	14	0		0		1			
312-314	13	0		0		1			
314-316	2	0		2		0			
330-332	5	0		0		0			
337-339	24	0		0		0			
350-352	5	0		0		0			
360-362	4	0		0		3			
370-372	4	0		0		2			
377-379	3	0		0		2			
390-392	4	0		0		1			
402-404	7	0		0		1			
417-419	4	0		0		2			
430-432	3	0		0		1			
441-443	4	0		0		2			
450-452	6	0		0		3			
462-464	2	0		0		3,5			
472-474	3	0		0		2			
484-486	10	0		0		1			
494-496	14	0		0		0			
501-503	10	0		0		0,5			
509-511	40	0		0		0			
527-529	16	0		0		0,5			
538-540	18	0		0		0			
548-550	15	0		0		0			
561-563	23	0		0		0			
574-576	28	0		0		0			
586-588	7	0		0		0,5			
600-602	0,5	0		0		0			
618-620	0,2	0		0		0			
642-643	0,2	0		0		0			
660-662	4	0		0		2			
672-674	5	0		0		2			
686-688	3	0		0		2,5			
706-708	2	0		0		2,5			
716-718	2	0		0		2			
738-740	3	0		0		1			
746,5-749,5	1	1		0		3			
756-759	2	0		0		2			

Tab. A5.5.6: Occurrence of agglutinated benthic foraminifer taxa in core PS87/070-1.
 R = rare (<5 specimen), F = frequent (5-10), C = common (10-50), A = abundant (> 50).

PS87/070 KAL (Depth in cmbstf)	<i>Pseudonodosinella nodulosa</i>	<i>Cribrostomoides subglobosus</i>	<i>Psammospaera fusca</i>	<i>Hyperammia rugosa</i>	<i>Placopsilinella aurantiaca</i>	<i>Glomospira gordialis</i>	<i>Rhabdammina</i> sp. 1	<i>Verrucina arctica</i>	<i>Haplophragmoides</i> sp. 1	Large agglutinated plates	<i>Hemisphaerammina</i> sp.	<i>Reticulophragmium pusillum</i>	<i>Evolutinella</i> sp. 1	<i>Trochammina</i> sp.	<i>Alveolophragmium polarensis</i>
3-5	R	C	F												
20-22	R	R													
30-32		R													
40-42															
48-50		R	R	R											
53-55				R	R										
67-69		C	R	F											
75-77		F	R	C											
90-92															
100-103															
110-112															
130-132															
150-152		C	R	C		R	R								
160-162		F	R	C			R								
175-177		C		C											
190-192															
200-202															
209-211															
217-219															
224-226															
231-233		C		R											
237-239		F													
246-248															
251-253							R								
255-257			F				F	R							
265-267	R	F	C	F				F							
274-276		C	F	C											
290-292		C		F					R						
300-302		F		F											
312-314		F		F											

314–316																	
320–322																	
330–332																	
337–339																	
350–352																	
360–362			C				F		F	F							
370–372				F		R			R	F							
377–379	R						C		C	F	R						
390–392							R		R								
402–404							R		R								
417–419							R			R							
430–432				F			R		F	R							
441–443			R				F		F	F		C	R				
450–452			R	F					C			C	F	R	F		
462–464			R	C		R			C			C				F	
472–474				C		R						C				R	
484–486			R	R								F					
494–496																	
501–503												F					
509–511																	
527–529																	
538–540																	
548–550																	
561–563																	
574–576																	
586–588												R					
600–602																	
618–620																	
642–644																	
660–662		C										C					
672–674		F										C				R	
686–688		F										C					
706–708	R		F	C	R	R	F		R	F		F					
716–718			R	F			F		R			C					
738–740												C					
746.5–749.5			R	C		R	F		F	R		C					
756–758		F		C		F	F					C					

Tab. A5.5.7: Summarized content of the > 63 μm fraction in core PS87/079-1.

For further details (scale ranging, calculation of sand content, etc.) see text.

PS87/079 KAL (Depth in cmbsf)	Sand particles (mm height in vials; ~ % of volume)	Planktic foraminifers (<i>N. pachyderma</i> l.)	Calcareous benthic foraminifers	Agglutinated benthic foraminifers
13-16	2	2	1	2
38-40	1	2	1	2
56-58	1	1	0	1
80-82	4	0	0	2
100-102	1	1	0	2
120-121	5	0	0	3
135-137	2	0	0	1
143-145	4	0	0	1
150-152	27	0	0	0
155-157	2	0	0	0
163-165	13	0	0	0
172-174	14	0	0	0
187-189	35	0	0	0
196-198	1	0	0	2
210-212	3	0	0	2
236-238	2	0	0	2
257-259	2	0	0	3
277-279	2	0	0	0
294-296	2	0	0	0
302-304	15	0	0	0
307-309	8	0	0	1

309-311	1	0	0	1
318-320	2	0	0	2
335-337	1	0	0	0
357-359	2	0	0	2
380-382	38	0	0	0
390-392	1	0	0	2
410-412	2	0	0	3
435-437	2	0	0	2
453-455	12	0	0	2
461-463	22	0	0	2
468-470	18	0	0	1
486-488	11	0	0	0
503-505	2	0	0	0
512-514	1	0	0	0
540-542	4	0	0	2
555-557	2	1	0	1
572-574	2	0	0	1
617-619	3	0	0	2
635-637	2	0	0	0
650-652	2	0	0	2

Tab. A5.5.8: Occurrence of agglutinated benthic foraminifer taxa in core PS87/079-1.																	
R = rare (<5 specimen), F = frequent (5-10), C = common (10-50).																	
PS87/079 KAL (Depth in cmbstf)	<i>Pseudonodosinella nodulosa</i>	<i>Cribrostomoides subglobosus</i>	<i>Glomospira gordialis</i>	<i>Ammodiscus catinus</i>	<i>Hyperammina rugosa</i>	<i>Psammospaera fusca</i>	<i>Hemisphaerammina</i> sp.	<i>Recurvoides</i> sp. (coarse)	<i>Reticulophragmium pusillum</i>	<i>Trochammina lomonosovensis</i>	<i>Rhabdammina</i> sp. 1	<i>Placopsilinella aurantiaca</i> large aggl plates	<i>Verrucina arctica</i>	<i>Haplophragmoides</i> sp. 1	<i>Capsammina</i>	<i>Reophax</i> sp.	<i>Glomospira irregularis</i>
13-16	F	R	R	R													
38-40	R																
56-58					R												
80-82	R					R											
100-102	R		R			R	R										
120-122		C			C		R	R	R								
135-137	R				F			R									
143-145		F			R				R	R							
150-152																	
155-157																	
163-165																	
172-174																	
187-189																	
196-198	F	R	R		C		R				C						
210-212	R	F	R		F												
236-238			R		R												
257-259	R	F			C	R	R										
277-279																	
294-296																	
302-304																	
307-309												R					
309-311											F						
318-320	R	R	R		C	R											
335-337																	
357-359		F			C		R										

380-382																		
390-392										F								
410-412		C	R		C	F				R	R	F	F	F	F			
435-437		C			C	R								R	R			
453-455		F	R		F													
461-463		R			F													
468-470						R		R		R								
486-488																		
503-505																		
512-514																		
540-542							R	R		C		R		C		R		
555-557	R		R		F	F				F								
572-574									R					R				R
617-619			R		C	R	R			F				F				
635-637			R		C		R				R			F				
650-652	R	R	R	R	F	R	R		C		C			C	F			

Die **Berichte zur Polar- und Meeresforschung** (ISSN 1866-3192) werden beginnend mit dem Band 569 (2008) als Open-Access-Publikation herausgegeben. Ein Verzeichnis aller Bände einschließlich der Druckausgaben (ISSN 1618-3193, Band 377-568, von 2000 bis 2008) sowie der früheren **Berichte zur Polarforschung** (ISSN 0176-5027, Band 1-376, von 1981 bis 2000) befindet sich im electronic Publication Information Center (**ePIC**) des Alfred-Wegener-Instituts, Helmholtz-Zentrum für Polar- und Meeresforschung (AWI); see <http://epic.awi.de>. Durch Auswahl "Reports on Polar- and Marine Research" (via "browse"/"type") wird eine Liste der Publikationen, sortiert nach Bandnummer, innerhalb der absteigenden chronologischen Reihenfolge der Jahrgänge mit Verweis auf das jeweilige pdf-Symbol zum Herunterladen angezeigt.

The **Reports on Polar and Marine Research** (ISSN 1866-3192) are available as open access publications since 2008. A table of all volumes including the printed issues (ISSN 1618-3193, Vol. 1-376, from 2000 until 2008), as well as the earlier **Reports on Polar Research** (ISSN 0176-5027, Vol. 1-376, from 1981 until 2000) is provided by the electronic Publication Information Center (**ePIC**) of the Alfred Wegener Institute, Helmholtz Centre for Polar and Marine Research (AWI); see URL <http://epic.awi.de>. To generate a list of all Reports, use the URL <http://epic.awi.de> and select "browse"/ "type" to browse "Reports on Polar and Marine Research". A chronological list in declining order will be presented, and pdf icons displayed for downloading.

Zuletzt erschienene Ausgaben:

Recently published issues:

688 (2015) The Expedition PS87 of the Research Vessel POLARSTERN to the Arctic Ocean in 2014, edited by Rüdiger Stein

687 (2015) The Expedition PS85 of the Research Vessel POLARSTERN to the Fram Strait in 2014, edited by Ingo Schewe

686 (2015) Russian-German Cooperation CARBOPERM: Field campaigns to Bol'shoy Lyakhovsky Island in 2014, edited by Georg Schwamborn and Sebastian Wetterich

685 (2015) The Expedition PS86 of the Research Vessel POLARSTERN to the Arctic Ocean in 2014, edited by Antje Boetius

684 (2015) Russian-German Cooperation SYSTEM LAPTEV SEA: The Expedition Lena 2012, edited by Thomas Opel

683 (2014) The Expedition PS83 of the Research Vessel POLARSTERN to the Atlantic Ocean in 2014, edited by Hartwig Deneke

682 (2014) Handschriftliche Bemerkungen in Alfred Wegeners Exemplar von: Die Entstehung der Kontinente und Ozeane, 1. Auflage 1915, herausgegeben von Reinhard A. Krause

681 (2014) Und sie bewegen sich doch ...Alfred Wegener (1880 – 1930): 100 Jahre Theorie der Kontinentverschiebung – eine Reflexion, von Reinhard A. Krause

680 (2014) The Expedition PS82 of the Research Vessel POLARSTERN to the southern Weddell Sea in 2013/2014, edited by Rainer Knust and Michael Schröder

679 (2014) The Expedition of the Research Vessel 'Polarstern' to the Antarctic in 2013 (ANT-XXIX/6), edited by Peter Lemke

678 (2014) Effects of cold glacier ice crystal anisotropy on seismic data, by Anja Diez



ALFRED-WEGENER-INSTITUT
HELMHOLTZ-ZENTRUM FÜR POLAR-
UND MEERESFORSCHUNG

BREMERHAVEN

Am Handelshafen 12
27570 Bremerhaven
Telefon 0471 4831-0
Telefax 0471 4831-1149
www.awi.de

